PHYSICAL REVIEW E **71**, 025104(R) (2005)

Power-law correlated processes with asymmetric distributions

Boris Podobnik,[1,2,3] Plamen Ch. Ivanov,[2] Vojko Jazbinsek,[4] Zvonko Trontelj,[4] H. Eugene Stanley,[2] and Ivo Grosse[3]
[1]*Faculty of Civil Engineering, University of Rijeka, Rijeka, Croatia*
[2]*Center for Polymer Studies and Department of Physics, Boston University, Boston, Massachusetts 02215, USA*
[3]*Institute of Plant Genetics and Crop Plant Research (IPK), 06466 Gatersleben, Germany*
[4]*Institute of Mathematics, Physics and Mechanics, University of Ljubljana, Ljubljana, Slovenia*
(Received 8 November 2004; published 28 February 2005)

Motivated by the fact that many physical systems display (i) power-law correlations together with (ii) an asymmetry in the probability distribution, we propose a stochastic process that can model both properties. The process depends on only two parameters, where one controls the scaling exponent of the power-law correlations, and the other controls the degree of asymmetry in the distributions leaving the correlations unaffected. We apply the process to air humidity data and find that the statistical properties of the process are in a good agreement with those observed in the data.

DOI: 10.1103/PhysRevE.71.025104 PACS number(s): 02.50.−r, 05.40.−a, 87.19.−j

Many physical phenomena exhibit temporal or spatial correlations that can be approximated by power laws. For example, long-range power-law correlations have been found in physical, biological, and social systems [1–8], and various stochastic processes [9–12] have been developed to model these power-law scaling properties. Recent studies have shown that in addition to power-law correlations empirical data often exhibit a significant skewness or asymmetry in their distributions. Asymmetric distributions have been found in astrophysical data [13], genome sequences [14], respiratory dynamics [15], brain dynamics [16], heartbeat dynamics [17], turbulence [18], physical activities, and finance [19].

With the goal of constructing a stochastic process that can generate time series with both power-law correlated and asymmetrically distributed variables x_i, we define the process $\mathcal{A}(\rho,\lambda)$ by

$$x_i = \lambda|x_{i-1}| + \sum_{n=1}^{\infty} a_n(\rho)(x_{i-n} - \lambda|x_{i-n-1}|) + \eta_i, \qquad (1)$$

where $\rho \in (0,0.5)$ and $\lambda \in (-1,1)$ are free parameters, $a_n(\rho)$ are weights defined by $a_n(\rho)=\Gamma(n-\rho)/[\Gamma(-\rho)\Gamma(1+n)]$, Γ denotes the Gamma function, and η_i denotes independent and identically distributed Gaussian variables with expectation value $\langle \eta_i \rangle = 0$ and variance $\langle \eta_i^2 \rangle = 1$. The parameter ρ controls the length of the memory, i.e., how rapidly the influence of past values x_{i-n} and $|x_{i-n-1}|$ on x_i decays in time, and the parameter λ controls the relative influence of x_{i-n} on x_i compared to the influence of $|x_{i-n-1}|$ on x_i.

$\mathcal{A}(\rho,\lambda)$ can be understood as a generalization [20,21] of the fractionally integrated process proposed in Refs. [9,10], to which $\mathcal{A}(\rho,\lambda)$ reduces for $\lambda=0$. While the fractionally integrated process $\mathcal{A}(\rho,0)$ is known to generate power-law correlated and symmetrically distributed time series [9,10], we will show in the following that, for $\lambda \neq 0$, $\mathcal{A}(\rho,\lambda)$ generates power-law correlations with an asymmetric distribution. Specifically, we will show that the parameter ρ controls the scaling exponent of the power-law correlations, and that the parameter λ controls the degree of asymmetry in the distributions, leaving the correlations almost unaffected.

Before studying the autocorrelation function of x_i, $C(n) \equiv \langle x_{i+n}x_i \rangle - \langle x_i \rangle^2$, and the probability distribution, $P(x)$, for different values of ρ and λ, we note that process $\mathcal{A}(\rho,\lambda)$ exhibits two invariance properties. Under the transformations $x_i \to -x_i$, $\eta_i \to -\eta_i$, $\lambda \to -\lambda$, one can see that $C(n|\rho,\lambda) = C(n|\rho,-\lambda)$ and $P(x|\rho,\lambda) = P(-x|\rho,-\lambda)$. That is, the autocorrelation functions calculated for opposite values of λ are identical, and the distributions for opposite values of λ are mirror images of each other. Hence, we focus on values of $\lambda \geqslant 0$ in the following study.

To quantify the autocorrelations in x_i generated by $\mathcal{A}(\rho,\lambda)$, we employ the method of detrended fluctuation analysis (DFA) [22]. In the DFA method one measures the standard deviation $F(n)$ of the detrended fluctuations as a function of the scale n. If $C(n)$ can be approximated by a power law with exponent γ, i.e., if $C(n) \propto n^{-\gamma}$, then $F(n)$ can also be approximated by a power law with exponent α, i.e., $F(n) \propto n^{\alpha}$, with $\alpha \approx 1 + \gamma/2$ [22]. Hence, the value of α represents the degree of autocorrelations in the time series: if $\alpha > 0.5$, the time series is power-law correlated; if $\alpha = 0.5$, the time series is uncorrelated or short-range correlated; and if $\alpha < 0.5$, the time series is power-law anticorrelated.

In order to study the influence of the parameter λ on autocorrelations and the degree of asymmetry in the distribution, we perform numerical simulations [23] of $\mathcal{A}(\rho,\lambda)$ with $\rho=0.3$ and varying λ. Figure 1(a) shows that, for $\lambda=0$, $F(n)$ can be approximated by a power law with scaling exponent α, i.e., $F(n) \propto n^{\alpha}$, where $\alpha \approx 0.5+\rho=0.8$, as expected from Refs. [9,10,24]. Figure 1(a) shows that, also for $\lambda \neq 0$, $F(n)$ can be approximated by a power law with scaling exponent α, where $\alpha \approx 0.5+\rho=0.8$, i.e., the value of λ has no visible effect on autocorrelations of x_i for asymptotically large values of n. We also find from Fig. 1(a) that, for $\lambda \neq 0$, the $F(n)$ curves exhibit a crossover at small time scales n, which becomes more pronounced and shifts to larger scales of n with increasing $|\lambda|$.

In Fig. 1(b) we see that, for $\lambda=0$, $P(x)$ is symmetric, as expected for the process of Refs. [9,10]. For $\lambda=0.6$ and $\lambda=0.9$, we find that $P(x)$ is asymmetric with positive skew-

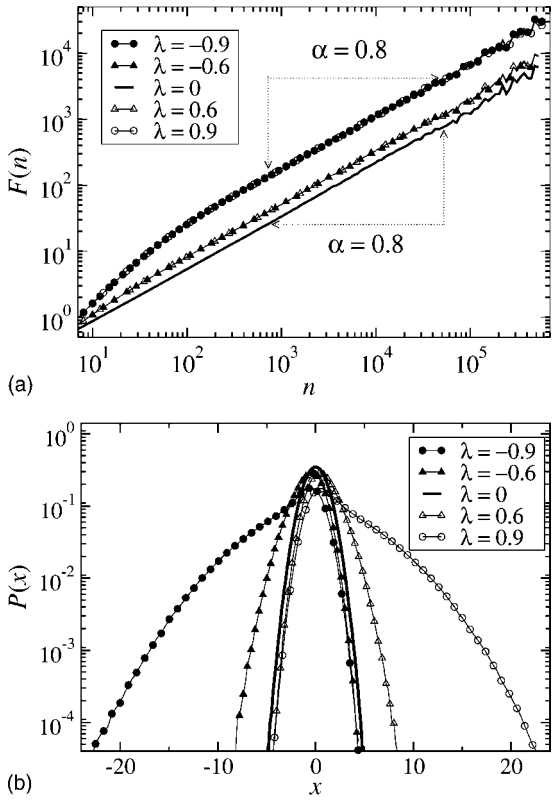

FIG. 1. Correlations and probability distributions obtained from numerical simulations of process $\mathcal{A}(\rho,\lambda)$ with $\rho=0.3$ and $\lambda=0$, ±0.6, and ±0.9. (a) Detrended fluctuation function $F(n)$. We see that the $F(n)$ curves for opposite values of λ are identical, and we find that, for all values of λ, $F(n)$ can be approximated by a power law for asymptotically large n, and the scaling exponent α in $F(n) \propto n^{\alpha}$ is virtually the same for all values of λ. (b) Probability distribution $P(x)$. We see that for opposite values of λ the distributions are mirror images of each other, and we find that $P(x)$ is symmetric for $\lambda=0$, $P(x)$ is asymmetric with positive skewness for $\lambda>0$, and the degree of asymmetry increases with increasing $|\lambda|$.

ness, where the left tail is almost identical to the left tail of the symmetric distribution, and the right tail is broader than the right tail of the symmetric distribution. Due to the invariance $P(x|\rho,\lambda)=P(-x|\rho,-\lambda)$, we find that the distributions for positive and negative values of λ are mirror images of each other for opposite values of λ.

In order to investigate how the correlation properties of $\mathcal{A}(\rho,\lambda)$ depend on ρ, we perform numerical simulations to obtain time series for $\lambda=0.6$ and ρ ranging from 0 to 0.4. We find from Fig. 2 that the $F(n)$ curves can be approximated by power laws with a scaling exponent of $\alpha\approx0.5+\rho$. This states that we obtain the same scaling law for the process $\mathcal{A}(\rho,\lambda)$ generating asymmetrical distributions as for the process $\mathcal{A}(\rho,0)$ generating symmetrical distributions. Numerically we find that, independently of λ, the relation $\alpha\approx0.5+\rho$ holds for all values of ρ and λ where $\rho\in(0,0.5)$ and $\lambda\in(-1,1)$ [24].

In order to model probability distributions with a different shape, particularly with tails broader than those generated by process $\mathcal{A}(\rho,\lambda)$, we propose the process $\mathcal{B}(\rho,\lambda)$ by substituting the term η_i in Eq. (1) by the term $\sigma_i\eta_i$, where the

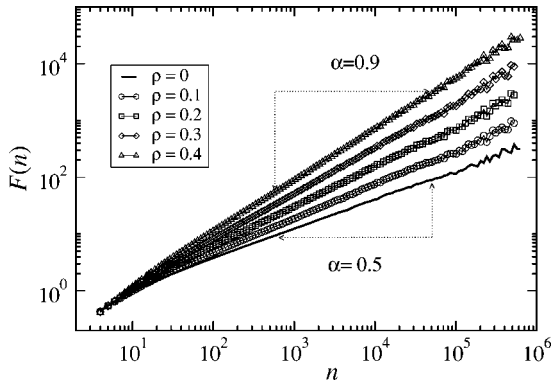

FIG. 2. Detrended fluctuation function $F(n)$ obtained from numerical simulations of process $\mathcal{A}(\rho,\lambda)$ with $\lambda=0.6$ and $\rho=0$, 0.1, 0.2, 0.3, and 0.4. For asymptotically large values of n, each of the $F(n)$ curves can be approximated by a power law $F(n)\propto n^{\alpha}$ with the scaling exponent $\alpha\approx0.5+\rho$.

time-dependent standard deviation σ_i is defined by [25]

$$\sigma_i=\sum_{n=1}^{\infty}a_n(\rho)\frac{|x_{i-n}|}{\langle|x_{i-n}|\rangle}. \tag{2}$$

$\mathcal{B}(\rho,\lambda)$ generates not only long-range autocorrelations in x_i, but also autocorrelations in the magnitudes $|x_i|$, and processes with autocorrelations in the magnitudes have been introduced to model broader tails in the distributions [26].

Figure 3(a) shows that, for asymptotically large n, each $F(n)$ curve can be approximated by a power law with scaling exponent $\alpha\approx0.5+\rho$. This states that the time-dependent standard deviation σ_i does not affect the relation between α and ρ observed for process $\mathcal{A}(\rho,\lambda)$ [24]. Figure 3(b) shows the distribution of x_i generated by $\mathcal{B}(\rho,\lambda)$ for $\rho=0.3$ and λ ranging from 0 to 0.3. As expected, the asymmetry vanishes for $\lambda=0$ even in the presence of the term $\sigma_i\eta_i$, meaning that this term alone does not create an asymmetry in the distribution of x_i but only broadens its tails [26]. For $\lambda>0$, we find that, as λ increases, the right tails of the distributions become broader, the left tails of the distributions become thinner, and thus the asymmetry becomes more pronounced. Comparing Figs. 3(b) and 1(b) we find that the time-dependent standard deviation σ_i broadens the tails and increases the skewness of $P(x)$.

To exemplify the utility of process $\mathcal{B}(\rho,\lambda)$ for modeling real-world data, we study air humidity data, which can be considered an output of a complex geophysical system. We analyze the relative air humidity recorded in 10-min intervals at the Institute of Plant Genetics and Crop Plant Research in Gatersleben [27]. We denote the differences of successive relative air humidity by $\tilde{x}_i$, and we show in Fig. 4(a) the time series $\tilde{x}_i$. Figures 4(b) and 4(c) show that the time series $\tilde{x}_i$ exhibits both power-law autocorrelations with a scaling exponent of $\alpha\approx0.87$ and an asymmetric distribution.

In order to investigate to which degree process $\mathcal{B}(\rho,\lambda)$ can approximate the statistical properties of the empirical time series $\tilde{x}_i$, we generate time series by numerical simulations of process $\mathcal{B}(\rho,\lambda)$ with $\rho=0.37$ and $\lambda=0.15$, where we

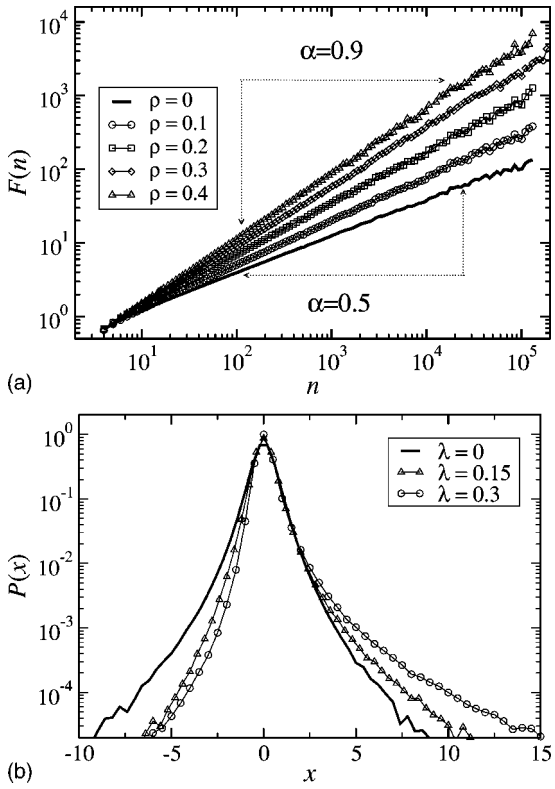

FIG. 3. Correlations and probability distributions of process $\mathcal{B}(\rho,\lambda)$. (a) Detrended fluctuation function $F(n)$ obtained from numerical simulations of process $\mathcal{B}(\rho,\lambda)$ with $\lambda=0.15$ and varying values of $\rho=0$, 0.1, 0.2, 0.3, and 0.4. We find that, independently of λ, $F(n)$ can be approximated by a power law $F(n)\propto n^{\alpha}$ with the scaling exponent $\alpha\approx 0.5+\rho$. (b) Probability distributions $P(x)$ obtained from numerical simulations with $\rho=0.3$ and $\lambda=0$, 0.15, and 0.3. We see that $P(x)$ is symmetric for $\lambda=0$, $P(x)$ is asymmetric with positive skewness for $\lambda>0$, and the skewness increases with increasing λ.

set ρ by using the relation $\alpha\approx 0.5+\rho$, and where we find λ based on a numerical least-square minimization. In Fig. 4, we present (a) the time series $\tilde{x}_i$ and x_i, (b) their detrended fluctuation functions $F(n)$, and (c) their distributions $P(\tilde{x})$ and $P(x)$. Figures 4(a)–4(c) show that the time series of $\tilde{x}_i$ and x_i look similar, that the autocorrelation behavior of the simulated time series x_i is in good agreement with that of the air humidity time series $\tilde{x}_i$, and that the distributions $P(\tilde{x})$ and $P(x)$ are asymmetric with positive skewness. Moreover, we find that even the shapes of both distributions are similar, which is surprising because the shape of $P(x)$ is not fitted to the shape of $P(\tilde{x})$, but the shape of $P(x)$ is entirely given by the values of ρ and λ.

One possible explanation for the positive skewness in the data is that it is very easy to increase the humidity rapidly, by rain for example, but it is hard to dry it rapidly. This simple physical fact could be one of the origins of the asymmetry observed in the distribution of $\tilde{x}_i$. The agreement of the statistical properties of $\tilde{x}_i$ and x_i observed in Fig. 4 might indicate that humidity changes at time i depend not only on past humidity changes x_{i-n} but also on their magnitudes $|x_{i-n-1}|$. The degree of asymmetry in the distribution of x_i reproduced

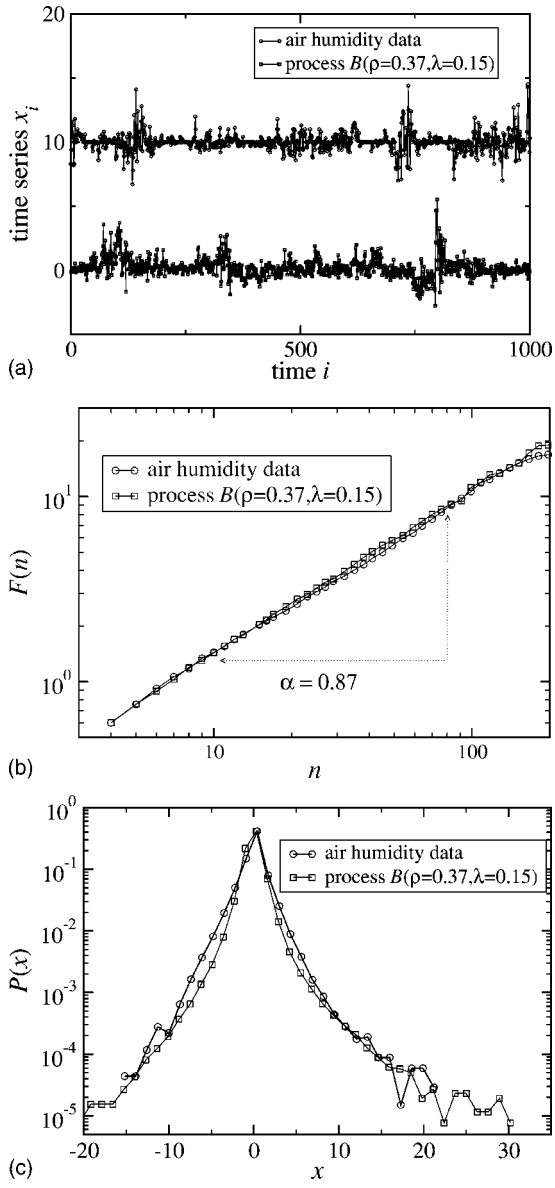

FIG. 4. Comparison of the changes of relative air humidity $\tilde{x}_i$ with the time series x_i generated by process $\mathcal{B}(\rho,\lambda)$ with $\rho=0.37$ and $\lambda=0.15$. (a) Time series $\tilde{x}_i$ and x_i. We find that both time series show sudden bursts of large fluctuations predominantly in the positive direction. (b) Detrended fluctuation functions $F(n)$. We find that autocorrelations of $\tilde{x}_i$ and x_i are very similar, and consistent with a power-law scaling of $F(n)\propto n^{\alpha}$ with the scaling exponent $\alpha\approx 0.87$. (c) Probability distributions $P(\tilde{x})$ and $P(x)$. We find that both distributions are asymmetric with positive skewness. Moreover, we find that even the shapes of both distributions are similar.

by process $\mathcal{B}(\rho,\lambda)$ with a small value of $\lambda\approx 0.15$ suggests that the influence of the past magnitudes $|x_{i-n-1}|$ on x_i is significantly smaller than the influence of the past humidity changes x_{i-n}. Specifically, we might speculate that the influence of the past humidity changes x_{i-n} on x_i is approximately seven times greater than the influence of their magnitudes $|x_{i-n-1}|$ on x_i. Even though both processes $\mathcal{A}(\rho,\lambda)$ and $\mathcal{B}(\rho,\lambda)$ can generate asymmetric distributions, we find that the empirical distribution cannot be reproduced by process

$\mathcal{A}(\rho,\lambda)$, but it can be almost perfectly reproduced by process $\mathcal{B}(\rho,\lambda)$. This surprising observation indicates that the environmental factors η_i at time i might be amplified by a multiplicative factor σ_i, which does not depend on past humidity changes x_{i-n} but on their magnitudes $|x_{i-n-1}|$.

In conclusion, we propose two stochastic processes, $\mathcal{A}(\rho,\lambda)$ and $\mathcal{B}(\rho,\lambda)$, that generate simultaneously power-law autocorrelations and asymmetric probability distributions. Both processes depend on only two parameters, ρ and λ, where ρ controls the scaling exponent of the power-law autocorrelations and λ controls the degree of asymmetry. We study air humidity time series, and we find that they display both power-law autocorrelations and asymmetric distributions. We find that process $\mathcal{B}(\rho,\lambda)$ is capable of reproducing—qualitatively and quantitatively—the autocorrelations and the distribution of the data. The quantitative agreement of the shape of the distribution generated by process $\mathcal{B}(\rho,\lambda)$ with the shape of the distribution of the air humidity changes is surprising, because the shape of the distribution is not fitted, but fully determined by the parameters ρ and λ controlling the scaling exponent of the power-law autocorrelations and the skewness of the distribution, respectively. The surprising agreement of the shapes of the distributions might suggest that air humidity changes at time i are possibly driven by (i) past air humidity changes at times $i-n$, (ii) their magnitudes at times $i-n$, and (iii) environmental factors at time i amplified by a multiplicative factor that itself depends on past magnitudes at times $i-n$. It is clear that processes $\mathcal{A}(\rho,\lambda)$ and $\mathcal{B}(\rho,\lambda)$ lack many important details necessary for realistic weather models, but the simplicity and generality of processes $\mathcal{A}(\rho,\lambda)$ and $\mathcal{B}(\rho,\lambda)$ might possibly make them useful for modeling diverse physical systems exhibiting both power-law correlations and asymmetric distributions.

We thank Stephan Posch, Roland Schnee, and Stephan Weise for valuable discussions and the Ministry of Science of Croatia (Grant No. 0119623), the NIH (Grant No. HL071972), and the German Federal Ministry of Education and Research (Grant No. 0312706A) for financial support.

[1] H. E. Hurst, Proc.-Inst. Civ. Eng. **1**, 519 (1951).
[2] M. Casandro and G. Jona-Lasinio, Adv. Phys. **27**, 913 (1978).
[3] *Correlations and Connectivity: Geometric Aspects of Physics, Chemisty and Biology*, edited by H. E. Stanley and N. Ostrowsky (Kluwer, Dordrecht, 1990).
[4] T. Vicsek, *Fractal Growth Phenomenon*, 2nd ed. (World Scientific, Singapore, 1993).
[5] *Fractals in Science*, edited by A. Bunde and S. Havlin (Springer, Berlin, 1994).
[6] J. B. Bassingthwaighte, L. S. Liebovitch, and B. J. West, *Fractal Physiology* (Oxford University Press, New York, 1994).
[7] J. Beran, *Statistics for Long-Memory Processes* (Chapman & Hall, New York, 1994).
[8] H. Takayasu, *Fractals in the Physical Sciences* (Manchester University Press, Manchester, 1997).
[9] C. W. J. Granger and R. Joyeux, J. Time Ser. Anal. **1**, 15 (1980).
[10] J. Hosking, Biometrika **68**, 165 (1981).
[11] C.-K. Peng *et al.*, Phys. Rev. A **44**, R2239 (1991).
[12] H. A. Makse *et al.*, Phys. Rev. E **53**, 5445 (1995).
[13] L. Hui and E. Gaztanaga, Astrophys. J. **519**, 622 (1999).
[14] International Human Genome Sequence Consortium, Nature (London) **409**, 860 (2001); J. C. Venter *et al.*, Science **291**, 1304 (2001).
[15] M. Samon and F. Curley, J. Appl. Physiol. **83**, 975 (1997).
[16] C. L. Ehlers *et al.*, J. Neurosci. **18**, 7474 (1998).
[17] C. Braun *et al.*, Am. J. Physiol. Heart Circ. Physiol. **275**, H1577 (1998).
[18] G. Boffetta, A. Celani, and M. Vergassola, Phys. Rev. E **61**, R29 (2000).
[19] K. Ohashi, L. A. N. Amaral, B. H. Natelson, and Y. Yamamoto, Phys. Rev. E **68**, 065204(R) (2003).
[20] J. D. Hamilton, *Time Series Analysis* (Princeton, New Jersey, 1994).
[21] To eliminate trends in empirical data, one commonly takes first-order differences $x_i - x_{i-1}$, or higher-order integer differences. This differencing procedure is accomplished through the linear operator $1-L$, defined by $(1-L)x_i = x_i - x_{i-1}$ [20], where L is the linear backward-shift operator defined by $L^n x_i = x_{i-n}$. Fractional processes [9,10] are obtained by allowing the order ρ in $(1-L)^\rho$ to take fractional values. After expanding the fractionally differencing operator $(1-L)^\rho$ as an infinite binomial series in powers of L, one can see that Eq. (1), including the definition of $a_n(\rho)$, can be expressed by $(1-L)^\rho(x_i - \lambda|x_{i-1}|) = \eta_i$.
[22] C.-K. Peng *et al.*, Phys. Rev. E **49**, 1685 (1994).
[23] We introduce a cutoff length $\ell = 30\,000$ in our numerical simulations, and we let the sum in Eq. (1) run from 1 to ℓ, i.e., we set $a_n = 0$ for $n \geq \ell$.
[24] Based on the relation $\alpha \approx 1 - \gamma/2$ [22], and based on the fact that the process $\mathcal{A}(\rho,0)$ is known to generate power-law correlated variables with exponent $\gamma = 1 - 2\rho$, we obtain the relation $\alpha \approx 0.5 + \rho$.
[25] C. W. J. Granger and Z. Ding, J. Econometr. **73**, 61 (1996).
[26] R. F. Engle, Econometrica **50**, 987 (1982).
[27] The data are publicly available at http://portal.bic-gh.de

Power-law correlated processes with asymmetric distributions

By: Podobnik, B (Podobnik, B); Ivanov, PC (Ivanov, PC); Jazbinsek, V (Jazbinsek, V); Trontelj, Z (Trontelj, Z); Stanley, HE (Stanley, HE); Grosse, I (Grosse, I)

View ResearcherID and ORCID

PHYSICAL REVIEW E
Volume: 71 **Issue:** 2 **Part:** 2
Article Number: 025104
DOI: 10.1103/PhysRevE.71.025104
Published: FEB 2005
Document Type: Article
View Journal Impact

Abstract

Motivated by the fact that many physical systems display (i) power-law correlations together with (ii) an asymmetry in the probability distribution, we propose a stochastic process that can model both properties. The process depends on only two parameters, where one controls the scaling exponent of the power-law correlations, and the other controls the degree of asymmetry in the distributions leaving the correlations unaffected. We apply the process to air humidity data and find that the statistical properties of the process are in a good agreement with those observed in the data.

Keywords

KeyWords Plus: VARIANCE

Author Information

Reprint Address: Podobnik, B (reprint author)

+ Univ Rijeka, Fac Civil Engn, Rijeka, Croatia.

Addresses:

+ [1] Univ Rijeka, Fac Civil Engn, Rijeka, Croatia
+ [2] Boston Univ, Ctr Polymer Studies, Boston, MA 02215 USA
+ [3] Boston Univ, Dept Phys, Boston, MA 02215 USA
+ [4] Inst Plant Genet & Crop Plant Res, D-06466 Gatersleben, Germany
+ [5] Univ Ljubljana, Inst Math Phys & Mech, Ljubljana, Slovenia

Funding

Funding Agency	Grant Number
NHLBI NIH HHS	HL071972

Publisher

AMER PHYSICAL SOC, ONE PHYSICS ELLIPSE, COLLEGE PK, MD 20740-3844 USA

Categories / Classification

Research Areas: Physics

Web of Science Categories: Physics, Fluids & Plasmas; Physics, Mathematical

See more data fields

Web of Science Core Collection

View Record in Other Databases:
View **medical data** (in MEDLINE®)

Suggest a correction

If you would like to improve the quality of the data in this record, please suggest a correction.

69 of 127

Cited References: 24

Showing 24 of 24 **View All in Cited References page** *(from Web of Science Core Collection)*

1. **Fractal physiology** — **Times Cited: 7**
   By: Bassinghtwaighte, J. B.; Leibovitch, L. S.; West, B. J.
   FRACTAL PHYSL Published: 1994
   Publisher: Oxford University Press, New York

2. Title: [not available] — **Times Cited: 1,713**
   By: Beran, J.
   Statistics for Long-Memory Processes Published: 1994
   Publisher: CRC Press

3. **Inverse energy cascade in two-dimensional turbulence: deviations from Gaussian behavior** — **Times Cited: 29**
   By: Boffetta, G; Celani, A; Vergassola, M.
   Phys Rev E Volume: 61 Pages: 29-32 Published: 2000

4. **Demonstration of nonlinear components in heart rate variability of healthy persons** — **Times Cited: 74**
   By: Braun, C; Kowallik, P; Freking, A; et al.
   AMERICAN JOURNAL OF PHYSIOLOGY-HEART AND CIRCULATORY PHYSIOLOGY Volume: 275 Issue: 5 Pages: H1577-H1584 Published: NOV 1998

5. **Fractals in science** — **Times Cited: 260**
   By: Bunde, A.
   Fractals in Science Published: 1994
   Publisher: Springer

6. Title: [not available] — **Times Cited: 1**
   By: CASANDRO M
   ADV PHYS Volume: 27 Pages: 913 Published: 1978

7. **Low doses of ethanol reduce evidence for nonlinear structure in brain activity** — **Times Cited: 87**
   By: Ehlers, CL; Havstad, J; Prichard, D; et al.
   JOURNAL OF NEUROSCIENCE Volume: 18 Issue: 18 Pages: 7474-7486 Published: SEP 15 1998

8. **AUTOREGRESSIVE CONDITIONAL HETEROSCEDASTICITY WITH ESTIMATES OF THE VARIANCE OF UNITED-KINGDOM INFLATION** — **Times Cited: 7,073**
   By: ENGLE, RF
   ECONOMETRICA Volume: 50 Issue: 4 Pages: 987-1007 Published: 1982

Quantifying signals with power-law correlations: A comparative study of detrended fluctuation analysis and detrended moving average techniques

Limei Xu,[1] Plamen Ch. Ivanov,[1] Kun Hu,[1] Zhi Chen,[1] Anna Carbone,[2] and H. Eugene Stanley[1]
[1]*Center for Polymer Studies and Department of Physics, Boston University, Boston, Massachusetts 02215, USA*
[2]*INFM and Physics Department, Politecnico di Torino, Corso Duca degli Abruzzi 24, 10129, Torino, Italy*
(Received 7 August 2004; revised manuscript received 14 February 2005; published 6 May 2005)

Detrended fluctuation analysis (DFA) and detrended moving average (DMA) are two scaling analysis methods designed to quantify correlations in noisy nonstationary signals. We systematically study the performance of different variants of the DMA method when applied to artificially generated long-range power-law correlated signals with an *a priori* known scaling exponent α_0 and compare them with the DFA method. We find that the scaling results obtained from different variants of the DMA method strongly depend on the type of the moving average filter. Further, we investigate the optimal scaling regime where the DFA and DMA methods accurately quantify the scaling exponent α_0, and how this regime depends on the correlations in the signal. Finally, we develop a three-dimensional representation to determine how the stability of the scaling curves obtained from the DFA and DMA methods depends on the scale of analysis, the order of detrending, and the order of the moving average we use, as well as on the type of correlations in the signal.

DOI: 10.1103/PhysRevE.71.051101 PACS number(s): 05.40.−a, 95.75.Wx, 95.75.Pq, 02.70.−c

I. INTRODUCTION

There is growing evidence that output signals of many physical [1–15], biological [16–19], physiological [20–35] and economic systems [36–43], where multiple component feedback interactions play a central role, exhibit complex self-similar fluctuations over a broad range of space and/or time scales. These fluctuating signals can be characterized by long-range power-law correlations. Due to nonlinear mechanisms controlling the underlying interactions, the output signals of complex systems are also typically nonstationary, characterized by embedded trends and heterogeneous segments (patches with different local statistical properties) [44–46]. Traditional methods such as power-spectrum and autocorrelation analysis [48–50] are not suitable for nonstationary signals.

Recently, new methods have been developed to address the problem of accurately quantifying long-range correlations in nonstationary fluctuating signals: (a) the detrended fluctuation analysis (DFA) [16,23,51], and (b) the detrended moving average method (DMA) [52–56]. An advantage of the DFA method [44–47] is that it can reliably quantify scaling features in the fluctuations by filtering out polynomial trends. However, trends may not necessarily be polynomial, and the DMA method was introduced to estimate correlation properties of nonstationary signals without any assumptions on the type of trends, the probability distribution, or other characteristics of the underlying stochastic process.

Here, we systematically compare the performance of the DFA and different variants of the DMA method. To this end we generate long-range power-law correlated signals with an *a priori* known correlation exponent α_0 using the Fourier filtering method [57]. Tuning the value of the correlation exponent α_0, we compare the scaling behavior obtained from the DFA and different variants of the DMA methods to determine: (1) how accurately these methods reproduce α_0; (2) what are the limitations of the methods when applied to signals with small or large values of α_0. Based on single realization as well as on ensemble averages of a large number of artificially generated signals, we also compare the best fitting range (i.e., the minimum and the maximum scales) over which the correlation exponent α_0 can be reliably estimated by the DFA and DMA methods.

The outline of this paper is as follows. In Sec. II, we review the DFA method and we introduce variants of the DMA method based on different types of moving average filters. In Sec. III we compare the performance of DFA and DMA on correlated and anticorrelated signals. We also test and compare the stability of the scaling curves obtained by these methods by estimating the local scaling behavior within a given window of scales and for different scaling regions. In Sec. IV we summarize our results and discuss the advantages and disadvantages of the two methods. In Appendix A we consider higher order weighted detrended moving average methods, and in Appendix B we discuss moving average techniques in the frequency domain.

II. METHODS

A. Detrended fluctuation analysis

The DFA method is a modified root-mean-square (rms) analysis of a random walk. Starting with a signal $u(i)$, where $i=1,\ldots,N$, and N is the length of the signal, the first step of the DFA method is to integrate $u(i)$ and obtain

$$y(i) = \sum_{j=1}^{i} [u(j) - \overline{u}], \tag{1}$$

where

$$\overline{u} \equiv \frac{1}{N}\sum_{j=1}^{N} u(j) \tag{2}$$

is the mean.

The integrated profile $y(i)$ is then divided into boxes of equal length n. In each box n, we fit $y(i)$ using a polynomial function $y_n(i)$, which represents the local trend in that box. When a different order of a polynomial fit is used, we have a different order DFA-ℓ (e.g., DFA-1 if $\ell=1$, DFA-2 if $\ell=2$, etc).

Next, the integrated profile $y(i)$ is detrended by subtracting the local trend $y_n(i)$ in each box of length n:

$$Y_n(i) \equiv y(i) - y_n(i). \tag{3}$$

Finally, for each box n, the rms fluctuation for the integrated and detrended signal is calculated:

$$F(n) \equiv \sqrt{\frac{1}{N}\sum_{i=1}^{N} [Y_n(i)]^2}. \tag{4}$$

The above calculation is then repeated for varied box length n to obtain the behavior of $F(n)$ over a broad range of scales. For scale-invariant signals with power-law correlations, there is a power-law relationship between the rms fluctuation function $F(n)$ and the scale n:

$$F(n) \sim n^{\alpha}. \tag{5}$$

Because power laws are scale invariant, $F(n)$ is also called the scaling function and the parameter α is the scaling exponent. The value of α represents the degree of the correlation in the signal: if $\alpha=0.5$, the signal is uncorrelated (white noise); if $\alpha>0.5$, the signal is correlated; if $\alpha<0.5$, the signal is anticorrelated.

B. Detrended moving average methods

The DMA method is a new approach to quantify correlation properties in nonstationary signals with underlying trends [52,53]. Moving average methods are widely used in fields such as chemical kinetics, biological processes, and finance [56,58–61] to quantify signals where large high-frequency fluctuations may mask characteristic low-frequency patterns. Comparing each data point to the moving average, the DMA method determines whether data follow the trend, and how deviations from the trend are correlated.

Step 1. The first step of the DMA method is to detect trends in data employing a moving average. There are two important categories of moving average: (I) simple moving average and (II) weighted moving average.

(I) Simple moving average. The simple moving average assigns equal weight to each data point in a window of size n. The position to which the average of all weighted data points is assigned determines the relative contribution of the "past" and "future" points. In the following we consider the backward and the centered moving average.

(a) Backward moving average. For a window of size n the simple backward moving average is defined as

$$\tilde{y}_n(i) \equiv \frac{1}{n}\sum_{k=0}^{n-1} y(i-k), \tag{6}$$

where $y(i)$ is the integrated signal defined in Eq. (1). Here, the average of the signal data points within the window refers to the last datapoint covered by the window. Thus, the operator $\tilde{y}_n$ in Eq. (6) is "causal," i.e., the averaged value at each data point i depends only on the past $n-1$ values of the signal. The backward moving average is however affected by a rather slow reaction to changes in the signal, due to a delay of length $n/2$ (half the window size) compared to the signal.

(b) Centered moving average. This is an alternative moving average method, where the average of the signal data points within a window of size n is placed at the center of the window. The moving average function is defined as

$$\tilde{y}_n(i) = \frac{1}{n}\sum_{k=-[(n+1)/2]+1}^{[n/2]} y(i+k), \tag{7}$$

where $y(i)$ is the integrated signal defined in Eq. (1) and $[x]$ is the integer part of x. The function $\tilde{y}_n$ defined in Eq. (7) is not "causal," since the centered moving average performs dynamic averaging of the signal by mixing data points lying to the left and to the right side of i. In practice, while the dynamical system under investigation evolves with time i according to $y(i)$, the output of Eq. (7) mixes past and future values of $y(i)$. However, this averaging procedure is more sensitive to changes in the signal without introducing delay in the moving average compared to the signal.

(II) Weighted moving average. In dynamical systems the most recent data points tend to reflect better the current state of the underlying "forces." Thus, a filter that places more emphasis on the recent data values may be more useful in determining reversals of trends in data. A widely used filter is the exponentially weighted moving average, which we employ in our study. In the following we consider the backward and the centered weighted moving average.

(a) Backward moving average. The weighted backward moving average is defined as

$$\tilde{y}_n(i) \equiv (1-\lambda)y(i) + \lambda\tilde{y}_n(i-1), \tag{8}$$

where the parameter $\lambda=n/(n+1)$, n is the window size, $i=2,3,\ldots,N$ and $\tilde{y}_n(1)\equiv y(1)$. Expanding the term $\tilde{y}_n(i-1)$ in Eq. (8), we obtain a recursive relation of step one with previous data points weighted by increasing powers of λ. Since $\lambda<1$, the contribution of the previous data points becomes exponentially small. The weighted backward moving average of higher order $\ell>1$ (WDMA-ℓ) where ℓ is the step size in the recursive Eq. (8) is defined in Appendix A.

(b) Centered moving average. The weighted centered moving average is defined as

$$\tilde{y}_n(i) = \frac{1}{2}[\tilde{y}_n^L(i) + \tilde{y}_n^R(i)], \tag{9}$$

where $\tilde{y}_n^L(i)$ is defined by Eq. (8), and $\tilde{y}_n^R(i)=(1-\lambda)y(i)+\lambda\tilde{y}_n^R(i+1)$, where $i=N-1,N-2,\ldots,1$ and $\tilde{y}_n^R(N)\equiv y(N)$. The term $\tilde{y}_n^R(i)$ is the weighted contribution of all data points to the right of i (from $i+1$ to the end of the signal N), and $\tilde{y}_n^L(i)$ is the weighted contribution of all data points to the left of i.

The exponentially weighted moving average reduces the correlation between the current data point at which the moving average window is positioned and the previous and future points.

Step 2. Once the moving average $\tilde{y}_n(i)$ is obtained, we next detrend the signal by subtracting the trend $\tilde{y}_n$ from the integrated profile $y(i)$

$$C_n(i) \equiv y(i) - \tilde{y}_n(i). \tag{10}$$

For the backward moving average, we then calculate the fluctuation for a window of size n as

$$F(n) = \sqrt{\frac{1}{N-n+1}\sum_{i=n}^{N}[C_n(i)]^2}. \tag{11}$$

For the centered moving average the fluctuation for a window of size n is calculated as

$$F(n) = \sqrt{\frac{1}{N-n+1}\sum_{i=[(n+1)/2]}^{N-[n/2]}[C_n(i)]^2}. \tag{12}$$

Step 3. Repeating the calculation for different n, we obtain the fluctuation function $F(n)$. A power law relation between the fluctuation function $F(n)$ and the scale n [see Eq. (5)] indicates a self-similar behavior.

When the moving average $\tilde{y}_n$ is calculated as in Eq. (6), Eq. (7), Eq. (8) and Eq. (9), we have the detrended moving method (DMA), the centered detrened moving average (CDMA), the weighted detrended moving average with order ℓ (WDMA-ℓ) and the weighted centered detrended moving average (WCDMA), respectively.

III. ANALYSIS AND COMPARISON

Using the modified Fourier filtering method [57], we generate uncorrelated, positively correlated, and anticorrelated signals $u(i)$, where $i=1,2,\ldots,N$ and $N=2^{20}$, with a zero mean and unit standard deviation. By introducing a designed power-law behavior in the Fourier spectrum [45,57], the method can efficiently generate signals with long-range power-law correlations characterized by an *a priori* known correlation exponent α_0.

A. Detrended moving average method and DFA

In this section we investigate the performance of the DMA and WDMA-1 methods when applied to signals with different type and degree of correlations, and compare them to the DFA method. Specifically, we compare the features of the scaling function $F(n)$ obtained from the DMA and WDMA-1 methods with the DFA method, and how accurately these methods estimate the correlation properties of the artificially generated signals $u(i)$. Ideally, the output scaling function $F(n)$ should exhibit a power-law behavior over all scales n, characterized by a scaling exponent α which is identical to the given correlation exponent α_0 of the artificial signals. Previous studies [44–46] show that the scaling behavior obtained from the DFA method depends on the scale n and the order ℓ of the polynomial fit when detrending the signal. We investigate if the results of the DMA and WDMA-1 method also have a similar dependence on the scale n. We also show how the scaling results depend on the order ℓ when WDMA-ℓ with $\ell=2,3,4,5$ are applied to the signals (see Appendix A).

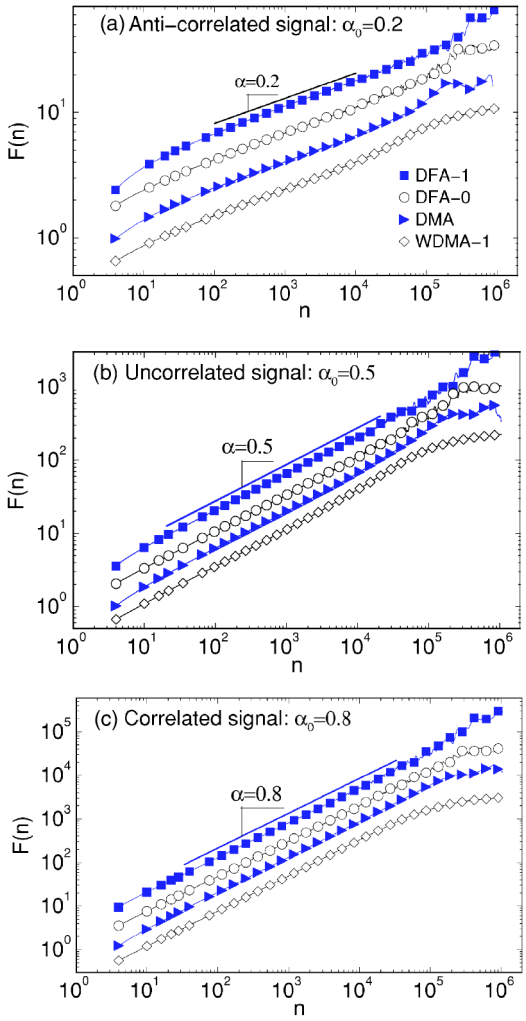

FIG. 1. A comparison of the scaling behavior obtained from the DMA, WDMA-1, DFA-0, and DFA-1 methods for artificially generated power-law correlated signals with a scaling exponent α_0. The length of the signals is $N=2^{20}$. Scaling curves $F(n)$ versus scale n for (a) an anticorrelated signal with $\alpha_0=0.2$, (b) an uncorrelated signal with $\alpha_0=0.5$, and (c) a positively correlated signal with $\alpha_0=0.8$. At small scales, all methods exhibit a weak crossover, which is more pronounced for anticorrelated signals. At large scales, the $F(n)$ curves obtained from DMA, WDMA-1, and DFA-0 exhibit a clear crossover to a flat region for all signals, independent of the type of correlations. No such crossover is observed for the scaling curves obtained from the DFA-1 method, suggesting a more accurate estimate of the scaling exponent α_0 at large scales.

To compare the performance of different methods, we first study the behavior of the scaling function $F(n)$ obtained from DFA-0, DFA-1, DMA, and WDMA-1. In Fig. 1 we show the rms fluctuation function $F(n)$ obtained from the different methods for an anti-correlated signal with correlation exponent $\alpha_0=0.2$, an uncorrelated signal with $\alpha_0=0.5$, and a posi-

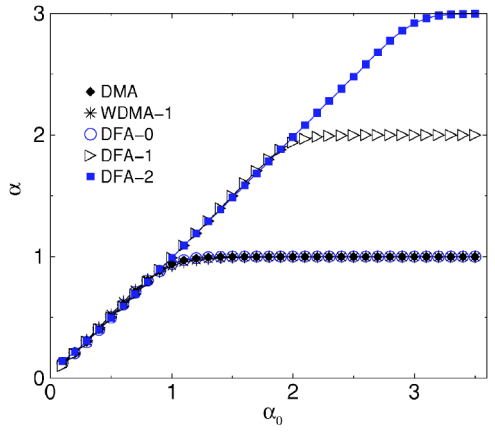

FIG. 2. A comparison of the performance of the different scaling methods (DMA, WDMA-1, DFA-0, DFA-1, and DFA-2) when applied to artificially generated signals with long-range power-law correlations. Here α_0 is the correlation exponent of the generated signals and α is the exponent value estimated using different methods. For all methods we obtain α by fitting the corresponding scaling curves $F(n)$ in the range $n \in [10^2, 10^4]$. Flat regions indicate the limitations of the methods in accurately estimating the degree of correlations in the generated signals, as the "output" exponent α remains unchanged when the "input" exponent α_0 is varied.

tively correlated signal with $\alpha_0=0.8$. We find that in the intermediate regime $F(n)$ (obtained from all methods) exhibits an approximate power-law behavior characterized by a single scaling exponent α. At large scales n for DFA-0, DMA, and WDMA-1, we observe a crossover in $F(n)$ leading to a flat regime. With increasing α_0 this crossover becomes more pronounced and moves to the intermediate scaling range. In contrast, such a crossover at large scales is not observed for DFA-1, indicating that the DFA-1 method can better quantify the correlation properties at large scales. At small scales n the scaling curves $F(n)$ obtained from all methods exhibit a crossover which is more pronounced for anticorrelated signals ($\alpha_0=0.2$) and becomes less pronounced for uncorrelated ($\alpha_0=0.5$) and positively correlated signals ($\alpha_0=0.8$).

We next systematically examine the performance of the DFA-0, DFA-1, DMA, and WDMA-1 methods by varying α_0 over a very broad range of values ($0.1 \leqslant \alpha_0 \leqslant 3.5$) (Fig. 2). For all four methods, we compare α_0 with the exponent α obtained from fitting the rms fluctuation function $F(n)$ in the scaling range $10^2 < n < 10^4$, i.e., the range where all methods perform well according to our observations in Fig. 1. If the methods work properly, for each value of the "input" exponent α_0 we expect the estimated "output" exponent to be $\alpha = \alpha_0$. We find that the scaling exponent α, obtained from different methods, saturates as the "input" correlation exponent α_0 increases, indicating the limitation of each method. The saturation of scaling exponent at $\alpha=1$ indicates that DMA and WDMA-1 do not accurately quantify the correlation properties of signals with $\alpha_0 > 1$.

In contrast, the DFA-ℓ method can quantify accurately the scaling behavior of strongly correlated signals if the appropriate order ℓ of the polynomial fit is used in the detrending procedure. Specifically, we find that the values of the scaling exponent α obtained from the DFA-ℓ are limited to $\alpha \leqslant \ell + 1$. Thus the DFA-$\ell$ can quantify the correlation properties of signals characterized by exponent $\alpha_0 \leqslant \ell + 1$. For signals with $\alpha_0 > \ell + 1$ we find that the output exponent α from the DFA-ℓ method remains constant at $\alpha = \ell + 1$. These findings suggest that in order to obtain a reliable estimate of the correlations in a signal one has to apply the DFA-ℓ for several increasing orders ℓ until the obtained scaling exponent α stops changing with increasing ℓ.

Since the accuracy of the scaling exponent obtained from the different methods depends on the range of scales n over which we fit the rms fluctuation function $F(n)$ (as seen in Fig. 1), and since different methods exhibit different limitations for the range of scaling exponent values (as demonstrated in Fig. 2), we next investigate the local scaling behavior of the $F(n)$ curves to quantify the performance of the different methods in greater details. To ensure a good estimation of the local scaling behavior, we calculate $F(n)$ at scales $n = 4 \times 2^{i/64}$, $i = 0, 1, 2, \ldots$, which in log scale provides 64 equidistant points for $F(n)$ per bin of size $\log 2$. To estimate the local scaling exponent α_{loc}, we locally fit $F(n)$ in a window of size $w = 3 \log 2$, e.g, α_{loc} is the slope of $F(n)$ in a window containing 3×64 points. To quantify the detailed features of the scaling curve $F(n)$ at different scales n, we slide the window w in small steps of size $\Delta = \frac{1}{4} \log 2$ starting at $n=4$, thus obtaining approximately 70 equidistant α_{loc} in log scale per each scaling curve. We consider the average value of α_{loc} obtained from 50 different realizations of signals with the same correlation exponent α_0.

In Fig. 3, we compare the behavior of α_{loc} as a function of the scale n to more accurately determine the best fitting range in the scaling curves $F(n)$ obtained from the DMA, WDMA-1, DFA-0, and DFA-1. A rms fluctuation function exhibiting a perfect scaling behavior would be characterized by $\alpha_{\mathrm{loc}} = \alpha_0$ for all scales n and for all values of α_0 denoted by horizontal lines in Fig. 3. A deviation of the α_{loc} curves from these horizontal lines indicates an inaccuracy in quantifying the correlation properties of a signal and the limitation of the methods. Our results show that the performance of different methods depends on the "input" α_0 and scale n. At small scales and for $\alpha_0 < 0.8$ we observe that α_{loc} for all methods deviates up from the horizontal lines suggesting an overestimation of the real correlation exponent α_0. This effect is less pronounced for uncorrelated and positively correlated signals. At intermediate scales α_{loc} exhibits a horizontal plateau indicating that all methods closely reproduce the input exponent for $\alpha_0 < 0.8$. This intermediate scaling regime changes for different types of correlations and for different methods. At large scales of $n > 10^4$, the DMA, WDMA-1, and DFA-0 methods strongly underestimate the actual correlations in the signal, with α_{loc} curves sharply dropping for all values of α_0 [Figs. 3(a)–3(c)]. In contrast, the DFA-1 method accurately reproduces α_0 at large scales with α_{loc} following the horizontal lines up to approximately $N/10$ [Fig. 3(d)]. In addition, the DFA-1 method accurately reproduces the correlation exponent at small and intermediate scales even when $\alpha_0 > 1$ [Fig. 3(d)], while the DMA, WDMA-1, and DFA-0 are limited to $\alpha_0 < 0.8$.

For a certain "input" correlation exponent α_0, we can estimate the good fitting regime of $F(n)$ to be the length of the

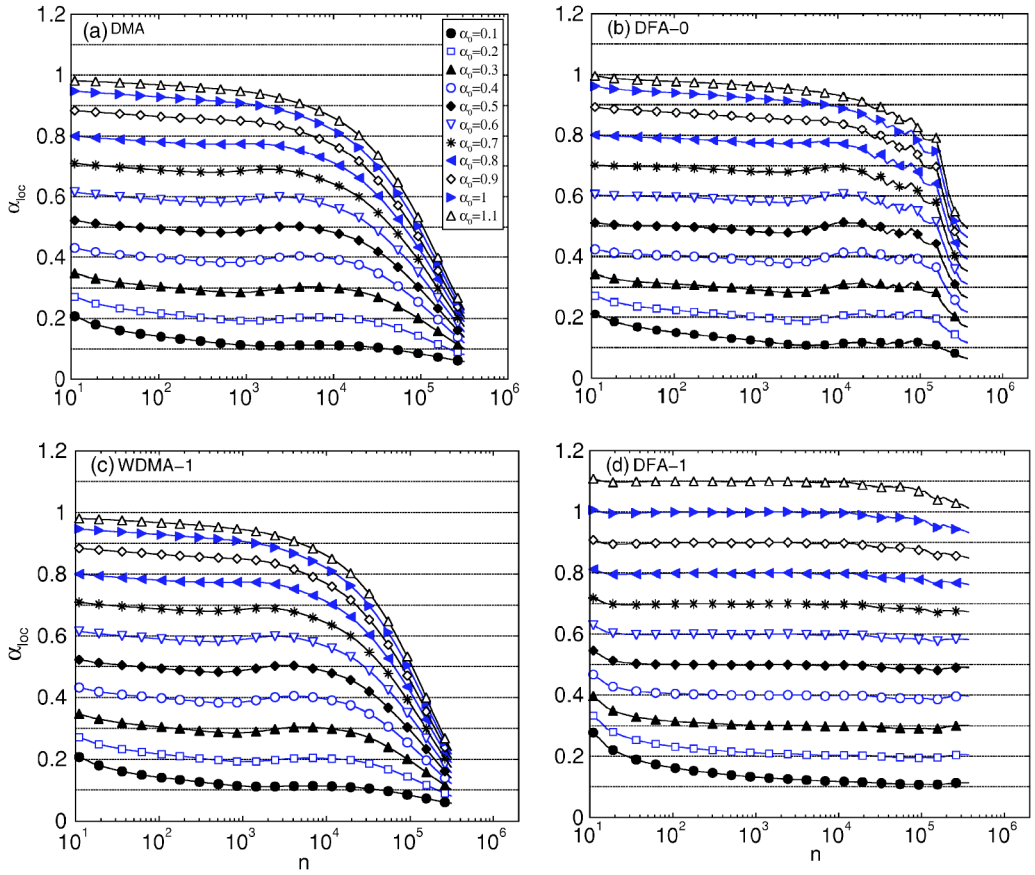

FIG. 3. A comparison of the local scaling exponent α_{loc} as a function of the scale n for the DMA, WDMA-1, DFA-0, and DFA-1 methods. We consider signals of length $N=2^{20}$ and varying values of the correlation exponent α_0. The local scaling exponent α_{loc} quantifies the stability of the scaling curves $F(n)$ (see Fig. 1) and is expected to exhibit small fluctuations around a constant value α_0 if $F(n)$ is well fitted by a power-law function. α_0 is denoted by horizontal dotted lines. Symbols denote the estimated values of α_{loc} and represent average results from 50 realizations of artificial signals for each value of the "input" scaling exponent α_0. Deviations from the horizontal lines at small or at large scales indicate limitations of the methods to accurately quantify the built-in correlations in different scaling ranges.

plateau in Fig. 3. For example, for $\alpha_0=0.2$ the calculated scaling exponent α_{loc} obtained from the DMA method is approximately equal to the expected value $\alpha_0=0.2$ within a range of two decades ($10^2<n<10^4$). Similarly, the good fitting range of $F(n)$ obtained from the DFA-0 for $\alpha_0=0.2$ is about three decades ($10^2<n<10^5$). However, the calculated local scaling exponent α_{loc} can fluctuate for different realizations of correlated signals. Although the mean value obtained from many independent realizations is close to the expected value, the fluctuation of the estimated scaling exponent can be very large. Thus, it is possible for α_{loc} to deviate from α_0 and the scaling range estimated from Fig. 3 may not be a good fitting range. Therefore, it is necessary to study the dispersion of the local scaling exponent to determine the reliability of the "good" fitting range estimated from Fig. 3. In Figs. 4–6 we show the results for α_{loc} from 20 different realizations of the correlated signal with $\alpha_0=0.2$, $\alpha_0=0.5$, and $\alpha_0=0.8$, respectively. For all methods, we observe that there is a large dispersion of α_{loc}, indicating strong fluctuations in the scaling function $F(n)$ at large scales n ($n\sim10^3$ for DMA and WDMA-1 and $n\sim10^4$ for DFA-0 and DFA-1) (Figs. 4–6). This suggests that the good fitting range obtained only from the mean value of α_{loc}, as shown in Fig. 3, may be overestimated.

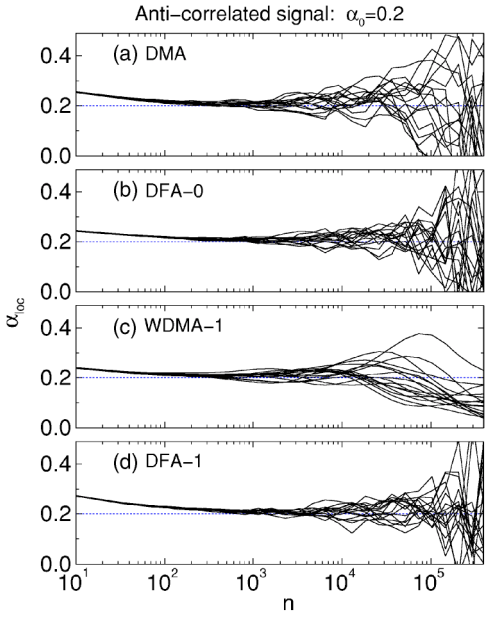

FIG. 4. Values of the local scaling exponent α_{loc} as a function of the scale n obtained from 20 different realizations of artificial anti-correlated signals with an identical scaling exponent $\alpha_0=0.2$.

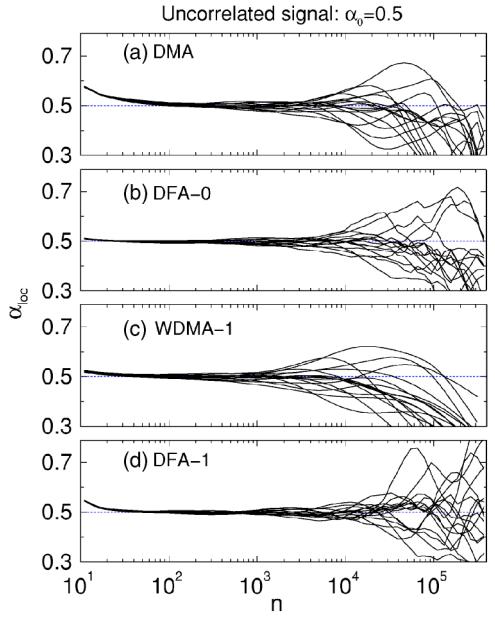

FIG. 5. Values of the local scaling exponent α_{loc} as a function of the scale n obtained from 20 different realizations of artificial uncorrelated signals with an identical scaling exponent $\alpha_0=0.5$.

To better quantify the best fitting range for different methods and for different types of correlations we develop a three-dimensional representation (Fig. 7). Based on 50 realizations of correlated signals with different values of $0.1<\alpha_0<1.1$, for each scale n we define the probability p (normalized frequency) to obtain values for $\alpha_0-\delta<\alpha_{loc}<\alpha_0+\delta$, where $\delta=0.02$ (arguments supporting this choice of δ are presented in Sec. III B). Again, as in Fig. 3, for each realization of correlated signals with a given α_0, we calculate α_{loc}

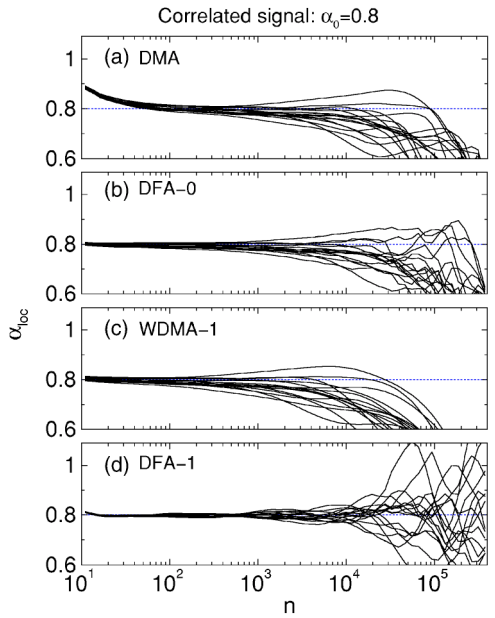

FIG. 6. Values of the local scaling exponent α_{loc} as a function of the scale n obtained from 20 different realizations of artificial positively correlated signals with an identical scaling exponent $\alpha_0=0.8$.

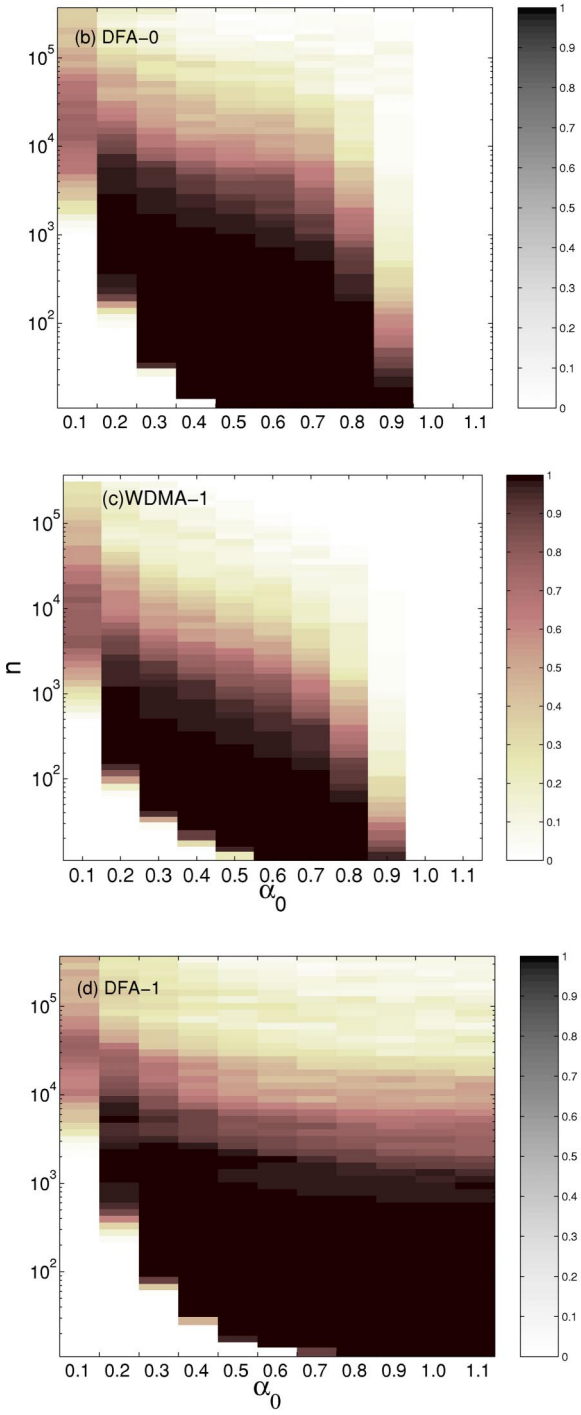

FIG. 7. Probability density of the estimated values of $\alpha_0-\delta<\alpha_{loc}<\alpha_0+\delta$, where $\delta=0.02$ for a varying scale range n and for different values of the "input" correlation exponent α_0. Separate panels show the performance of the DMA, WDMA-1, DFA-0 and DFA-1 methods, respectively, based on 50 realizations of correlated signals for each value of α_0. The probability density values p are presented in color, with the darker color corresponding to higher values as indicated in the vertical columns next to each panel. A perfect scaling behavior would correspond to dark-colored columns spanning all scales n for each value of α_0.

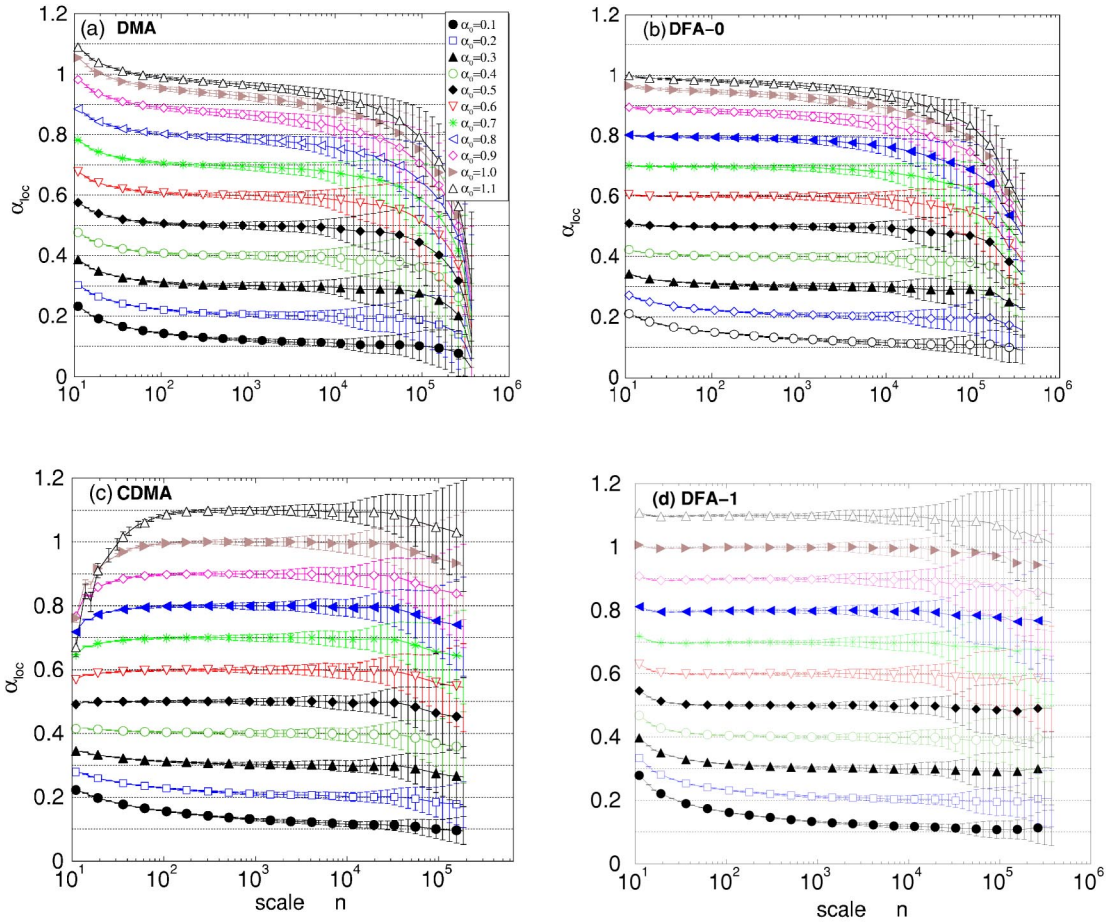

FIG. 8. A comparison of the local scaling exponent α_{loc} as a function of the scale n for the DMA, CDMA, DFA-0, and DFA-1 methods. We consider signals of length $N=2^{20}$ and varying values of the correlation exponent α_0. The local scaling exponent α_{loc} quantifies the stability of the scaling curves $F(n)$ and is expected to exhibit small fluctuations around a constant value α_0 if $F(n)$ is well fitted by a power-law function. α_0 is denoted by horizontal dotted lines. Symbols denote the estimated values of α_{loc} and represent average results from 50 realizations of artificial signals for each value of the "input" scaling exponent α_0. Deviations from the horizontal lines at small or at large scales indicate limitations of the methods to accurately quantifying the built-in correlations in different scaling ranges. Error bars represent the standard deviation for each average value of α_{loc} at different scales n, and determine the accuracy of each method.

by fitting the rms fluctuation function $F(n)$ in a window of size $w=3\log 2$ sliding in steps of $\Delta=\frac{1}{4}\log 2$. Vertical color bars in Fig. 7 represent the value of the probability p—darker colors corresponding to higher probability to obtain accurate values for α_{loc}. Thus dark-colored columns in the panels of Fig. 7 represent the range of scales n where the methods perform best.

For the DMA and WDMA-1 methods, we find that with high probability ($p>0.7$), accurate scaling results can be obtained in the scaling range of two decades for $0.4\leqslant\alpha_0\leqslant 0.6$. However, WDMA-1 performs better at small scales compared to DMA. For an explanation of why the WDMA-1 performs better at small scales compared to DMA, see Appendix B. In contrast, DFA-0 exhibits an increased fitting range of about three decades for $0.4\leqslant\alpha_0\leqslant 0.8$, while for the DFA-1 we find the best fitting range to be around three decades for $\alpha_0>0.5$. For strongly anticorrelated signals ($\alpha_0<0.2$), all methods do not provide an accurate estimate of the scaling exponents α_0. However, by integrating anticorrelated signals with $\alpha_0<0.3$ and applying the DFA-1 method, we can reliably quantify the scaling exponent, since DFA-1 has the advantage to quantify signals with $\alpha_0>1$ [Fig. 7(d)]. This cannot be obtained by the other three methods [Figs. 7(a)–7(c)].

B. Centered moving average method and DFA

To test the accuracy of the CDMA method we perform the same procedure as shown in Fig. 3. We calculate the local scaling exponent α_{loc} for signals with different "input" correlation exponent α_0 and for a broad range of scales n (Fig. 8). We find that for $0.3<\alpha_0<0.8$ the CDMA method performs better than the DMA for all scales n, and the average value of α_{loc} follows very closely the expected values of α indicated by horizontal lines in Fig. 8. For anticorrelated signals with $\alpha_0\leqslant 0.3$, both DMA and CDMA overestimate the value of α_0 at small scales $n<10^2$. For strongly correlated signals with $\alpha_0>0.8$, CDMA underestimates α_0 at small scales $n<10^2$, in contrast to DMA which overestimates α_0. For correlated signals with $\alpha_0>1.1$ [not shown in

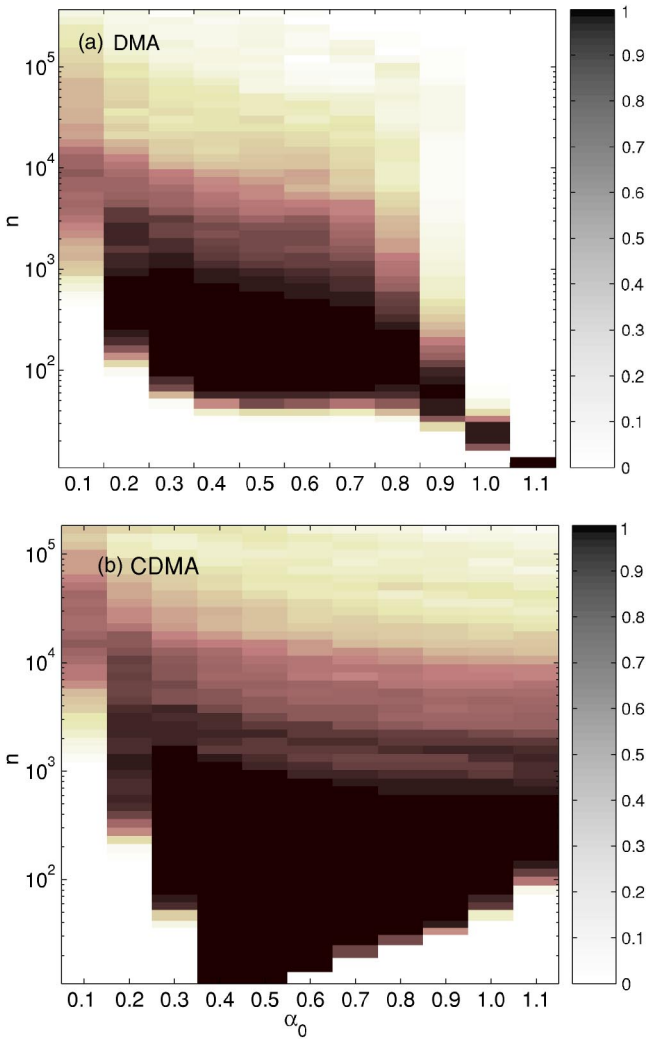

FIG. 9. Probability density of the estimated values of $\alpha_0-\delta < \alpha_{\rm loc} < \alpha_0+\delta$, where $\delta=0.02$ for a varying scale range n and for different values of the "input" correlation exponent α_0. The two panels show the performance of the DMA and CDMA methods, respectively, based on 50 realizations of correlated signals for each value of α_0. The probability density values p are presented in color, with the darker color corresponding to higher values, as indicated in the vertical columns next to each panel. A perfect scaling behavior would correspond to dark-colored columns spanning all scales n for each value of α_0.

Fig. 8(c)] the deviation of α_{loc} from the expected value α_0 for the CDMA method becomes even more pronounced and spreads to large scales. At intermediate and large scales CDMA performs much better—α_{loc} closely follows the horizontal lines [Figs. 8(a)–8(c)]. These differences in the performance of the DMA and CDMA methods are also clearly seen in the probability density plots shown in Fig. 9.

Next, we compare the stability of the DMA, CDMA, DFA-0, and DFA-1 methods in reproducing the same "input" value of α_0 for different realizations of correlated signals. We generate 50 realizations of signals for each α_0, and we obtain the average value and the standard deviation of α_{loc} for a range of scales n. The values of the standard deviation are represented by error bars in Fig. 8 for each value of α_{loc} at all

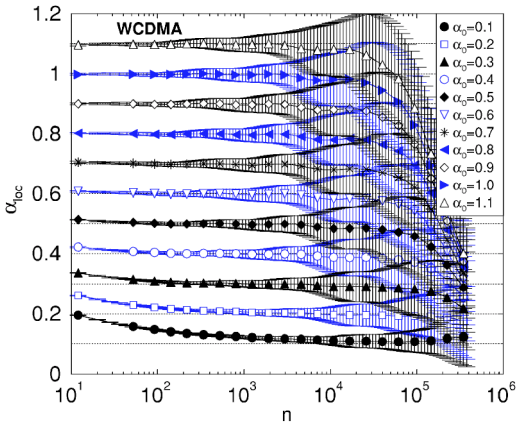

FIG. 10. Local scaling exponent $\alpha_{\rm loc}$ as a function of the scale n for the WCDMA method. We consider signals of length $N=2^{20}$ and varying values of the correlation exponent α_0. The expected value of the exponent α_0 is denoted by horizontal dotted lines. Symbols denote the estimated values of $\alpha_{\rm loc}$ and represent average results from 50 realizations of artificial signals for each value of the "input" scaling exponent α_0. Deviations from the horizontal lines at small or at large scales indicate limitations of the methods to accurately quantify the built-in correlations in different scaling ranges. Error bars represent the standard deviation for each average value of $\alpha_{\rm loc}$ at different scales n, and determine the accuracy of the method.

scales n. We find that with increasing scales n, the standard deviation gradually increases, and that for DMA the standard deviation is less than 0.02 while for DFA the standard deviation is less than 0.01 in the range of scales n up to $N/100$ (N is the signal length). For all methods at scales $n>N/100$, the standard deviation increases more rapidly, and thus the stability of the methods in reproducing the same value of the exponent for different realizations decreases.

In Fig. 10 we present the dependence of α_{loc} on the scale n for the weighted centered detrended moving average method. Compared to the CDMA method, the WCDMA method weakens the overestimation of α_{loc} at small scale for anticorrelated signals and provides accurate results of α_{loc} at small scales for positively correlated signals with $0.5<\alpha_0<1$. Compared to the DFA method, the WCDMA performs better at small scales for $0.5<\alpha_0<1.0$. However, at larger scales $n>10^2$, the standard deviation of DFA-1 is smaller than that of WCDMA [Figs. 8(d), 10, and 11], indicating more reliable results for the local scaling exponent α_{loc} obtained from DFA-1.

Finally, we test how the choice of the parameter δ will affect the probability density plots shown in Fig. 7 and Fig. 9. To access the precision of the methods one has to increase the confidence level by decreasing δ. In Fig. 7 and Fig. 9 we have chosen $\delta=0.02$ to correspond to the value of the standard deviation for α_{loc} at scales $n<10^4$ as estimated by the DMA method (Fig. 8). We demonstrate that the distribution plot for DMA with $\delta=0.02$ (shown in Fig. 7) changes dramatically when we choose $\delta=0.01$ [as shown in Fig. 12(b)]. This result confirms the observation from Figs. 8(a) and 8(d) that the DFA-1 method is more stable (smaller standard

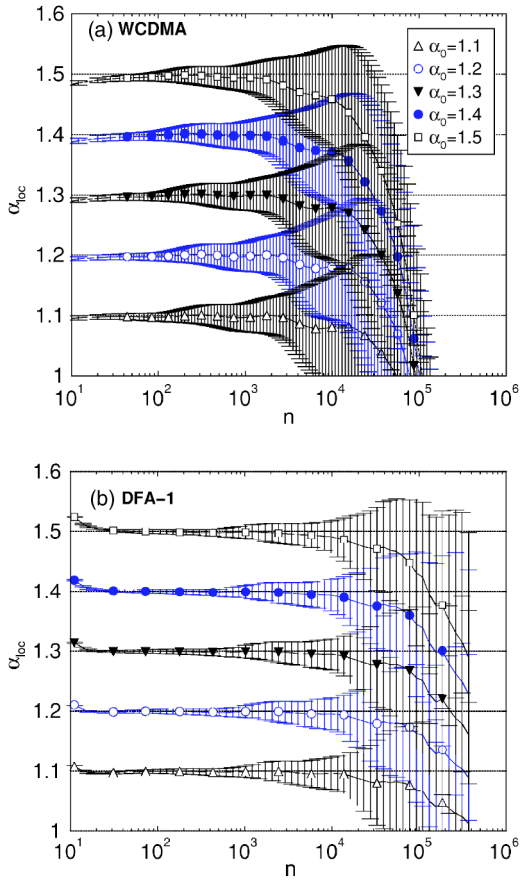

FIG. 11. A comparison of the local scaling exponent α_{loc} as a function of the scale n obtained from (a) the WCDMA method and (b) the DFA-1 method. Symbols denote the estimated values of α_{loc} calculated as in Fig. 10 for different "input" scaling exponents $\alpha_0 > 1$. Error bars representing the standard deviation around the average α_{loc} are smaller for the DFA-1 method at all scales n, indicating that the DFA-1 method provides more reliable results.

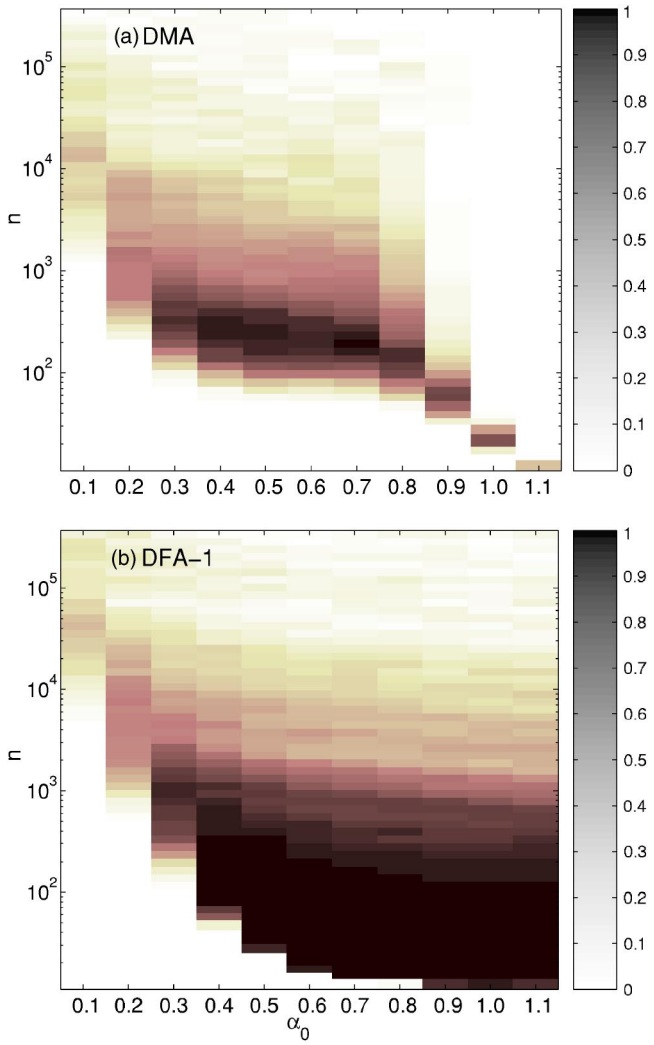

FIG. 12. Probability density of estimated values of $\alpha_0 - \delta < \alpha_{\mathrm{loc}} < \alpha_0 + \delta$, where $\delta = 0.01$ for varying scale range n and for different values of the "input" correlation exponent α_0. The two panels show the performance of the DMA and DFA-1 methods, respectively, based on 50 realizations of correlated signals for each value of α_0. The probability density values p are presented in color, with darker color corresponding to higher values as indicated in the vertical columns next to each panel. A perfect scaling behavior would correspond to dark-colored columns spanning all scales n for each value of α_0.

deviation) and more accurate (average of α_{loc} closer to the theoretically expected value α_0) than the DMA method.

IV. DISCUSSION

We have systematically studied the performance of the different variants of DMA method when applied to signals with long-range power-law correlations, and we have compared them to the DFA method. Specially, we have considered two categories of detrended moving average methods—the simple moving average and the weighted moving average—in order to investigate the effect of the relative contribution of data points included in the moving average window when estimating correlations in signals. To investigate the role of "past" and "future" data points in the dynamic averaging process for signals with different correlations, we have also considered the cases of backward and centered moving average within each of the above two categories. Finally, we have introduced a three-dimensional representation to compare the performance of different variants of the DMA method and the DFA methods over different scaling ranges based on an ensemble of multiple signal realizations.

We find that the simple backward moving average DMA method and the weighted backward moving average method WDMA-ℓ have limitations when applied to signals with very strong correlations characterized by scaling exponent $\alpha_0 > 0.8$. A similar limitation is also found for the $\ell = 0$ order of the DFA method. However, for higher order ℓ, the DFA-ℓ method can accurately quantify correlations with $\alpha_0 < \ell + 1$. We also find that at large scales the DMA, WDMA-ℓ, and DFA-0 methods underestimate the correlations in signals with $0.5 < \alpha_0 < 1.0$, while the DFA-ℓ method can more accurately quantify the scaling behavior of such signals. Further, we find that the scaling curves obtained from the DFA-1

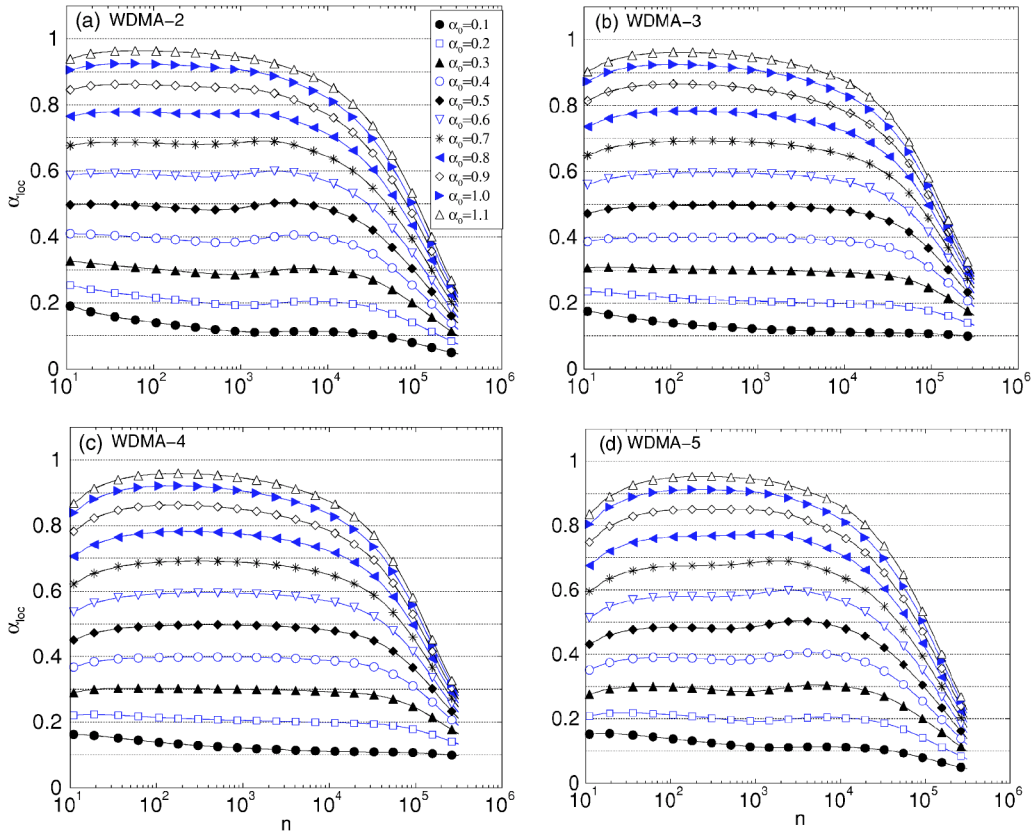

FIG. 13. A comparison of the local scaling exponent α_{loc} as a function of the scale n for the WDMA-ℓ method with different order $\ell=2,\ldots,5$ of the weighted moving average. We consider signals of length $N=2^{20}$ and varying values of the correlation exponent α_0. The local scaling exponent α_{loc} quantifies the stability of the scaling curves $F(n)$ (see Fig. 1), and is expected to exhibit small fluctuations around a constant value α_0 if $F(n)$ is well fitted by a power-law function. α_0 is denoted by horizontal dotted lines. Symbols denote the estimated values of α_{loc} and represent average results from 50 realizations of artificial signals for each value of the "input" scaling exponent α_0. For small values of ℓ at small and intermediate scales n, WDMA-ℓ accurately reproduces the scaling behavior of signals with $0.4<\alpha_0<0.8$, while for large ℓ, the scaling behavior of anticorrelated signals with $\alpha_0<0.4$ are better reproduced at small scales.

method are stable over a much broader range of scales compared to the DMA, WDMA-1, and DFA-0 methods, indicating a better fitting range to quantify the correlation exponent α_0. In contrast, we find that WDMA-ℓ with a higher order ℓ, more accurately reproduce the correlation properties of anticorrelated signals ($\alpha_0<0.5$) at small scales. Accurate results for anticorrelated signals can also be obtained from the DFA-1 method after first integrating the signal and thus reducing the value of the estimated correlation exponent by 1.

In contrast to the simple backward moving average (DMA) and DFA-0 methods, the centered moving average CDMA provides a more accurate estimate of the correlations in signals with $0.3<\alpha_0<0.7$ at small scales $n<10^2$, and in signals with $\alpha_0>0.7$ at intermediate scales $10^2<n<10^4$. However, the CDMA method strongly underestimates correlations in signals with $\alpha_0>0.7$ at small scales ($n<10^2$), while the DFA-1 method reproduces quite accurately the correlations of signals with $\alpha_0>0.7$ at both small and intermediate scales. We also find that by introducing weighted centered moving average WCDMA, one can overcome the limitation of the CDMA method in estimating correlations in signals with $\alpha_0>0.5$ at small scales ($n<10^2$). On the other hand, the WCDMA method is characterized by larger error bars for α_{loc} at intermediate scales compared to the CDMA method. Further, we find that the performance of the WCDMA is comparable to the DFA-1 method for signals with $0.5<\alpha_0<1$. At small scales the WCDMA performs better than the DFA-1 method, while at the intermediate scales $10^2<n<10^4$, DFA-1 provides more reliable local scaling exponent with smaller standard deviation based on 50 independent realizations for each α_0. For very strongly correlated signals with $\alpha_0>1$, we find that the DFA-1 method performs much better at all scales compared to WCDMA and all other variants of the DMA method.

ACKNOWLEDGMENTS

This work was supported by NIH Grant HL071972 and by the MIUR (PRIN 2003029008).

APPENDIX A

1. Higher order weighted moving average

To account for different types of correlations in signals, we consider the ℓ-order weighted moving average (WDMA-ℓ), defined as

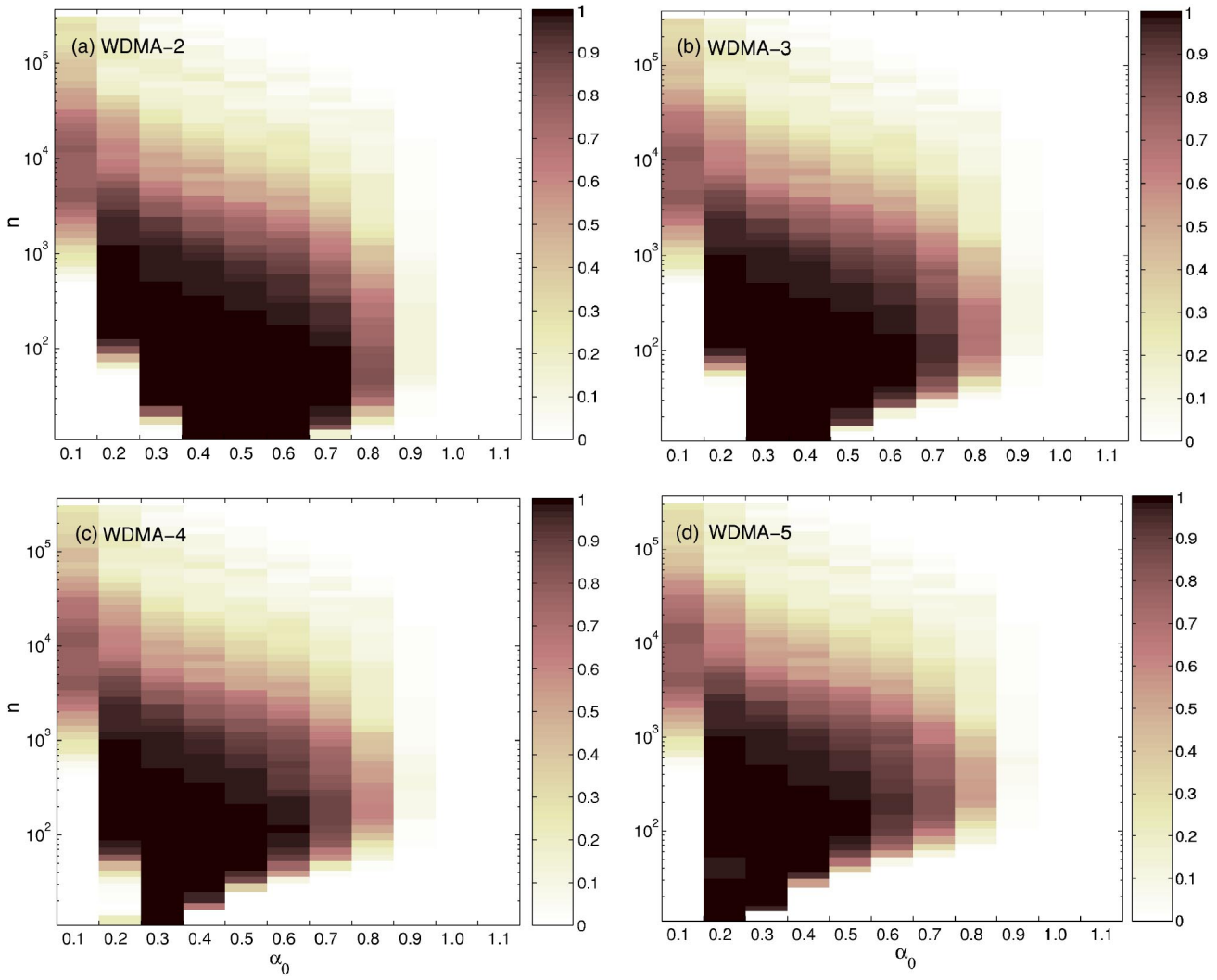

FIG. 14. Probability density of estimated values of $\alpha_0-\delta<\alpha_{\rm loc}<\alpha_0+\delta$, where $\delta=0.02$ for the varying scale range n and for different values of the "input" correlation exponent α_0. Separate panels show the performance of the WDMA-2, WDMA-3, WDMA-4, and WDMA-5 methods, respectively, based on 50 realizations of correlated signals for each value of α_0. The probability density values p are presented in color, with the darker color corresponding to higher values, as indicated in the vertical columns next to each panel. A perfect scaling behavior would correspond to dark-colored columns spanning all scales n for each value of α_0.

$$\tilde{y}_n(i) \equiv \frac{(1-\lambda)}{\ell}\sum_{k=0}^{\ell-1} y(i-k) + \lambda \tilde{y}_n(i-\ell), \qquad \text{(A1)}$$

where $\lambda=n/(n+\ell)$, ℓ is the order of the moving average, $y(i)$ is defined in Eq. (1). The relative importance of the two terms entering the function in Eq. (A1) can be further understood by analyzing the properties of the transfer function $H(f)$ in the frequency domain (see Appendix B).

Compared to the traditional exponentially weighted moving average (of order $\ell=1$) where the terms in Eq. (A1) decrease exponentially, the higher order $\ell>1$ allows for a slower, step-size decrease of the terms in Eq. (A1) with a "step" of size ℓ. The fluctuation function $F(n)$ is obtained following Eq. (10) and Eq. (11). The WDMA-ℓ allows for a more gradual decrease in the distribution of weights in the moving average box, and thus may be more appropriate when estimating the scaling behavior of anticorrelated and uncorrelated signals.

We apply the WDMA-ℓ method for increasing values of ℓ to correlated signals with varied values of the scaling exponent α_0. To study the performance of the WDMA-ℓ methods, we estimate the scaling behavior of the rms fluctuation function $F(n)$ at different scales n by calculating the local scaling exponent $\alpha_{\rm loc}$ in the same way as discussed in Fig. 3. We find that at large scales for $\ell=2,\ldots,5$, the $\alpha_{\rm loc}$ curves deviate significantly from the expected values α_0—presented with horizontal dashed lines in Fig. 13. This indicates that the WDMA-ℓ method significantly underestimates the strength of the correlations in our artificially generated signals. Further, as for $\ell=1$, we find that for higher order $\ell>1$ the WDMA-ℓ methods exhibit an inherent limitation to accurately quantify the scaling behavior of positively correlated signals with $\alpha_0>0.7$. This behavior is also clear from our three-dimensional presentation in Fig. 14. For anticorrelated

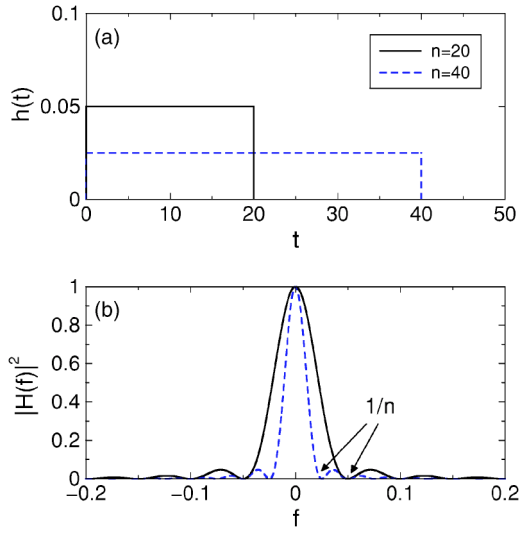

FIG. 15. Plot of the moving average filter kernel in the time (a) and in the frequency domain (b), respectively.

signals, however, the WDMA-ℓ performs better at small and intermediate scales for increasing order ℓ as α_0 decreases (Fig. 13) (see Appendix B). These observations are also confirmed from the three-dimensional probability histograms in Fig. 14, where it is clear that the scaling range for the best fit shrinks for positively correlated signals ($\alpha_0 > 0.5$) for increasing order ℓ, while for anticorrelated signals ($\alpha_0 < 0.5$), there is a broader range of scales over which a best fit (with a probability of $p > 0.7$) is observed.

APPENDIX B

1. Moving average methods in frequency domain

In this appendix, the performance of the DMA algorithm is discussed in the frequency domain. The interest of the frequency domain derives from the simplification designed to describe the effect of the detrending function $\tilde{y}_n(i)$ in terms of the product of the square modulus of the transfer function $H_n(f)$ and of $S(f)$, the power spectral density of the noisy signal $y(i)$.

The simple moving average $\tilde{y}_n(i)$ of window size n is defined as

$$\tilde{y}_n(i) \equiv \frac{1}{n}\sum_{k=0}^{n-1} y(i-k), \tag{B1}$$

corresponding to the discrete form of the causal convolution integral, where the convolution kernel introduces the memory effect. Equation (B1) is a sum with a constant memory kernel $h(t)$, i.e., a step function with an amplitude $1/n$ [Fig. 15(a)]. The function $h(t)$ uniformly weights the contribution of all the past events in the window $[0,n)$, thus it works better for random paths with a correlation exponent centered around 0.5. For higher degrees of correlation or anticorrelation, it should be taken into account (as already explained in the section describing the DMA function) that each data point is more correlated to the most recent points than to the points further away.

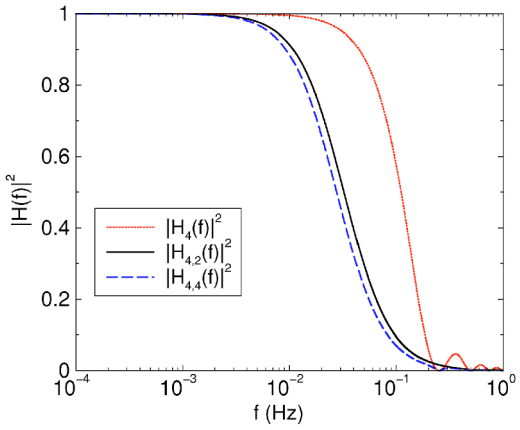

FIG. 16. Plot of the function $|H(f)|^2$ for the simple moving average with $n=4$, $|H_4(f)|^2$; for the weighted moving average, with $n=4$ and $\ell=2$, $|H_{4,2}(f)|^2$, respectively; for the weighted moving average with $n=4$ and $\ell=4$ $|H_{4,4}(f)|^2$, respectively.

In the frequency domain, $\tilde{y}_n(i)$ is characterized by the transfer function $H_n(f)$ (the Dirichlet kernel), which is

$$H_n(f) = \frac{\sin(n\pi f)}{n\pi f} e^{-in\pi f}. \tag{B2}$$

$H_n(f)$ takes the values $H_n(0)=1$ and $H_n(kf_0)=0$ for $k=1,2,\ldots n$.

The transfer function $H(f)$ of any filter should ideally be a window of constant amplitude, going to zero very quickly above the cutoff frequency $1/n$. By observing the curves of Fig. 15(b) and Fig. 16, it is clear that the filtering performance of $H_n(f)$ is affected by the presence of the side lobes at frequency higher than $1/n$.

As observed in Fig. 16, $|H_4(f)|^2$ presents a side lobe allowing the components of the signal $y(i)$, with a frequency between $1/n$ and $2/n$ (i.e., time scales between $n/2$ and n) to pass through the filter, thus giving a spurious contribution to $\tilde{y}_n(i)$. These components contribute to the rms $F(n)$ [defined in Eq. (11)] less than what should correspond to n on the basis of the scaling law $F(n) \sim n^{\alpha}$, with the consequence of increasing the slope $F(n)$ at small scales.

We next discuss the reasons why the weighted moving average might reduce this effect. The exponentially weighted moving average (WDMA-ℓ) weights recent data more than older data. It is defined as

$$\tilde{y}_{n,\ell}(i) \equiv \frac{(1-\lambda)}{\ell}\sum_{k=0}^{\ell-1} y(i-k) + \lambda \tilde{y}_{n,\ell}(i-\ell). \tag{B3}$$

The coefficients are commonly indicated as *weights* of the filter and are given by

$$\lambda = \frac{n}{\ell + n}. \tag{B4}$$

Taking the Fourier transform on Eq. (B3), we obtain

$$\tilde{Y}_{n,\ell}(f) = (1-\lambda)H_\ell(f)Y(f) + \lambda\tilde{Y}_{n,\ell}(f)e^{-i2\pi\ell f}, \qquad \text{(B5)}$$

where $Y(f)$, $\tilde{Y}_{n,\ell}(f)$ are the Fourier transforms of $y(i)$ and $\tilde{y}_{n,\ell}(i)$, respectively. Further, we have

$$\tilde{Y}_{n,\ell}(f) = \frac{1-\lambda}{1-\lambda e^{-i2\pi\ell f}}H_\ell(f)Y(f). \qquad \text{(B6)}$$

Thus the transfer function is

$$H_{n,\ell}(f) = \frac{1-\lambda}{1-\lambda e^{-i2\pi\ell f}}H_\ell(f). \qquad \text{(B7)}$$

From Eq. (B7), one can find that the cutoff frequency for $|H_{n,\ell}(f)|^2$ is $\min\{1/[2\pi\sqrt{n(n+\ell)}], 1/\ell\}$. In Fig. 16, the transfer function of the weighted moving averages with $n=4$ and $\ell=2$ and with $n=4$ and $\ell=4$, respectively, are shown. It can be observed that the effect of the side lobe to the performance of $|H_{4,2}(f)|^2$ and $|H_{4,4}(f)|^2$ has become negligible compared to that of $|H_4(f)|^2$, with the consequence of reducing the high frequency components in the detrended signal and thus reducing the deviation of the α_{loc}, as discussed in the paper.

[1] P. A. Robinson, Phys. Rev. E **67**, 032902 (2003).
[2] K. Ivanova, T. P. Ackerman, E. E. Clothiaux, P. Ch. Ivanov, H. E. Stanley, and M. Ausloos, J. Geophys. Res., [Atmos.] **108**, 4268 (2003).
[3] Z. Siwy, M. Ausloos, and K. Ivanova, Phys. Rev. E **65**, 031907 (2002).
[4] P. A. Varotsos, N. V. Sarlis, and E. S. Skordas, Phys. Rev. E **67**, 021109 (2003).
[5] P. A. Varotsos, N. V. Sarlis, and E. S. Skordas, Phys. Rev. E **68**, 031106 (2003).
[6] E. Koscielny-Bunde, A. Bunde, S. Havlin, H. E. Roman, Y. Goldreich, and H. J. Schellnhuber, Phys. Rev. Lett. **81**, 729 (1998).
[7] P. Talkner and R. O. Weber, Phys. Rev. E **62**, 150 (2000).
[8] J. F. Eichner, E. Koscielny-Bunde, A. Bunde, S. Havlin, and H. J. Schellnhuber, Phys. Rev. E **68**, 046133 (2003).
[9] K. Fraedrich and R. Blender, Phys. Rev. Lett. **90**, 108501 (2003).
[10] M. Pattantyus-Abraham, A. Kiraly, and I. M. Janosi, Phys. Rev. E **69**, 021110 (2004).
[11] A. Montanari, R. Rosso, and M. S. Taqqu, Water Resour. Res. **36**, 1249 (2000).
[12] C. Matsoukas, S. Islam, and I. Rodriguez-Iturbe, J. Geophys. Res., [Atmos.] **105**, 29 165 (2000).
[13] M. A. Moret, G. F. Zebende, E. Nogueira, and M. G. Pereira, Phys. Rev. E **68**, 041104 (2003).
[14] R. G. Kavasseri and R. Nagarajan, IEEE Trans. Circuits Syst., I: Fundam. Theory Appl. **51**, 2255 (2004).
[15] G. F. Zebende, M. V. S. da Silva, A. C. P. Rosa, A. S. Alves, J. C. O. de Jesus, and M. A. Moret, Physica A **342**, 322 (2004).
[16] C.-K. Peng, S. V. Buldyrev, S. Havlin, M. Simons, H. E. Stanley, and A. L. Goldberger, Phys. Rev. E **49**, 1685 (1994).
[17] S. V. Buldyrev, A. L. Goldberger, S. Havlin, C.-K. Peng, H. E. Stanley, and M. Simons, Biophys. J. **65**, 2673 (1993).
[18] R. N. Mantegna, S. V. Buldyrev, A. L. Goldberger, S. Havlin, C.-K. Peng, M. Simons, and H. E. Stanley, Phys. Rev. Lett. **76**, 1979 (1996).
[19] P. Carpena, P. Bernaola-Galván, P. Ch. Ivanov, and H. E. Stanley, Nature (London) **418**, 955 (2002).
[20] N. Iyengar, C.-K. Peng, R. Morin, A. L. Goldberger, and L. A. Lipsitz, Am. J. Physiol. **40**, R1078 (1996).
[21] P. Ch. Ivanov, A. Bunde, L. A. Nunes Amaral, S. Havlin, J. Fritsch-Yelle, R. M. Baevsky, H. E. Stanley, and A. L. Goldberger, Europhys. Lett. **48**, 594 (1999).
[22] S. M. Pikkujamsa, T. H. Makikallio, L. B. Sourander, I. J. Raiha, P. Puukka, J. Skytta, C.-K. Peng, A. L. Goldberger, and H. V. Huikuri, Circulation **100**, 393 (1999).
[23] C.-K. Peng, S. Havlin, H. E. Stanley, and A. L. Goldberger, Chaos **5**, 82 (1995).
[24] D. Toweill, K. Sonnenthal, B. Kimberly, S. Lai, and B. Goldstein, Crit. Care Med. **28**, 2051 (2000).
[25] A. Bunde, S. Havlin, J. W. Kantelhardt, T. Penzel, J. H. Peter, and K. Voigt, Phys. Rev. Lett. **85**, 3736 (2000).
[26] Y. Ashkenazy, P. Ch. Ivanov, S. Havlin, C.-K. Peng, A. L. Goldberger, and H. E. Stanley, Phys. Rev. Lett. **86**, 1900 (2001).
[27] P. Ch. Ivanov, L. A. Nunes Amaral, A. L. Goldberger, M. G. Rosenblum, H. E. Stanley, and Z. R. Struzik, Chaos **11**, 641 (2001).
[28] M. Cernelc, B. Suki, B. Reinmann, Graham L. Hall, and Urs Frey, J. Appl. Physiol. **92**, 1817 (2002).
[29] J. W. Kantelhardt, Y. Ashkenazy, P. Ch. Ivanov, A. Bunde, S. Havlin, T. Penzel, J.-H. Peter, and H. E. Stanley, Phys. Rev. E **65**, 051908 (2002).
[30] R. Karasik, N. Sapir, Y. Ashkenazy, P. Ch. Ivanov, I. Dvir, P. Lavie, and S. Havlin, Phys. Rev. E **66**, 062902 (2002).
[31] J. C. Echeverria, M. S. Woolfson, J. A. Crowe, B. R. Hayes-Gill, G. D. H. Croaker, and H. Vyas, Chaos **13**, 467 (2003).
[32] K. Hu, P. Ch. Ivanov, Z. Chen, M. F. Hilton, H. E. Stanley, and S. A. Shea, Physica A **337**, 307 (2004).
[33] D. N. Baldwin, B. Suki, J. J. Pillow, H. L. Roiha, S. Minocchieri, and U. Frey, J. Appl. Physiol. **97**, 1830 (2004).
[34] J. W. Kantelhardt, S. Havlin, and P. Ch. Ivanov, Europhys. Lett. **62**, 147 (2003).
[35] R. C. Hwaand T. C. Ferree, Physica A **338**, 246 (2004).
[36] N. Vandewalle and M. Ausloos, Phys. Rev. E **58**, 6832 (1998).
[37] Y. Liu, P. Gopikrishnan, P. Cizeau, M. Meyer, C.-K. Peng, and H. E. Stanley, Phys. Rev. E **60**, 1390 (1999).
[38] I. M. Janosi, B. Janecsko, and I. Kondor, Physica A **269**, 111 (1999).
[39] M. Ausloos, N. Vandewalle, P. Boveroux, A. Minguet, and K. Ivanova, Physica A **274**, 229 (1999).
[40] M. Roberto, E. Scalas, G. Cuniberti, and M. Riani, Physica A **269**, 148 (1999).

[41] P. Grau-Carles, Physica A **287**, 396 (2000).
[42] M. Ausloos and K. Ivanova, Phys. Rev. E **63**, 047201 (2001).
[43] P. Ch. Ivanov, A. Yuen, B. Podobnik, and Y. Lee, Phys. Rev. E **69**, 056107 (2004).
[44] K. Hu, P. Ch. Ivanov, Z. Chen, P. Carpena, and H. E. Stanley, Phys. Rev. E **64**, 011114 (2001).
[45] Z. Chen, P. Ch. Ivanov, K. Hu, and H. E. Stanley, Phys. Rev. E **65**, 041107 (2002).
[46] Z. Chen, K. Hu, P. Carpena, P. Bernaola, H. E. Stanley, and P. Ch. Ivanov, Phys. Rev. E **71**, 011104 (2005).
[47] P. S. Wilson, A. C. Tomsett, and R. Toumi, Phys. Rev. E **68**, 017103 (2003).
[48] R. L. Stratonovich, *Topics in the Theory of Random Noise Vol. 1* (Gordon & Breach, New York, 1981).
[49] H. E. Hurst, Trans. Am. Soc. Civ. Eng. **116**, 770 (1951).
[50] B. B. Mandelbrot and J. R. Wallis, Water Resour. Res. **5**, No. 2, 321 (1969).
[51] M. S. Taqqu, V. Teverovsky, and W. Willinger, Fractals **3**, 785 (1995).
[52] E. Alessio, A. Carbone, G. Castelli, and V. Frappietro, Eur. Phys. J. B **27**, 197 (2002).
[53] A. Carbone, G. Castelli, and H. E. Stanley, Phys. Rev. E **69**, 026105 (2004).
[54] A. Carbone and H. E. Stanley, *Noise in Complex Systems and Stochastic Dynamics*, Proc. SPIE Vol. 5471 (SPIE, Bellingham, WA, 2004), p. 1.
[55] A. Carbone, G. Castelli, and H. E. Stanley, Physica A **340**, 540 (2004).
[56] A. Carbone and H. E. Stanley, Physica A **344**, 267 (2004).
[57] H. A. Makse, S. Havlin, M. Schwartz, and H. E. Stanley, Phys. Rev. E **53**, 5445 (1996).
[58] K. Kwon and R. J. Kish, Appl. Financ. Econ. **12**, 273 (2002).
[59] S. Talluri and J. Sarkis, Int. J. Prod. Res. **74**, 47 (2004).
[60] D. Q. Cai, M. Xie, and T. N. Goh, Int. J. Comput. Vis. **14**, 206 (2001).
[61] A. B. Yeh, D. K. J. Lin, H. Zhou, and C. Renkataramani, J. App. Stat. **30**, 507 (2003).

Quantifying signals with power-law correlations: A comparative study of detrended fluctuation analysis and detrended moving average techniques

By: Xu, LM (Xu, LM); Ivanov, PC (Ivanov, PC); Hu, K (Hu, K); Chen, Z (Chen, Z); Carbone, A (Carbone, A); Stanley, HE (Stanley, HE)

View ResearcherID and ORCID

PHYSICAL REVIEW E
Volume: 71 **Issue:** 5 **Part:** 1
Article Number: 051101
DOI: 10.1103/PhysRevE.71.051101
Published: MAY 2005
Document Type: Article
View Journal Impact

Abstract

Detrended fluctuation analysis (DFA) and detrended moving average (DMA) are two scaling analysis methods designed to quantify correlations in noisy nonstationary signals. We systematically study the performance of different variants of the DMA method when applied to artificially generated long-range power-law correlated signals with an a priori known scaling exponent alpha(0) and compare them with the DFA method. We find that the scaling results obtained from different variants of the DMA method strongly depend on the type of the moving average filter. Further, we investigate the optimal scaling regime where the DFA and DMA methods accurately quantify the scaling exponent alpha(0), and how this regime depends on the correlations in the signal. Finally, we develop a three-dimensional representation to determine how the stability of the scaling curves obtained from the DFA and DMA methods depends on the scale of analysis, the order of detrending, and the order of the moving average we use, as well as on the type of correlations in the signal.

Keywords

KeyWords Plus: LONG-RANGE CORRELATIONS; FRACTIONAL BROWNIAN PATHS; TIME-SERIES; CROSSOVER PHENOMENA; HEARTBEAT DYNAMICS; HEALTHY INFANTS; VARIABILITY; SLEEP; TRANSITION; EXPONENT

Author Information

Reprint Address: Xu, LM (reprint author)

+ Boston Univ, Ctr Polymer Studies, Boston, MA 02215 USA.

Addresses:

+ [1] Boston Univ, Ctr Polymer Studies, Boston, MA 02215 USA
+ [2] Boston Univ, Dept Phys, Boston, MA 02215 USA
+ [3] Politecn Torino, INFM, I-10129 Turin, Italy
+ [4] Politecn Torino, Dept Phys, I-10129 Turin, Italy

Publisher

AMER PHYSICAL SOC, ONE PHYSICS ELLIPSE, COLLEGE PK, MD 20740-3844 USA

Journal Information

Impact Factor: Journal Citation Reports

Categories / Classification

Research Areas: Physics

Web of Science Categories: Physics, Fluids & Plasmas; Physics, Mathematical

Suggest a correction

If you would like to improve the quality of the data in this record, please suggest a correction.

See more data fields

70 of 127

Cited References: 61

Showing 30 of 61 **View All in Cited References page** *(from Web of Science Core Collection)*

1. **Second-order moving average and scaling of stochastic time series** **Times Cited: 248**
   By: Alessio, E; Carbone, A; Castelli, G; et al.
   EUROPEAN PHYSICAL JOURNAL B Volume: 27 Issue: 2 Pages: 197-200 Published: MAY 2002

2. **Magnitude and sign correlations in heartbeat fluctuations** **Times Cited: 299**
   By: Ashkenazy, Y; Ivanov, PC; Havlin, S; et al.
   PHYSICAL REVIEW LETTERS Volume: 86 Issue: 9 Pages: 1900-1903 Published: FEB 26 2001

3. **Applications of statistical physics to economic and financial topics** **Times Cited: 67**
   By: Ausloos, M; Vandewalle, N; Boveroux, P; et al.
   PHYSICA A Volume: 274 Issue: 1-2 Pages: 229-240 Published: DEC 1 1999

4. **Power-law correlations in the southern-oscillation-index fluctuations characterizing El Nino** **Times Cited: 55**
   By: Ausloos, M; Ivanova, K
   PHYSICAL REVIEW E Volume: 63 Issue: 4 Article Number: 047201 Part: 2 Published: APR 2001

5. **Effect of sighs on breathing memory and dynamics in healthy infants** **Times Cited: 45**
   By: Baldwin, DN; Suki, B; Pillow, JJ; et al.
   JOURNAL OF APPLIED PHYSIOLOGY Volume: 97 Issue: 5 Pages: 1830-1839 Published: NOV 2004

6. **FRACTAL LANDSCAPES AND MOLECULAR EVOLUTION - MODELING THE MYOSIN HEAVY-CHAIN GENE FAMILY** **Times Cited: 112**
   By: BULDYREV, SV; GOLDBERGER, AL; HAVLIN, S; et al.
   BIOPHYSICAL JOURNAL Volume: 65 Issue: 6 Pages: 2673-2679 Published: DEC 1993

7. **Correlated and uncorrelated regions in heart-rate fluctuations during sleep** **Times Cited: 367**
   By: Bunde, A; Havlin, S; Kantelhardt, JW; et al.
   PHYSICAL REVIEW LETTERS Volume: 85 Issue: 17 Pages: 3736-3739 Published: OCT 23 2000

8. **SPC in an automated manufacturing environment** **Times Cited: 7**
   By: Cai, DQ; Xie, M; Goh, TN
   INTERNATIONAL JOURNAL OF COMPUTER INTEGRATED MANUFACTURING Volume: 14 Issue: 2 Pages: 206-211 Published: MAR-APR 2001

9. **Spatio-temporal complexity in the clusters generated by fractional Brownian paths** **Times Cited: 5**
   By: Carbone, A; Stanley, HE
   NOISE IN COMPLEX SYSTEMS AND STOCHASTIC DYNAMICS II Book Series: Proceedings of SPIE Volume: 5471 Pages: 1-12 Published: 2004

PHYSICAL REVIEW E **73**, 065201(R) (2006)

Spurious detection of phase synchronization in coupled nonlinear oscillators

Limei Xu,[1] Zhi Chen,[1,2] Kun Hu,[1,3] H. Eugene Stanley,[1] and Plamen Ch. Ivanov[1]
[1]*Center for Polymer Studies and Department of Physics, Boston University, Boston, Massachusetts 02215 USA*
[2]*Department of Physics and Astronomy, University of California, Irvine, California 92697, USA*
[3]*Division of Gerontology, Harvard Medical School, Beth Israel Deaconess Medical Center, Boston, Massachusetts 02215, USA*
(Received 24 January 2006; published 26 June 2006)

Coupled nonlinear systems under certain conditions exhibit phase synchronization, which may change for different frequency bands or with the presence of additive system noise. In both cases, Fourier filtering is traditionally used to preprocess data. We investigate to what extent the phase synchronization of two coupled Rössler oscillators depends on (1) the broadness of their power spectrum, (2) the width of the bandpass filter, and (3) the level of added noise. We find that for identical coupling strengths, oscillators with broader power spectra exhibit weaker synchronization. Further, we find that within a broad bandwidth range, bandpass filtering reduces the effect of noise but can lead to a spurious increase in the degree of phase synchronization with narrowing bandwidth, even when the coupling between the two oscillators remains the same.

DOI: 10.1103/PhysRevE.73.065201 PACS number(s): 05.45.Xt, 05.45.Tp, 05.45.Pq

In recent years both theoretical and experimental studies of coupled nonlinear oscillators have demonstrated that such oscillators can exhibit phase synchronization [1–5]. Analysis of experimental data has also indicated the presence of phase synchronization in a range of coupled physical, biological, and physiological systems [6–17]. In many of these studies, an important practical question is how multivariate time series characterized by a relatively broad power spectrum are phase synchronized in a specific frequency range [18–24]. The presence of internal or external noise may also be an obstacle when quantifying phase synchronization from experimental data [18,19,25–27]. In both cases a bandpass filter is traditionally applied either to reduce the noise effect or to extract the frequency range of interest. Thus, it is important to know to what extent the width of the bandpass filter influences the results of the phase synchronization analysis, as well as what is the range of the index values obtained from the analysis that indicate a statistically significant phase synchronization.

To address these questions, we consider a system of two coupled Rössler oscillators (1,2) defined as

$$\dot{x}_{1,2} = -\omega_{1,2} y_{1,2} - z_{1,2} + C(x_{2,1} - x_{1,2}),$$

$$\dot{y}_{1,2} = \omega_{1,2} x_{1,2} + a y_{1,2},$$

$$\dot{z}_{1,2} = f + z_{1,2}(x_{1,2} - b) \qquad (1)$$

with parameter values $a=0.165$, $f=0.2$, and $b=10$. For the mismatch of natural frequencies, we choose $\omega_{1,2}=\omega_0 \pm \Delta\omega$, with $\omega_0=0.6$ and $\Delta\omega=0.005$ [Fig. 1(a)]. The time step in our simulation is $\Delta t = 2\pi/10^3$, and the signal length $n=\text{int}[t/\Delta t]$ with $t=10^4$, where int$[x]$ denotes the integer part of x.

We first investigate the characteristics of the system defined in Eq. (1) by comparing them with the characteristics of a second set of two coupled Rössler oscillators (3,4) studied in [3]. The system (3,4) is also described by Eq. (1), and has the same values for the parameters a, f, and b as system (1,2). The only differences are the natural frequency $\omega_0=1$ and the frequency mismatch $\Delta\omega=0.015$ [Fig. 1(b)]. We observe a significantly broader power spectrum for system (1,2) with $\omega_0=0.6$ and frequency mismatch $\Delta\omega=0.005$ [Fig. 1(c)]. Further, we observe that the instantaneous phase differences $\Delta\psi_{1,1}=[\phi_{x_1}(t)-\phi_{x_2}(t)] \bmod(2\pi)$ for system (1,2) exhibits larger fluctuations [Fig. 1(d)], described by a broader distribution [Fig. 1(e)], compared to system (3,4), suggesting a weaker 1:1 phase synchronization for system (1,2). To quantify the degree of phase synchronization in the two Rössler systems we use the synchronization index $\rho=(S_{\max}-S)/S_{\max}$ [18], where $S \equiv -\Sigma_{k=1}^{N} P_k \ln P_k$ is the Shannon entropy [28] of the distribution $P(\Delta\psi_{1,1})$ of $\Delta\psi_{1,1}$, and $S_{\max}=\ln N$, where $N=\text{int}\{\exp[0.626+0.4\ln(n-1.0)]\}$ is the optimized number of bins over which the distribution is obtained [29]. For system (3,4) with a narrow power spectrum we obtain a significantly larger value of ρ compared to the system (1,2) characterized by a broader power spectrum [Fig. 1(f)]. Varying the values of the coupling strength C, we find that the phase synchronization index ρ is consistently higher for system (3,4) characterized by the narrower power spectrum. Thus, for the same coupling strength C and for identical other parameters, system (1,2) with $\omega_0=0.6$, which has a broader power spectrum, exhibits weaker synchronization compared to system (3,4) with $\omega_0=1$, which has a narrow power spectrum. These findings are complementary to a recent study indicating a different degree of phase synchronization for the spectral components of coupled chaotic oscillators [30].

Recent work has shown that coupled Rössler oscillators may exhibit different degrees of synchronization for different ranges of time scales obtained via wavelet transform [31]. Here, we ask to what extent the width of a bandpass filter affects the degree of phase synchronization between two coupled Rössler oscillators. While the output observables $x_1$and x_2 of system (1,2) are clearly not in phase [Fig. 2(a)], after Fourier bandpass filtering in the range of $\Delta f=0.01$ centered at the peak of the power spectrum $2\pi f \approx 0.54$ [Fig. 1(c)], the observables x_1 and x_2 appear 1:1 synchronized with well-aligned peaks [Fig. 2(b)]. The effect of the bandpass filter can be clearly seen in the behavior of the instantaneous

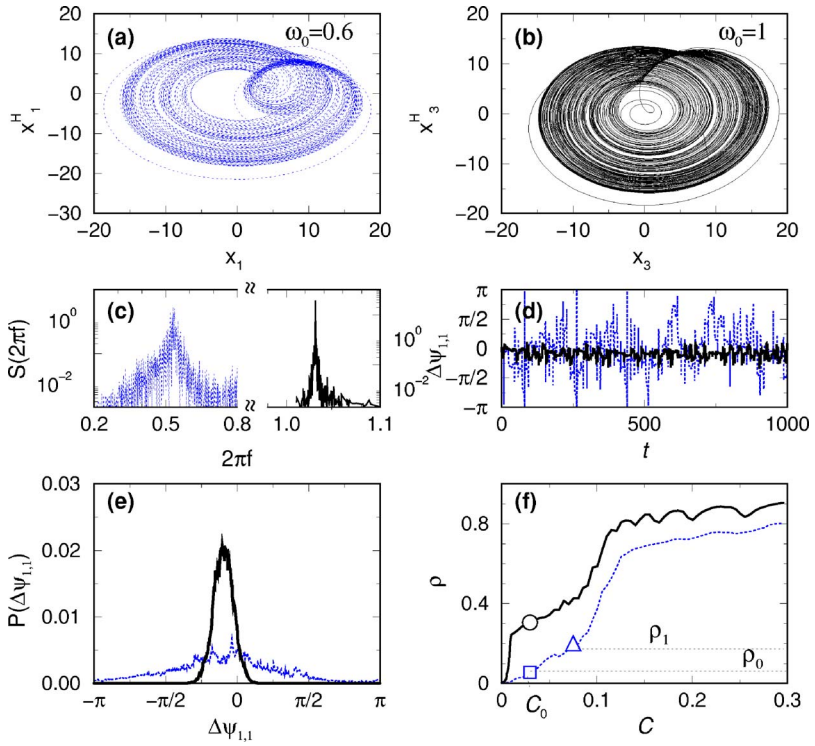

FIG. 1. (Color online) Differences in the synchronization of two Rössler systems with identical coupling strengths and different power spectra. Phase plot trajectories of the variables x vs their Hilbert transform x^H for (a) system (1,2), with x_1 corresponding to $\omega_1=\omega_0+\Delta\omega$, where $\omega_0=0.6$ and $\Delta\omega=0.005$; (b) system (3,4), with x_3 corresponding to $\omega_3=\omega_0+\Delta\omega$, where now $\omega_0=1$ and $\Delta\omega=0.015$. For both Rössler systems $C=0.03$. (c) Power spectra of the time sequence x_1 (dashed line) and x_3 (solid line). A broader spectrum is observed for system (1,2) compared to system (3,4). (d) Instantaneous phase difference $\Delta\psi_{1,1}\equiv(\phi x_1(t)-\phi x_2(t))$ mod(2π) for system (1,2) (dashed line), and $\Delta\psi_{1,1}\equiv(\phi x_3(t)-\phi x_4(t))$ mod(2π) for system (3,4) (solid line), and (e) their corresponding distributions $P(\Delta\psi_{1,1})$. System (1,2) exhibits larger fluctuations in $\Delta\psi_{1,1}$ and is characterized by a broader distribution $P(\Delta\psi_{1,1})$. (f) Synchronization index ρ as a function of the coupling strength C. For identical values of C, system (3,4) (solid line), which is characterized by a narrower power spectrum, exhibits stronger synchronization (larger index ρ) compared to system (1,2) with a broader power spectrum. Specifically, for identical coupling strength $C=C_0=0.03$, the index $\rho=\rho_0$ (□) for system (1,2), while $\rho=0.3>\rho_0$ (○) for system (3,4) although the frequency mismatch for system (3,4) is much larger. The effect of a Fourier bandpass filter applied to the system (1,2) while keeping $C=0.03$ fixed is equivalent to an increase of the coupling strength of the system leading to a larger index $\rho_1>\rho_0$ (Δ) as also shown in Fig. 2(e).

phase difference $\Delta\psi_{1,1}$ [Fig. 2(c)] and in the shape of the probability density function $P(\Delta\psi_{1,1}(t))$ [Fig. 2(d)]. After bandpass filtering, $\Delta\psi_{1,1}$ becomes smoother with fewer fluctuations, and the distribution $P(\Delta\psi_{1,1})$ exhibits a more pronounced peak. To quantify how the degree of synchronization changes with the width Δf of the bandpass filter, we calculate the synchronization index ρ [Fig. 2(e)]. We find that for very large values of the bandwidth Δf, the index ρ is the same as the value ρ_0 obtained for the system (1,2) without any filtering, and that ρ remains unchanged for intermediate values of Δf. However, for decreasing Δf, the index ρ increases rapidly from the expected value ρ_0 [Figs. 1(f) and 2(c)]. Such deviation to higher values of $\rho>\rho_0$, while the coupling constant C in Eq. (1) remains fixed, indicates a spurious effect of synchronization due to the bandpass filter. Thus, applying a bandpass filter with a too narrow bandwidth when preprocessing empirical data may lead to overestimation of the phase synchronization (as defined by index ρ) between two empirical systems where the coupling strength is not known *a priori*.

Many physical and biological systems are influenced by external noise, which can mask their intrinsic properties. Recent studies have shown that noise can bias the estimation of the driver-response relationship in coupled nonlinear oscillators leading to change in synchronization measures [32]. Specifically, external noise may weaken the detection of the coupling and reduce the synchronization between two coupled dynamical systems. To address this problem, we next test the effect of external noise on the degree of phase synchronization of the two coupled Rössler oscillators defined in Eq. (1). Adding uncorrelated and unfiltered Gaussian noise η to the output observables x_1 and x_2, while keeping the coupling constant C in Eq. (1) fixed, we find that the synchronization index ρ decreases with increasing noise strength σ_η (i.e., higher standard deviation σ_η compared to the standard deviation σ of the output signals x_1 and x_2) [Fig. 3(a)]. The dependence of ρ on the value of the coupling constant C for different noise strength is shown in Fig. 3(b). We find that the transition to the state of maximum degree of synchronization [indicated by a horizontal plateau for ρ in Fig. 3(b)] occurs at decreasing values of the coupling constant C for increasing noise strength σ_η. For very strong noise ($\sigma_\eta=\sigma=8.3$), the two Rössler oscillators in Eq. (1) appear not to be synchronized, characterized by low values for the index ρ, even for very large values of the coupling

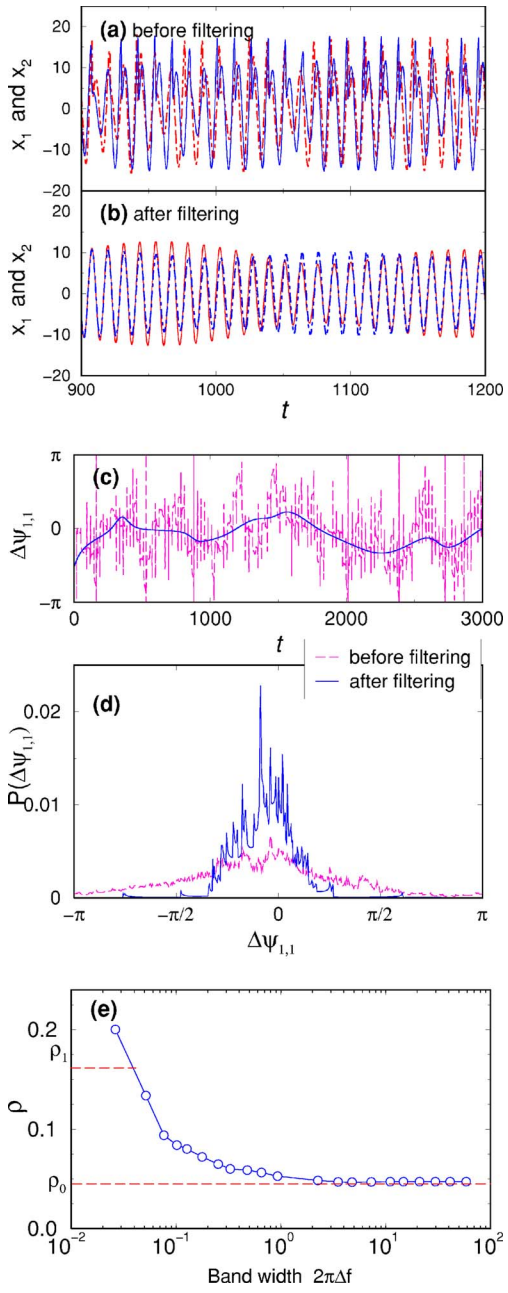

FIG. 2. (Color online) Effects of bandpass filtering on synchronization. Time sequence of the variables x_1 and x_2 of system (1,2) (a) before and (b) after applying a bandpass Fourier filter with bandwidth $\Delta f=0.01$. After bandpass filtering the sequences x_1 and x_2 are better aligned in time (with almost matching peaks). (c) Instantaneous phase difference $\Delta\psi_{1,1}$ and (d) the distribution $P(\Delta\psi_{1,1})$ before (dashed line) and after (solid line) the Fourier bandpass filtering. After filtering, $\Delta\psi_{1,1}$ is characterized by fewer fluctuations and a much narrower distribution $P(\Delta\psi_{1,1})$, indicating a stronger synchronization, although the coupling strength $C=0.03$ remains constant. (e) Dependence of the index ρ on the bandwidth $2\pi\Delta f$ for fixed $C=0.03$. A filter with a relatively broader bandwidth ($2\pi\Delta f>1$) leaves the synchronization index ρ practically unchanged, $\rho=\rho_0$, where ρ_0 characterizes the synchronization between x_1 and x_2 before filtering. Narrowing Δf leads to a sharp increase in ρ, which is an artifact of the Fourier filtering as the coupling C and all other parameters remain unchanged, e.g., for $\Delta f=0.005$, $\rho=\rho_1\approx 4\rho_0$.

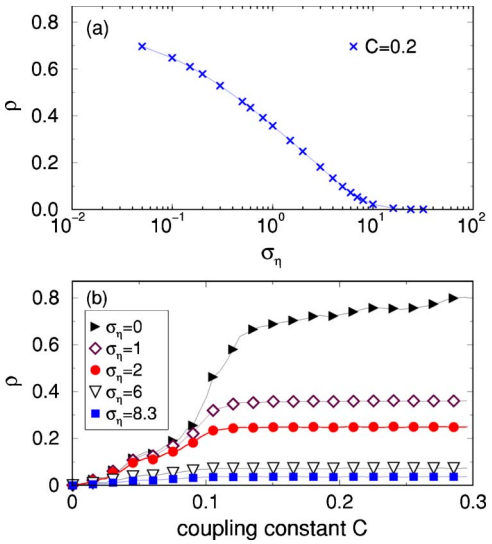

FIG. 3. (Color online) Effect of external additive white noise on phase synchronization for system (1,2) defined in Eq. (1). (a) Dependence of the synchronization index ρ on the noise strength σ_η for fixed value of the coupling constant C. (b) Dependence of the synchronization index ρ on the coupling strength C for different levels of white noise which are defined through the standard deviation σ_η.

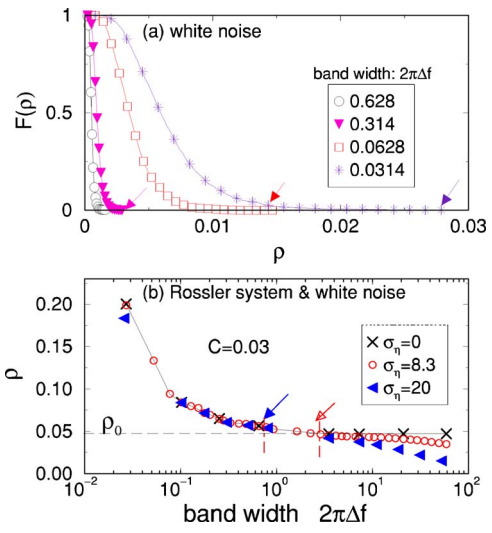

FIG. 4. (Color online) Combined effects of external noise and Fourier bandpass filtering on the synchronization. (a) Cumulative distribution function $F(\rho)\equiv 1-\int_0^\rho P(\rho')d\rho'$ for the synchronization index ρ obtained from 100 different realizations of pairs of white noise signals without coupling. The length of the noise signals is int$[10^7/2\pi]$. Tails of the distributions for each bandwidth indicate the maximum values of ρ one can obtain simply as a result of bandpass filtering when there is no synchronization between two white noise signals. (b) Synchronization index ρ obtained for system (1,2) defined in Eq. (1) with additive white noise as a function of the bandwidth Δf for $C=0.03$. While the effect of noise is gradually reduced by the Fourier bandpass filter with decreasing bandwidth Δf, there is an artificially increased synchronization (sharp increase in ρ) when $2\pi\Delta f<1$, as also shown in Fig. 2(e).

constant C [Fig. 3(b)]. We note, that with increasing noise strength σ_η the position of the crossover to the plateau of maximum synchronization shifts to smaller values of C in Fig. 3(b), indicating that with increasing σ_η the level of the plateau drops faster compared to the decline in the growth of ρ with increasing coupling C.

To reduce the effect of noise in data analysis, a common approach is to apply a bandpass filter. In the case of the coupled Rössler oscillators defined in Eq. (1), we next ask to what extent a bandpass filter can reduce the effect of external noise while preserving the expected "true" phase synchronization as presented by ρ_0 in Fig. 1(e). To answer this question, we first need to determine what are the limits to which spurious phase synchronization can be obtained purely as a result of bandpass filtering of two uncorrelated and not coupled Gaussian noise signals. Our results for the synchronization index ρ obtained from multiple realizations of pairs of uncoupled white noise signals show that the synchronization index ρ can reach different maximum values $\rho_{\max}$, indicated by arrows in Fig. 4(a), for different bandwidth Δf—with decreasing bandwidth $\rho_{\max}$ increases. The values of $\rho_{\max}$ provide an estimate of the maximum possible effect additive noise may have on the spurious "detection" of phase synchronization in coupled nonlinear oscillators. Thus, empirical observations of synchronization index $\rho > \rho_{\max}$ may indicate presence of a genuine phase synchronization between the outputs of two coupled oscillators, which is not an artifact of external noise. Our simulations show that the value of $\rho_{\max}$ does not change significantly with the length of the uncorrelated noise signals. In Fig. 4(b) we show how the synchronization index ρ for system (1,2) depends on the strength of the added noise and on the width Δf of the bandpass filter. For very broad bandwidth Δf the noise is not sufficiently filtered, and the synchronization between the two oscillators decreases (ρ decreases) with increasing noise strength σ_η. With decreasing band width Δf, i.e., applying a stronger filter, the effect of the noise is reduced, and correspondingly the index ρ increases—approaching the value ρ_0 expected for the system (1,2) without noise. On the other hand, applying a filter with too narrow bandwidth Δf leads to a spurious synchronization effects with $\rho > \rho_0$ [Fig. 4(b)], following closely the dependence of ρ on Δf shown in Fig. 2(e) for a Rössler system without noise.

In summary, our results indicate that phase synchronization between coupled nonlinear oscillators may strongly depend on the width of the power spectrum of these oscillators. Further, we find that while external noise can affect the degree of phase synchronization, bandpass filtering can reduce noise effects but can also lead to a spurious overestimation of the actual degree of phase synchronization in the system. This is of importance when analyzing empirical data in specific narrow frequency ranges, for which the coupling strength may not be known *a priori*.

We thank NIH (Grant No. 2R01 HL 071972) for support.

[1] M. G. Rosenblum *et al.*, Phys. Rev. Lett. **76**, 1804 (1996).
[2] U. Parlitz *et al.*, Phys. Rev. E **54**, 2115 (1996).
[3] M. G. Rosenblum *et al.*, Phys. Rev. Lett. **78**, 4193 (1997).
[4] A. S. Pikovsky *et al.*, Physica D **104**, 219 (1997).
[5] A. S. Pikovsky, M. G. Rosenblum, and J. Kurths, *Synchronization: A Universal Concept in Nonlinear Sciences* (Cambridge University Press, Cambridge, U.K., 2001).
[6] D. Y. Tang and N. R. Heckenberg, Phys. Rev. E **55**, 6618 (1997).
[7] S. Boccaletti *et al.*, Phys. Rev. E **61**, 3712 (2000).
[8] C. Schafer *et al.*, Nature (London) **392**, 153 (2000).
[9] V. S. Anishchenko *et al.*, Int. J. Bifurcation Chaos Appl. Sci. Eng. **10**, 2339 (2000).
[10] A. Stefanovska *et al.*, Phys. Rev. Lett. **85**, 4831 (2000).
[11] S. Boccaletti *et al.*, Phys. Rep. **366**, 1 (2002).
[12] Z. Chen *et al.*, Phys. Rev. E **73**, 031915 (2006).
[13] S. Bahar and F. Moss, Chaos **13**, 138 (2003).
[14] D. Rybski *et al.*, Physica A **320**, 601 (2003).
[15] S. Moshel *et al.*, Ann. N.Y. Acad. Sci. **1039**, 484 (2005).
[16] K. Nagai *et al.*, Phys. Rev. E **71**, 036217 (2005).
[17] E. Pereda *et al.*, Prog. Neurobiol. **77**, 1 (2005).
[18] P. Tass *et al.*, Phys. Rev. Lett. **81**, 3291 (1998).
[19] A. Neiman *et al.*, Phys. Rev. Lett. **82**, 660 (1999).
[20] L. Gross *et al.*, J. Physiol. (London) **527**, 623 (2000).
[21] F. Mormann *et al.*, Physica D **144**, 358 (2000).
[22] R. Q. Qiuan Quiroga *et al.*, Phys. Rev. E **65**, 041903 (2002).
[23] L. Angelini *et al.*, Phys. Rev. Lett. **93**, 038103 (2004).
[24] E. Gysels, P. Renevey, and P. Celka, Signal Process. **85**, 2178 (2005).
[25] B. Lindner *et al.*, Phys. Rep. **392**, 321 (2004).
[26] X. Q. Feng and Z. G. Zheng, Int. J. Mod. Phys. B **19**, 3501 (2005).
[27] P. F. Gora, Physica A **354**, 153 (2005).
[28] C. E. Shannon and W. Weaver, *The Mathematical Theory of Information* (Illinois University Press, Urbana, IL, 1949).
[29] R. Otnes and L. Enochson, *Digital Time Series Analysis* (Wiley, New York, 1972).
[30] A. E. Hramov *et al.*, Phys. Rev. E **71**, 056204 (2005).
[31] A. E. Hramov and A. A. Koronovskii, Physica D **206**, 252 (2005).
[32] R. Quian Quiroga, J. Arnhold, and P. Grassberger, Phys. Rev. E **61**, 5142 (2000).

Spurious detection of phase synchronization in coupled nonlinear oscillators

By: Xu, LM (Xu, Limei); Chen, Z (Chen, Zhi); Hu, K (Hu, Kun); Stanley, HE (Stanley, H. Eugene); Ivanov, PC (Ivanov, Plamen Ch.)

View ResearcherID and ORCID

PHYSICAL REVIEW E
Volume: 73 **Issue:** 6 **Part:** 2
Article Number: 065201
DOI: 10.1103/PhysRevE.73.065201
Published: JUN 2006
Document Type: Article
View Journal Impact

Abstract

Coupled nonlinear systems under certain conditions exhibit phase synchronization, which may change for different frequency bands or with the presence of additive system noise. In both cases, Fourier filtering is traditionally used to preprocess data. We investigate to what extent the phase synchronization of two coupled Rossler oscillators depends on (1) the broadness of their power spectrum, (2) the width of the bandpass filter, and (3) the level of added noise. We find that for identical coupling strengths, oscillators with broader power spectra exhibit weaker synchronization. Further, we find that within a broad bandwidth range, bandpass filtering reduces the effect of noise but can lead to a spurious increase in the degree of phase synchronization with narrowing bandwidth, even when the coupling between the two oscillators remains the same.

Keywords

KeyWords Plus: CHAOTIC OSCILLATORS; EXCITABLE SYSTEMS; MAGNETOENCEPHALOGRAPHY; LOCKING; SIGNALS; NOISE; EEG

Author Information

Reprint Address: Xu, LM (reprint author)

+ Boston Univ, Ctr Polymer Studies, Boston, MA 02215 USA.

Addresses:

+ [1] Boston Univ, Ctr Polymer Studies, Boston, MA 02215 USA
+ [2] Boston Univ, Dept Phys, Boston, MA 02215 USA
+ [3] Univ Calif Irvine, Dept Phys & Astron, Irvine, CA 92697 USA
+ [4] Harvard Univ, Beth Israel Deaconess Med Ctr, Sch Med, Div Gerontol, Boston, MA 02215 USA

Funding

Funding Agency	Grant Number
NHLBI NIH HHS	2R01 HL 071972

Publisher

AMERICAN PHYSICAL SOC, ONE PHYSICS ELLIPSE, COLLEGE PK, MD 20740-3844 USA

Categories / Classification

Research Areas: Physics

Web of Science Categories: Physics, Fluids & Plasmas; Physics, Mathematical

If you would like to improve the quality of the data in this record, please suggest a correction.

See more data fields

77 of 127

Cited References: 32

Showing 30 of 32 **View All in Cited References page** *(from Web of Science Core Collection)*

1. **Steady-state visual evoked potentials and phase synchronization in migraine patients** **Times Cited: 64**
   By: Angelini, L; Tommaso, MD; Guido, M; et al.
   PHYSICAL REVIEW LETTERS Volume: 93 Issue: 3 Article Number: 038103 Published: JUL 16 2004

2. **Entrainment between heart rate and weak noninvasive forcing** **Times Cited: 48**
   By: Anishchenko, VS; Balanov, AG; Janson, NB; et al.
   INTERNATIONAL JOURNAL OF BIFURCATION AND CHAOS Volume: 10 Issue: 10 Pages: 2339-2348 Published: OCT 2000

3. **Stochastic phase synchronization in the crayfish mechanoreceptor/photoreceptor system** **Times Cited: 17**
   By: Bahar, S; Moss, F
   CHAOS Volume: 13 Issue: 1 Pages: 138-144 Published: MAR 2003

4. **Synchronization of chaotic structurally nonequivalent systems** **Times Cited: 53**
   By: Boccaletti, S; Valladares, DL; Kurths, J; et al.
   PHYSICAL REVIEW E Volume: 61 Issue: 4 Pages: 3712-3715 Part: A Published: APR 2000

5. **The synchronization of chaotic systems** **Times Cited: 1,632**
   By: Boccaletti, S; Kurths, J; Osipov, G; et al.
   PHYSICS REPORTS-REVIEW SECTION OF PHYSICS LETTERS Volume: 366 Issue: 1-2 Pages: 1-101 Article Number: PII S0370-1573(02)00137-0 Published: AUG 2002

6. **Cross-correlation of instantaneous phase increments in pressure-flow fluctuations: Applications to cerebral autoregulation** **Times Cited: 35**
   By: Chen, Z; Hu, K; Stanley, HE; et al.
   PHYSICAL REVIEW E Volume: 73 Issue: 3 Article Number: 031915 Part: 1 Published: MAR 2006

7. **Coherent resonance and phase locking in noise-driven excitable systems** **Times Cited: 6**
   By: Feng, XQ; Zheng, ZG
   INTERNATIONAL JOURNAL OF MODERN PHYSICS B Volume: 19 Issue: 22 Pages: 3501-3509 Published: SEP 10 2005

8. **Linear transmitter with correlated noises** **Times Cited: 6**
   By: Gora, PF
   PHYSICA A-STATISTICAL MECHANICS AND ITS APPLICATIONS Volume: 354 Pages: 153-170 Published: AUG 15 2005

9. **Cortico-muscular synchronization during isometric muscle contraction in humans as revealed by magnetoencephalography** **Times Cited: 182**
   By: Gross, J; Tass, PA; Salenius, S; et al.
   JOURNAL OF PHYSIOLOGY-LONDON Volume: 527 Issue: 3 Pages: 623-631 Published: SEP 15 2000

10. **SVM-based recursive feature elimination to compare phase synchronization computed from broadband** **Times Cited: 28**

and narrowband EEG signals in Brain-Computer Interfaces
By: Gysels, E; Renevey, P; Celka, P
SIGNAL PROCESSING Volume: 85 Issue: 11 Pages: 2178-2189 Published: NOV 2005

11. **Time scale synchronization of chaotic oscillators** **Times Cited: 72**
By: Hramov, AE; Koronovskii, AA
PHYSICA D-NONLINEAR PHENOMENA Volume: 206 Issue: 3-4 Pages: 252-264 Published: JUL 1 2005

12. **Synchronization of spectral components and its regularities in chaotic dynamical systems** **Times Cited: 35**
By: Hramov, AE; Koronovskii, AA; Kurovskaya, MK; et al.
PHYSICAL REVIEW E Volume: 71 Issue: 5 Article Number: 056204 Part: 2 Published: MAY 2005

13. **Effects of noise in excitable systems** **Times Cited: 895**
By: Lindner, B; Garcia-Ojalvo, J; Neiman, A; et al.
PHYSICS REPORTS-REVIEW SECTION OF PHYSICS LETTERS Volume: 392 Issue: 6 Pages: 321-424 Published: MAR 2004

14. **Mean phase coherence as a measure for phase synchronization and its application to the EEG of epilepsy patients** **Times Cited: 628**
By: Mormann, F; Lehnertz, K; David, P; et al.
PHYSICA D Volume: 144 Issue: 3-4 Pages: 358-369 Published: OCT 1 2000

15. **Phase-synchronization decay of fixational eye movements** **Times Cited: 11**
By: Moshel, S; Liang, JR; Caspi, A; et al.
CLINICAL AND BASIC OCULOMOTOR RESEARCH: IN HONOR OF DAVID S. ZEE Book Series: ANNALS OF THE NEW YORK ACADEMY OF SCIENCES Volume: 1039 Pages: 484-488 Published: 2005

16. **Synchrony of neural Oscillators induced by random telegraphic currents** **Times Cited: 25**
By: Nagai, K; Nakao, H; Tsubo, Y
PHYSICAL REVIEW E Volume: 71 Issue: 3 Article Number: 036217 Part: 2 Published: MAR 2005

17. **Synchronization of the noisy electrosensitive cells in the paddlefish** **Times Cited: 158**
By: Neiman, A; Pei, X; Russell, D; et al.
PHYSICAL REVIEW LETTERS Volume: 82 Issue: 3 Pages: 660-663 Published: JAN 18 1999

18. Title: [not available] **Times Cited: 356**
By: Otnes, R. K.; Enochson, L. D.
DIGITAL TIME SERIES Published: 1972
Publisher: Wiley, NewYork, NY

19. **Experimental observation of phase synchronization** **Times Cited: 202**
By: Parlitz, U; Junge, L; Lauterborn, W; et al.
PHYSICAL REVIEW E Volume: 54 Issue: 2 Pages: 2115-2117 Published: AUG 1996

20. **Nonlinear multivariate analysis of neurophysiological signals** **Times Cited: 566**
By: Pereda, E; Quiroga, RQ; Bhattacharya, J
PROGRESS IN NEUROBIOLOGY Volume: 77 Issue: 1-2 Pages: 1-37 Published: SEP-OCT 2005

21. Title: [not available] **Times Cited: 2,716**
By: Pikovsky, A; Rosenblum, M; Kurths, J.
Synchronization, a universal concept in nonlinear sciences Published: 2001
Publisher: Cambridge University Press, England

22. **Phase synchronization of chaotic oscillators by external driving** **Times Cited: 451**

By: Pikovsky, AS; Rosenblum, MG; Osipov, GV; et al.
PHYSICA D Volume: 104 Issue: 3-4 Pages: 219-238 Published: JUN 1 1997

23. **Performance of different synchronization measures in real data: A case study on electroencephalographic signals** **Times Cited: 417**
By: Quiroga, RQ; Kraskov, A; Kreuz, T; et al.
PHYSICAL REVIEW E Volume: 65 Issue: 4 Article Number: 041903 Part: 1 Published: APR 2002

24. **Learning driver-response relationships from synchronization patterns** **Times Cited: 145**
By: Quiroga, RQ; Arnhold, J; Grassberger, P
PHYSICAL REVIEW E Volume: 61 Issue: 5 Pages: 5142-5148 Published: MAY 2000

25. **From phase to lag synchronization in coupled chaotic oscillators** **Times Cited: 991**
By: Rosenblum, MG; Pikovsky, AS; Kurths, J
PHYSICAL REVIEW LETTERS Volume: 78 Issue: 22 Pages: 4193-4196 Published: JUN 2 1997

26. **Phase synchronization of chaotic oscillators** **Times Cited: 1,933**
By: Rosenblum, MG; Pikovsky, AS; Kurths, J
PHYSICAL REVIEW LETTERS Volume: 76 Issue: 11 Pages: 1804-1807 Published: MAR 11 1996

27. **Phase synchronization in temperature and precipitation records** **Times Cited: 39**
By: Rybski, D; Havlin, S; Bunde, A
PHYSICA A-STATISTICAL MECHANICS AND ITS APPLICATIONS Volume: 320 Pages: 601-610 Article Number: PII S0378-4371(02)01509-1 Published: MAR 15 2003

28. Title: [not available] **Times Cited: 1**
By: SCHAFER C
NATURE Volume: 392 Pages: 153 Published: 2000

29. Title: [not available] **Times Cited: 213**
By: Shannon, C.; Weaver, W.
The Mathematical Theory of Information Published: 1949
Publisher: University of Illinois Press.

30. **Reversible transitions between synchronization states of the cardiorespiratory system** **Times Cited: 119**
By: Stefanovska, A; Haken, H; McClintock, PVE; et al.
PHYSICAL REVIEW LETTERS Volume: 85 Issue: 22 Pages: 4831-4834 Published: NOV 27 2000

Showing 30 of 32 **View All in Cited References page**

Eur. Phys. J. B **56**, 157–166 (2007)
DOI: 10.1140/epjb/e2007-00098-2

THE EUROPEAN PHYSICAL JOURNAL B

Quantitative relations between corruption and economic factors

Jia Shao[1,a], Plamen Ch. Ivanov[1,2], Boris Podobnik[1,3,4], and H. Eugene Stanley[1]

[1] Center for Polymer Studies and Department of Physics, Boston University, MA 02215, Boston, USA
[2] Institute of Solid State Physics, Bulgarian Academy of Sciences, 1784 Sofia, Bulgaria
[3] Zagreb School of Economics and Management, Zagreb, Croatia
[4] Faculty of Civil Engineering, University of Rijeka, Croatia

Received 21 December 2006 / Received in final form 6 March 2007
Published online 12 April 2007 –

Abstract. We report quantitative relations between corruption level and economic factors, such as country wealth and foreign investment per capita, which are characterized by a power law spanning multiple scales of wealth and investment per capita. These relations hold for diverse countries, and also remain stable over different time periods. We also observe a negative correlation between level of corruption and long-term economic growth. We find similar results for two independent indices of corruption, suggesting that the relation between corruption and wealth does not depend on the specific measure of corruption. The functional relations we report have implications when assessing the relative level of corruption for two countries with comparable wealth, and for quantifying the impact of corruption on economic growth and foreign investment.

PACS. 89.90.+n Other topics in areas of applied and interdisciplinary physics – 05.45.Tp Time series analysis – 05.40.Fb Random walks and Levy flights

1 Introduction

Corruption influences important aspects of social and economic life. The level of corruption in a given country is widely believed to be an important factor to consider when projecting economic growth, estimating the effectiveness of the government administration, making decisions for strategic investments, and forming international policies. The relation between corruption level and key parameters of economic performance is largely qualitative [1–8]. Corruption has become increasingly important with the globalization of the international economic and political relations between countries, which has led various governmental and non-governmental organizations to search for adequate measures to quantify levels of corruption [1,2,9–12].

Systematic studies of corruption have been hampered because of the complexity and secretive nature of corruption, making it difficult to quantify. There have been concerted efforts to introduce quantitative measures suitable for describing levels of corruption across diverse countries [13–15]. However, a specific functional dependence between quantitative measures of corruption and economic performance has not been established.

Previous studies have suggested a negative association between corruption level and country wealth [1–3]. There is active debate concerning the relation between corruption level and economic growth [16,17]. Some earlier studies suggest that corruption may help the most efficient firms bypass bureaucratic obstacles and rigid laws [4,5] leading to a positive effect on economic growth, while more recent works do not find a significant negative dependence between corruption and growth [1,2]. Further, studies of net flow of foreign investment report conflicting results. Some studies find no significant correlation between inward foreign investment and corruption level in host countries [6,7], while others indicate a negative association between corruption and foreign investments [2,8]. This debate reflects the inherent complexity of the problem as countries in the world vary dramatically in their social and economic development [18]. Thus, an open question remains whether there is a general functional relation between corruption level and key aspects of the economic performance of different countries.

We develop and test the hypothesis that there may be a power-law dependence between corruption level and economic performance which holds across diverse countries regardless of differences in specific country characteristics such as country wealth (defined in our paper as gross domestic product per capita) or foreign direct investment. Recent studies show that diverse social and economic systems exhibit scale invariant behavior — e.g.,

[a] To whom correspondence may be addressed:
e-mail: jiashao@bu.edu or e-mail: plamen@buphy.bu.edu

size ranking and growth of firms, universities, urban centers, countries and even people's personal fortunes follow a power law over a broad range of scales [19–26]. Since countries in the world greatly differ in their wealth and foreign investments, we test the possibility that there may be an underlying organization, such that the cross-country relations between corruption level and country wealth, and corruption level and foreign investments exhibit a significant negative correlation characterized by scale-invariant properties over multiple scales, and thus they can be described by power laws. Specifically, we test if this scale-invariant behavior remains stable over different time periods, as well as its validity for different subgroups of countries. Finally, we demonstrate a strong correlation between corruption level and past long-term economic growth.

2 Data and methods

We analyze the Corruption Perceptions Index (CPI) [14,27] introduced by *Transparency International* [14], a global civil organization supported by a wide network of government agencies, developmental organizations, foundations, public institutions, the private sector, and individuals. The CPI is a composite index based on independent surveys of business people and on assessments of corruption in different countries provided by more than ten independent institutions around the world, including the *World Economic Forum*, *United Nations Economic Commission for Africa*, the *Economist Intelligence Unit*, the *International Institute for Management Development* [27]. The CPI spans 10-year period 1996–2005. The different surveys and assessments use diverse sampling frames and different methodologies. Some of the institutions consult a panel of experts to assess the level of corruption, while others, such as the *International Institute for Management Development* and the *Political and Economic Risk Consultancy*, turn to elite businessmen and businesswomen from different industries. Further, certain institutions gather information about the perceptions of corruption from *residents* with respect to the performance of their home countries, while other institutions survey the perceptions of *non-residents* in regard to foreign countries or specifically in regard to neighboring countries. All sources employ a homogeneous definition of corruption as the misuse of public power for private benefit, such as bribing public officials, kickbacks in public procurement, or embezzlement of public funds. Each of these sources also assesses the "extent" of corruption among public officials and politicians in different countries. Transparency International uses non-parametric statistics for standardizing the data and for determining the precision of the scores [27]. While there is a certain subjectivity in people's perceptions of corruption, the large number of independent surveys and assessments based on different methodologies averages out most of the bias. The CPI ranges from 0 (highly corrupt) to 10 (highly transparent).

We also analyze a different measure of corruption, the Control of Corruption Index (CCI) [9,15] provided by the *World Bank* [15]. The CCI ranges from –2.5 to 2.5, with positive numbers indicating low levels of corruption. As a measure of country wealth, we use the *gdp*, defined to be the annual nominal gross domestic product per capita in current prices in US dollars, provided by the *International Monetary Fund* (IMF) [28] over the 26-year period 1980–2005. As a measure of foreign direct investment we use annual data from the *Bureau of Economic Analysis* [29] of the United States (US) government, which represents the direct investment received by different countries from the US over the period 2000–2004. These data are appropriate for our study since (i) the US has been the dominant source of foreign investment in the past decades, and (ii) the 1977 Foreign Corrupt Practices Act (FCPA) [30] holds US companies legally liable for bribing foreign government officials, which makes the US a source country which penalizes its multinational companies for corruption practices [8].

3 Results and discussion

3.1 Relation between corruption level and country wealth

To test if there is a common functional dependence between corruption level and country wealth, we plot the CPI versus *gdp* for different countries (Figs. 1a–e). We find a positive correlation between CPI and country wealth, which can be well approximated by a power law

$$CPI \sim (gdp)^{\mu}, \tag{1}$$

where $\mu > 0$, indicating that richer countries are less corrupt. Most countries fall close to the power-law fitting line shown in Figure 1, consistent with specific functional relation between corruption and country wealth even for countries characterized by levels of wealth ranging over a factor of 10^3. This finding in equation (1) indicates that the relative corruption level between two countries should be considered not only in terms of *CPI* values but also in the context of country wealth. For example, two countries with a large difference in their *gdp* on average will not have the same level of corruption, as our results quantify the degree to which poorer countries with lower *gdp* have higher levels of corruption.

The quantitative relation between *CPI* and *gdp* for all countries in the world — represented by the power-law fitting curves in Figure 1 — indicates where is the "expected" level of corruption for a given level of wealth. A country above (or below) the fitting line is less (or more) corrupt than expected for its level of wealth. For example, comparing the relative corruption level of two countries with similar *gdp* such as Bulgaria and Romania, one can assess that Bulgaria is less corrupt than Romania (Fig. 3). Depending whether a specific country is above (e.g., Bulgaria) or below (e.g., Romania) the power-law fit, one can assess if this country is less (or more) corrupt relative to the average level of corruption corresponding to the wealth of this country.

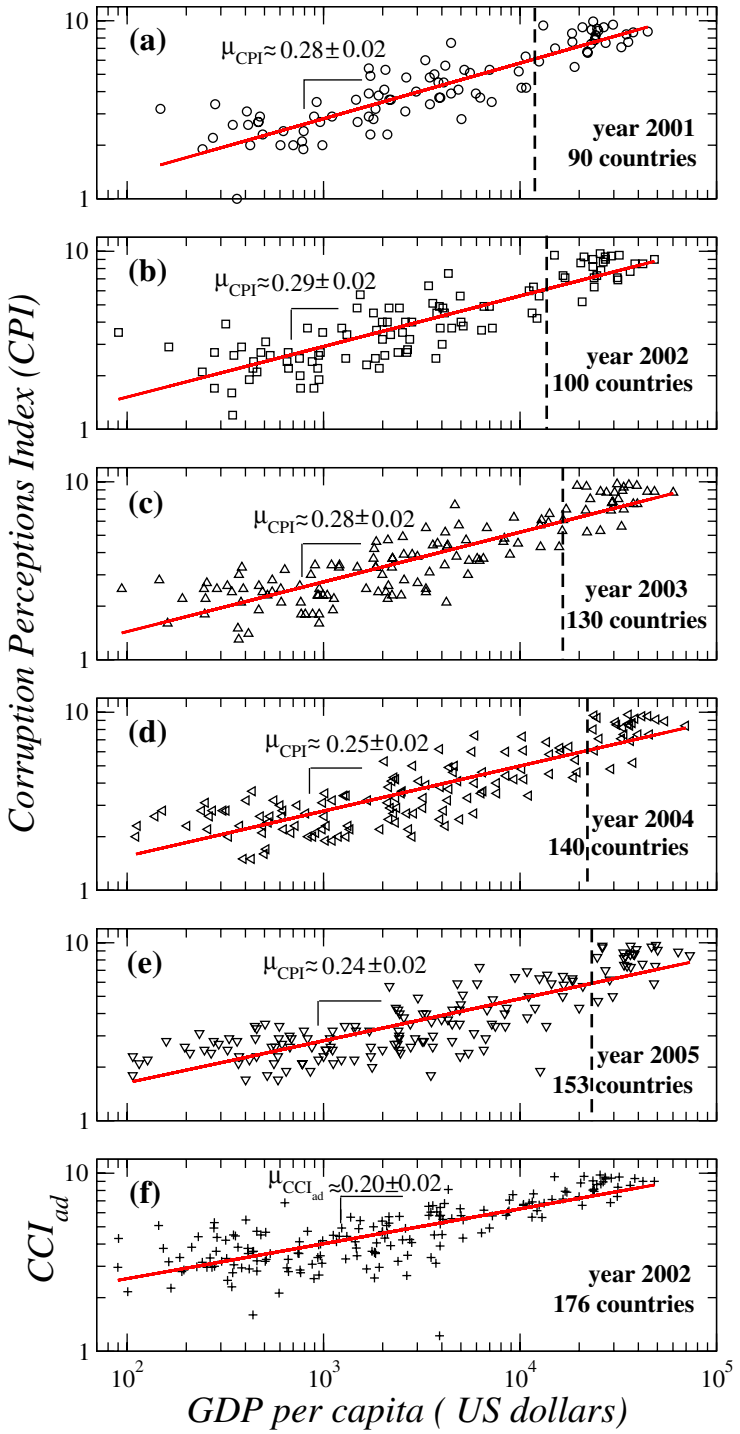

Fig. 1. Log-log plots of the corruption perceptions index (*CPI*) versus *GDP* per capita (*gdp*) indicating a power-law functional dependence. A low value of *CPI* corresponds to a high level of corruption [14]. Data on *gdp* are obtained as current prices in US dollars [28]. (a–e) The power-law functional dependence remains stable over different time periods, and is characterized by similar values of the exponent μ for different years and different number of countries. The power-law fit indicates the expected level of corruption for given country wealth. Note that, comparing two countries with a similar *gdp*, the country placed above the power-law fit is less corrupt than one would expect for its level of wealth, while the country below the power-law curve has a relatively higher level of corruption than one would expect for its wealth. (f) We obtain similar results for the *adjusted* control of corruption index CCI_{ad} [15], which is independent of *CPI*, indicating that the scale-invariant relation between corruption and wealth does not depend on the specific measure of corruption. Vertical dashed lines in the panels separate the top 30 wealthiest countries (see Figs. 5 and 6).

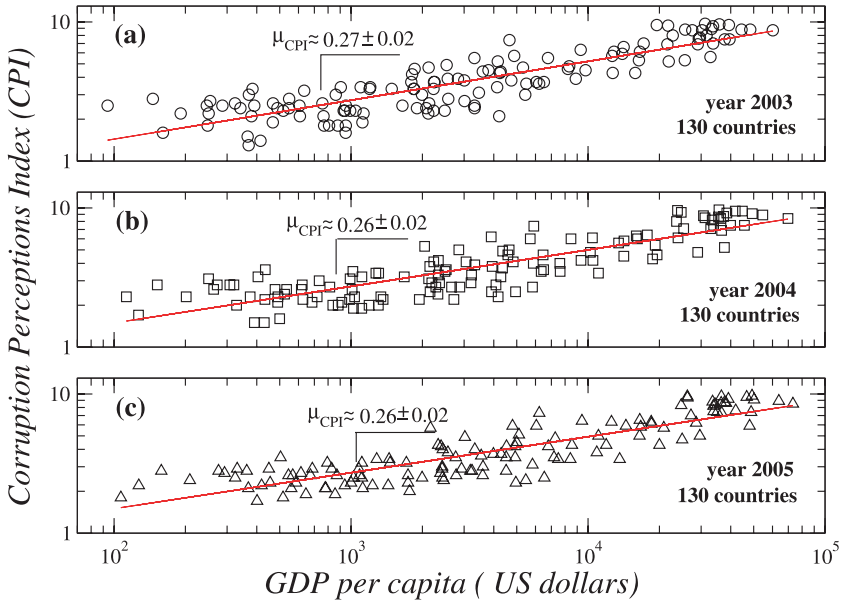

Fig. 2. Log-log plots of the corruption perceptions index (*CPI*) versus *GDP* per capita (*gdp*) for a subset of 130 countries over the period 2003–2005. The same set of countries is presented in each plot, indicating that the power-law exponent μ characterizing the relation between *CPI* and *gdp* remains relatively stable over the considered period. As rich countries have a relatively higher *gdp* growth rate compared to poor countries (see Fig. 9 below), and because *CPI* is defined in a bounded interval, we expect the value of the exponent μ to decrease slightly with time when considering time horizons larger than a decade.

Moreover, the quantitative dependence we find in equation (1) allows us to compare the relative levels of corruption between two countries which belong to two different wealth brackets. Specifically, two countries with a very different *gdp* should not be compared only by the value of their *CPI*, but also by their relative distances from the power-law fitting line which indicates the expected level of corruption. For example, Bulgaria and Slovenia differ significantly in their wealth (Slovenia has ≈5 times higher *gdp*), but both countries are at equal distances above the fitting line, indicating (i) that both countries are less corrupt than the corruption level expected for their corresponding wealth, and (ii) that the relative level of corruption of Slovenia within the group of countries falling in the same *gdp* bracket as Slovenia is similar to the relative corruption level of Bulgaria within the group of countries falling in the same *gdp* bracket as Bulgaria (Fig. 3).

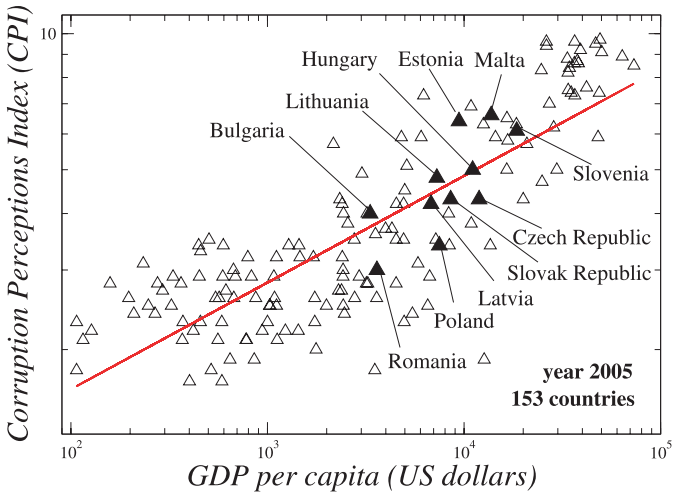

Fig. 3. Same as panel (e) in Figure 1 except we now identify by filled symbols the subset of the 153 countries, which are recently-accepted members of the European Union and candidates. Although this subset varies greatly in wealth and corruption level, data also follow a similar scale-invariant behavior.

To test how robust is the power-law dependence between corruption and country wealth, we analyze groups containing different numbers of countries for the period 2000–2005, and we find that equation (1) holds, with similar values of μ (Figs. 1a–e). Averaging the power-law exponent μ for different years and for different number of countries we find $\overline{\mu} \approx 0.27 \pm \Delta$, where $\Delta = 0.02$ is the standard deviation. For the *CPI* and *gdp* data we find an average correlation coefficient of 0.86. We also note that the inverse relation of *gdp* as a function of *CPI* is characterized by an exponent $\hat{\mu}$ which is not equal to $1/\mu$ as one might expect, since the correlation coefficient of the data fit is less than 1. Next, we analyze data comprising the same set of countries for different years (Fig. 2), and we find that the power-law dependence of equation (1) remains stable in time over periods shorter than a decade, with similar and slightly decreasing values for μ (Figs. 1 and 2). Similar results we obtain also for the period 1996–2000 (not shown in the figures as available data cover much smaller number of countries for that earlier period).

Given the facts that (i) the number of countries we analyze changes from 90 to 153, and (ii) that the time horizon of 5–6 years we consider could be sufficient for significant changes in both corruption level and wealth

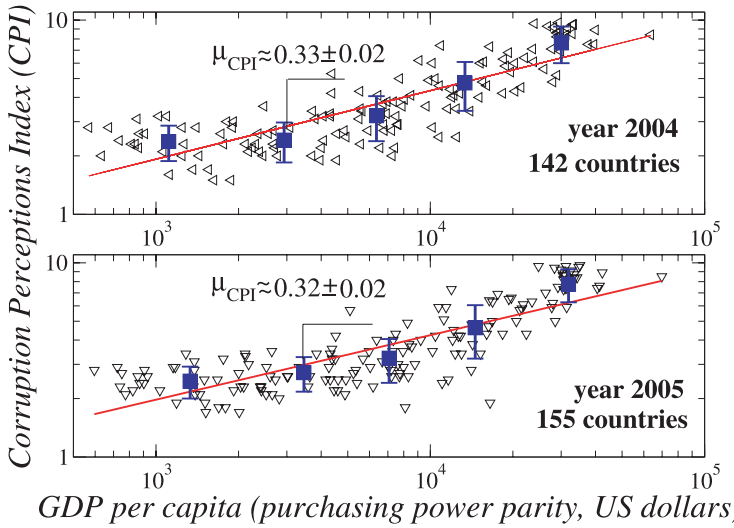

Fig. 4. Log-log plots of the corruption perceptions index (*CPI*) versus *GDP* per capita (*gdp*) for the same years as shown in panels (d) and (e) in Figure 1, indicating a power-law functional dependence similar to Figure 1. Data on *gdp* are obtained based on purchasing power parity in US dollars [28]. A low value of *CPI* corresponds to a high level of corruption [14]. The power-law relation between *CPI* and *gdp* remains stable also for constant prices across different years and different number of countries, and is characterized by a similar value of the exponent μ as for current prices. We note that the slightly higher value of μ_{CPI} observed here compared with Figures 1 and 2 is due to the slight reduction in the difference between wealthy and poor countries when *gdp* is measured based on purchasing power parity. The group average and standard deviation of the *CPI* for five subgroups of countries for both years are shown with filled squares. The power-law fit across all countries indicates the expected level of corruption for a given range of country wealth.

(e.g., the case of Eastern European countries), our finding of a power-law relationship in equation (1) is consistent with a universal dependence between *gdp* and *CPI* across diverse countries. We note that the power-law relation in equation (1) holds when *gdp* is calculated both as current prices in US dollars (Figs. 1 and 2), as well as the value based on purchasing power parity (Fig. 4). Further, equation (1) implies that lowering the corruption level of a country would lead to an increase in its *gdp* and vice versa — e.g., for a country with *gdp* $\approx$ \$4000 an increase in CPI of 0.25 units would lead to increase in the *gdp* of approximately \$700 (Figs. 1 and 2).

To confirm that our findings do not depend on the specific choice of the measure of corruption, we repeat our analysis for a different index, the CCI [9,15]. As the CCI is defined in the interval [–2.5, 2.5] we use a linear transformation to obtain the *adjusted* CCI, $CCI_{ad} \equiv 2\times(CCI+2.5)$, so that both CCI_{ad} and *CPI* are defined in the same interval from 0 to 10. We find that CCI_{ad} also exhibits a power-law behavior as a function of *gdp* with a similar value of the power-law exponent μ as obtained for *CPI* (Fig. 1f). Thus, the specific interval in which the corruption index is defined does not affect the nature of our findings. We note that there is no artificially imposed scale on the values of the *CPI* or CCI index for different countries. While the upper and lower bounds for the *CPI* or CCI index are indeed pre-determined, the intrinsic relative relation between the index values for different countries is inherent to the data. There is no logarithmic scale artificially imposed on the index values of each country (see details on the *CPI* and CCI methodology in [14,15,27]). The fact that we obtain practically identical results (power-law dependence with similar values of the exponent μ) for two independent indices *CPI* and CCI, which are provided by different institutions and are calculated using different methodologies, indicates that the quantitative relation of equation (1) is not an artifact of subjective evaluation of corruption. In summary, our empirical results indicate that the power-law relation between corruption and *gdp* across countries (i) does not depend on the specific subset of chosen countries (provided they span a broad range of *gdp*), (ii) does not depend on the specific measure of corruption (*CPI* and CCI), and (iii) does not change significantly over time horizons shorter than a decade.

3.2 Corruption level and country wealth rank curves

We next rank countries by their *gdp* and by their *CPI*. We find that *gdp* versus rank exhibits an exponential behavior for countries with rank larger than 30, and a pronounced crossover to a power-law behavior for the wealthiest 30 countries (Fig. 5). We further find that the shape of *gdp* versus rank curve remains unchanged for different years, and that increasing the number of countries we consider only extends the range of the exponential tail. Our findings for the shape of the *gdp* versus rank curve differ from earlier reports [31,32]. We find that the *CPI* versus rank curve exhibits a behavior similar to that of the *gdp* versus rank curve, with a crossover from a power law to an exponential tail for countries with rank larger than 30 (Fig. 5 and Fig. 6). The shape of the *CPI* versus rank curve also remains unchanged when we repeat the analysis for different years (Fig. 6). We find that the ranking of countries based on *gdp* practically matches the ranking based

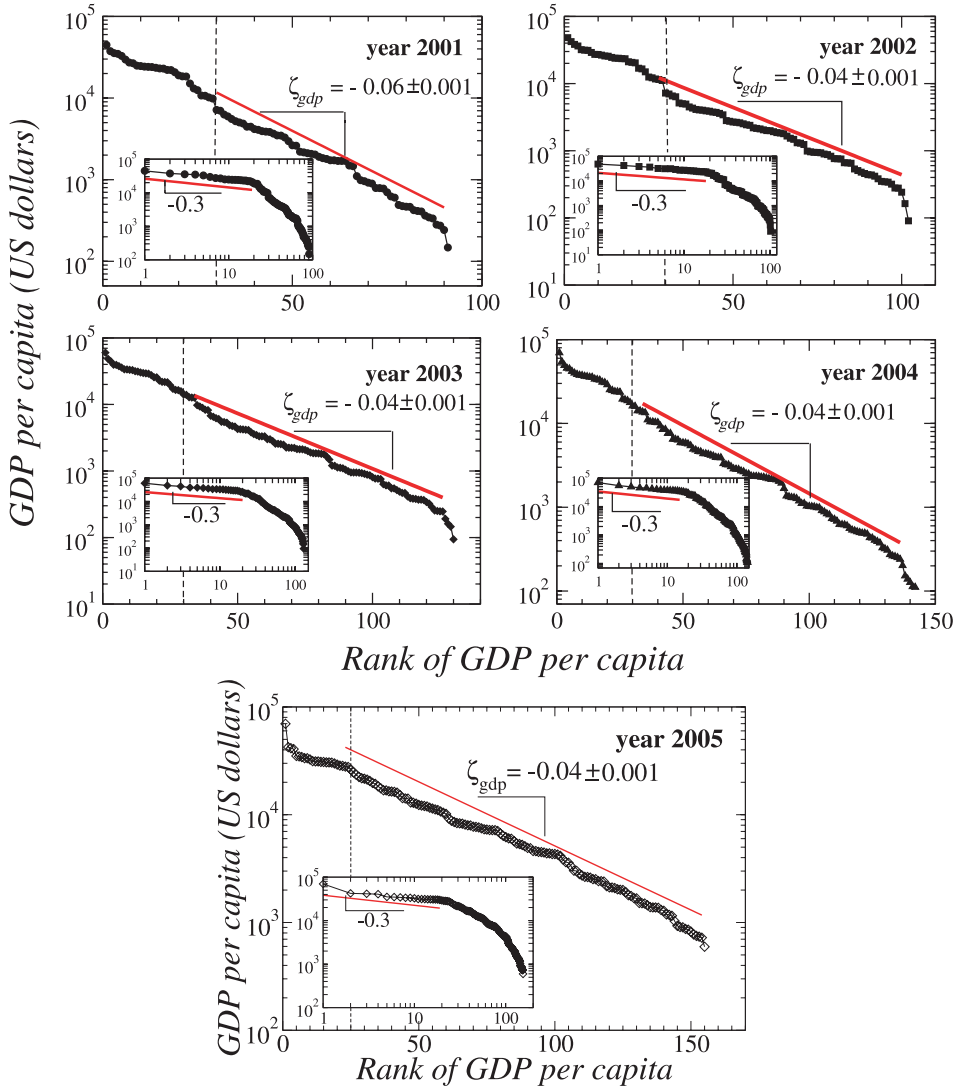

Fig. 5. Zipf plots ranking in decreasing order the *GDP* per capita (*gdp*) for the same groups of countries and for the same years as shown in Figure 1. Data on *GDP* per capita are obtained from the International Monetary Fund as current prices in US dollars [28]. Fitting lines indicate exponential behavior for the *GDP* per capita for countries below rank 30 (vertical dashed line, shown also in Figure 1), characterized by the exponential decay constant ζ_{gdp}. Log-log plots of the ranking curves (shown in the insets) indicate a crossover from an exponential to a power-law behaviour for the top 30 wealthiest countries. We note that the top 30 wealthiest countries cluster above the fitting curves in Figures 1, 2 and 4.

on the *CPI* index. This is evidence of a strong and positive correlation between the ranking of wealth and the ranking of corruption. Since the *gdp* rank is an unambiguous result of an *objective* quantitative measure, the evidence of a strong correlation of the *CPI* rank with the *gdp* rank we observe in Figures 5 and 6 indicates that the *CPI* values are *not subjective*, and that our finding of a power-law relation between *CPI* and *gdp* in Figures 1 and 2 is not an artifact of an arbitrary scale imposed on the *CPI* or on the CCI. Further, we compare the values of the decay parameters ζ_{CPI} and ζ_{gdp} characterizing the exponential behavior of the *CPI* and *gdp* rank curves,

$$CPI \sim \exp(\zeta_{CPI} \cdot R_{CPI}), \tag{2}$$

and

$$gdp \sim \exp(\zeta_{gdp} \cdot R_{gdp}), \tag{3}$$

where R_{CPI} and R_{gdp} is the rank order of *CPI* and *gdp* respectively.

We find that for each year the ratio ζ_{CPI}/ζ_{gdp} reproduces the value of the power-law exponent μ defined in equation (1) for the same year — an insightful result since it would hold only when R_{CPI} is similar to R_{gdp}. Indeed, only when $R_{CPI} \approx R_{gdp}$ we obtain from equation (2) and equation (3) the relation between $\log(CPI)$ and $\log(gdp)$,

$$log(CPI) \approx (\zeta_{CPI}/\zeta_{gdp}) \cdot log(gdp). \tag{4}$$

Combining equations (1) and (4), we see that

$$\mu = \zeta_{CPI}/\zeta_{gdp}. \tag{5}$$

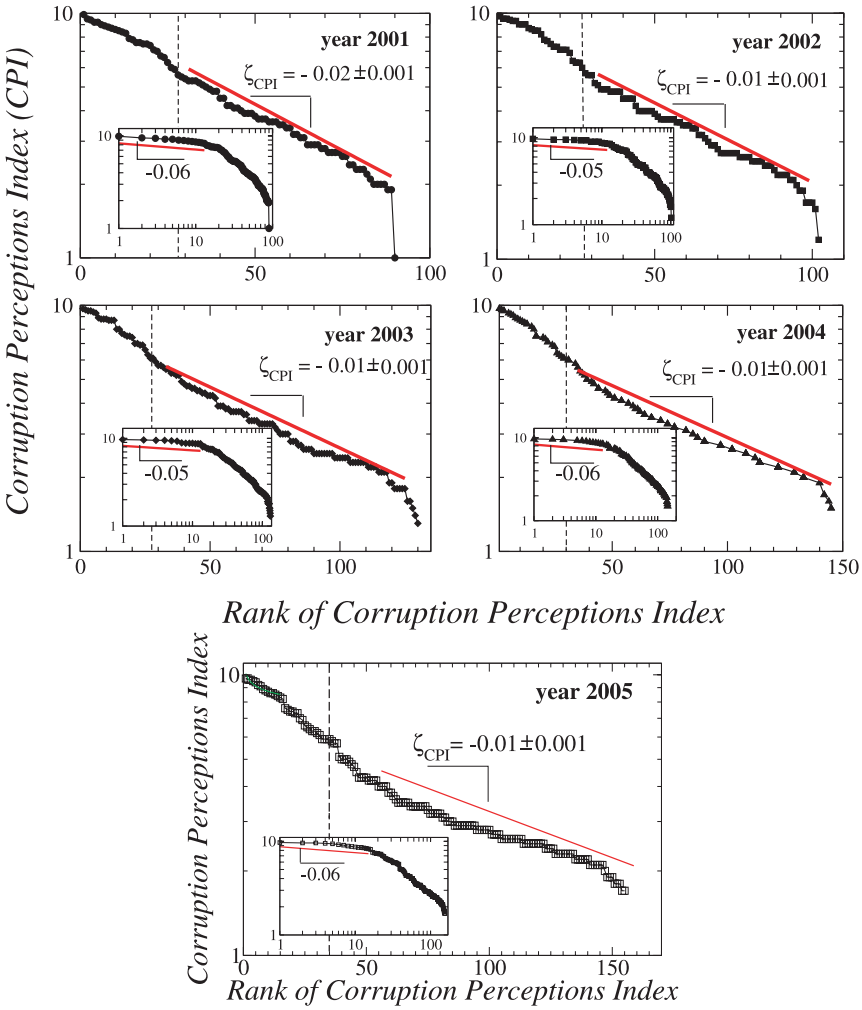

Fig. 6. Zipf plots ranking in decreasing order the *CPI* for the same groups of countries and for the same years as shown in Figures 1 and 5. Fitting lines indicate exponential behavior for the *CPI* for countries below rank 30 (vertical dashed line, shown also in Figs. 1 and 5), characterized by the exponential decay constant ζ_{CPI}. The ratio ζ_{CPI}/ζ_{gdp} consistently reproduces the value of the power-law exponent μ in Figures 1a–d for each corresponding year and each group of countries. This indicates that a necessary condition for the power-law relation between *CPI* and *GDP* per capita is that the *GDP* per capita rank order of countries is similar to the rank order based on CPI. Log-log plots of the ranking curves (shown in the insets) indicate a crossover from an exponential to a power-law behaviour for the top 30 least corrupt countries, similar to the crossover behaviour observed for *gdp* in Figure 5.

Thus, for each year the power-law dependence between *CPI* and *gdp* in equation (1) is directly related to the exponential relations of the *CPI* and *gdp* as a function of the rank shown in equation (2) and equation (3). We note that equation (5) does not hold for the top 30 wealthiest countries, for which there is an enhanced economic interaction in a globalization sense, perhaps leading to similarities in development patterns and to an overall decrease in the *gdp* growth difference between these countries [33,34].

3.3 Relation between corruption level and foreign direct investment

We next investigate how the corruption level relates to foreign direct investment. We consider the amount of inward investment received by different countries from the United States (US). Investments originating from the US are sensitive to corruption, since US legislation holds American investors in other countries liable for corruption practices [30]. We find a strong dependence of the amount of US direct investment in a given country on the corruption level in that country (Fig. 7). Specifically, we find that the functional dependence between US direct investment per capita, I, and the corruption level across countries exhibits scale-invariant behavior characterized by a power law ranging over at least a factor of 10^3 (Fig. 7)

$$CPI \sim I^{\lambda}. \tag{6}$$

We find that less corrupt countries have received more US investment per capita, and that equation (6) also holds for different years. In particular, we find that groups of countries from different continents, which differ both in *gdp* and in average *CPI*, are characterized by different values

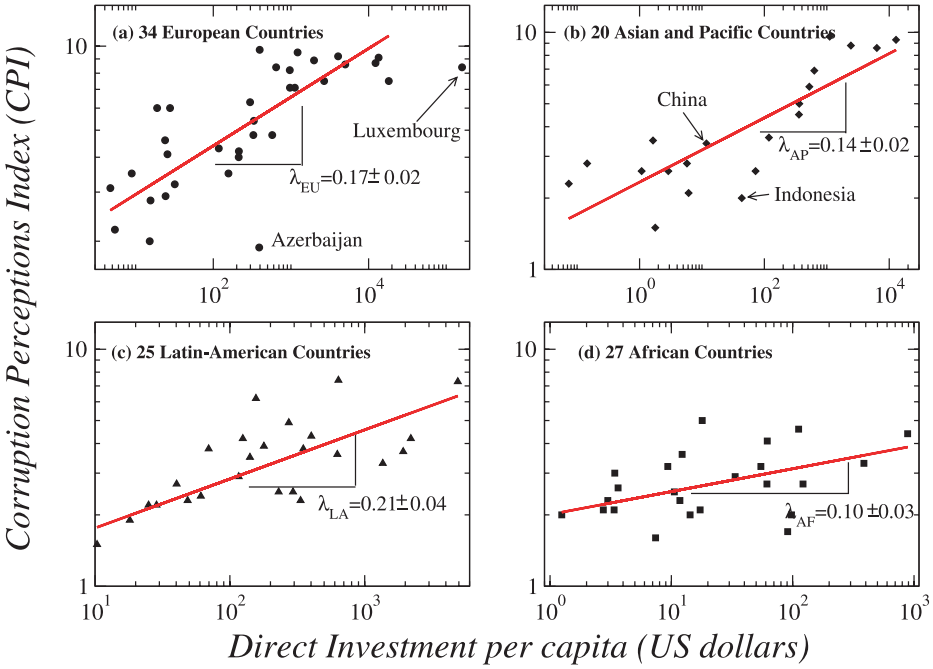

Fig. 7. Log-log plots of the *CPI* versus the amount of direct investment on a historical-cost basis from the United States received by different countries for the year 2004 [29]. We observe strong positive correlation between level of investment per capita and level of corruption — countries with high *CPI* receive also larger investment. Shown are (a) 34 European countries, (b) 20 Asian-Pacific countries, (c) 25 Latin-American countries and (d) 27 African countries. Note the striking difference between the typical values of direct investment per capita when comparing, say, European countries and African countries, with typical values of $CPI \approx 5$ and $CPI \approx 2.5$ respectively. The correlation coefficients of the fits in (a–d) are 0.74, 0.83, 0.69 and 0.37 respectively. Note that although China receives a huge net inflow of US investment each year, the per capita investment from the US is not very high, and is quite similar to the US per capita investment for countries with a *CPI* value similar to that of China.

of λ (Fig. 7). We obtain similar results when repeating our analysis for the CCI, suggesting that the power-law relation in equation (6) between corruption level and foreign direct investment per capita does not depend on the specific measure of corruption. We also note that the 1977 Foreign Corrupt Practices Act [30] only precludes American firms from entering corruption deals, but does not dictate in which country and how much money the American firms should invest. Therefore, the statistical regularities we find in Figure 7 cannot arise from legislatory measures against foreign corruption.

3.4 Relation between corruption level and growth rate

Finally, we investigate whether there is a relation between corruption level and long-term growth rate. Since the *CPI* reflects the quality of governing and administration in a given country, which traditionally requires considerable time to change, we hypothesize that there may be relation between the current corruption level of a country and its growth rate over a wide range of time horizons. To test this hypothesis we estimate the long-term growth rate for each country as the slope of the least square fit to the plot of $\log(gdp)$ versus year over the past several decades, where the *gdp* is taken as constant prices in national currency (Fig. 8). We divide all countries into four groups according to the World Bank classification based on *gdp* [35]. We find a strong positive dependence between country group average of *CPI* and the group average long-term growth

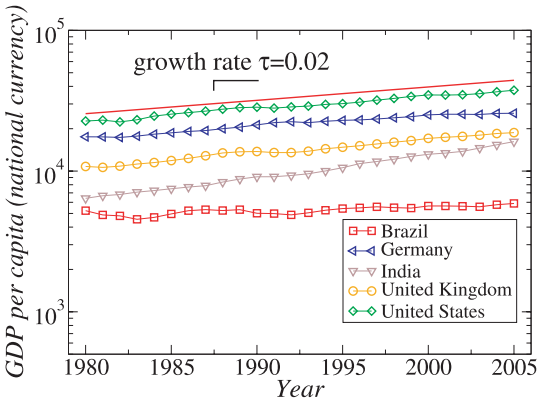

Fig. 8. Long-term growth rate of the *GDP* per capita (*gdp*) measured as constant prices in national currency [28] over the period 1980 to 2005. Separate curves represent countries of different wealth and corruption level from different continents. All countries exhibit exponential growth characterized by average long-term growth rate τ, estimated for each country as the slope of the least square fit to the plot of $\log(gdp)$ versus year over the period 1980 to 2005. The fitting line indicates the long-term growth rate τ of the United States over the period 1980 to 2005.

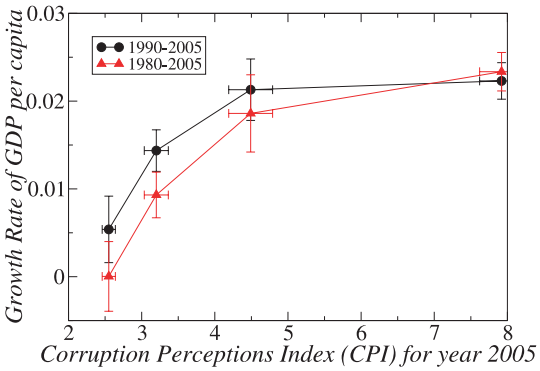

Fig. 9. Relation between the *CPI* for the year 2005 [14] and the long-term growth rate of *GDP* per capita (*gdp*) measured as constant prices in national currency [28]. Each curve represents 120 countries divided into 4 groups based on their level of wealth according to the World Bank's classification [35]. Excluded are countries with population less than two million and countries for which the *GDP* per capita records extend back fewer than 15 years starting from 2005. The long-term growth rate is estimated over the periods 1980–2005 and 1990–2005. Symbols represent the group average value of *CPI* and long-term growth rate of *GDP* per capita. The error bars represent the group standard error. The plot indicates that the corruption level of a country at present is strongly related to the past long-term growth rate of the *GDP* per capita. Countries which are presently more corrupt exhibit on average negligible or even negative growth rates. In contrast, less corrupt countries exhibit higher growth rates. This strong correlation between corruption level and growth rate of *GDP* per capita remains valid for a broad range of past time horizons.

rate, showing that less corrupt countries exhibit significant economic growth while more corrupt countries display insignificant growth rates (or even display negative growth rates) (Fig. 9). Repeating our analysis for different time horizons (1990–2005;1980–2005) we find similar relations between the *CPI* and the long-term growth, indicating a link between corruption and economic growth.

In summary, the functional relations we report here can have implications when determining the relative level of corruption between countries, and for quantifying the impact of corruption when planning foreign investments and economic growth. These quantitative relations may further facilitate current studies on spread of corruption across social networks [36], the emergence of endogenous transitions from one level of corruption to another through cascades of agent-based micro-level interactions [37,38], as well as when considering corruption in the context of certain cultural norms [39].

We thank F. Liljeros for valuable suggestions and discussions, and we thank D. Schmitt and F. Pammolli for helpful comments. We also thank Merck Foundation, NSF, and NIH for financial support.

References

1. J. Svensson, J. Economic Perspectives **19**, 19 (2005)
2. P. Mauro, Quarterly Journal of Economics **110**, 681 (1995)
3. V. Tanzi, H.R. Davoodi, *Corruption, Growth, and Public Finance*, Working Paper of the International Monetary Fund, Fiscal Affairs Department (2000)
4. N.H. Leff, American Behavioral Scientist **82**, 337 (1964)
5. S.P. Huntington, *Political Order in Changing Societies* (Yale University Press, New Haven, 1968)
6. D. Wheeler, A. Mody, J. International Economics **33**, 57 (1992)
7. J. Hines, *Forbidden Payment: Foreign Bribery and American Business After 1977*, NBER Working Paper 5266, (1995)
8. S.J. Wei, The Review of Economics and Statistics **82**, 1 (2000)
9. D. Kaufmann et al., *Governance Matters III: Governance Indicators for 1996–2002*, World Bank Policy Research Working Paper, 3106 (2003)
10. S. Knack, P. Keefer, Economics and Politics **7**, 207 (1995)
11. D. Treisman, J. Public Economics **76**, 399 (2000)
12. A.K. Jain, J. Economic Surveys **15**, 71121 (2001)
13. *International Country Risk Guide's Corruption Indicator*, published by Political Risk Services, `http://www.prsgroup.com/countrydata/countrydata.html`
14. *The Corruption Perceptions Index (CPI)*, is published by Transparency International, `http://www.transparency.org/policy_research/surveys_indices/cpi`
15. *The Control of Corruption Index (CCI)*, published by the World Bank, `http://info.worldbank.org/governance/kkz2002/tables.asp`
16. P. Bardhan, J. Economic Literature **35**, 1320 (1997)
17. J.G. Lambsdorff, *Corruption in Empirical Research - A Review*, Transparency International Working Paper, (1999)
18. F. Schneider, D.H. Enste, J. Economic Literature **38**, 77 (2000)
19. H.A. Makse et al. Nature **377**, 608 (1995)
20. R.L. Axtell, Science **293**, 1818 (2001)
21. M.H.R. Stanley et al., Nature **379**, 804 (1996)
22. Y. Lee et al., Phys. Rev. Lett. **81**, 3275 (1998)
23. D. Fu et al., Proc. Natl. Acad. Sci. **102**, 18801 (2005)
24. V. Plerou et al., Nature **400**, 433 (1999)
25. P.Ch. Ivanov et al., Phys. Rev. E **69**, 056107 (2004)
26. M.E.J. Newman, Contemporary Physics **46**, 323 (2005)
27. For details on the methodology in computing the *CPI* see *The Methodology of the 2005 Corruption Perceptions Index*, `http://www.transparency.org/policy_research/surveys_indices/cpi/2005/methodology`
28. GDP per capita data as current prices in US dollars and as constant prices in national currency are provided by the International Monetary Fund, WORLD ECONOMIC OUTLOOK Database, September 2005, `http://www.imf.org/external/pubs/ft/weo/2005/02/data/index.htm`
29. US Direct Investment Position data are obtained from `http://www.bea.gov/bea/di/usdctry/longctry.htm`
30. Information regarding the Foreign Corrupt Practices Act (FCPA) of 1977 is available at `http://www.usdoj.gov/criminal/fraud/fcpa.html`

31. C. Di Guilmi et al. Economics Bulletin **15**, 1 (2003)
32. R. Iwahashi, T. Machikita, Economics Bulletin **6**, 1 (2004)
33. J, Miskiewicz, M. Ausloos, Acta Physica Polonica B **36**, 2477
34. J, Miskiewicz, M. Ausloos, Int. J. Modern Phys. C **17**, 317 (2006)
35. Information regarding the classification of countries based on their gross domestic product per capita is provided by the World Bank, at: `http://www.worldbank.org`
36. Ph. Blanchard et al., e-print `arXiv.org/abs/physics/0505031`, (2005)
37. R. Hammond, *Endogenous Transition Dynamics in Corruption: An Agent-Based Computer Model*, CSED Working Paper No. 19, (2000)
38. H. Situngkir, *Money-Scape: A Generic Agent-Bases Model of Corruption*, Working Paper WPD2003, Bandung Fe Institute Press (2003)
39. R. Fisman, E. Miguel, *Cultures of Corruption: Evidence from Diplomatic Parking Tickets*, NBER working paper No. 2312 (2006)

Quantitative relations between corruption and economic factors

By: Shao, J (Shao, Jia); Ivanov, PC (Ivanov, Plamen Ch.); Podobnik, B (Podobnik, Boris); Stanley, HE (Stanley, H. Eugene)

View ResearcherID and ORCID

EUROPEAN PHYSICAL JOURNAL B
Volume: 56 **Issue:** 2 **Pages:** 157-166
DOI: 10.1140/epjb/e2007-00098-2
Published: MAR 2007
Document Type: Article
View Journal Impact

Abstract

We report quantitative relations between corruption level and economic factors, such as country wealth and foreign investment per capita, which are characterized by a power law spanning multiple scales of wealth and investment per capita. These relations hold for diverse countries, and also remain stable over different time periods. We also observe a negative correlation between level of corruption and long-term economic growth. We find similar results for two independent indices of corruption, suggesting that the relation between corruption and wealth does not depend on the specific measure of corruption. The functional relations we report have implications when assessing the relative level of corruption for two countries with comparable wealth, and for quantifying the impact of corruption on economic growth and foreign investment.

Keywords

KeyWords Plus: GROWTH DYNAMICS; FIRMS

Author Information

Reprint Address: Shao, J (reprint author)

+ Boston Univ, Ctr Polymer Studies, Boston, MA 02215 USA.

Addresses:

+ [1] Boston Univ, Ctr Polymer Studies, Boston, MA 02215 USA
+ [2] Boston Univ, Dept Phys, Boston, MA 02215 USA
+ [3] Bulgarian Acad Sci, Inst Solid State Phys, BU-1784 Sofia, Bulgaria
[4] Zagreb Sch Econ & Management, Zagreb, Croatia
+ [5] Univ Rijeka, Fac Civil Engn, Rijeka, Croatia

E-mail Addresses: jiashao@bu.edu; plamen@buphy.bu.edu

Publisher

SPRINGER, 233 SPRING STREET, NEW YORK, NY 10013 USA

Journal Information

Impact Factor: Journal Citation Reports

Categories / Classification

Research Areas: Physics

Web of Science Categories: Physics, Condensed Matter

If you would like to improve the quality of the data in this record, please suggest a correction.

See more data fields

82 of 127

Cited References: 31

Showing 30 of 31 **View All in Cited References page** *(from Web of Science Core Collection)*

1. **Zipf distribution of US firm sizes** **Times Cited: 627**
   By: Axtell, RL
   SCIENCE Volume: 293 Issue: 5536 Pages: 1818-1820 Published: SEP 7 2001

2. **Corruption and development: A review of issues** **Times Cited: 765**
   By: Bardhan, P
   JOURNAL OF ECONOMIC LITERATURE Volume: 35 Issue: 3 Pages: 1320-1346 Published: SEP 1997

3. Title: [not available] **Times Cited: 1**
   By: BLANCHARD P
   ARXIVORGABSPHYSICS05 Published: 2005

4. **Power law scaling in the world income distribution** **Times Cited: 16**
   By: Di Guilmi, C.; Gaffeo, E.; Gallegati, M.
   Econ. Bull Volume: 15 Pages: 1-7 Published: 2003

5. Title: [not available] **Times Cited: 1**
   By: FISMAN R
   2312 NBER Published: 2006

6. **The growth of business firms: Theoretical framework and empirical evidence** **Times Cited: 95**
   By: Fu, DF; Pammolli, F; Buldyrev, SV; et al.
   PROCEEDINGS OF THE NATIONAL ACADEMY OF SCIENCES OF THE UNITED STATES OF AMERICA Volume: 102 Issue: 52 Pages: 18801-18806 Published: DEC 27 2005

7. Title: [not available] **Times Cited: 5**
   By: HAMMOND R
   ENDOGENOUS TRANSITIO Published: 2000

8. **Forbidden Payment: Foreign Bribery and American Business After 1977** **Times Cited: 54**
   By: Hines, James R.
   NBER Working Paper 5266 Published: 1995
   Publisher: National Bureau of Economic Research, Cambridge, MA

9. Title: [not available] **Times Cited: 3,171**
   By: Huntington, Samuel P.
   Political order in changing societies Published: 1968
   Publisher: Yale Univeristy Press, New Haven

10. **Common scaling patterns in intertrade times of US stocks** **Times Cited: 124**

Patterns of spiral wave attenuation by low-frequency periodic planar fronts

Miguel A. de la Casa and , F. Javier de la Rubia, and Plamen Ch. Ivanov

Citation: Chaos **17**, 015109 (2007); doi: 10.1063/1.2404640
View online: http://dx.doi.org/10.1063/1.2404640
View Table of Contents: http://aip.scitation.org/toc/cha/17/1
Published by the American Institute of Physics

Patterns of spiral wave attenuation by low-frequency periodic planar fronts

Miguel A. de la Casa and F. Javier de la Rubia
Departamento de Física Fundamental, UNED, 28040 Madrid, Spain

Plamen Ch. Ivanov[a)]
Center for Polymer Studies and Department of Physics, Boston University, Boston, Massachusetts 02215 and Institute of Solid State Physics, Bulgarian Academy of Sciences, 1784 Sofia, Bulgaria

(Received 17 August 2006; accepted 13 November 2006; published online 30 March 2007)

There is evidence that spiral waves and their breakup underlie mechanisms related to a wide spectrum of phenomena ranging from spatially extended chemical reactions to fatal cardiac arrhythmias [A. T. Winfree, *The Geometry of Biological Time* (Springer-Verlag, New York, 2001); J. Schutze, O. Steinbock, and S. C. Muller, Nature **356**, 45 (1992); S. Sawai, P. A. Thomason, and E. C. Cox, Nature **433**, 323 (2005); L. Glass and M. C. Mackey, *From Clocks to Chaos: The Rhythms of Life* (Princeton University Press, Princeton, 1988); R. A. Gray *et al.*, Science **270**, 1222 (1995); F. X. Witkowski *et al.*, Nature **392**, 78 (1998)]. Once initiated, spiral waves cannot be suppressed by periodic planar fronts, since the domains of the spiral waves grow at the expense of the fronts [A. N. Zaikin and A. M. Zhabotinsky, Nature **225**, 535 (1970); A. T. Stamp, G. V. Osipov, and J. J. Collins, Chaos **12**, 931 (2002); I. Aranson, H. Levine, and L. Tsimring, Phys. Rev. Lett. **76**, 1170 (1996); K. J. Lee, Phys. Rev. Lett. **79**, 2907 (1997); F. Xie, Z. Qu, J. N. Weiss, and A. Garfinkel, Phys. Rev. E **59**, 2203 (1999)]. Here, we show that introducing periodic planar waves with long excitation duration and a period longer than the rotational period of the spiral can lead to spiral attenuation. The attenuation is not due to spiral drift and occurs periodically over cycles of several fronts, forming a variety of complex spatiotemporal patterns, which fall into two distinct general classes. Further, we find that these attenuation patterns only occur at specific phases of the descending fronts relative to the rotational phase of the spiral. We demonstrate these dynamics of phase-dependent spiral attenuation by performing numerical simulations of wave propagation in the excitable medium of myocardial cells. The effect of phase-dependent spiral attenuation we observe can lead to a general approach to spiral control in physical and biological systems with relevance for medical applications.
 [DOI: 10.1063/1.2404640]

The dynamics of waves in excitable media[1–11] have been studied in physical, chemical, and biological systems under a variety of conditions including noise and inhomogeneities in the medium[12–14] and mechanical deformation.[15] Of particular interest is the problem of nonlinear wave interaction in the excitable medium of the heart muscle, as loss of wave stability and spiral wave breakup lead to spatiotemporal patterns associated with adverse cardiac events such as ventricular fibrillation and sudden cardiac death.[5,6,16,17] While different approaches to prevent spiral breakup have been proposed,[18–22] it is widely accepted that stable spiral waves cannot be suppressed by periodic planar wave fronts, since the frequency of the spiral is higher than the frequency of the fronts, and thus the domains of the spiral waves grow at the expense of the slower wave fronts.[7–11] Here, we focus on the attenuation of a single stable spiral wave. We show that it is possible to attenuate spiral waves by planar wave fronts with period longer than the rotational period of the spiral, and we address the problem of how to control spiral attenuation in excitable media. We find that when the fronts have long excitation duration, and are delivered at a specific phase relative to the rotational phase of the spiral, the spiral-front interaction is characterized by periodic patterns of spiral attenuation, which remain stable in time and over a broad range of physiologically meaningful parameter values. While spiral drift has been shown under similar conditions,[23] we do not aim to achieve spiral drift but to attenuate a stable spiral, i.e., to reduce the area covered by the spiral and the number of cells involved in the propagation of the spiral wave.

I. PHYSIOLOGICAL CONSIDERATIONS AND MODELING

We perform numerical simulations on a two-dimensional (2D) square lattice by considering interactions between the cells of the lattice, based on physiologically motivated rules representing the excitation dynamics of myocardial cells in the heart muscle (Fig. 1). The transmembrane potential of a myocardial cell represents the state of excitation of that cell. We model the state of the cell in position (i,j) in the lattice by an integer number E_{ij} as follows: (i) Resting (equilibrium) state: this state is represented in our model by $E_{ij}=0$, which corresponds to the experimentally observed transmembrane

a)Electronic address: plamen@buphy.bu.edu

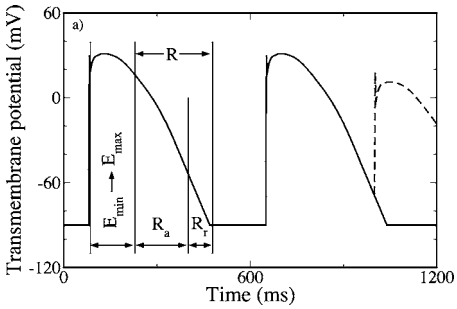

FIG. 1. Time evolution of the transmembrane potential of a ventricular myocite. After a superthreshold perturbation, the potential sharply increases from the resting state, of ≈−90 mV, to the excited state, with a plateau of positive potential of ≈30 mV. The duration of the excitation ranges from $E_{\min}$ to $E_{\max}$. The excited state is followed by a smooth decrease of the potential during the absolute refractory period, R_a. The decrease in the transmembrane potential continues during the relative refractory period, R_r, when a cell can be excited again but to a lower potential, and for shorter excitation duration compared to an excitation started during the resting state (dashed line).

potential ≈−90 mV.[24] A cell remains in the resting state for an unlimited time until a superthreshold perturbation occurs in the medium, which brings the cell to the excited state. This threshold for ventricular cells in guinea pigs was experimentally found to be ≈4–8 V/cm,[25] and is represented in our model by the parameter $\mathrm{Th}_{\mathrm{rest}}$ [Fig. 2(a)]. (ii) Excited state: when a cell enters the excited state, it takes a value in the interval $E_{\min} \leq E_{ij} \leq E_{\max}$, where $E_{\min} > 1$. For an excited

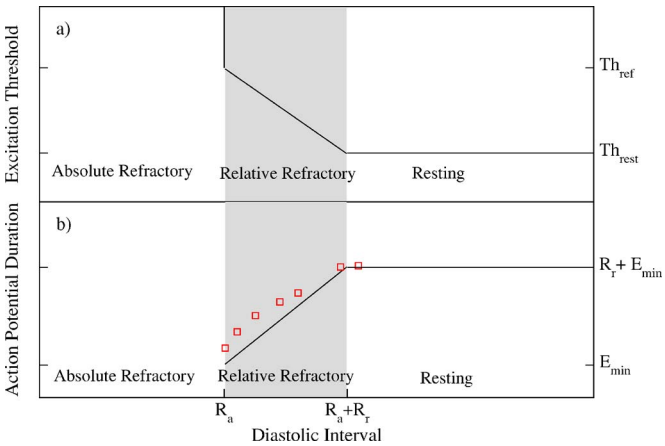

FIG. 2. Schematic presentation of the model. (a) Excitation threshold vs time past after the last excitation of a cell [also called diastolic interval (DI)]. For short DI, during the absolute refractory period, the cell cannot be excited and the excitation threshold is infinite. When the cell enters the relative refractory period, the excitation threshold is $\mathrm{Th}_{\mathrm{ref}}$, and with increasing DI the threshold decreases linearly in agreement with experimental observations (Ref. 29) until it reaches the value $\mathrm{Th}_{\mathrm{rest}}$ at the end of the relative refractory period. For long DI, during the resting state, the threshold remains constant and equal to $\mathrm{Th}_{\mathrm{rest}}$ (Ref. 27) We choose $\mathrm{Th}_{\mathrm{rest}}=20$ and $\mathrm{Th}_{\mathrm{ref}}=48$ to maintain the movement of the spiral tip in our simulations within a small area in agreement with experimental observations (Ref. 29). (b) Restitution curve—relation between the excitation duration [action potential duration (APD)] vs DI. There are no action potentials in the absolute refractory period. During the relative refractory period, the APD increases linearly with time, and in the resting state the APD is constant. We use the experimental restitution curve (denoted by □) and the conduction speed for guinea pig ventricular myocites (Ref. 29) to calibrate the parameter values, so that the restitution curve in our simulations reproduces the experimental one.

cell, in every time step τ, E_{ij} decreases by 1. Thus, in our simulations E_{ij} represents not only the transmembrane potential but also has a meaning of excitation duration [Fig. 2(b)], where at the beginning of the excitation the lowest excitation level a cell can assume is $E_{\min}$, corresponding to the shortest possible action potential duration (APD), while the highest excitation level is $E_{\max}$, which corresponds to the longest APD. At the end of the excitation period, $E_{ij}=1$ before the cell becomes absolute refractory. (iii) Absolute refractory state: when a cell enters this state, $E_{i,j}$ falls to $-R_a-R_r$, where R_a is the duration of the absolute refractory state when a cell cannot be excited. For an absolute refractory cell, in every time step τ, E_{ij} increases by 1. After R_a time steps, the cell becomes relative refractory (at $E_{ij}=-R_r$) before it reaches the resting state. (iv) Relative refractory state: this state is represented by $-R_r \leq E_{ij} \leq -1$, where R_r is the duration of the relative refractory state. A cell in this state can be excited with an excitation threshold experimentally observed to decrease in time as the cell approaches the resting state.[26] This threshold remains higher than the excitation threshold of cells in the resting state,[26] and in our model, it decreases linearly in time from the value $\mathrm{Th}_{\mathrm{ref}}$, when $E_{ij}=-R_r$, to the value $\mathrm{Th}_{\mathrm{rest}}$ in the resting state [Fig. 2(a)]. For every time step τ in which a relative refractory cell does not become excited, E_{ij} is increased by 1, until the cell reaches the resting state $E_{ij}=0$.

We define the excitation stimulus received by a cell in position (i,j) from the neighboring cells as $S_{ij}=\Sigma_{k,l}W_{kl}\sigma_{kl}$, where $k \in [i-\epsilon, i+\epsilon]$, $l \in [j-\epsilon, j+\epsilon]$, and ϵ defines the range of interaction. W_{kl} is a rotationally symmetric interaction kernel,[27] and $\sigma_{kl}=1$ if the cell in position (k,l) is excited and $\sigma_{kl}=0$ otherwise. To preserve a proper relation between the speed of propagation and the curvature of the wave front,[28] we set $\epsilon=5$. To account for the weaker effects of more distant neighbors, we choose values of the kernel elements W_{kl} decreasing with increasing distance from the center of the kernel.[27] A cell in position (i,j) that is excitable at time t will become excited in the next time step $t+1$ if it receives a stimulus S_{ij} larger than the excitation threshold of the cell. In this case, the new excited state of the cell is given by $E_{ij}^{t+1}=E_{ij}^{t}+R_r+E_{\min}$ [Fig. 2(b)], so that a cell at the beginning of the relative refractory state, with $E_{ij}^{t}=-R_r$, will reach an excitation level $E_{ij}^{t+1}=E_{\min}$. This is in accordance with the experimentally observed behavior of the restitution curve.[29] To account for the ion leakage from excited neighboring cells, we allow for an excitable cell to reach the longest APD, $E_{ij}^{t+1}=E_{\max}$, if (i) there is a cell (k,l) included in the kernel that is in the state $E_{kl}^{t}=E_{\max}$, and (ii) at the same time the perturbation S_{ij} is larger than the excitation threshold.

We consider a square lattice of $N \times N$ cells. To avoid effects of the lattice edge on the dynamics of wave propagation, and to account for experimental settings[30] we introduce no-flux boundary conditions, i.e., the lattice is surrounded by a strip of cells of width ϵ where the cells mirror the state of the cells neighboring the edge of the lattice.

The values of the parameters and the rules in our model match well the excitation dynamics in the ventricular cells of the guinea pig, traditionally used in experimental settings and theoretical studies:[29] (a) The experimentally observed

excitable gap (time between the end of the absolute refractory period and the next excitation) is $G=12\pm4$ ms,[29] which corresponds to one time step τ in our simulations, so we have $\tau=12$ ms; (b) comparing the experimental propagation speed of $v\approx75$ cm/s (Ref. 29) with the wave propagation of three lattice cells per time unit τ in our model, we have that our spatial unit is $\delta=0.3$ cm (≈100 myocite cells); (c) the experimentally found refractory period, $R^{\mathrm{exp}}=R_a^{\mathrm{exp}}+R_r^{\mathrm{exp}}\approx200$ ms, and relative refractory period $R_r^{\mathrm{exp}}\approx120$ ms,[29] are approximated in our simulation by the parameter values $R=R_a+R_r\in[18,30]$ and $R_r\in[7,10]$, in units of the time step τ; (d) the minimum and maximum APD experimentally observed are $E_{\mathrm{min}}^{\mathrm{exp}}\approx40$ ms and $E_{\mathrm{max}}^{\mathrm{exp}}\approx160$ ms,[29] which correspond to our parameters $E_{\mathrm{min}}\in[2,4]$ and $E_{\mathrm{max}}\in[10,20]$, in units of the time step τ; (e) the prolongation of the APD due to ion leakage has been physiologically estimated as $\Delta(\mathrm{APD})^{\mathrm{exp}}\approx D(\mathrm{APD})\partial_{xx}(\mathrm{APD})$, where $D\approx1$ cm^2/s is a diffusion constant.[31] Since typically $\mathrm{APD}\approx(E_{\mathrm{max}}^{\mathrm{exp}}+E_{\mathrm{min}}^{\mathrm{exp}})/2$ and $\partial_{xx}(\mathrm{APD})\approx(E_{\mathrm{max}}^{\mathrm{exp}}-E_{\mathrm{min}}^{\mathrm{exp}})/\delta^2$, we find $\Delta(\mathrm{APD})^{\mathrm{exp}}\approx130$ ms, which compares to the maximum prolongation in our model $\Delta(\mathrm{APD})^{\mathrm{model}}=E_{\mathrm{max}}-E_{\mathrm{min}}\in[6,18]$ in units of τ. The shape of the model restitution curve shown in Fig. 2(b) mimics the experimental data.[29] Thus, our model is based on experimentally relevant parameter values.

We generate the spiral according to a standard procedure, by propagating a planar front with one end close to the center of the lattice and the other end on the lattice edge.[32] We wait for 300 time steps τ (≈15 spiral rotations) until the spiral reaches a stable rotation with the tip moving only within a small approximately linear area of ≈30 cells near the center of the lattice, as observed in experimental settings.[33] We next introduce planar fronts with a period T, starting from the edge of the lattice. Each front is generated as a line of excited cells with maximum APD, $E_{1j}=E_{\mathrm{max}}$, for $j=1,\ldots,N$. To test whether it is possible to attenuate spiral waves with slow fronts, we choose the period T of the fronts to be longer than the rotational period of the spiral. We release the first front at time T_0 (in units τ) after the stabilization period of the spiral. The width of the front is proportional to the parameter E_{max} and to the speed of propagation, which depends on the excitation thresholds $\mathrm{Th}_{\mathrm{rest}}$ and $\mathrm{Th}_{\mathrm{ref}}$. Under these conditions, the position of the spiral tip remains stable and localized within a small area, and thus the patterns of spiral attenuation we find are not the result of spiral drift. To track if the spiral is attenuated, we follow the time evolution of every individual cell in the lattice. To survey the system, we also measure the total number of excited cells in the lattice as a function of time.

II. RESULTS

In contrast to previous studies showing that spiral waves cannot be attenuated by fronts of lower frequency,[7–11] we hypothesize that the interaction of a stable spiral wave and lower-frequency periodic planar fronts with sufficiently long excitation duration and with period T larger than the rotational period of the spiral can lead to spiral attenuation. Specifically, we hypothesize that spiral attenuation can only occur for an appropriate timing of the descending fronts (as measured by T_0) relative to the rotational phase of the spiral. We find that the interaction between the fronts and the spiral leads to complex patterns where, after several passing fronts, the spiral is attenuated (Fig. 3). These patterns repeat in time and remain stable for a broad range of physiologically meaningful parameter values (Fig. 7). Further, we find that the system exhibits a variety of different patterns that fall into two general classes: (i) Class I, where there is one spiral attenuation within a cycle of several passing fronts [Figs. 3(a)–3(c)], and (ii) Class II, where there are two nonconsecutive spiral attenuations within a cycle of several passing fronts [Figs. 3(d)–3(f)]. Repeating our simulations for $N=60,80,100,\ldots,200$, and for $N\times N$ and $N\times2N$ lattices, we find identical dynamics with the same periodic patterns of spiral attenuation. This also allows us to study the effect of the distance from the area where the fronts are introduced to the spiral core. In Fig. 4, we provide a color-coded representation of the spiral-front interaction on the lattice for the Class I and Class II patterns shown in Fig. 3.

The spatiotemporal patterns of spiral attenuation we present in Fig. 3 are a result of a complex nonlinear interaction between the spiral and the descending fronts. Without the fronts, the rotational period of the spiral is uniform in both space and time, i.e., the excitation of every cell in the lattice has a period equal to the rotational period of the spiral. In our simulations, the APD of a cell that becomes excited is $E_{ij}^{t+1}=E_{ij}^t+R_r+E_{\mathrm{min}}$. Since the excitable gap in experimental settings is $G\approx12$ ms,[29] which corresponds to one time step τ in our simulations, a cell in the relative refractory state $E_{ij}^t=-R_r$ is excited within a single time step to $E_{ij}^{t+1}=E_{\mathrm{min}}$. Thus, the APD of a cell in the isolated spiral is always E_{min}. The period of the spiral equals the sum of the duration of all states a cell undergoes during a single spiral rotation, $T_{sp}^-=E_{\mathrm{min}}+R_a+G$. In the presence of fronts, where the excited cells have maximum APD given by $E_{ij}=E_{\mathrm{max}}$, after a collision of a front with the spiral, a thin layer of maximum APD excitations propagates from the front along the advancing contour of the spiral (as shown in Fig. 5, frames 2–4). When these excitations reach the tip of the spiral before the next spiral rotation, the period of the spiral increases to $T_{sp}^+=E_{\mathrm{max}}+R_a+G$, which is also the period of the cells with maximum APD. In this situation, the spiral survives (Fig. 5, frame 6), and we observe a peak in the total number of excited cells in the lattice (Fig. 3). When the layer of cells with maximum APD excitations that propagates from the front to the spiral does not reach the tip of the spiral before the next spiral rotation (i.e., it does not cover the entire contour of the spiral), the period of the spiral remains T_{sp}^-. In this case, the cells at the tip of the spiral continue to have short APD given by $E_{ij}=E_{\mathrm{min}}$ (Fig. 5, frame 11). Due to the short APD, the spiral cannot propagate through the absolute refractory areas left by the layer of cells with long APD (given by $E_{ij}=E_{\mathrm{max}}$) formed between the front and the spiral, and the spiral is attenuated (Fig. 5, frame 12). This spiral attenuation corresponds to a reduced or absent peak in the total number of excited cells in the lattice (Fig. 3). In our simulations, the period of the fronts is $T=T_{sp}^++2$. Thus, the spiral attenuation we observe in Figs. 3 and 4 is achieved for planar fronts with a period longer than the period of the spiral.

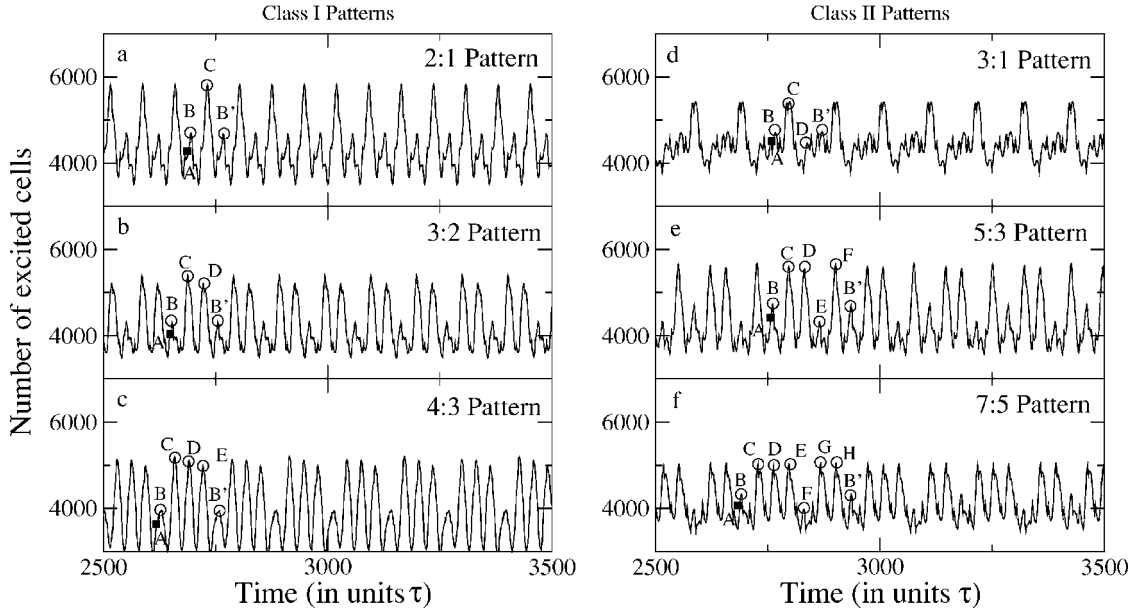

FIG. 3. Time evolution of the total number of excited cells from simulations on a square lattice of size $N=100$. Time is presented in units of the simulation time step τ. Data show a variety of robust patterns of spiral attenuation that remain stable in time. Absent and reduced peaks correspond to attenuation of the spiral. We find that these patterns belong to two general classes. (i) Class I $(n:n-1)$, where within a cycle of n fronts we have $n-1$ consecutive spiral rotations followed by one spiral attenuation. Examples of Class I patterns are presented in (a) pattern 2:1—out of the collision of the spiral with two consecutive fronts there is first a spiral attenuation (denoted by B) followed by one surviving spiral (denoted by C); (b) pattern 3:2—for each cycle of three consecutive fronts there is first a spiral attenuation (B) followed by two surviving spirals (C and D); (c) pattern 4:3—for each cycle of four consecutive fronts there is a spiral attenuation (B) and three surviving spirals (C, D, and E). The Class I patterns in (a), (b), and (c) are obtained for the following parameter values: $R_a=16$, $R_r=8$, $E_{\min}=2$, $E_{\max}=17,15,13$, $T_0=73,39,64$, respectively. (ii) Class II $(2n+1:2n-1)$, where within a cycle of $2n+1$ fronts there are $2n-1$ spiral rotations and two spiral attenuations. Examples of Class II patterns are presented in (d) pattern 3:1—for each cycle of three fronts there are two spiral attenuations (B and D) and one surviving spiral (C); (e) pattern 5:3—for each cycle of five fronts there are two spiral attenuations (B and E) and three surviving spirals (C, D, and F); (f) pattern 7:5—for each cycle of seven fronts we have two attenuations (B and F) and five surviving spirals (C, D, E, G, and H). The Class II patterns in (d), (e), and (f) are obtained for the following parameter values: $R_a=15,16,17$, $R_r=8$, $E_{\min}=2$, $E_{\max}=17,16,15$, $T_0=65,70,70$, respectively. In all panels, the instant in which a spiral attenuation is initiated is denoted by A, and the beginning of the next cycle is denoted by B', repeating the spiral attenuation in B. We find the same attenuation patterns independently of the size of the lattice and for a broad range of parameter values (Fig. 7).

We find that this mechanism of nonlinear interaction between the spiral and planar fronts comprised of cells with long APD and with frequency lower than the spiral rotation leads to the attenuation patterns in Figs. 3 and 4. We demonstrate that these patterns cannot be matched by a linear superposition of the number of excited cells of the isolated spiral and the number of excited cells in the isolated fronts, as we show in Fig. 6. Such a linear superposition exhibits periodic pulses with a higher number of excited cells, and cannot account for the missing peaks associated with spiral attenuation. Moreover, the pulses observed in the linear superposition of spiral and front form a cycle that repeats with a different duration compared to the duration of the cycle of spiral attenuation (Fig. 6).

Further, we observe that these complex front-spiral interactions lead to rich dynamics characterized by a variety of temporal patterns. We find that all patterns belong to two general classes. For Class I $(n:n-1)$ patterns, we observe that within a cycle of n fronts, we have $n-1$ slow spiral rotations with period T_{sp}^{+}, followed by two fast rotations with period T_{sp}^{-}:

$$\text{Class I:}\quad nT=(n-1)T_{sp}^{+}+2T_{sp}^{-}, \tag{2.1}$$

where the two fast rotations correspond to a single episode of spiral attenuation [Figs. 3(a)–3(c)].

For Class II $(2n+1:2n-1)$ patterns, we observe that within a cycle of $2n+1$ fronts, we have $2n-1$ slow spiral rotations, with period T_{sp}^{+}, and four fast rotations, with period T_{sp}^{-}:

$$\text{Class II:}\quad (2n+1)T=(2n-1)T_{sp}^{+}+4T_{sp}^{-}, \tag{2.2}$$

where the four fast rotations correspond to two separate nonconsecutive episodes of spiral attenuation [Figs. 3(d)–3(f)].

Solving for n in Eqs. (2.1) and (2.2), we obtain

$$\text{Class I:}\quad n=\frac{4T_{sp}^{-}-2T_{sp}^{+}}{2(T-T_{sp}^{+})}=\frac{1}{2}(2E_{\min}-E_{\max}+R_a+G), \tag{2.3}$$

$$\text{Class II:}\quad n=\frac{4T_{sp}^{-}-T_{sp}^{+}-T}{2(T-T_{sp}^{+})}=\frac{1}{2}(2E_{\min}-E_{\max}+R_a+G-1). \tag{2.4}$$

Based on the choice of parameter values for the system, the above expressions allow us to predict (i) the specific attenuation pattern, and (ii) the class to which a given pattern belongs. Parameter values for which we do not obtain integer n in either Eq. (2.3) or (2.4) cannot lead to spiral attenuation patterns. Thus, we can control the dynamical behavior of the

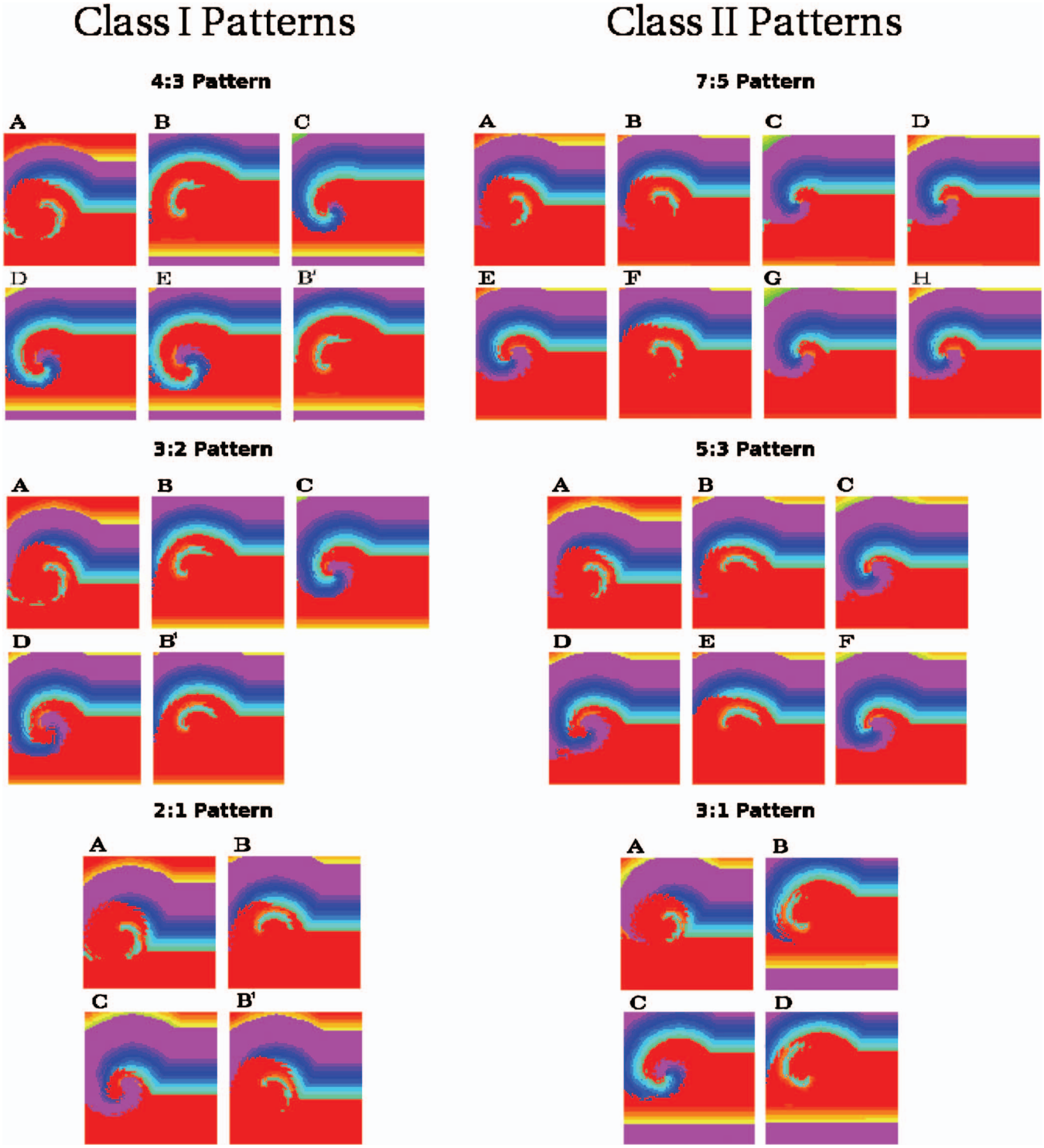

FIG. 4. (Color) Color-coded representation of the spiral-front interaction corresponding to the Class I and Class II patterns shown in Fig. 3. For increasing values of E_{ij} we have absolute refractory cells in red, relative refractory cells in orange and yellow, and excited cells in cyan, blue, and violet (highest values of E_{ij}). Snapshots for each pattern represent the same stages of the dynamics in time, as indicated by the corresponding capital letters in the panels of Fig. 3.

system in generating desired patterns of spiral attenuation.

Our simulations of up to 10^5 time steps τ (corresponding to $\approx$1500 seconds in experimental settings) show no change in the dynamics, which indicates that the spiral attenuation patterns remain stable in time. Further, we find that both Class I and Class II patterns can be obtained for a broad range of parameter values showing a robust effect of spiral attenuation. Specifically, we observe a particular structure in parameter space where individual patterns are organized along parallel straight lines, with every even line corresponding to a Class I pattern and every odd line corresponding to a Class II pattern (Fig. 7). This regular structure in parameter space is also predicted by Eqs. (2.3) and (2.4). In the upper left corner of the parameter diagram, for increasing values of R_a and decreasing values of $E_{\max}$, an attenuation becomes less frequent for increasing n, since we have only one attenu-

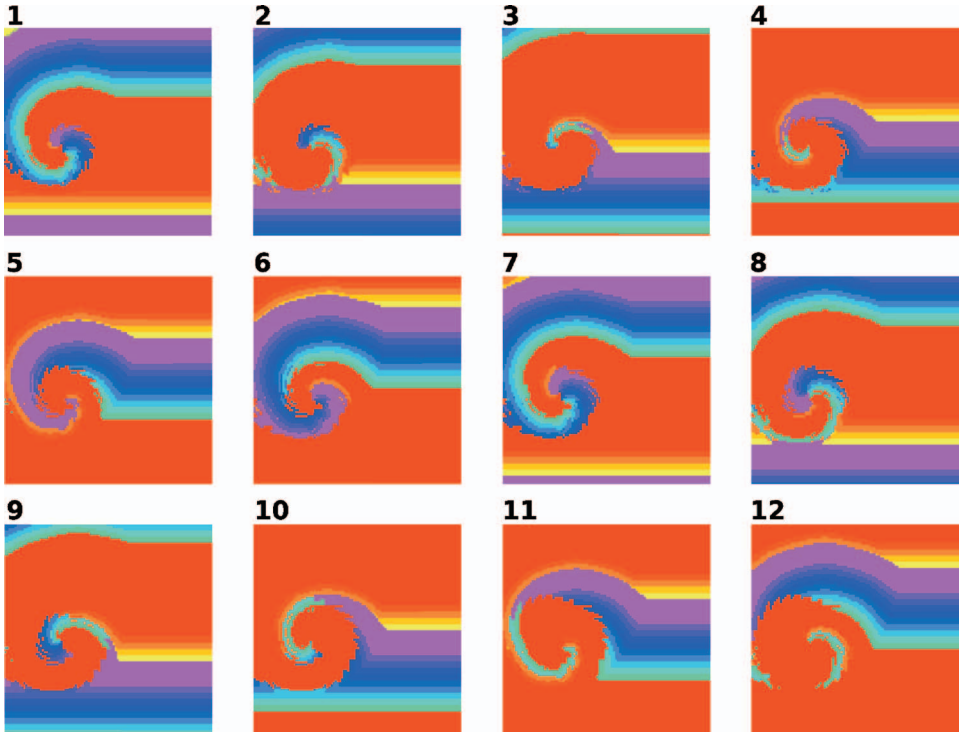

FIG. 5. (Color) Color-coded representation of the time evolution for the Class I 4:3 pattern obtained for the same parameter values as in Fig. 3(c). Snapshots represent the state of the lattice in intervals of five time steps τ. Snapshots 1, 7, and 12 correspond to D, E, and A in Fig. 3(c). For increasing values of E_{ij} we have absolute refractory cells in red, relative refractory cells in orange and yellow, and excited cells in cyan, blue, and violet (highest values of E_{ij}).

ation per cycle of n fronts for Class I patterns, and two attenuations per cycle for $2n+1$ fronts for Class II. In the upper right (large R_a and $E_{\max}$) and lower left (small R_a and $E_{\max}$) corners of the diagram, we find alternating patterns in a broad range of parameter values extending beyond the physiologically meaningful region (not shown in the diagram in Fig. 7). Finally, in the lower right corner of the diagram (small R_a and large $E_{\max}$) we do not observe patterns. This is in agreement with Eqs. (2.3) and (2.4), which do not allow $n<2$ for Class I (a cycle of at least two fronts is needed to have one attenuation within the cycle), and $n<1$ for Class II (a cycle of at least three fronts is needed to have two attenuations within the cycle).

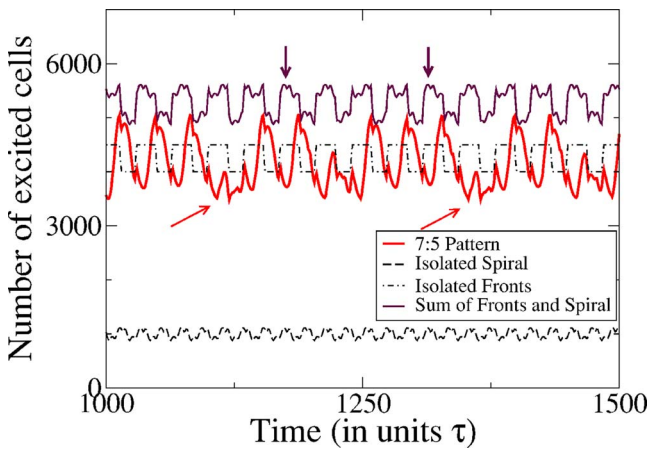

FIG. 6. Time evolution of the total number of excited cells in a square lattice of size $N=100$ for isolated fronts (without a spiral), isolated spiral (without fronts), linear superposition of fronts and spiral, and the Class II pattern 7:5, generated for the same parameter values as in Fig. 3(f) (arrows inclined to the right indicate one cycle of the 7:5 pattern). It is apparent that the 7:5 attenuation pattern cannot be a result of the linear superposition of periodic fronts and the spiral wave. This linear superposition is characterized by absence of attenuation, much higher average value of the number of excited cells, different profile of the periodic peaks, and shorter cycle (indicated by vertical arrows) compared to the 7:5 attenuation pattern, generated by the nonlinear interaction of the spiral wave and lower frequency fronts with maximum APD.

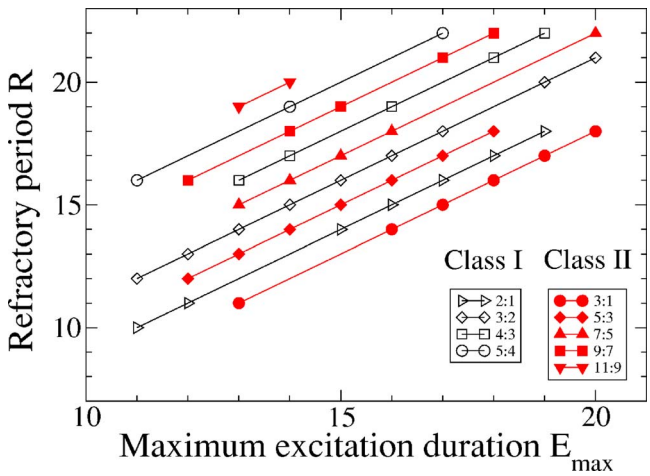

FIG. 7. Diagram of spiral attenuation patterns in parameter space R_a vs $E_{\max}$, for a square lattice of $N=100$ and fixed parameter values $R_r=8$ and $E_{\min}=2$. We observe attenuation patterns for a broad range of parameter values where each pattern can be found along a single straight line, in accordance with Eqs. (2.3) and (2.4). Patterns of Class I $(n:n-1)$ and Class II $(2n+1:2n-1)$ alternate in a series of parallel lines, where n increases with increasing R_a. To assess the intensity of the attenuation effect in different regions of the parameter diagram, we estimate for each cycle the ratio between the average number of excited cells when there is no spiral attenuation (large peaks in Fig. 3) and during spiral attenuation (reduced or absent peaks in Fig. 3). We find that this ratio is (i) characterized by a broad maximum in the central region of the parameter diagram and (ii) it exhibits a monotonic decrease in all directions of the parameter space for both classes of patterns, indicating a common behavior in the intensity of spiral attenuation.

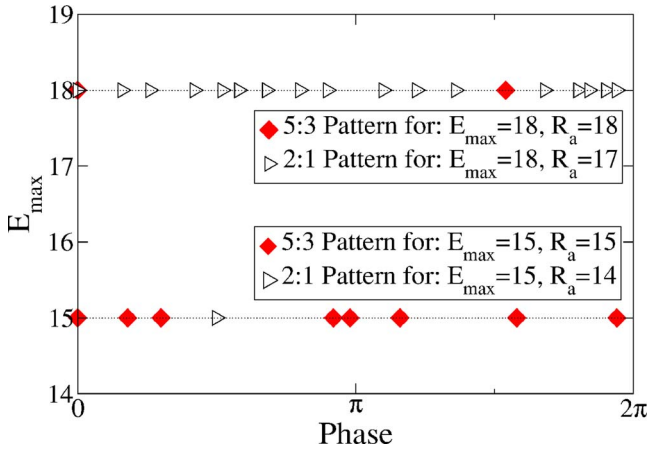

FIG. 8. Dependence of the attenuation patterns on the relative phase between the first released front and the spiral. Presented are only the patterns 2:1 (Class I) and 5:3 (Class II) for two sets of parameter values $E_{\max}$ and R_a, with the same symbols as in Fig. 7. Our results show that, for each set of parameter values on the diagram in Fig. 7, the patterns can appear only for specific values of the relative phase between the front and the spiral, indicating that the phase in which the front hits the spiral is crucial to achieve spiral attenuation.

We finally investigate how the front-spiral interaction depends on the relative phase between the spiral and the fronts. To answer this question, we perform several tests by releasing the first front at a time T_0 after the stabilization period of the spiral (which is 300 time steps τ), followed by a train of fronts with period T. We repeat the simulations for every value of $T_0 \in [0,T]$, for every point in the parameter space shown in Fig. 7. Surprisingly, we find that the patterns we observe in the parameter diagram of Fig. 7 occur only for specific values of T_0 (Fig. 8). For example, the Class I, 2:1 pattern generated for $E_{\max}=15$ and $R_a=14$ occurs only for phase $2\pi/4$, corresponding to $T_0=T/4$, while the same pattern, for $E_{\max}=18$ and $R_a=17$, occurs for several values of T_0 (Fig. 8). Thus, the observed dynamical patterns of spiral attenuation shown in Figs. 3 and 4 depend not only on the parameter values, but also on the relative phase between the spiral wave and the first released front. These findings indicate the presence of particular "vulnerable" phases during the spiral rotation when planar fronts can lead to spiral attenuation patterns.

III. SUMMARY

In summary, we find that the interaction of a spiral wave with planar fronts of sufficiently long excitation duration and a period longer than the period of the spiral can lead to spiral attenuation. The spiral attenuation only occurs for an appropriate timing of the descending fronts relative to the rotational phase of the spiral. This phase-dependent spiral attenuation is not a result of spiral drift and is characterized by different spatiotemporal patterns, each of them observed for a broad range of physiologically meaningful parameter values. Further, we find that these hitherto unknown patterns of phase-dependent spiral attenuation fall into two general classes, where each class is defined by a specific mathematical relation, and is represented by a structured diagram in parameter space. The spiral attenuation patterns we observe remain stable in time and do not change during the evolution of the system. These dynamics of phase-dependent spiral attenuation could be utilized for practical applications, and in the context of cardiac dynamics may lead to general approaches for controlling and preventing fatal arrhythmias.

ACKNOWLEDGMENT

Miguel de la Casa and Javier de la Rubia acknowledge partial support by the Ministerio de Educacion y Ciencia (Spain), Project No. FIS2005-01729, and Plamen Ch. Ivanov acknowledges support from NIH Grant No. 2RO1 HL071972.

[1] A. T. Winfree, *The Geometry of Biological Time* (Springer-Verlag, New York, 2001).
[2] J. Schutze, O. Steinbock, and S. C. Muller, "Forced vortex interaction and annihilation in an active medium," Nature (London) **356**, 45–47 (1992).
[3] S. Sawai, P. A. Thomason, and E. C. Cox, "An autoregulatory circuit for long-range self-organization in Dictyostelium cell populations," Nature (London) **433**, 323–326 (2005).
[4] L. Glass and M. C. Mackey, *From Clocks to Chaos: The Rhythms of Life* (Princeton University Press, Princeton, 1988).
[5] R. A. Gray, J. Jalife, A. V. Panfilov, W. T. Baxter, C. Cabo, J. M. Davidenko, A. M. Pertsov, P. Hogeweg, and A. T. Winfree, "Mechanism of cardiac fibrillation," Science **270**, 1222–1223 (1995).
[6] F. X. Witkowski, L. J. Leon, P. A. Penkoske, W. R. Giles, M. L. Spano, W. L. Ditto, and A. T. Winfree, "Spatiotemporal evolution of ventricular fibrillation," Nature (London) **392**, 78–82 (1998).
[7] A. N. Zaikin and A. M. Zhabotinsky, "Concentration wave propagation in two-dimensional liquid-phase self-oscillating system," Nature (London) **225**, 535–537 (1970).
[8] A. T. Stamp, G. V. Osipov, and J. J. Collins, "Suppressing arrhythmias in cardiac models using overdrive pacing and calcium channel blockers," Chaos **12**, 931–940 (2002).
[9] I. Aranson, H. Levine, and L. Tsimring, "Spiral competition in three-component excitable media," Phys. Rev. Lett. **76**, 1170–1173 (1996).
[10] K. J. Lee, "Wave pattern selection in an excitable system," Phys. Rev. Lett. **79**, 2907–2910 (1997).
[11] F. Xie, Z. Qu, J. N. Weiss, and A. Garfinkel, "Interactions between stable spiral waves with different frequencies in cardiac tissue," Phys. Rev. E **59**, 2203–2205 (1999).
[12] F. Moss, "Chemical dynamics—Noisy waves," Nature (London) **391**, 743–744 (1998).
[13] S. Kadar, J. C. Wang, and K. Showalter, "Noise-supported travelling waves in sub-excitable media," Nature (London) **391**, 770–772 (1998).
[14] A. Mikhailov and V. Zykov, "Rotating spiral waves in a simple model of excitable medium," Dokl. Akad. Nauk SSSR **286**, 341–344 (1986).
[15] M. P. Nash and A. V. Panfilov, "Electromechanical model of excitable tissue to study reentrant cardiac arrhythmias," Prog. Biophys. Mol. Biol. **85**, 501–522 (2004).
[16] A. T. Winfree, *When Time Breaks Down* (Princeton University Press, Princeton, 1987).
[17] H. M. Hastings, S. J. Evans, W. Q. Martha, L. Chong, and O. Nwasokwa, "Non-linear dynamics in ventricular fibrillation," Proc. Natl. Acad. Sci. U.S.A. **93**, 10495–10499 (1996).
[18] V. Petrov, V. Gáspár, J. Masere, and K. Showalter, "Controlling chaos in the Belousov-Zhabotinsky reaction," Nature (London) **361**, 240–243 (1993).
[19] V. S. Zykov, A. S. Mikhailov, and S. C. Müller, "Controlling spiral waves in confined geometries by global feedback," Phys. Rev. Lett. **78**, 3398–3401 (1997).
[20] S. J. Evans, H. M. Hastings, S. Nangia, J. Chin, M. Smolow, O. Nwasokwa, and A. Garfinkel, "Ventricular fibrillation: One spiral or many?," Proc. R. Soc. London, Ser. B **265**, 2167–2170 (1998).
[21] W. L. Ditto, M. L. Spano, V. In, J. Neff, and B. Meadows, "Control of human atrial fibrillation," Int. J. Bifurcation Chaos Appl. Sci. Eng. **10**, 593–601 (2000).
[22] S. Sitabhra, A. Pande, and R. Pandit, "Defibrillation via the elimination of spiral turbulence in a model for ventricular fibrillation," Phys. Rev. Lett. **86**, 3678–3681 (2001).

[23]G. Gottwald, A. Pumir, and V. Krinsky, "Spiral drift induced by stimulating wave trains," Chaos **11**, 487–494 (2001).
[24]G. W. Beeler and H. Reuter, "Reconstruction of the action potential of ventricular myocardial fibers," J. Physiol. (London) **268**, 177–210 (1977).
[25]V. Sharma, L. Susil, and R. Tung, "Paradoxical loss of excitation with high intensity pulses during electric field stimulation of single cardiac cells," Biophys. J. **88**, 3038–3049 (2005).
[26]*Essential Medical Physiology*, edited by L. R. Johnson (Lippincott-Raven, Philadelphia, 1998).
[27]V. G. Fast, I. R. Efimov, and V. I. Krinsky, "Transition from circular to linear rotation of a vortex in an excitable medium," Phys. Lett. A **151**, 157–161 (1990).
[28]V. S. Zykov, *Modeling of Wave Processes in Excitable Media* (Manchester University Press, Manchester, 1988).
[29]S. D. Girouard, "Optical mapping in a new guinea pig model of ventricular tachycardia reveals mechanisms for multiple wavelengths in a single reentrant circuit," Circulation **93**, 603–613 (1996).
[30]J. M. Starobin and C. F. Starmer, "Boundary-layer analysis of waves propagating in an excitable medium: Medium conditions for wave-front—Obstacle separation," Phys. Rev. E **54**, 430–437 (1996).
[31]A. Karma and F. Fenton, "Vortex dynamics in three-dimensional continuous myocardium with fiber rotation: Filament instability and fibrillation," Chaos **8**, 20–47 (1998).
[32]V. N. Biktashev and A. V. Holden, "Reentrant waves and their elimination in a model of mammalian ventricular tissue," Chaos **8**, 48–56 (1998).
[33]V. I. Krinsky, I. R. Efimov, and J. Jalife, "Vortices with linear cores in excitable media," Proc. R. Soc. London, Ser. A **437**, 645–655 (1992).

Patterns of spiral wave attenuation by low-frequency periodic planar fronts

By: de la Casa, MA (de la Casa, Miguel A.); de la Rubia, FJ (de la Rubia, F. Javier); Ivanov, PC (Ivanov, Plamen Ch.)

View ResearcherID and ORCID

CHAOS
Volume: 17 **Issue:** 1
Article Number: 015109
DOI: 10.1063/1.2404640
Published: MAR 2007
Document Type: Article
View Journal Impact

Abstract

There is evidence that spiral waves and their breakup underlie mechanisms related to a wide spectrum of phenomena ranging from spatially extended chemical reactions to fatal cardiac arrhythmias [A. T. Winfree, The Geometry of Biological Time (Springer-Verlag, New York, 2001); J. Schutze, O. Steinbock, and S. C. Muller, Nature 356, 45 (1992); S. Sawai, P. A. Thomason, and E. C. Cox, Nature 433, 323 (2005); L. Glass and M. C. Mackey, From Clocks to Chaos: The Rhythms of Life (Princeton University Press, Princeton, 1988); R. A. Gray , Science 270, 1222 (1995); F. X. Witkowski , Nature 392, 78 (1998)]. Once initiated, spiral waves cannot be suppressed by periodic planar fronts, since the domains of the spiral waves grow at the expense of the fronts [A. N. Zaikin and A. M. Zhabotinsky, Nature 225, 535 (1970); A. T. Stamp, G. V. Osipov, and J. J. Collins, Chaos 12, 931 (2002); I. Aranson, H. Levine, and L. Tsimring, Phys. Rev. Lett. 76, 1170 (1996); K. J. Lee, Phys. Rev. Lett. 79, 2907 (1997); F. Xie, Z. Qu, J. N. Weiss, and A. Garfinkel, Phys. Rev. E 59, 2203 (1999)]. Here, we show that introducing periodic planar waves with long excitation duration and a period longer than the rotational period of the spiral can lead to spiral attenuation. The attenuation is not due to spiral drift and occurs periodically over cycles of several fronts, forming a variety of complex spatiotemporal patterns, which fall into two distinct general classes. Further, we find that these attenuation patterns only occur at specific phases of the descending fronts relative to the rotational phase of the spiral. We demonstrate these dynamics of phase-dependent spiral attenuation by performing numerical simulations of wave propagation in the excitable medium of myocardial cells. The effect of phase-dependent spiral attenuation we observe can lead to a general approach to spiral control in physical and biological systems with relevance for medical applications. (c) 2007 American Institute of Physics.

Keywords

KeyWords Plus: VENTRICULAR-FIBRILLATION; EXCITABLE MEDIA; DYNAMICS; TISSUE; VORTEX; MODEL; ARRHYTHMIAS; MECHANISMS; ROTATION; CIRCUIT

Author Information

Reprint Address: de la Casa, MA (reprint author)

+ Univ Nacl Educ Distancia, Dept Fis Fundamental, Madrid 28040, Spain.

Addresses:

+ [1] Univ Nacl Educ Distancia, Dept Fis Fundamental, Madrid 28040, Spain

+ [2] Boston Univ, Dept Phys, Boston, MA 02215 USA

[3] Boston Univ, Ctr Polymer Studies, Boston, MA 02215 USA

[4] Bulgarian Acad Sci, Inst Solid State Phys, BU-1784 Sofia, Bulgaria

E-mail Addresses: plamen@buphy.bu.edu

Suggest a correction

If you would like to improve the quality of the data in this record, please suggest a correction.

Funding

Funding Agency	Grant Number
NHLBI NIH HHS	2R01 HL071972

Publisher

AMER INST PHYSICS, CIRCULATION & FULFILLMENT DIV, 2 HUNTINGTON QUADRANGLE, STE 1 N O 1, MELVILLE, NY 11747-4501 USA

Journal Information

Impact Factor: Journal Citation Reports

Categories / Classification

Research Areas: Mathematics; Physics

Web of Science Categories: Mathematics, Applied; Physics, Mathematical

See more data fields

Cited References: 33

Showing 30 of 33 View All in Cited References page *(from Web of Science Core Collection)*

1. **Spiral competition in three-component excitable media** **Times Cited: 44**
By: Aranson, I; Levine, H; Tsimring, L
PHYSICAL REVIEW LETTERS Volume: 76 Issue: 7 Pages: 1170-1173 Published: FEB 12 1996

2. **RECONSTRUCTION OF ACTION POTENTIAL OF VENTRICULAR MYOCARDIAL FIBERS** **Times Cited: 1,042**
By: BEELER, GW; REUTER, H
JOURNAL OF PHYSIOLOGY-LONDON Volume: 268 Issue: 1 Pages: 177-210 Published: 1977

3. **Reentrant waves and their elimination in a model of mammalian ventricular tissue** **Times Cited: 90**
By: Biktashev, VN; Holden, AV
CHAOS Volume: 8 Issue: 1 Pages: 48-56 Published: MAR 1998

4. **Control of human atrial fibrillation** **Times Cited: 51**
By: Ditto, WL; Spano, ML; In, V; et al.
INTERNATIONAL JOURNAL OF BIFURCATION AND CHAOS Volume: 10 Issue: 3 Pages: 593-601 Published: MAR 2000

5. **Ventricular fibrillation: one spiral or many?** **Times Cited: 3**
By: Evans, SJ; Hastings, HM; Nangia, S; et al.
PROCEEDINGS OF THE ROYAL SOCIETY B-BIOLOGICAL SCIENCES Volume: 265 Issue: 1411 Pages: 2167-2170 Published: NOV 22 1998

6. **TRANSITION FROM CIRCULAR TO LINEAR ROTATION OF A VORTEX IN AN EXCITABLE CELLULAR MEDIUM** **Times Cited: 40**
By: FAST, VG; EFIMOV, IR; KRINSKY, VI
PHYSICS LETTERS A Volume: 151 Issue: 3-4 Pages: 157-161 Published: DEC 3 1990

Am J Physiol Regul Integr Comp Physiol 293: R1923–R1937, 2007.
First published August 1, 2007; doi:10.1152/ajpregu.00372.2007.

Fractal scale-invariant and nonlinear properties of cardiac dynamics remain stable with advanced age: a new mechanistic picture of cardiac control in healthy elderly

Daniel T. Schmitt[1,2] and Plamen Ch. Ivanov[2,3]

[1]*Theoretische Physik, Universität Ulm, Ulm, Germany;* [2]*Center for Polymer Studies and Department of Physics, Boston University, Boston; and* [3]*Harvard Medical School and Division of Sleep Medicine, Brigham and Women's Hospital, Boston, Massachusetts*

Submitted 26 May 2007; accepted in final form 10 July 2007

Schmitt DT, Ivanov PC. Fractal scale-invariant and nonlinear properties of cardiac dynamics remain stable with advanced age: a new mechanistic picture of cardiac control in healthy elderly. *Am J Physiol Regul Integr Comp Physiol* 293: R1923–R1937, 2007. First published August 1, 2007; doi:10.1152/ajpregu.00372.2007.—Heart beat fluctuations exhibit temporal structure with robust long-range correlations, fractal and nonlinear features, which have been found to break down with pathologic conditions, reflecting changes in the mechanism of neuroautonomic control. It has been hypothesized that these features change and even break down also with advanced age, suggesting fundamental alterations in cardiac control with aging. Here we test this hypothesis. We analyze heart beat interval recordings from the following two independent databases: *1*) 19 healthy young (average age 25.7 yr) and 16 healthy elderly subjects (average age 73.8 yr) during 2 h under resting conditions from the Fantasia database; and *2*) 29 healthy elderly subjects (average age 75.9 yr) during ≈8 h of sleep from the sleep heart health study (SHHS) database, and the same subjects recorded 5 yr later. We quantify: *1*) the average heart rate (<R-R>); *2*) the SD $\sigma_{R\text{-}R}$ and $\sigma_{\Delta R\text{-}R}$ of the heart beat intervals R-R and their increments ΔR-R; *3*) the long-range correlations in R-R as measured by the scaling exponent $\alpha_{R\text{-}R}$ using the Detrended Fluctuation Analysis; *4*) fractal linear and nonlinear properties as represented by the scaling exponents α^{sgn} and α^{mag} for the time series of the sign and magnitude of ΔR-R; and *5*) the nonlinear fractal dimension $D(k)$ of R-R using the fractal dimension analysis. We find: *1*) No significant difference in ($P > 0.05$); *2*) a significant difference in $\sigma_{R\text{-}R}$ and $\sigma_{\Delta R\text{-}R}$ for the Fantasia groups ($P < 10^{-4}$) but no significant change with age between the elderly SHHS groups ($P > 0.5$); and *3*) no significant change in the fractal measures $\alpha_{R\text{-}R}$ ($P > 0.15$), α^{sgn} ($P > 0.2$), α^{mag} ($P > 0.3$), and $D(k)$ with age. Our findings do not support the hypothesis that fractal linear and nonlinear characteristics of heart beat dynamics break down with advanced age in healthy subjects. Although our results indeed show a reduced SD of heart beat fluctuations with advanced age, the inherent temporal fractal and nonlinear organization of these fluctuations remains stable. This indicates that the coupled cascade of nonlinear feedback loops, which are believed to underlie cardiac neuroautonomic regulation, remains intact with advanced age.

aging; dynamics; heart rate; nervous system; autonomic; physiology; sleep; fractals; nonlinearity; scaling

THE OUTPUTS OF PHYSIOLOGICAL systems under neural regulation exhibit *1*) high degree of variability, *2*) spacial and temporal fractal organization that remains invariant at different scales of observation, and *3*) complex nonlinear properties (6, 46). These inherent features of physiological dynamics change significantly with different physiological states such as wake and sleep, exercise and rest, circadian rhythms, as well as with pathological conditions. Because different physiological states and pathological perturbations correspond to changes or even break down in the mechanism of the underlying neural regulation, alterations in certain dynamic properties of physiological signals have been found to be reliable markers of changes in physiological control.

Aging is traditionally associated with the process of decline of physiological function and reduction of physiological complexity (2, 35). One major hypothesis is that physiological aging results from a gradual change in the underlying mechanisms of physiological control (a regulatory network of neural and metabolic pathways interacting through coupled cascades of nonlinear feedback loops on a range of time and length scales), leading to changes of physiological dynamics. Under this hypothesis, even ostensibly healthy elderly subjects would exhibit: *1*) loss of sensitivity and decreased responsiveness to external and internal stimuli, leading to reduced physiological variability (2) and *2*) breakdown of certain feedback loops acting at different time scales in the regulatory mechanism of various physiological systems. This breakdown would lead to loss of physiological complexity as reflected in certain scale-invariant and nonlinear temporal characteristics of physiological dynamics (35, 41). This hypothesis of a breakdown of physiological complexity with healthy aging has recently been challenged (68). Furthermore, earlier studies have linked various pathological states with breakdown of the scale-invariant fractal organization in physiological dynamics, which is likely to result from disintegration of coupled feedback loops in the regulatory mechanism (15, 27, 28, 54, 61, 71). Thus, based on this hypothesis, mechanistically, physiological processes under healthy aging would be categorized in the same class as pathological dynamics where fractal organization and nonlinear complexity is lost.

A second hypothesis is that, while aging may lead to reduced variability, certain temporal fractal, scale-invariant and nonlinear structures embedded in physiological dynamics may remain unchanged. These two alternative hypotheses represent different notions about which aspects of the physiological control mechanisms are expected to change in the process of aging in contrast to the changes accompanying certain pathological conditions.

Address for reprint requests and other correspondence: P. Ch. Ivanov, Center for Polymer Studies and Dept. of Physics, Boston University, Boston, MA 02215 (e-mail: plamen@buphy.bu.edu).

The costs of publication of this article were defrayed in part by the payment of page charges. The article must therefore be hereby marked "*advertisement*" in accordance with 18 U.S.C. Section 1734 solely to indicate this fact.

To test these two hypotheses, we analyze cardiac dynamics, a typical example of an output of an integrated physiological system under autonomic neural regulation. Previous studies have shown that heart rate variability decreases with certain pathological conditions (46, 69) and with advanced age (51, 65). Studies based on approaches from statistical physics and nonlinear dynamics revealed that heart beat fluctuations in healthy subjects possess a self-similar fractal structure characterized by long-range power-law correlations over a range of time scales (37, 54, 61). The scaling exponent associated with these power-law correlations was shown to change significantly with rest and exercise (13, 36, 48), posture (66, 72), sleep and wake state (29), across sleep stages (8, 32, 33, 55) and circadian phases (23, 49), and to be a reliable marker of cardiac vulnerability under pathological conditions (21, 53). Furthermore, studies have found that turbulence-like multifractal and nonlinear features in heart beat dynamics are reduced and even lost with disease (25, 27, 39). Several studies have also reported reduced heart rate variability (67; as also shown in Fig. 1), apparent loss of fractal organization, as well as breakdown of scale-invariant correlations and certain nonlinear properties with advanced age (17, 18, 31, 41, 56), suggesting that healthy aging is associated with changes in the neuroautonomic mechanism of cardiac regulation related to disintegration of coupled feedback loops across a range of time scales.

Here, we investigate how cardiac dynamics change with advanced age by analyzing scale-invariant, linear, and nonlinear characteristics of heart beat fluctuations recorded from subjects during rest and sleep from two independent databases.

DATA AND METHODS

We analyze heart beat interval recordings from two independent databases.

Fantasia Database

The Fantasia database (15a) contains 20 young and 20 elderly subjects. We carefully selected 19 healthy young subjects (9 male; 10 female) with an average age of 25.7 yr (youngest 21; oldest 34) and 16 healthy elderly subjects (6 male; 10 female) with an average age 73.8 yr (youngest 68; oldest 85). All subjects were recorded while watching the movie Fantasia (Disney, 1940) in a relaxed supine or semirecumbent posture. These conditions were chosen to avoid the effect that differences in the level of physical activity between young and elderly subjects during daily routine might have on cardiac dynamics (Fig. 1). The continuous electrocardiogram (ECG) and respiration signals were digitized at 250 Hz. Each heart beat was annotated using the ARISTOTLE arrhythmia detector (50), and each beat annotation was verified by visual inspection. Only intervals between two normal beats were considered. One young and four elderly subjects (shown in Fig. 8) were excluded from our analysis because of artifacts in the data.

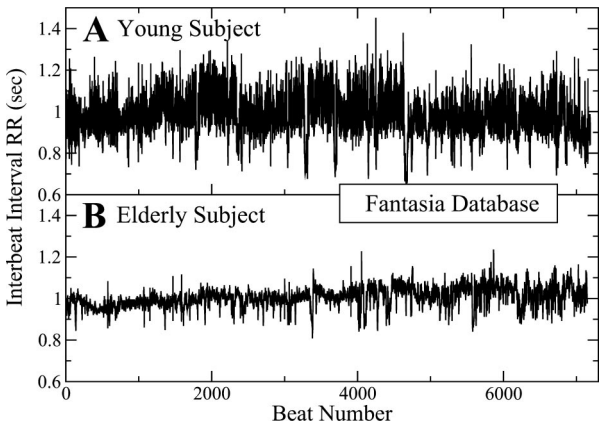

Fig. 1. Consecutive heart beat R-R intervals from a representative young healthy (*A*) and elderly (*B*) healthy subject from the Fantasia database. Under the same resting conditions elderly subjects exhibit significantly reduced heart rate variability.

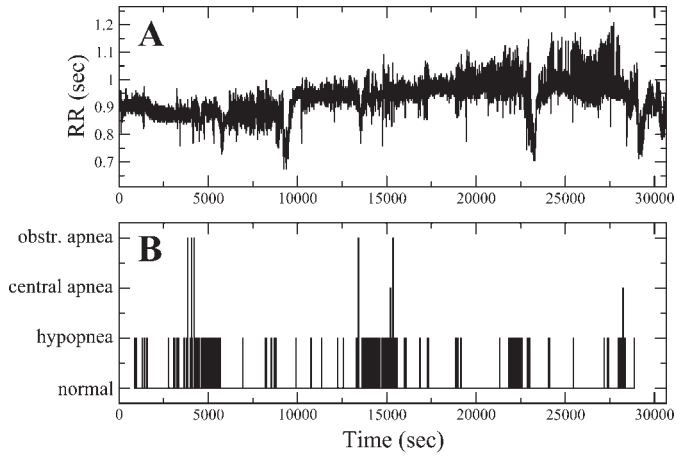

Fig. 2. Representative elderly subject from the Sleep Heart Health Study (SHHS) database. Consecutive heart beat R-R intervals (*A*) and apnea scoring (*B*).

Sleep Heart Health Study Database

The Sleep Heart Health Study (SHHS) is a prospective cohort study designed to investigate the relationship between sleep-disordered breathing and cardiovascular disease. Subjects were recorded during their habitual sleep periods of ≈8 h, and continuous ECG were recorded with 250 Hz (Fig. 2). Full details of the study design and cohort are provided in (40, 59). Details about obtaining the ECG and polysomnographic recordings are outlined (60). Sleep apnea episodes were annotated, and heart rate data during apnea (obstructive and central) were excluded from our analysis (Fig. 2). We selected a subset of 29 subjects (8 males; 21 females) with average age at the time of the first recording 75.9 yr (youngest 72; oldest 84). The recordings were repeated 5 yr later when the subjects were again screened and categorized as healthy.

Detrended Fluctuation Analysis

We use the detrended fluctuation analysis (DFA) method (52), which has been developed to quantify fractal correlations embedded in nonstationary signals, to estimate dynamic scale-invariant characteristics in heart beat fluctuations. Compared with traditional correlation analyzes such as autocorrelation, power-spectrum analysis, and Hurst analysis, the advantage of the DFA method is that it can accurately quantify the correlation property of signals masked by polynomial trends; it is described in detail in Refs. 9, 10, 22, 34, and 70.

The DFA method quantifies the detrended fluctuations $F(n)$ of a signal at different time scales n. A power-law functional form $F(n) \sim n^{\alpha}$ indicates the presence of self-similar organization in the fluctuations. The parameter α, called the scaling exponent, quantifies the correlation properties of the heart beat signal: if $\alpha = 0.5$, there is no correlation and the signal is white noise; if $\alpha = 1.5$, the signal is a random walk (Brownian motion); if $0.5 < \alpha < 1.5$, there are positive correlations, where large heart beat intervals are more likely

to be followed by large intervals (and the same is true for small heart beat intervals); if $\alpha < 0.5$ the signal is anticorrelated.

One advantage of the DFA method is that it can quantify signals with $\alpha > 1$, which cannot be done using the traditional autocorrelation and R/S analyses (14). In contrast to the conventional methods, the DFA method avoids spurious detection of apparent long-range correlations that are an artifact of nonstationary (63). Thus the DFA method is able to detect subtle temporal structures in highly heterogeneous physiological time series.

An inherent limitation of the DFA analysis is the maximum time scale $n_{\max}$ for which the fluctuation function $F(n)$ can be reliably calculated. To ensure sufficient statistics at large scales, it was shown that $n_{\max}$ should be chosen by $n_{\max} \leq N/6$, where N is the length of the signal (12, 22, 70). For time scales $n < n_{max}$ there is no bias in estimating the scaling exponent α. Thus recordings >1 h ($N \approx 3{,}600$ beats) are sufficient to reliably quantify α up to time scales $n = 600$ beats, and differences in the length of the recordings between the Fantasia database (2 h) and SHHS database (8 h) do not affect the estimate of α. Recent studies have tested the performance of the DFA method when applied to correlated signals with patches of missing data, random spikes, and superposed trends related to different activity levels and patches with different standard deviation and local correlations, as often found in heart beat data (10, 22).

Both the Fantasia database and the National Institutes of Health SHHS database have used 250-Hz sampling rate for the ECG recordings. A precision of 0.004 s (250 Hz) is more than sufficient for our analysis, since the DFA method as well as the magnitude and sign analyses (MSA) and fractal dimension analysis (FDA) analyses we employ (see below) are robust in that respect. Use of a lower sampling rate (i.e., lower precision in the estimate of the R-R intervals) acts effectively as added random noise with an amplitude proportional to the sampling interval; in our case, the amplitude of this sampling noise is more than two orders of magnitude smaller than the R-R interval. It has been shown that adding noise with such a small amplitude to a fractal correlated signal does not effect the correlation scaling and fractal properties (10).

MSA

Because the DFA method quantifies linear fractal characteristics related to two-point correlations, we have selected the MSA method to probe for long-term nonlinear properties in the data. Specifically, it has been shown that signals with identical temporal organization, quantified by the DFA-scaling exponent α, can exhibit very different nonlinear properties captured by the MSA method (5).

The MSA method (3, 4) consists of the following steps: *1*) given R-R$_i$ series we obtain the increment series, ΔR-R$_i$ = R-R$_{i+1}$ − R-R$_i$; *2*) we decompose the increment series into a magnitude series ΔR-R and a sign series (ΔR-R); *3*) to avoid artificial trends, we subtract the average from the magnitude series; *4*) because of limitations in the accuracy of the DFA method for estimating the scaling exponents of anticorrelated signals ($\alpha < 0.5$), we integrate the magnitude series (22); *5*) we perform a scaling analysis using DFA; and *6*) to obtain the scaling exponents for the magnitude series, we measure the slope of $F(n)/n$ on a log-log plot, where $F(n)$ is the fluctuation function and n is the time scale of analysis.

This approach is sensitive to nonlinear features in signals (64). We find that positive correlations in the magnitude series ($\alpha_{\text{mag}} > 0.5$) are a reliable marker of long-term nonlinear properties. Thus we employ the MSA as a complementary method to the DFA, because it can distinguish physiological signals with identical long-range correlations, as quantified by the DFA method, but with different nonlinear properties and different temporal organization for the sign(ΔR-R) series.

FDA

The fractal dimension $D(k)$ is a local nonlinear measure used to quantify the irregularity of a time series (47). We estimate the fractal dimension using an algorithm proposed previously (19).

Starting from a discrete time series, $x(i)$, with $i \in [1,N]$, a new sparse time series x_k^m is constructed in the following way

$$x_k^m;\ x(m),\ x(m+k),\ \ldots,\ x\left(m + \left\lfloor \frac{N-m}{k} \right\rfloor k\right), \qquad (1)$$

with $m \in [1,k]$ where m and k are integers, and $\lfloor (N-m)/k \rfloor$ denotes the largest integer number smaller than $(N-m)/k$. Then a length measure for this sparse time series is defined as

$$L_m(k) = \frac{N-1}{hk^2}\left(\sum_{i=1}^{h} \left| x_{ik}^m - x_{(i-1)k}^m \right|\right), \qquad (2)$$

with $h \equiv \lfloor (N-m)/k \rfloor$. For a time series $x(i)$ with a fractal dimension D the length $L_m(k)$ averaged over m is a power-law function of the scale k: $L(k) \equiv \langle L(k) \rangle_m \sim k^{-D}$. In the general case D can depend on the scale k. In this case, the local fractal dimension $D(k)$ of the time series $x(i)$ is defined as the negative local derivative of log $L(k)$ as a function of log k (Table 1).

RESULTS

Variability in Heart Beat Intervals and Their Increments

We first test the possibility that advanced age in ostensibly healthy subjects would lead to an increase in the average heart rate and to a significant reduction in heart rate variability, a behavior previously observed in subjects with congestive heart failure where under suppressed vagal tone increased heart rate is associated with reduced heart rate variability (69, 71). We find that both young and elderly healthy subjects in the Fantasia database exhibit very similar group average interbeat intervals: $\langle$R-R$\rangle \pm \sigma = 0.9 \pm 0.14$ for the young group and $\langle$R-R$\rangle \pm \sigma = 1.06 \pm 0.17$ for the elderly group, where σ is the standard deviation (Table 2). This is in agreement with

Table 1. *Overview of measures used*

Abbreviation	Measure	Significance
	Static measures	
$\langle$R-R$\rangle$ (AVNN)	Mean of R-R intervals	Inversely proportional to heart rate
$\sigma_{\text{R-R}}$ (SDNN)	SD of R-R	Para- and sympathetic HRV measure sensitive to trends
$\sigma_{\Delta\text{R-R}}$ (RMSSD)	SD of ΔR-R	Parasympathetic HRV measure insensitive to trends
	Dynamic measures	
α	Scaling exponent of R-R	Linear scale-invariant correlations
α^{mag}	Scaling exponent of $\lvert\Delta$R-R$\rvert$	Nonlinear scale-invariant correlations
α_1^{sgn}	Scaling exponent of sgn(ΔR-R)	Fractal measure of directionality
$D(k)$	Fractal dimension of R-R	Nonlinear fractal measure

Table 2. *Average values and SD of <R-R>, $\sigma_{R\text{-}R}$ (SDNN), $\sigma_{\Delta R\text{-}R}$ (RMSSD), and DFA-2 scaling exponents for subjects from the Fantasia database and the SHHS database*

	Fantasia Database			SHHS Database		
Measure	Young	Elderly	*P* Value	Elderly	Elderly + 5 yr	*P* Value
<R-R>	0.9±0.14	1.06±0.17	0.11	0.92±0.08	0.92±0.1	0.92
$\sigma_{R\text{-}R}$	0.089±0.034	0.051±0.017	**3.3×10^{-4}**	0.077±0.027	0.081±0.024	0.50
$\sigma_{\Delta R\text{-}R}$	0.061±0.031	0.027±0.012	**9.9×10^{-5}**	0.028±0.015	0.028±0.013	0.74
α_1	1.09±0.24	1.22±0.29	0.16	1.12±0.27	1.09±0.28	0.78
α_2	0.76±0.08	0.78±0.12	0.47	0.88±0.12	0.97±0.12	0.01
α_1^{mag}	0.53±0.1	0.56±0.08	0.36	0.57±0.13	0.60±0.13	0.49
α_2^{mag}	0.64±0.11	0.68±0.11	0.45	0.70±0.12	0.72±0.13	0.58
α_1^{sgn}	0.24±0.15	0.3±0.2	0.28	0.23±0.19	0.21±0.19	0.74
α_2^{sgn}	0.47±0.09	0.44±0.08	0.37	0.38±0.07	0.39±0.07	0.77

Data are averages ± SD. AVNN, average normal to normal heartbeat interval; SDNN, SD of normal to normal heartbeat interval; RMSSD, root mean square SD of normal to normal heartbeat interval. For the Fantasia database, detrended fluctuation at the time scale $n \in F(n)$] was fitted in the interval $n \in [6,16]$ for α_1 and $n \in [60,(N/6)]$ for α_2. For the Sleep Heart Health Study (SHHS) database, $F(n)$ was fitted in the interval n ∈ [6,16] for α_1 and n ∈ [60,600] for α_2. A two-tailed Student's *t*-test was performed to obtain the *P* values. *P* values that indicate significant differences between young and elderly groups are shown in bold.

previous studies (11, 31, 56). A Student's *t*-test shows no significant difference between the two groups with a *P* value = 0.11. A very similar average heart beat interval was observed for the healthy elderly subjects in the SHHS database with <R-R> ± σ = 0.92 ± 0.075, indicating no significant difference (*P* value = 0.07) compared with the group of young Fantasia subjects (Table 2). Furthermore, comparing the group average heart beat interval of the elderly subjects from the SHHS database with the same subjects recorded 5 yr later, we find again no significant difference: <R-R> ± σ = 0.92 ± 0.08 at the first recording and <R-R> ± σ = 0.92 ± 0.1 after 5 yr (*P* value = 0.92; Table 2). Thus we do not observe a significant change in the average heart rate with advanced age.

To test whether there is a reduction in heart rate variability with aging, we next estimate for each subject the standard deviation of the heart beat intervals $\sigma_{R\text{-}R}$ (often denoted as SDNN) and the standard deviation of the increments in the consecutive heart beat intervals $\sigma_{\Delta R\text{-}R}$ (often denoted as RMSSD) (Table 2). For the young and elderly subjects in the Fantasia database, we find a statistically significant difference with *1*) a higher value for the group average $<\sigma_{R\text{-}R}>$ and *2*) larger inter-subject variability for the young group: $<\sigma_{R\text{-}R}> \pm \sigma = 0.089 \pm 0.034$ for the young compared with $<\sigma_{R\text{-}R}> \pm \sigma = 0.051 \pm 0.017$ for the elderly subjects (*P* value = 3.3×10^{-4}; Table 2). Similarly, we observe a significantly higher value for the group average $<\sigma_{\Delta R\text{-}R}>$ for the young subjects in the Fantasia database ($<\sigma_{\Delta R\text{-}R}> \pm \sigma = 0.061 \pm 0.031$) compared with the elderly subjects ($<\sigma_{\Delta R\text{-}R}> \pm \sigma = 0.027 \pm 0.012$; *P* value = 9.9×10^{-5}), again with a larger intersubject variability for the young group (Table 2). We note that the sampling rate of 250 Hz does not effect the significance of the difference in $\sigma_{\Delta R\text{-}R}$ between the young and elderly groups, since this difference is ~0.034 s, i.e., one magnitude larger than the sampling precision of 0.004 s.

For the group of healthy elderly subjects from the SHHS database, we find a higher value of $<\sigma_{R\text{-}R}> \pm \sigma = 0.077 \pm 0.027$ compared with the elderly group from the Fantasia database, a difference that could be attributed to the fact that the SHHS subjects were recorded during sleep where transitions between sleep stages are associated with trends and larger fluctuations in the interbeat interval time series (32, 55), whereas the elderly Fantasia subjects were recorded during rest. In contrast, for $<\sigma_{\Delta R\text{-}R}>$, we do not observe a significant difference between the elderly groups from the Fantasia and SHHS database (*P* value = 0.74; Table 2). However, we find a significant difference between young and elderly subjects, indicating a clear reduction in the heart rate variability with aging.

Fractal Correlations

We next test whether the temporal organization in the heart beat fluctuations changes in ostensibly healthy elderly compared with young subjects. Earlier studies have shown that heart beat fluctuations exhibit self-similar power-law correlations over a broad range of time scales ranging from seconds to many hours (37, 62) and that the scaling exponents associated with these power-law correlations change significantly with sleep and wake state (29) and with pathological conditions (53, 54), reflecting changes in the underlying mechanism of cardiac regulation. Specifically, heart beat fluctuations of healthy subjects during daily activity exhibit 1/*f*-like power spectrum (37, 54, 61) with a scaling exponent $\alpha \approx 1$ (see DATA AND METHODS). During sleep, this behavior changes to exponent $\alpha \approx 0.8$ at time scales >60 beats, indicating stronger anticorrelations in the interbeat increments ΔR-R during sleep compared with the wake state (29 and Fig. 3*A*). In contrast, for pathological conditions such as congestive heart failure, earlier studies have reported a value for the exponent α closer to 1.5, which is typical for random walk behavior (Brownian motion) and associated with loss of cardiac control (53).

Applying the DFA method, we obtain a very similar scaling behavior for a representative healthy young and a healthy elderly subject from the Fantasia database, both characterized by a scaling exponent $\alpha_2 \approx 0.8$ at intermediate and large time scales (Fig. 3, *B* and *C*). At small time scales for both representative subjects, we observe a crossover to a higher exponent of $\alpha_1 \approx 1.1$ (Fig. 3, *B* and *C*). Although there is certain intersubject variability in the scaling functions $F(n)$, this crossover behavior remains robust with a group average scaling exponent $\alpha_1 \approx 1.1$ at small scales and $\alpha_2 \approx 0.75$ at large scales for the young subjects, and, respectively, $\alpha_1 \approx 1.2$ and $\alpha_2 \approx 0.8$ for the elderly subjects (see APPENDIX and Fig. 12). Our analysis indicates no significant difference in the scaling behavior between healthy young and healthy elderly subjects

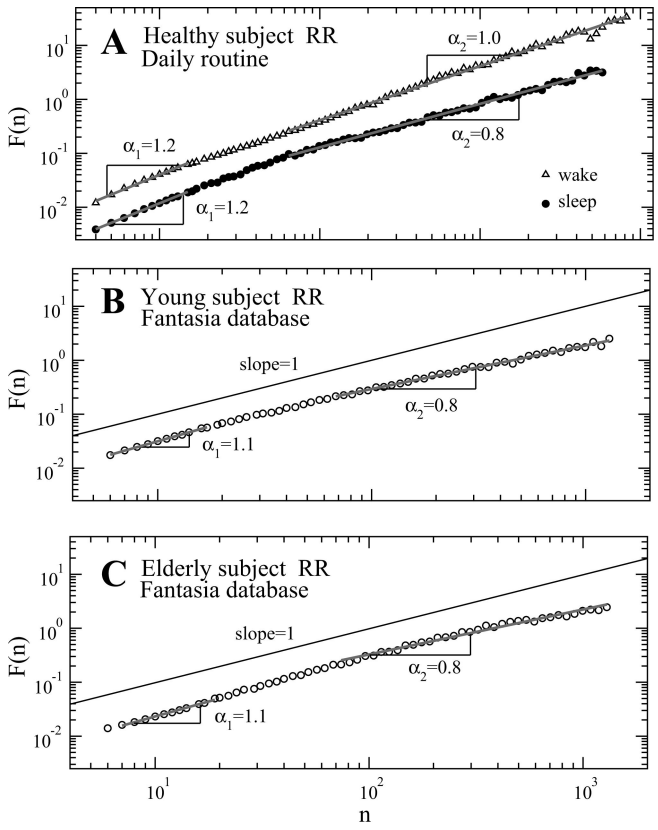

Fig. 3. Fluctuation function $F(n)$ vs. time scale n (in heart beat number) obtained using DFA-2 for 6 h-long record of R-R heart beat intervals during wake and sleep from a representative healthy subject [MIT-BIH Normal Sinus Rhythm Database (15a); *A*], as well as 2 h-long records of a representative healthy young subject (*B*) and healthy elderly subject (*C*) from the Fantasia database. A very similar scaling behavior is observed for the representative young (*B*) and elderly (*C*) subjects that closely resembles the scaling behavior of the healthy subjects during sleep shown in *A* [MIT-BIH Normal Sinus Rhythm Database (15a)], indicating no *change* in the scale-invariant temporal correlations of heart beat intervals with advanced age under healthy resting conditions. Scaling curves for all individuals are shown in APPENDIX and Fig. 12.

under the resting conditions in the Fantasia study protocol (Table 2). We note that our findings for the young and elderly Fantasia subjects (Fig. 3, *B* and *C*) are very similar to the scaling behavior in heart beat fluctuations previously reported for healthy subjects during sleep (29), which exhibit a crossover from $\alpha_1 \approx 1.2$ at small time scales to $\alpha_2 \approx 0.8$ at intermediate and large time scales (Fig. 3*A*). This similarity in the scaling properties of heart beat dynamics of healthy subjects during sleep (Fig. 3*A*) and the Fantasia database subjects (Fig. 3, *B* and *C*) may be attributed to the fact that, under the Fantasia study protocol, subjects are resting in a semirecumbent/supine posture, watching a relaxing movie, physiological conditions that more closely resemble sleep than daytime activity.

To confirm the validity of these findings, we further investigate the scale-invariant correlation properties of cardiac dynamics for healthy elderly subjects from the SHHS database, where heart rate data were recorded during sleep, a protocol that differs from the Fantasia study (see DATA AND METHODS). In Fig. 4, we show the DFA scaling curves for a representative SHHS subject with a crossover in the scaling behavior from $\alpha_1 \approx 1.1$ at small time scales to $\alpha_2 \approx 0.9$ above 60 beats. This scaling behavior is very similar to the one we find for both young and elderly subjects from the Fantasia database (Fig. 3). Furthermore, comparing the scaling behavior of the elderly subjects from the SHHS database with the same subjects recorded five years later, we do not find a significant difference in the correlation scaling exponents α_1 and α_2 (Fig. 4 and Table 2). The results shown in Figs. 3 and 4, the APPENDIX, and Fig. 12 indicate that the fractal correlation properties of healthy heart beat dynamics remain stable and do not significantly change with advanced age.

MSA

Recent studies have demonstrated that scale-invariant processes with identical long-range power-law correlations may be characterized by very different dynamics for the magnitude and sign of their fluctuations (5, 32) and that the information contained in the temporal organization of the magnitude and the sign time series is independent from the correlation properties of the original time series (3). Specifically, for cardiac dynamics of healthy subjects, it was shown (5) that heart beat intervals during routine daily activity exhibit correlation properties at intermediate and large time scales characterized by scaling exponent $\alpha_2 \approx 1$ while at the same time scales the magnitude series of the increments in consecutive heart beat intervals is characterized by $\alpha_2^{mag} \approx 0.8$. Furthermore, although correlations reflect the linear properties of heart beat dynamics, the temporal structure of the magnitude of interbeat increments has been shown to relate to the nonlinear properties encoded in the Fourier phases (3, 5, 64). For certain pathological conditions such as congestive heart failure, previous studies have reported loss of nonlinearity (57) associated with a breakdown of the multifractal spectrum (25), and reduced scaling exponent α_{mag} for the magnitude series (3).

For the magnitude time series of the interbeat increments, we obtain $\alpha_1^{mag} \approx 0.53$ at small time scales and $\alpha_2^{mag} \approx 0.68$ at intermediate and large time scales for a representative young subject (Fig. 5*A*) and very similar results with $\alpha_1^{mag} \approx 0.53$ and

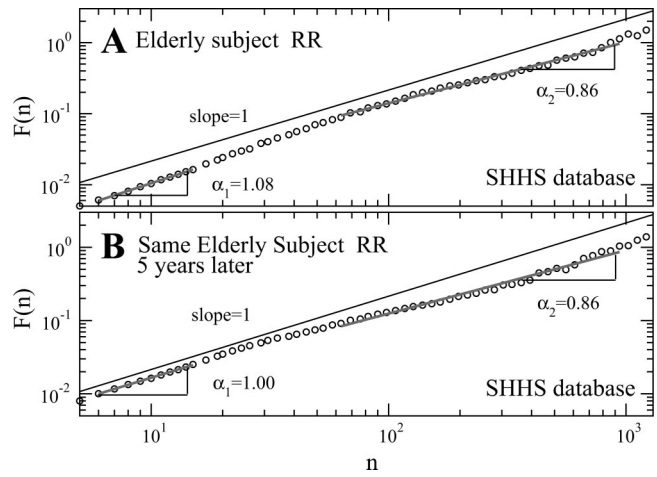

Fig. 4. Fluctuation function $F(n)$ vs. time scale n (in heart beat number) obtained from detrended fluctuation analysis (DFA)-2 for ≈8-h long records of R-R heart beat intervals during sleep for representative healthy elderly subject from the SHHS database (*A*) and the same elderly subject 5 yr later (*B*). The very similar values for the exponents α_1 and α_2 indicate no breakdown of linear fractal correlations with advanced age under healthy conditions. Note the similarity with the scaling behavior for the young subjects, shown in Fig. 3, the APPENDIX, and Fig. 12, which is not consistent with the hypothesis of a gradual loss of scale-invariant complexity in the process of aging.

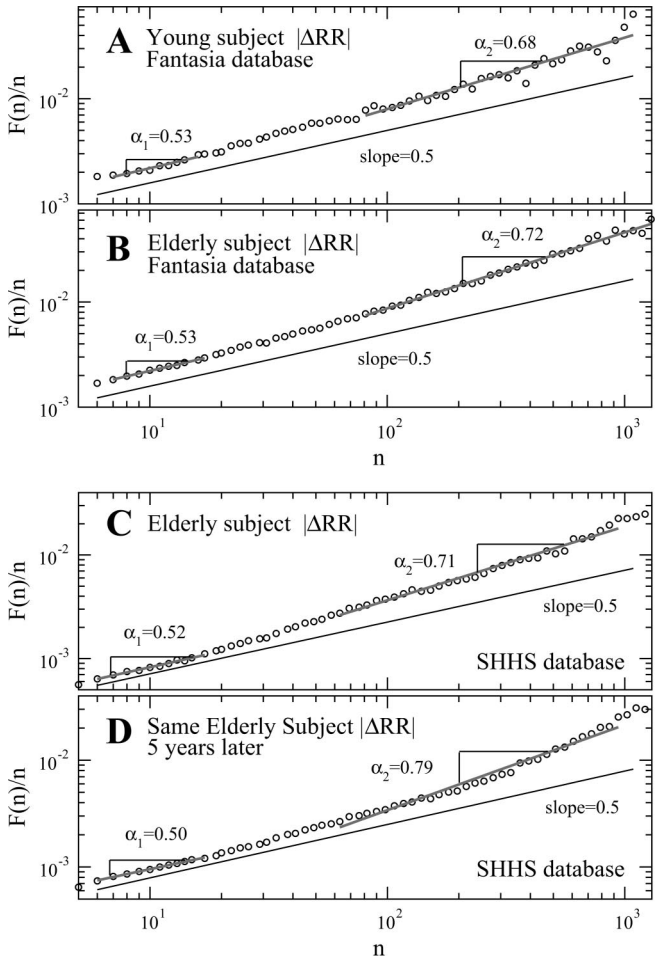

Fig. 5. Fluctuation function $F(n)$ vs. time scale n (in beat number) obtained for the magnitude of the interbeat increments (ΔR-R) using DFA-2 for a representative healthy young (*A*) and healthy elderly (*B*) subject from the Fantasia database, and for a representative healthy elderly subject from the SHHS database (*C*) and the same subject recorded 5 yr later (*D*). All subjects exhibit a very similar scaling behavior characterized by an exponent $\alpha_2^{mag} \approx 0.7$ at intermediate and large time scales, very different from $\alpha_{mag} = 0.5$ characteristic for linear processes with no correlations in the Fourier phases (3, 5), which indicates that the long-term nonlinear properties of heart beat dynamics do not break down with advanced age under healthy resting conditions. This is in contrast to the hypothesis linking the process of healthy aging with a gradual loss of nonlinearity. Scaling curves for all individuals from the Fantasia database are shown in the APPENDIX and Fig. 13.

$\alpha_2^{mag} \approx 0.72$ for a representative elderly subject from the Fantasia database (Fig. 5*B*). The DFA scaling functions $F(n)$ for all young and elderly subjects, shown in APPENDIX and Fig. 13, exhibit a consistent behavior among the subjects in each group with a smooth crossover from a group average magnitude exponent $\alpha_1^{mag} \approx 0.53$ at small and intermediate time scales to $\alpha_2^{mag} \approx 0.64$ at large scales for the young group, and a similar crossover from a group average exponent $\alpha_1^{mag} \approx 0.6$ at small and intermediate time scales to $\alpha_2^{mag} \approx 0.7$ at large scales for the elderly group (Table 2).

To confirm these findings, we next calculate the magnitude scaling exponent of the interbeat increments for the elderly subjects from the SHHS database. Again we observe a crossover from $\alpha_1^{mag} \approx 0.52$ at small scales to $\alpha_2^{mag} \approx 0.7$ at large time scales shown in Fig. 5*C* for a representative elderly subject, a behavior very similar to the one observed for both young and elderly Fantasia subjects shown in Fig. 5, *A* and *B*. Our analysis does not show a statistically significant difference in the group average magnitude scaling exponents α_1^{mag} (with P value = 0.71) and α_2^{mag} (with P value = 0.57) between the elderly SHHS subjects and the elderly Fantasia subjects. Moreover, we find no significant difference in α_1^{mag} (with P value = 0.24) and α_2^{mag} (with P value = 0.16) between the elderly SHHS subjects and the young Fantasia subjects.

For the sign of the interbeat increments time series, we again find no significant difference in the scaling behavior between the young and elderly subjects in the Fantasia database with practically identical exponents of $\alpha_1^{sgn} \approx 0.2$ at short time scales and $\alpha_2^{sgn} \approx 0.4$ at intermediate and large time scales (Fig. 6, *A* and *B*). We observed a consistently similar behavior for all subjects in the young and elderly group in the Fantasia database (APPENDIX and Fig. 14), where the scaling function $F(n)$ exhibits a crossover from strongly anticorrelated behavior at

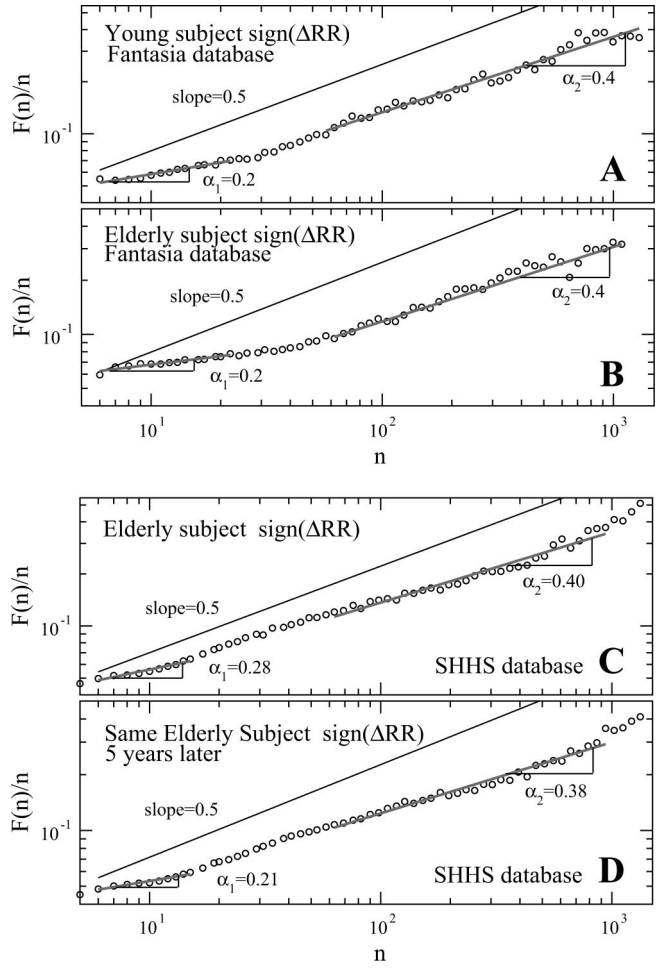

Fig. 6. Fluctuation function $F(n)$ vs. time scale n (in beat number) obtained for the sign of the interbeat increments [sign(ΔR-R)] using DFA-2 for a representative healthy young (*A*) and healthy elderly subject (*B*) in the Fantasia database, and for representative healthy elderly subject from the SHHS database (*C*) and the same elderly SHHS subject recorded 5 yr later (*D*). All subjects exhibit a very similar scaling behavior for the sign with a crossover from strong anticorrelations with $\alpha_1^{sgn} \approx 0.2$ at small time scales to weaker anticorrelations with $\alpha_2^{sgn} \approx 0.4$ at large scales, indicating a similar fractal organization of sympathetic and parasympathetic control in both young and elderly subjects under healthy resting conditions. Scaling curves for all individuals in the Fantasia database are shown in the APPENDIX and Fig. 14.

short time scales to weaker anticorrelations at larger scales, respectively, characterized by group average sign exponents $\alpha_1^{sgn} \approx 0.24$ for the young and $\alpha_1^{sgn} \approx 0.3$ for the elderly subjects at small scales and $\alpha_2^{sgn} \approx 0.47$ for the young and $\alpha_2^{sgn} \approx 0.43$ for the elderly subjects at large scales. These results indicate no significant difference in the temporal organization of the sign series between the young and the elderly subjects in the Fantasia database (Table 2).

Repeating our sign scaling analysis for the SHHS database, we observe a crossover from strongly anticorrelated behavior with an exponent $\alpha_1^{sgn} \approx 0.2$ at small time scales to weaker anticorrelations with $\alpha_2^{sgn} \approx 0.4$ at intermediate and large time scales, as shown in Fig. 6, *C* and *D*. This crossover behavior is very similar to the one we find for both young and elderly Fantasia subjects (Fig. 6, *A* and *B*, APPENDIX, and Fig. 14). Moreover, we do not find a significant difference in the scaling of the sign series for the elderly SHHS subjects and the same subjects 5 yr later (Fig. 6, *C* and *D* and Table 2).

FDA

Finally, we employ the FDA method (see DATA AND METHODS) to estimate the fractal dimension $D(k)$ of a time series (14, 19, 47). It has been demonstrated that the fractal dimension is a measure that represents the nonlinear properties in the output of a dynamical system so that two signals with identical scale-invariant correlations may be quantified by different fractal dimension depending on the degree of nonlinearity encoded in the Fourier phases (20, 64). Our analysis shows no significant difference in the group average of the nonlinear fractal dimension measure $D(k)$ between the young and the elderly subjects in the Fantasia database for the whole range of time scales except for a very short time interval of six to eight heart beats (Fig. 7*A*), which are time scales typical for sleep apnea (see Fig. 8). At smaller and larger time scales, the average fractal dimension $D(k)$ converges for both groups (Fig. 7*A*). Furthermore, we do not observe a statistically significant difference between the elderly subjects from the SHHS database and the same subjects recorded 5 yr later (Fig. 7*B*). These findings do not support the hypothesis that nonlinearity is reduced in healthy elderly subjects.

Summary of the Results

In agreement with previous studies (11, 31, 56, 65), we observe a certain degree of reduction in heart rate variability, as measured by $\sigma_{R\text{-}R}$ (SDNN) and $\sigma_{\Delta R\text{-}R}$ (RMSSD), when comparing young with elderly subjects (Table 2). In contrast to previous studies (31, 41, 56), however, we do not find a significant difference in the scaling exponents α_1 and α_2 characterizing the fractal scale-invariant temporal organization of heart beat fluctuations between young and elderly subjects (Table 2). For the scaling properties of the magnitude and the sign of heart beat fluctuations, which have been shown to carry additional independent information about the nonlinear and linear properties of a time series (3, 5, 32), we find that these measures also remain unchanged when comparing young and healthy elderly subjects (Table 2). Finally, for the fractal dimension $D(k)$ of the heart beat interval time series, an independent nonlinear measure, again contrary to previous reports (18), we do not find significant differences between young and elderly subjects. Furthermore, comparing longitudinal data from a group of elderly subjects who were also recorded 5 yr later, we find that the heart rate variability is not further reduced (Table 2) and that the scaling exponents α_1 and α_2 of the heart beat fluctuations, as well as the nonlinear features as measured by the magnitude exponent α_{mag} and the fractal dimension $D(k)$, remain stable.

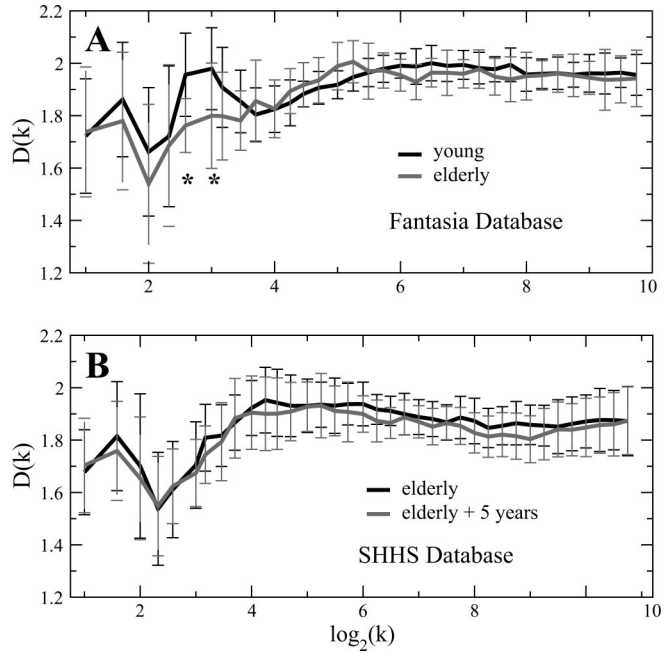

Fig. 7. Group average nonlinear fractal dimension $D(k)$ vs. time scale $\log_2 k$, where k is measured in beat numbers for young and elderly healthy Fantasia subjects (*A*) and healthy elderly SHHS subjects and the same subjects 5 yr later (*B*). There is no significant difference in the group averages indicated by the overlapping SDs except for the interval of scales $k \in [3,6]$ marked by * in *A* (P value $= 1.94 \times 10^{-4}$ and 6×10^{-3} correspondingly). Note the very similar profile of $D(k)$ for all groups, indicating no apparent loss of nonlinearity with aging, in agreement with our findings for the long-term nonlinear properties represented by the magnitude exponent α_2^{mag} shown in Fig. 5.

These findings indicate that, in the process of aging, the alterations in the underlying mechanisms of cardiac autonomic regulation are not likely to involve breakdown of coupling between feedback loops at different time scales or dominance of a particular feedback loop at a given time scale, as often observed with pathological perturbations (21, 26, 30, 38, 42, 44). Rather, our findings suggest a reduced reflexiveness of the neuroautonomic regulation with aging while the nonlinear feedback interactions across time scales between elements of the cardiac regulatory system remain unchanged.

INTERPRETATION AND MODELING

Our findings indicate that scale-invariant correlation and nonlinear properties do not significantly change in healthy elderly subjects compared with young subjects. This is in contrast to some earlier studies, based on the same Fantasia database (or on a subset of it), which have reported loss of fractal organization in heart beat fluctuations, a behavior resembling Brownian motion (random walk process) with $\alpha = 1.5$ at small scales and white noise with $\alpha = 0.5$ over large scales (31, 56), as well as a significant loss of nonlinearity (18) with healthy aging. A possible reason for these different findings may be the presence of artifacts in the data such as

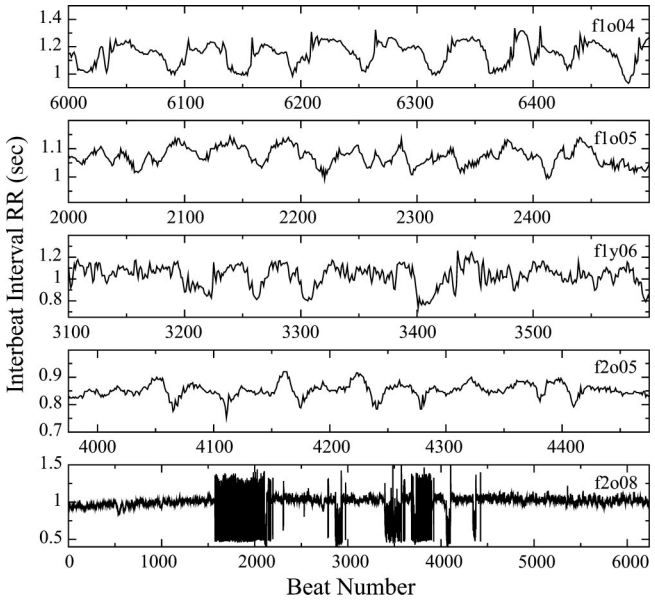

Fig. 8. Recordings of heart beat intervals from one young and four elderly subjects in the Fantasia database excluded from our analysis. The first four recordings contain many segments with well-pronounced periodic patterns, the period and amplitude of which are typical for sleep apnea (see Fig. 9). The last recording contains segments of corrupted data. These artifacts strongly influence scaling and fractal and nonlinear measures (see Figs. 10 and 11) and can lead to spurious differences between young and elderly subjects.

segments of corrupted recordings or certain periodic patterns (Fig. 8). These periodic patterns strongly resemble episodes of sleep apnea, as shown in Fig. 9*A*. Indeed, sleep apnea may be present in the elderly subjects from the Fantasia database, since they have not been specifically screened for sleep apnea. Furthermore, ECG recordings were taken when subjects were watching a calming movie for 2 h in a semirecumbent or supine posture during which subjects may have fallen asleep for periods of time, when apnea episodes are likely to occur.

The periodic patterns we observe in wide segments of the interbeat interval recordings shown in Figs. 8 and 9*A* have a period of ~30 to 60 s, typical for apnea episodes (Fig. 9*B* and Refs. 26, 30, and 58). Similar apnea-like patterns are also present in the breathing records of some Fantasia subjects (Figs. 8 and 9*A*). These periodic patterns have a very strong effect on the scaling analysis, as shown in earlier studies (22), leading to a pronounced crossover at the time scale corresponding to the period of the patterns. This crossover separates a regime of apparent Brownian-motion-type behavior with $\alpha \approx 1.5$ at smaller scales from a second regime of apparent white noise behavior $\alpha \approx 0.5$ at larger scales (Figs. 10*F* and 11), a behavior that in earlier studies (31, 56) has been spuriously attributed to changes in the cardiac neuroautonomic control due to aging.

To model the effect that periodic patterns of sleep apnea have on the scaling properties of heart beat intervals, we first generate a fractal correlated signal X_η using the Makse et al. (45) algorithm. To account for the statistical properties observed in heart beat intervals, we rescale the signal to have the mean value $<X_\eta(i)> = 1$, standard deviation $\sigma_{X\eta} = 0.05$, and correlation scaling exponent $\alpha_{X\eta} = 0.8$ (Fig. 10*A*), which match the group mean <R-R>, standard deviation $<\sigma_{R\text{-}R}>$ (Table 2), and scaling exponent value $<\alpha_2>$ (APPENDIX and Fig. 12, *C* and *D*) of the elderly subjects in the Fantasia database. To model the periodic influence of sleep apnea on the heart beat intervals, we generate a sinusoidal signal, $X_s(i) = A \sin(2\pi i/T)$, with a period $T = 50$ (similar to the average period of 50 heart beats in apnea patterns) and amplitude $A = 0.1$ (as observed in apnea patterns; Fig. 10*B*), and we superpose the sinusoidal signal X_s with the fractal correlated signal $X_\eta(i)$ to obtain $X_{\eta s}(i) = X_\eta(i) + X_s(i)$ (Fig. 10*C*). We note that $X_{\eta s}(i)$ strongly resembles the data shown in Figs. 8 and 9.

Applying the DFA analysis to the fractal signal X_η we obtain the scaling function $F_\eta(n)$ with a slope of 0.8 across all scales, in agreement with the scaling exponent $\alpha = 0.8$ we have found for healthy subjects (Fig. 10*D*). For the sinusoidal signal X_s the scaling function $F_s(n)$ exhibits a crossover at scale $n_x \approx T$, corresponding to the period of X_s. For scales $n_x < T$, the fluctuation function $F_s(n)$ exhibits an apparent scaling, $F_s(n) \sim (A/T)n^{\alpha_s}$, with an exponent $\alpha_s = 2$. For scales $n_x > T$, because of the periodic property of the sinusoidal signal X_s, the fluctuation function $F_s(n)$ is constant and independent of the scale n, i.e., $F_s(n) \sim ATn^{\alpha_s}$ where $\alpha_s = 0$. Thus changing the amplitude A leads to a vertical shift in $F_s(n)$ (Fig. 10*E* and Ref. 22).

Applying the DFA analysis to our model signal $X_{\eta s}$, we observe that $F_{\eta s}(n)$ exhibits a very pronounced kink [not present in $F_\eta(n)$] with a crossover at $n_x \approx T$ because of the sinusoidal trend (Fig. 10*F*). The behavior of $F_{\eta s}(n)$ around the kink is very similar to $F_s(n)$ around $n_x \approx T$. At small scales $n_x < T$ and at large scales $n_x > T$ the fluctuation function $F_{\eta s}(n)$ converges to the scaling behavior expected for $F_\eta(n)$. Testing our model for signals X_η with different values for α, we find that the position of the crossover n_x for $F_{\eta s}(n)$ does not depend on α. Thus this type of crossover behavior in the scaling for different subjects depends only on the period T of the periodic patterns embedded in the heart beat signals.

We find that our model in Fig. 10*F* reproduces well the crossover behavior in $F(n)$ observed for the sleep apnea subject [Apnea-ECG Database (15a) shown in Fig. 9*B*]. Indeed, a very similar kink in $F(n)$ is observed at scale $n \approx 50$ beats for this

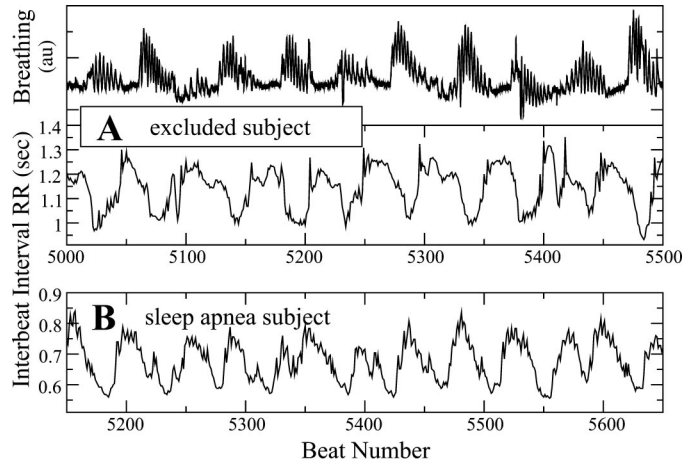

Fig. 9. Segments of interbeat R-R interval time series for (*A*) an elderly subject from the Fantasia database excluded from this study (shown in Fig. 8, *top*) and (*B*) a subject diagnosed with sleep apnea from the apnea-ECG database (see Ref. 15a). Both subjects show very similar and pronounced periodic patterns with a period of about 50 beats, matching the periodic patterns in the breathing record in *A*. These patterns strongly affect the scaling analysis as demonstrated in Figs. 10 and 11.

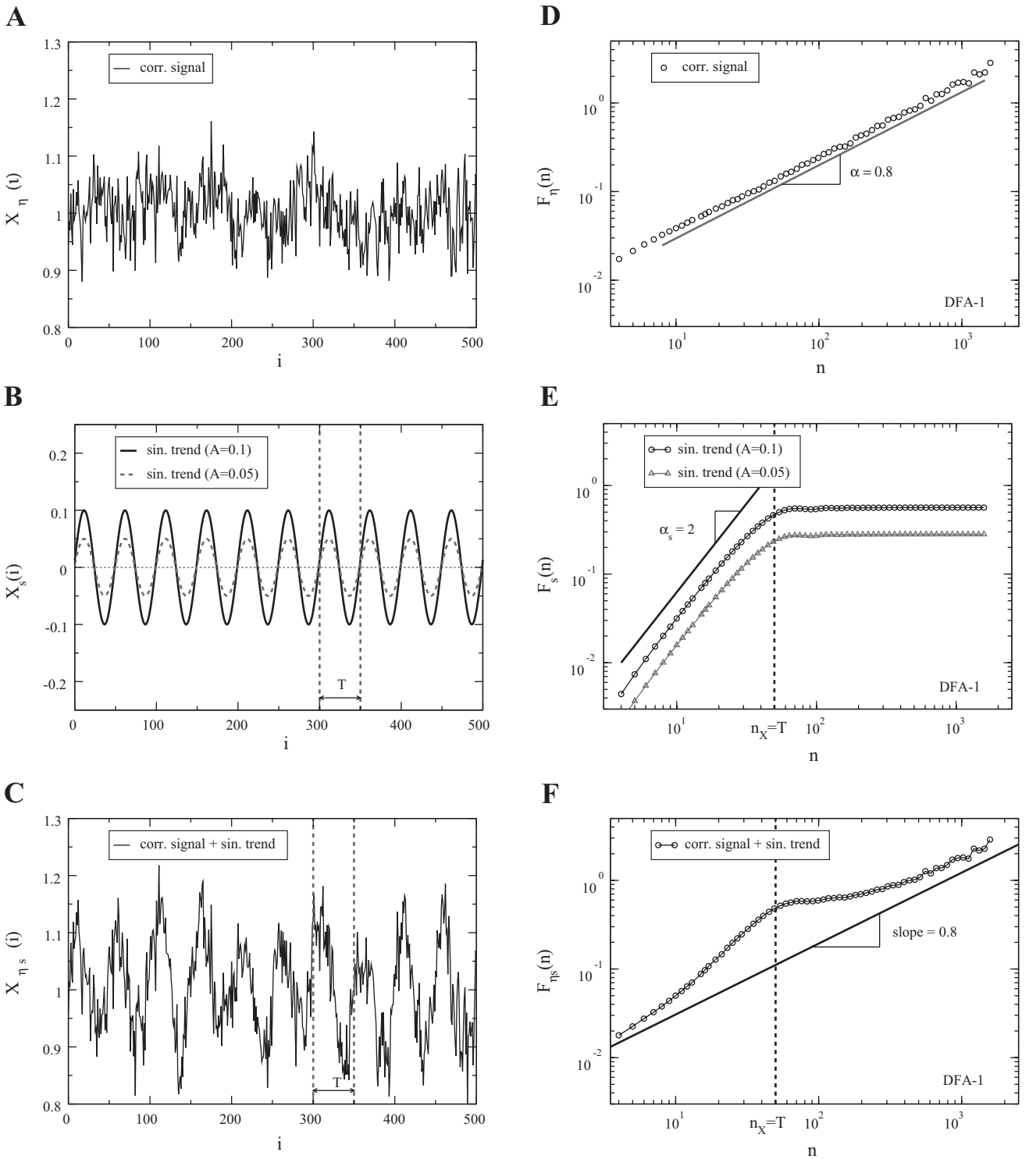

Fig. 10. Modeling crossover behavior in the scaling of heart beat dynamics associated with periodic patterns. *A*: artificially generated fractal signal X_η with long-range power-law correlations (corr), average value, and SDs as observed in healthy heart beat data. *B*: sinusoidal (sin) signal X_s with period and amplitude matching the period T and amplitude A of typical sleep apnea patterns embedded in heart beat interval time series as shown in Fig. 9. *C*: superposition of the signals X_η in *A* and X_s in *B*. Note the apparent similarity between the signal $X_{\eta s}$ and the time series shown in Fig. 9. *D*: fluctuation function $F_\eta(n)$ obtained using DFA-1 for the signal X_η in *A*. *E*: fluctuation function $F_s(n)$ obtained using DFA-1 for the signal X_s in *B*. The position of the crossover n_x corresponds to the period T in X_s. Changing the amplitude A leads to a vertical shift of $F_s(n)$. *F*: fluctuation function $F_{\eta s}(n)$ obtained using DFA-1 for the signal $X_{\eta s}$ in *C*. Note the appearance of a kink with a crossover at $n_x \approx T$ as observed in *E*.

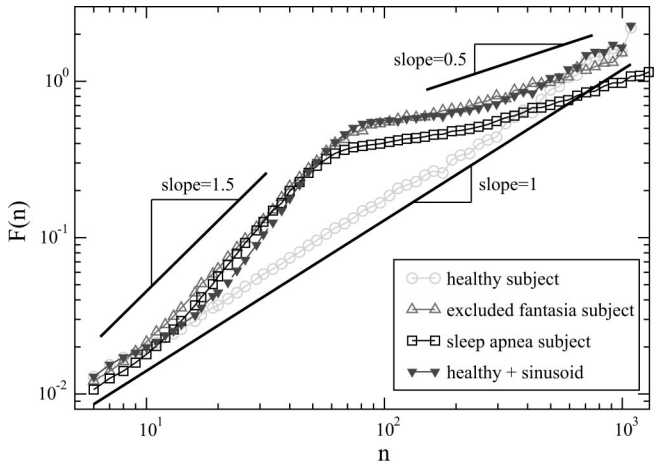

Fig. 11. Scaling functions $F(n)$ vs. time scale n obtained for the heart beat intervals using DFA-2 for a healthy subject taken from the MIT-BIH Normal Sinus Rhythm Database (15a), a Fantasia database subject we excluded from this study (15a) (shown in Fig. 9*A*), a subject with diagnosed sleep apnea (shown in Fig. 9*B*), and a healthy subject with a superposed sinusoidal signal. A period of $T = 50$ beats and an amplitude of $A = 0.1$ s were chosen for the sinusoidal signal to model the effect of periodic patterns resulting from sleep apnea on the scaling function $F(n)$. This effect leads to a change in the scaling exponent to $\alpha \approx 1.5$ (left of the crossover at T) and to $\alpha \approx 0.5$ (right of the crossover), which may be the reason why earlier studies have reported loss of fractal organization in heart beat fluctuations with healthy aging (31, 56).

apnea subject, as shown in Fig. 11. Moreover, we find that this behavior is also closely followed (as shown in Fig. 11) by the Fantasia subject in Fig. 9*A*. Adding the same sinusoidal trend to a real heart beat signal from a healthy subject [MIT-BIH Normal Sinus Rhythm Database (15a)] also leads to a very similar kink in $F(n)$ (Fig. 11).

As we demonstrate in Fig. 11, the excluded Fantasia subject shown in Fig. 9*A* exhibits a scaling curve very similar to the curve obtained from a recording during sleep from a subject diagnosed with sleep apnea [Apnea-ECG Database (15a)]. Furthermore, our model reproduces well the crossover in the scaling behavior of $F(n)$ and demonstrates that this crossover is because of the superposition of healthy heart rate dynamics and a sinusoidal trend with approximately the same period and amplitude as the periodic apnea patterns shown in Fig. 9. Our model reproduces also the scaling curve $F(n)$ obtained for the elderly Fantasia subject excluded from this study and shown in Fig. 9*A*, suggesting that artifacts may have been the reason why earlier studies (18, 31, 56) have reported scaling differences in heart beat dynamics between young and elderly subjects.

Our modeling results confirm that the presence of pronounced crossovers for some of the elderly subjects in the Fantasia database are because of periodic patterns embedded in the heart rate that strongly resemble sleep apnea episodes and, thus, cannot be attributed to changes in the underlying mechanism of cardiac neuroautonomic regulation associated with healthy aging. Because apnea is more prominent in elderly subjects, our modeling results (Figs. 10 and 11) explain why earlier studies using the same Fantasia database have reported higher values for the scaling exponent α_1 at small scales n and lower values for α_2 at large scales n for the elderly subjects compared with the group of young subjects (18, 31), claiming changes in cardiac regulation with healthy aging.

DISCUSSION

Our investigations demonstrate the presence of robust correlation, fractal, and nonlinear properties in cardiac dynamics of healthy elderly subjects that remain surprisingly stable compared with healthy young subjects. Specifically, we find that key dynamic characteristics such as the correlation scaling exponent of heart beat fluctuations, the scaling exponent of the magnitude and sign of interbeat increments, and the nonlinear fractal dimension measure do not significantly change with advanced age. Because the scaling exponents α and the fractal dimension measure D quantify a robust scale-invariant fractal and nonlinear structure in heart beat fluctuations (25, 29, 30, 53), and have been shown to reflect underlying mechanisms of cardiac control (1, 16, 27, 28), our findings indicate that important aspects of heart beat regulation do not break down with healthy aging. Moreover, we observe no significant change in these scaling and nonlinear measures when comparing healthy elderly subjects with the same subjects recorded 5 yr later.

These findings do not support the hypothesis that healthy aging may be associated with such a change in the mechanism of cardiac neuroautonomic control that would lead to a loss of all aspects of physiological complexity. In contrast, we find that fundamental scale-invariant and nonlinear properties of heart beat dynamics remain unchanged. Furthermore, our findings do not support the hypothesis of a gradual change of cardiac dynamics under healthy conditions with advanced age, since key properties of these dynamics, including heart rate variability (Table 2), remain stable in healthy elderly subjects with advancing age. Indeed, in agreement with previous studies (11, 31, 56, 65), we find a significant reduction in heart rate variability as measured by $\sigma_{R\text{-}R}$ (SDNN) and $\sigma_{\Delta R\text{-}R}$ (RMSSD) (although not in the average heart rate) in healthy elderly subjects compared with healthy young subjects (Table 2). The observed reduction in heart rate variability is also in agreement with decrease of the commonly used approximate entropy measure with aging, as reported earlier (11) and often interpreted as loss of complexity. However, comparing elderly subjects with the same subjects years later, we do not find a further reduction in interbeat variability. Moreover, we do not observe a loss in the scale-invariant fractal and nonlinear features in healthy elderly compared with healthy young subjects, indicating that the process of aging, even in elderly healthy subjects, may not result in a gradual change of the mechanism of control. Our findings support the hypothesis that *1*) only certain aspects of cardiac regulation may change with advanced age. These aspects are related to decreased responsiveness to external and internal stimuli, leading to reduced heart rate variability and *2*) other fundamental features of the neuroautonomic cardiac control may remain stable and unchanged with healthy aging. These features are related to the network of nonlinear feedback loops responsible for the neuroautonomic regulation at different time scales, leading to scale-invariant cascades in heart beat fluctuations (27, 28, 39).

This new emerging picture of healthy aging is fundamentally different from the changes in neural regulation of cardiac dynamics under pathological conditions (21, 24, 42, 43) and also differs from previous studies reporting breakdown of the scale-invariant and nonlinear features of heart beat dynamics in elderly (17, 18, 31, 41). Indeed, suppression of parasympa-

thetic tone and dominance of sympathetic inputs, typical for subjects with congestive heart failure, lead to changes in cardiac dynamics associated with higher heart rate (62, 71), lower heart rate variability (69), relative loss of the scale-invariant long-range correlations in the heart beat fluctuations with scaling exponent α between 1.25 and 1.4 (closer to $\alpha = 1.5$ corresponding to Brownian motion, i.e., random walk; see Ref. 53), reduced responsiveness (7), and breakdown of nonlinearity and multifractality (1, 25, 27, 57). In contrast to such pathological perturbations, healthy aging appears to be accompanied only by a reduction in heart rate variability as measured by $\sigma_{R\text{-}R}$ and $\sigma_{\Delta R\text{-}R}$, whereas the heart rate and the scaling and nonlinear properties remain on average unchanged. This important dissociation between heart rate variability on one side and the scale-invariant and nonlinear temporal organization of heart beat fluctuations on the other side may be specific for the process of aging and suggests that the alterations in the cardiac control mechanism with advanced age differ conceptually from the mechanistic changes in the autonomic regulation associated with pathological conditions. More specifically, the reduced heart rate variability with advanced age suggests a reduced responsiveness of cardiac control to external and internal stimuli and thus a reduced strength of feedback interactions. However, the cascade of nonlinear feedback loops (27, 28, 39) controlling the dynamics across different time scales may remain intact in healthy elderly subjects without breaking down at a particular scale or across a range of scales, since the scale-invariant fractal and nonlinear properties appear to remain stable with advanced age (Table 2). This is not the case with pathological conditions such as congestive heart failure where the self-organization of neural feedback interactions indeed breaks down across time scales, shifting the dynamics closer to a process that is more random (loss of long-range power-law correlations) and closer to a linear process (loss of nonlinearity and multifractality).

The value of the correlation exponent $\alpha_2 \approx 0.8$ we observe at intermediate and large time scales for both young and elderly Fantasia subjects (Figs. 3 and 4) is consistent with earlier reports of a very similar value of $\alpha_2 \approx 0.85$ for healthy subjects during sleep, compared with $\alpha \approx 1$ for the same subjects during wake and daily activity (29). This is also in agreement with studies of heart beat dynamics of healthy subjects during rest and exercise, with $\alpha \approx 0.8$ for rest and $\alpha \approx 1.1$ during exercise (13, 36, 48). Indeed, the Fantasia subjects were recorded under conditions of rest (see DATA AND METHODS Section I) (15a). Our findings of $\alpha \approx 0.8$ consistently for both healthy young and healthy elderly subjects from the Fantasia database are further supported by our analysis of data from the longitudinal SHHS study, where the same elderly subjects were recorded during sleep several year later. These observations of $\alpha < 1$ are not because of artifacts in the heart beat time series related to sleep apnea, since full polysomnographic data were recorded for the SHHS subjects, indicating the apnea episodes, and we have excluded the apnea segments in the data from our analysis. Moreover, our preliminary results (a focus of a subsequent study) indicate no significant differences between young and elderly subjects even when we account for rapid eye movement (REM) and non-REM (NREM) sleep stages. Because there is no statistically significant difference in the value of the scaling exponent α between the young and elderly subjects from both databases, the α value <1 is not likely to be

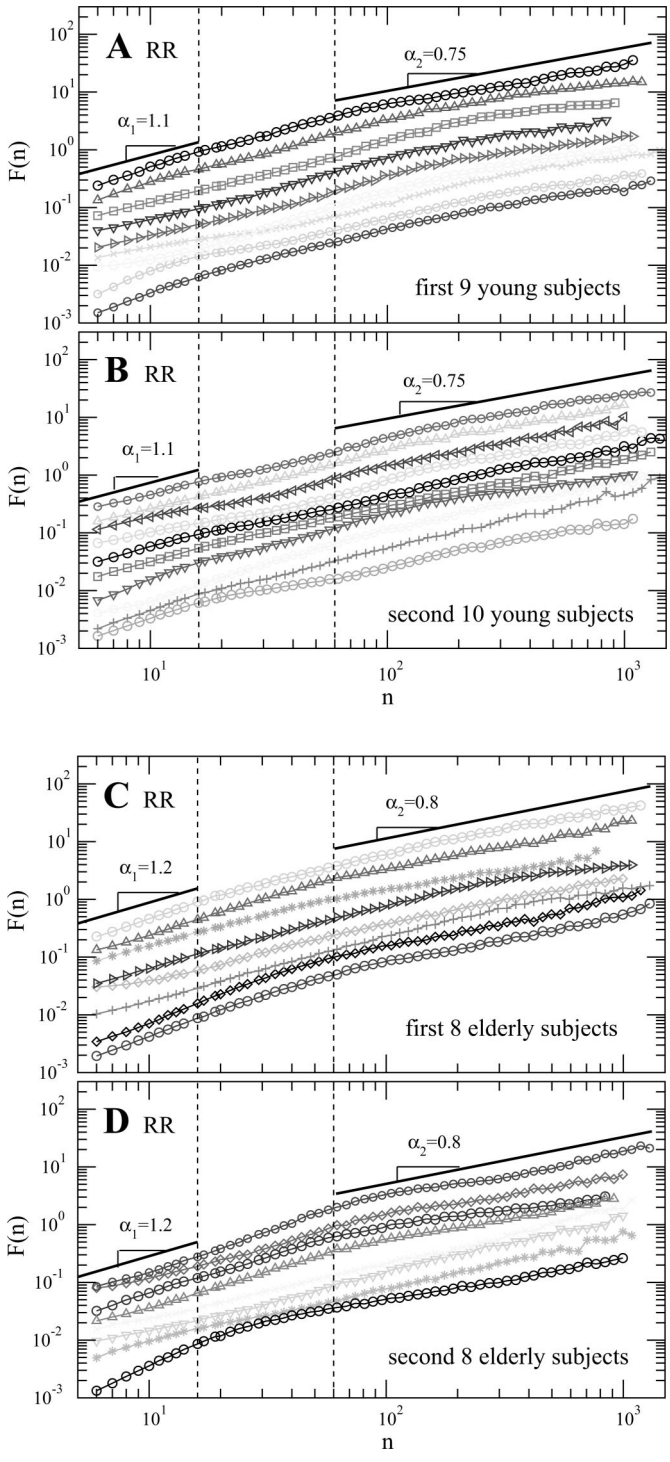

Fig. 12. Scaling curves $F(n)$ vs. time scale n (in beat numbers) obtained for the R-R heart beat intervals using DFA-2 for 19 young healthy subjects (*A* and *B*) and 16 elderly healthy subjects (*C* and *D*) in the Fantasia database. Despite certain intersubject variability, there is a very common scaling behavior with a crossover from a higher average slope α_1 at small time scales to a lower average slope α_2 at large scales as represented by the solid lines and consistent with Figs. 3 and 4. Individual curves are vertically shifted to aid visual comparison. Group average statistics are presented in Table 2. Vertical dashed lines indicate the range of fit.

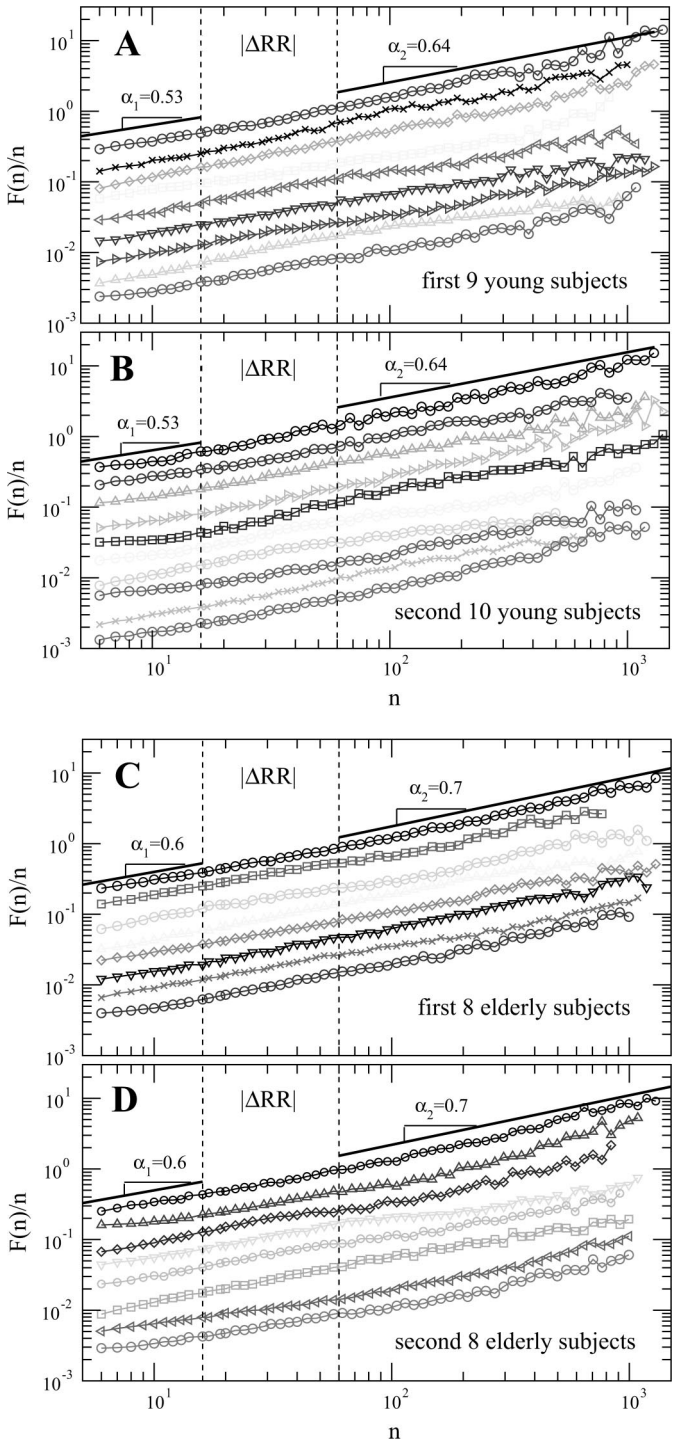

Fig. 13. Scaling curves $F(n)$ vs. time scale n (in beat numbers) obtained for the magnitude of the interbeat increments ΔR-R using DFA-2 for 19 healthy young subjects (*A* and *B*) and 16 healthy elderly subjects (*C* and *D*) in the Fantasia database. Despite certain intersubject variability, there is a common scaling behavior characterized by a group average exponent $\alpha_2 \approx 0.7$ at large scales for all groups as represented by the solid lines, indicating presence of long-term nonlinear properties encoded in the Fourier phases of the heart beat time series similar to those shown in Fig. 5. Curves are vertically shifted for clarity. Vertical dashed lines indicate the range of fit.

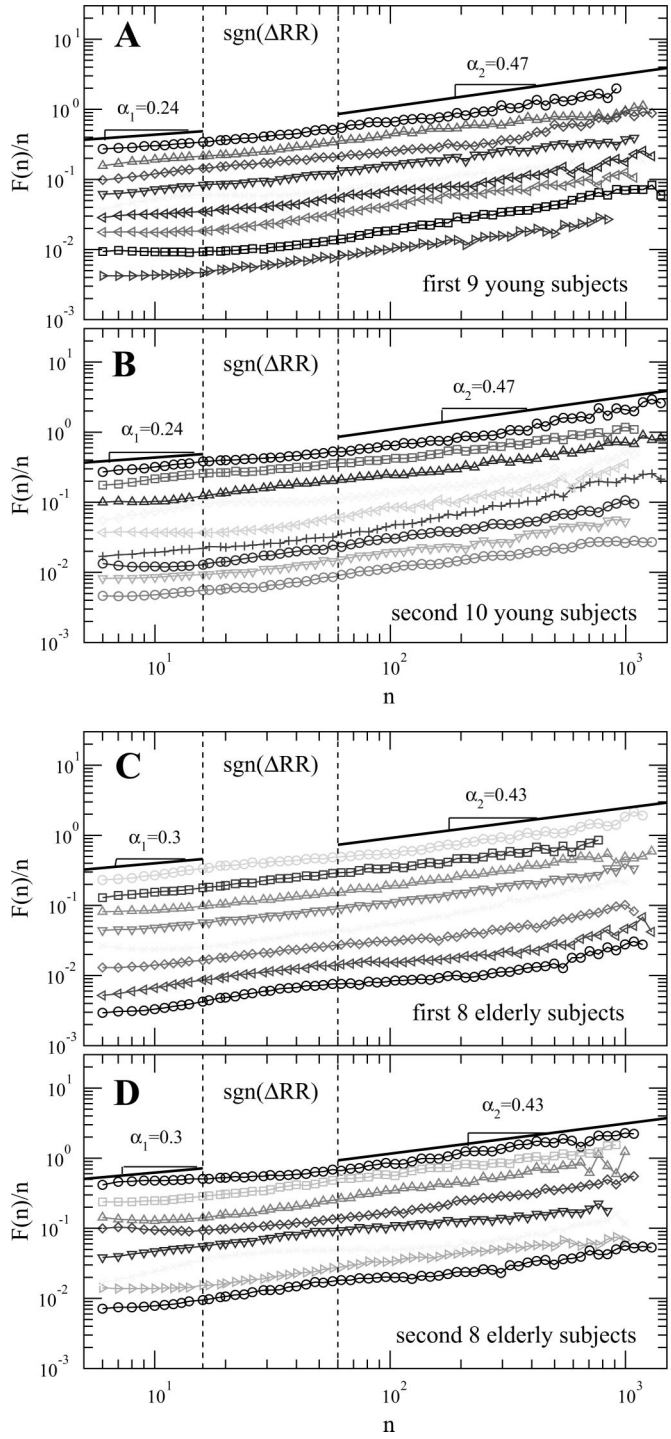

Fig. 14. Scaling curves $F(n)$ vs. time scale n (in beat numbers) obtained for the sign time series of the interbeat increments sign(ΔR-R) using DFA-2 for 19 healthy young subjects (*A* and *B*) and 16 healthy elderly subjects (*C* and *D*) in the Fantasia database. All subjects exhibit a crossover from strongly (at small scales) to weakly (at large scales) anticorrelated behavior with no significant statistical difference between the young and elderly groups (Table 2). Scaling curves are vertically shifted for clarity. Vertical dashed lines indicate the range of fit.

related to a mechanistic breakdown of cardiac control with advanced age as previously suggested (31, 56). Rather, this decrease in α is most likely to be related to the normal regime of cardiac regulation during rest and sleep when parasympa-

thetic tone dominates during NREM sleep stages, leading to stronger anticorrelations with $\alpha \approx 0.8$ in the heart beat fluctuations (8, 28, 29, 33, 36).

We find very similar results for the scaling exponent α_{mag} for the magnitude of the interbeat increments between young and elderly subjects in the Fantasia database (Table 2), as well as between the young Fantasia subjects and the elderly subjects from the SHHS database (see *P* values reported in RESULTS Section II C). These findings do not support the hypotheses that the nonlinear properties, as measured by the magnitude scaling exponent α_{mag} and encoded in the Fourier phases (64), are lost with advanced age in healthy subjects under resting conditions. We note that our results for the magnitude exponents for the young and elderly subjects from both databases are in agreement with previous studies reporting nonlinear magnitude correlations in healthy heart beat dynamics (5) and more specifically with the magnitude exponent values found in the heart rate of healthy subjects during sleep (32, 33).

Furthermore, because the dynamics of the sign (directionality) of the interbeat increments is directly related to inputs of the sympathetic and parasympathetic branches of the autonomic nervous system modulating the heart rate in opposite directions, our findings of similar scaling for the sign series for both young and elderly healthy subjects (Table 2) indicate that fundamental features of the cardiac control mechanism remain unchanged with advanced age. We also note that our results for the sign scaling exponent α^{sgn} for the young and elderly subjects from both databases are in agreement with the values reported in previous studies for healthy subjects during rest (36) and sleep (32).

Although our results do not show a significant difference in the scaling and nonlinear properties of heart beat dynamics between healthy young and healthy elderly subjects during rest and sleep, we note that, under conditions of high levels of physical activity and stress, which are associated with a different regime of the neuroautonomic control, these properties may differ between young and elderly subjects.

In summary, the observations reported here do not support the hypothesis of a continuous gradual loss of the scaling and nonlinear properties of cardiac dynamics with advanced age under healthy conditions, since we do not find a statistically significant change in these properties between the young and elderly subjects from the Fantasia and the SHHS databases as well as for the elderly subjects from the SHHS database and the same subjects recorded five years later. Although cardiac dynamics in healthy elderly subjects is characterized by markedly reduced variability compared with healthy young subjects, the stability we observe in key fractal and nonlinear characteristics with advanced age does not support the mechanistic view of a breakdown of specific feedback loops at given time scales in the neuroautonomic regulation (which would lead to appearance of dominant time scales in the dynamics) or of a breakdown of the feedback interactions in cardiac control across multiple time scales (which would lead to random-like behavior in the dynamics). Indeed, both dominant time scales and close-to-random behavior in cardiac dynamics have been observed under various pathological conditions. In contrast, cardiac dynamics under healthy aging appears not to belong to this class of processes. Instead, our results indicate that the inherent structure and temporal organization in the cascades of nonlinear feedback loops underlying the cardiac neuroautonomic regulation remain intact in healthy elderly subjects, thus preserving the fractal and nonlinear features in heart beat dynamics across all time scales. The coupling strength of these neuronal feedback interactions, however, is likely to diminish with advanced age, leading to the observed reduction in heart rate variability and dampened responsiveness in elderly compared to young healthy subjects.

APPENDIX

Results of DFA and MSA Analyses for the Heartbeat Interval Recordings for All Young and Elderly Subjects in the Fantasia Database

All subjects show a consistent behavior with: *1*) a smooth crossover from $\alpha_1 \approx 1.1$ at small time scales to $\alpha_2 \approx 0.8$ at large scales for the heart beat intervals R-R for both the young and the elderly group (Fig. 12); *2*) a smooth crossover from $\alpha_1^{mag} \approx 0.6$ at small time scales to $\alpha_2^{mag} \approx 0.7$ at large scales for the magnitude of the interbeat increments ΔR-R for both the young and the elderly group (Fig. 13); and *3*) a crossover from $\alpha_1^{sgn} \approx 0.3$ at small time scales to $\alpha_2^{sgn} \approx 0.45$ at large scales for the sign of the interbeat increments sign(ΔR-R) for both the young and the elderly group (Fig. 14).

The results show that these fractal correlation and nonlinear properties of heartbeat dynamics do not break down with healthy aging.

ACKNOWLEDGMENTS

We thank George B. Moody for discussions and help with the ARISTOTLE ECG-annotator.

This paper represents the work of the authors and not the Sleep Heart Health Study.

GRANTS

This work was supported by National Heart, Lung, and Blood Institute Grant 2 RO1 HL-071972 and the Volkswagen Foundation.

REFERENCES

1. **Amaral LAN, Ivanov PCh, Aoyagi N, Hidaka I, Tomono S, Goldberger AL, Stanley HE, Yamamoto Y.** Behavioral-independent features of complex heartbeat dynamics. *Phys Rev Lett* 86: 6026–6029, 2001.
2. **Arking R.** *Biology of Aging: Observations and Principles* (3rd ed). Oxford, UK: Oxford Univ Press, 2006.
3. **Ashkenazy Y, Havlin S, Ivanov PCh, Peng CK, Schulte-Frohlinde V, Stanley HE.** Magnitude and sign scaling in power-law correlated time series. *Physica A* 323: 19–41, 2003.
4. **Ashkenazy Y, Ivanov PCh, Havlin S, Peng CK, Yamamoto Y, Goldberger AL, Stanley HE.** Decomposition of heartbeat time series: scaling analysis of the sign sequence. *Comput Cardiol* 27: 139–142, 2000.
5. **Ashkenazy Y, Ivanov PCh, Havlin S, Peng CK, Goldberger AL, Stanley HE.** Magnitude and Sign Correlations in Heartbeat Fluctuations. *Phys Rev Lett* 86: 1900–1903, 2001.
6. **Bassingthwaighte JB, Liebovitch L, West BJ.** *Fractal Physiology*. Osford, UK: Oxford Univ Press, 1994.
7. **Bernaola-Galván P, Ivanov PCh, Amaral LAN, Stanley HE.** Scale invariance in the nonstationarity of human heart rate. *Phys Rev Lett* 87: 168105, 2001.
8. **Bunde A, Havlin S, Kantelhardt JW, Penzel T, Peter JH, Voigt K.** Correlated and Uncorrelated Regions in Heart-Rate Fluctuations during Sleep. *Phys Rev Lett* 85: 3736–3739, 2000.
9. **Chen Z, Hu K, Carpena P, Bernaola-Galvan P, Stanley HE, Ivanov PCh.** Effect of nonlinear filters on detrended fluctuation analysis. *Phys Rev E* 71: 011104, 2005.
10. **Chen Z, Ivanov PCh, Hu K, Stanley HE.** Effect of nonstationarities on detrended fluctuation analysis. *Phys Rev E* 65: 041107, 2002.
11. **Corino VDA, Matteuccib M, Cravelloc L, Ferraric E, Ferrarid AA, Mainardi LT.** Long-term heart rate variability as a predictor of patient age. *Comp Method Prog Biomed* 82: 248–257, 2006.
12. **Coronado AV, Carpena P.** Size effects on correlation measures. *J Biol Phys* 31: 121–133, 2005.

13. **Echeverria JC, Aguilar SD, Ortiz MR, Alvarez-Ramirez J, González-Camarena R.** Comparison of R-R-interval scaling exponents derived from long and short segments at different wake periods. *Physiol Meas* 27: N19–N25, 2006.
14. **Feder J.** *Fractals*. New York, NY: Plenum, 1988.
15. **Glass L, Malta CP.** Chaos in multiloop negative feedback-systems (Abstract). *J Theor Biol* 145: 217, 1990.
15a. **Goldberger AL, Amaral LAN, Glass L, Hausdorff JM, Ivanov PCh, Mark RG, Mietus JE, Moody GB, Peng CK, Stanley HE.** PhysioBank, PhysioToolkit, and Physionet: components of a new research resource for complex physiologic signals. *Circulation* 101: e215–e220, 2000 (http://physionet.org/physiobank/).
16. **Goldberger AL, Amaral LAN, Hausdorff JM, Ivanov PCh, Peng CK, Stanley HE.** Fractal dynamics in physiology: alterations with disease and aging. *Proc Natl Acad Sci USA* 99: 2466–2472, 2002.
17. **Goldberger AL, Peng CK, Lipsitz LA.** What is physiological complexity and how does it change with aging and disease? *Neurobiol Aging* 23: 23–26, 2002.
18. **Guzmán-Vargas L, Angulo-Brown F.** Simple model of the aging effect in heart interbeat time series. *Phys Rev E* 67: 052901, 2003.
19. **Higuchi T.** Approach to an irregular time series on the basis of the fractal theory. *Physica D* 31: 277–283, 1988.
20. **Higuchi T.** Relationship between the fractal dimension and the power law index for a time series: a numerical investigation. *Phys D* 46: 254–264, 1990.
21. **Ho KKL, Moody GB, Peng CK, Mietus JE, Larson MG, Levy D, Goldberger AL.** Predicting survival in heart failure cases and controls using fully automated methods for deriving nonlinear and conventional indices of heart rate dynamics. *Circulation* 96: 842–848, 1997.
22. **Hu K, Ivanov PCh, Chen Z, Carpena P, Stanley HE.** Effects of trends on detrended fluctuation analysis. *Phys Rev E* 64: 011114, 2001.
23. **Hu K, Ivanov PCh, Hilton MF, Chen Z, Ayers RT, Stanley HE, Shea SA.** Endogenous circadian rhythm in an index of cardiac vulnerability independent of changes in behavior. *Proc Natl Acad Sci USA* 101: 18223–18227, 2004.
24. **Huikuri HV, Mäkikallio TH, Peng CK, Goldberger AL, Hintze U, Moller M.** Fractal correlation properties of R-R interval dynamics and mortality in patients with depressed left ventricular function after an acute myocardial infarction. *Circulation* 101: 47–53, 2000.
25. **Ivanov PCh, Rosenblum MG, Amaral LAN, Struzik ZR, Havlin S, Goldberger AL, Stanley HE.** Multifractality in human heartbeat dynamics. *Nature* 399: 461–465, 1999.
26. **Ivanov PCh, Rosenblum MG, Peng CK, Mietus J, Havlin S, Stanley HE, Goldberger AL.** Scaling and universality in heart rate variability distributions. *Physica A* 249: 587–593, 1998.
27. **Ivanov PCh, Amaral LAN, Goldberger AL, Havlin S, Rosenblum MG, Stanley HE, Struzik Z.** From 1/*f* noise to multifractal cascades in heartbeat dynamics. *Chaos* 11: 641–652, 2001.
28. **Ivanov PCh, Amaral LAN, Goldberger AL, Stanley HE.** Stochastic feedback and the regulation of biological rhythms. *Europhys Lett* 43: 363–368, 1998.
29. **Ivanov PCh, Bunde A, Amaral LAN, Havlin S, Fritsch-Yelle J, Baevsky RM, Stanley HE, Goldberger AL.** Sleep-wake differences in scaling behavior of the human heartbeat: analysis of terrestrial and long-term space flight data. *Europhys Lett* 48: 594–600, 1999.
30. **Ivanov PCh, Rosenblum MG, Peng CK, Mietus J, Havlin S, Stanley HE, Goldberger AL.** Scaling behaviour of heartbeat intervals obtained by wavelet-based time-series analysis. *Nature* 383: 323–327, 1996.
31. **Iyengar N, Peng CK, Morin R, Goldberger AL, Lipsitz LA.** Age-related alterations in the fractal scaling of cardiac interbeat interval dynamics. *Am J Physiol Regul Integr Comp Physiol* 271: R1078–R1084, 1996.
32. **Kantelhardt JW, Ashkenazy Y, Ivanov PCh, Bunde A, Havlin S, Penzel T, Peter J, Stanley HE.** Characterization of sleep stages by correlations in the magnitude and sign of heartbeat increments. *Phys Rev E* 65: 051908, 2002.
33. **Kantelhardt JW, Havlin S, Ivanov PCh.** Modeling transient correlations in heartbeat dynamics during sleep. *Europhys Lett* 62: 147–153, 2003.
34. **Kantelhardt JW, Koscielny-Bunde E, Rego HHA, Havlin S, Bunde A.** Detecting long-range correlations with detrended fluctuation analysis. *Physica A* 295: 441–454, 2001.
35. **Kaplan DT, Furman MI, Pincus SM, Ryan SM, Lipsitz LA, Goldberger AL.** Aging and the complexity of cardiovascular dynamics. *Biophys J* 59: 945–949, 1991.
36. **Karasik R, Sapir N, Ashkenazy Y, Ivanov PCh, Dvir I, Lavie Pz, Havlin S.** Correlation differences in heartbeat fluctuations during rest and exercise. *Phys Rev E* 66: 062902, 2002.
37. **Kobayashi M, Musha T.** 1/*f* fluctuation of heartbeat period. *IEEE Trans Biomed Eng* 29: 456–457, 1982.
38. **Kurths J, Voss A, Saparin P, Witt A, Kleiner HJ, Wessel N.** Quantitative analysis of heart rate variability. *Chaos* 5: 88–94, 1995.
39. **Lin DC, Hughson RL.** Modeling heart rate variability in healthy humans: a turbulence analogy. *Phys Rev Lett* 86: 1650–1653, 2001.
40. **Lind BK, Goodwin JL, Hill JG, Ali T, Redline S, Quan SF.** Recruitment of healthy adults into a study of overnight sleep monitoring in the home: experience of the sleep heart health study. *Sleep Breath* 7: 13–24, 2003.
41. **Lipsitz LA, Goldberger AL.** Loss of "complexity" aging. Potential applications of fractals and chaos theory to senescence. *J Am Med Assoc* 267: 1806–1809, 1992.
42. **Mäkikallio TH, Seppänen T, Airaksinen KEJ, Koistinen J, Tulppo MP, Peng CK.** Dynamic analysis of heart rate may predict subsequent ventricular tachycardia after myocardial infarction. *Am J Cardiol* 80: 779–783, 1997.
43. **Mäkikallio TH, Jalonen JR, Helenius H, Sariola-Heinonena K, Yli-Mayry S, Scheinin H.** Correlation properties and complexity of perioperative R-R-interval dynamics in coronary artery bypass surgery patients. *Anesthesiology* 93: 69–80, 2000.
44. **Mäkikallio TH, Ristimäe T, Airaksinen KEJ, Peng CK, Goldberger AL, Huikuri HV.** Heart rate dynamics in patients with stable angina pectoris and utility of fractal and complexity measures. *Am J Cardiol* 81: 27–31, 1998.
45. **Makse HA, Havlin S, Schwartz M, Stanley HE.** Method for generating long-range correlations for large systems. *Phys Rev E* 53: 5445–5449, 1996.
46. **Malik M, Camm AJ.** *Heart Rate Variability*. Armonk, NY: Futura, 1995.
47. **Mandelbrot Benoit B.** *Fractals: Form, Chance and Dimension*. San Francisco, CA: Freeman, 1977.
48. **Martinis M, Knezevic A, Krstacic G, Vargovic E.** Changes in the Hurst exponent of heartbeat intervals during physical activity. *Phys Rev E* 70: 012903, 2004.
49. **Moelgaard H, Soerensen KE, Bjerregaard P.** Circadian variation and influence of risk factors on heart rate variability in healthy subjects. *Am J Cardiol* 68: 777–784, 1991.
50. **Moody GB, Mark RG.** Development and evaluation of a 2-lead ECG analysis program. *Comp Cardiol* 9: 39–44, 1982.
51. **O'Brien IA, O'Hare P, Corrall RJ.** Heart rate variability in healthy subjects: effect of age and the derivation of normal ranges for tests of autonomic function. *Brit Heart J* 55: 348–354, 1986.
52. **Peng CK, Buldyrev SV, Havlin S, Simons M, Stanley HE, Goldberger AL.** Mosaic organization of DNA nucleotides. *Phys Rev E* 49: 1685–1689, 1994.
53. **Peng CK, Havlin S, Stanley HE, Goldberger AL.** Quantification of scaling exponents and crossover phenomena in nonstationary heartbeat time series. *Chaos* 5: 82–87, 1995.
54. **Peng CK, Mietus J, Hausdorff JM, Havlin S, Stanley HE, Goldberger AL.** Long-range anticorrelations and non-Gaussian behavior of the heartbeat. *Phys Rev Lett* 70: 1343–1346, 1993.
55. **Penzel T, Kantelhardt JW, Grote L, Peter JH, Bunde A.** Comparison of detrended fluctuation analysis and spectral analysis for heart rate variability in sleep and sleep apnea. *IEEE Trans Biomed Eng* 50: 1143–1151, 2003.
56. **Pikkujämsä SM, Mäkikallio TH, Sourander LB, Räihä IJ, Puukka P, Skyttä J, Peng C, Goldberger AL, Huikuri HV.** Cardiac interbeat interval dynamics from childhood to senescence—comparison of conventional and new measures based on fractals and chaos theory. *Circulation* 100: 393–399, 1999.
57. **Poon CS, Merrill CK.** Decrease of cardiac chaos in congestive heart failure. *Nature* 389: 492–495, 1997.
58. **Quan SF, Gillin JC, Littner MR, Shepard JW.** Sleep-related breathing disorders in adults: recommendations for syndrome definition and measurement techniques in clinical research. *Sleep* 22: 662–689, 1999.
59. **Quan S, Howard B, Iber C, Kiley J, Nieto F, O'Connor G, Rapoport D, Redline S, Robbins J, Samet J, Wahl P.** The Sleep Heart Health Study: design, rationale, and methods. *Sleep* 20: 1077–1085, 1997.
60. **Redline S, Sanders MH, Lind BK, Quan SF, Iber C, Gottlieb DJ, Bonekat WH, Rapoport DM, Smith PL, Kiley JP.** Methods for obtaining and analyzing unattended polysomnography data for a multicenter study. Sleep Heart Health Research Group. *Sleep* 21: 759–767, 1998.

61. **Saul JP, Albrecht P, Berger RD, Cohen RJ.** Analysis of long term heart rate variability: methods, 1/f scaling, and implications. *Comput Cardiol* 14: 419–422, 1988.
62. **Saul JP, Arai Y, Berger RD, Lilly LS, Colucci WS, Cohen RJ.** Assessment of autonomic regulation in chronic congestive heart failure by heart rate spectral analysis. *Am J Cardiol* 61: 1292–1299, 1988.
63. **Taqqu M, Teverovsky V, Willinger W.** Estimators for long-range dependence: an empirical study. *Fractals* 3: 785–788, 1995.
64. **Theiler J, Eubank S, Longtin A, Galdrikian B, Garmer DJ.** Testing for nonlinearity in time series: the method of surrogate data. *Physica D* 58: 77–94, 1992.
65. **Tsuji H, Venditti FJ, Manders ES, Evans JC, Larson MG, Feldman CL, Levy D.** Reduced heart rate variability and mortality risk in an elderly cohort. The Framingham Heart Study. *Circulation* 90: 878–883, 1994.
66. **Tulppo MP, Hughson RL, Mäkikallio TH, Airaksinen KEJ, Seppänen T, Huikuri HV.** Effects of exercise and passive head-up tilt on fractal and complexity properties of heart rate dynamics. *Am J Physiol Heart Circ Physiol* 280: H1081–H1087, 2001.
67. **Umetani K, Singer DH, McCraty R, Atkinson M.** Twenty-four hour time domain heart rate variability and heart rate: relations to age and gender over nine decades. *J Am Coll Cardiol* 31: 593–601, 1998.
68. **Vaillancourt DE, Newell KM.** Changing complexity in human behavior and physiology through aging and disease. *Neurobiol Aging* 23: 1–11, 2002.
69. **Wolf MM, Varigos GA, Hunt D, Sloman JG.** Sinus arrhythmia in acute myocardial infarction. *Med J Austral* 2: 52–53, 1978.
70. **Xu L, Ivanov PCh, Hu K, Chen Z, Carbone A, Stanley HE.** Quantifying signals with power-law correlations: a comparative study of detrended fluctuation analysis and detrended moving average techniques. *Phys Rev E* 71: 051101, 2005.
71. **Yamamoto Y, Nakamura Y, Sato H, Yamamoto M, Kato K, Hughson RL.** On the fractal nature of heart rate variability in humans: effects of vagal blockade. *Am J Physiol Regul Integr Comp Physiol* 269: R830–R837, 1995.
72. **Yeragani VK, Berger R, Balon R, Srinivasan K.** Relationship between age and heart rate variability in supine and standing postures: a study of spectral analysis of heart rate. *Pediatr Cardiol* 15: 14–20, 1994.

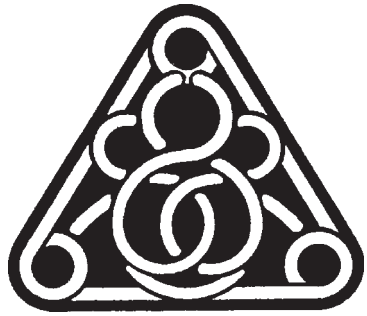

Fractal scale-invariant and nonlinear properties of cardiac dynamics remain stable with advanced age: a new mechanistic picture of cardiac control in healthy elderly

By: Schmitt, DT (Schmitt, Daniel T.); Ivanov, PC (Ivanov, Plamen Ch.)

View ResearcherID and ORCID

AMERICAN JOURNAL OF PHYSIOLOGY-REGULATORY INTEGRATIVE AND COMPARATIVE PHYSIOLOGY

Volume: 293 **Issue:** 5 **Pages:** R1923-R1937

DOI: 10.1152/ajpregu.00372.2007

Published: NOV 2007

Document Type: Article

View Journal Impact

Abstract

Heart beat fluctuations exhibit temporal structure with robust long-range correlations, fractal and nonlinear features, which have been found to break down with pathologic conditions, reflecting changes in the mechanism of neuroautonomic control. It has been hypothesized that these features change and even break down also with advanced age, suggesting fundamental alterations in cardiac control with aging. Here we test this hypothesis. We analyze heart beat interval recordings from the following two independent databases: 1) 19 healthy young (average age 25.7 yr) and 16 healthy elderly subjects (average age 73.8 yr) during 2 h under resting conditions from the Fantasia database; and 2) 29 healthy elderly subjects (average age 75.9 yr) during approximate to 8 h of sleep from the sleep heart health study (SHHS)database, and the same subjects recorded 5 yr later. We quantify: 1) the average heart rate (< R-R >); 2) the SD sigma(R-R) and sigma(Delta R-R) of the heart beat intervals R- R and their increments Delta R-R; 3) the long-range correlations in R- R as measured by the scaling exponent < R-R using the Detrended Fluctuation Analysis; 4) fractal linear and nonlinear properties as represented by the scaling exponents alpha(sgn) and alpha(mag) for the time series of the sign and magnitude of Delta R-R; and 5) the nonlinear fractal dimension D(k) of R-R using the fractal dimension analysis. We find: 1) No significant difference in (P > 0.05); 2) a significant difference in sigma(R-R) and sigma(Delta R-R) for the Fantasia groups (P < 10 (-4)) but no significant change with age between the elderly SHHS groups (P > 0.5); and 3) no significant change in the fractal measures alpha(R-R) (P > 0.15), alpha(sgn) (P > 0.2), alpha(mag) (P > 0.3), and D(k) with age. Our findings do not support the hypothesis that fractal linear and nonlinear characteristics of heart beat dynamics break down with advanced age in healthy subjects. Although our results indeed show a reduced SD of heart beat fluctuations with advanced age, the inherent temporal fractal and nonlinear organization of these fluctuations remains stable. This indicates that the coupled cascade of nonlinear feedback loops, which are believed to underlie cardiac neuroautonomic regulation, remains intact with advanced age.

Keywords

Author Keywords: aging; dynamics; heart rate; nervous system; autonomic; physiology; sleep; fractals; nonlinearity; scaling

KeyWords Plus: HEART-RATE-VARIABILITY; DETRENDED FLUCTUATION ANALYSIS; ACUTE MYOCARDIAL-INFARCTION; LONG-RANGE CORRELATIONS; TIME-SERIES; INTERVAL DYNAMICS; SPECTRAL-ANALYSIS; CHAOS THEORY; COMPLEXITY; SLEEP

Author Information

Reprint Address: Ivanov, PC (reprint author)

+ Boston Univ, Ctr Polymer Studies, Boston, MA 02215 USA.

Addresses:

+ [1] Boston Univ, Ctr Polymer Studies, Boston, MA 02215 USA
+ [2] Boston Univ, Dept Phys, Boston, MA 02215 USA
+ [3] Univ Ulm, Ulm, Germany
+ [4] Harvard Univ, Sch Med, Boston, MA USA
+ [5] Brigham & Womens Hosp, Div Sleep Med, Boston, MA 02115 USA

E-mail Addresses: plamen@buphy.bu.edu

Funding

Funding Agency	Grant Number
NHLBI NIH HHS	2 R01 HL-071972

Publisher

AMER PHYSIOLOGICAL SOC, 9650 ROCKVILLE PIKE, BETHESDA, MD 20814 USA

Journal Information

Impact Factor: Journal Citation Reports

Categories / Classification

Research Areas: Physiology

Web of Science Categories: Physiology

See more data fields

Cited References: 73

Showing 30 of 73 **View All in Cited References page** *(from Web of Science Core Collection)*

1. **Behavioral-independence features of complex heartbeat dynamics** **Times Cited: 186**
By: Amaral, LAN; Ivanov, PC; Aoyagi, N; et al.
PHYSICAL REVIEW LETTERS Volume: 86 Issue: 26 Pages: 6026-6029 Published: JUN 25 2001

2. Title: [not available] **Times Cited: 70**
By: Arking, R.
Biology of Aging: Observations and Principles Published: 2006
Publisher: Oxford University Press, Oxford, UK

3. **Decomposition of heartbeat time series: Scaling analysis of the sign sequence** **Times Cited: 27**
By: Ashkenazy, Y; Ivanov, PC; Havlin, S; et al.
COMPUTERS IN CARDIOLOGY 2000, VOL 27 Book Series: COMPUTERS IN CARDIOLOGY Volume: 27 Pages: 139-142 Published: 2000

4. **Magnitude and sign scaling in power-law correlated time series** **Times Cited: 108**
By: Ashkenazy, Y; Havlin, S; Ivanov, PC; et al.
PHYSICA A-STATISTICAL MECHANICS AND ITS APPLICATIONS Volume: 323 Pages: 19-41 Published: MAY 15 2003

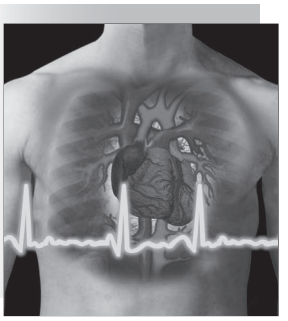

Scale-Invariant Aspects of Cardiac Dynamics

Observing Sleep Stages and Circadian Phases

BY PLAMEN CH. IVANOV

The normal electrical activity of the heart is usually described as a regular sinus rhythm. However, cardiac interbeat intervals fluctuate in an irregular manner in healthy subjects—even at rest or during sleep. In recent years, the intriguing statistical properties of interbeat interval sequences have attracted the attention of researchers from different fields. Analysis of heartbeat fluctuations focused initially on short-time oscillations associated with breathing, blood pressure, and neuroautonomic control [1], [2]. Studies of longer heartbeat records revealed $1/f$-like behavior [3], [4]. Recent analyses of very long time series (up to 24 h) show that under healthy conditions interbeat interval increments exhibit power-law anticorrelations [5], [6], follow a universal scaling form in their distributions [7], and exhibit turbulence-like dynamics characterized by a broad multifractal spectrum [8]. These scaling features change with disease and advanced age [9]–[12].

Sleep-wake cycles and the endogenous circadian rhythms are associated with periodic changes in key physiological processes [13]–[15]. Here, we ask the question if there are characteristic differences in the behavior between sleep and wake cardiac dynamics across multiple time scales. We hypothesize that, in addition to the known periodic rhythms with a characteristic time scale, the endogenous mechanisms of sleep and circadian regulation may influence cardiac dynamics over a broad range of time scales, and thus could lead to systematic changes in the scaling properties of the heartbeat fluctuations. Elucidating the nature of these interactions could lead to a better understanding of the neuroautonomic mechanisms of cardiac regulation.

Results

Sleep-Wake Differences in Heart Rate Distributions

Typically, the differences in the cardiac dynamics during sleep and wake phases are reflected in the average and standard deviation of the heartbeat intervals (Figure 1) [15].

To analyze the statistical properties of human cardiac activity we introduced the cumulative variation amplitude analysis (CVAA), designed to quantify probability distributions of physiologic fluctuations embedded in nonstationary signals [7]. This method comprises sequential application of a set of algorithms based on wavelet and Hilbert transform analyses. The first step is the wavelet transform [16], which extracts the cumulative variations in the heartbeat intervals over a spacific wavelet (time) scale by simultaneously removing polynomial trends associated with the nonstationarity in the data. The second step of the CVAA method is to extract the amplitudes of the variations in the beat-to-beat signal by means of an analytic signal approach (Hilbert transform) [17], which provides a measure for the duration of segments with different amplitudes of heartbeat variations. The CVAA method for nonstationary time series analysis has been consequently applied to different physiological systems [18]–[21].

We studied the distribution of the amplitudes of the beat-to-beat variations for a group of healthy subjects ($N = 18$: five males and 13 females; age: 20–50, mean: 34 years). We begin by considering night phase records (sleep between midnight—6:00 a.m.). Inspection of the distribution functions of the amplitudes of the cumulative variations reveals marked differences between individuals. To test the hypothesis that there is a possibly universal structure to these heterogeneous time series, we rescale the distributions and find for all healthy subjects that the data conform to a single-scaled plot [7]. Further, we find the rescaled data are well fit with a homogeneous Gamma distribution (Figure 2), defines with a single parameter for all healthy subjects, and that the form of the probability distribution of the cumulative heartbeat variations is preserved when changing the time scale of the analysis over a very broad range of time scales from seconds to hours [7]. This stability of the from of the probability distribution at various time scales has been confirmed by follow-up studies [23]. Such robust scaling behavior is reminiscent of a wide class of well-studied physical systems with universal scaling properties [24], [25]. The collapse of the individual distributions for all healthy subjects after rescaling their individual parameter is indicative of a universal structure, in the sense that there is a closed mathematical scaling form describing in a unified quantitative way the cardiac dynamics of healthy subjects over a broad range of time scales [26].

We next analyzed heart rate dynamics for healthy subjects during the daytime (wake state between noon—6 p.m.). The apparently universal behavior we find holds not only for the night phase but for the day phase as well. However, semilog plots of the averaged distributions show a slower decay in the tail for the sleep-state, whereas the wake-state distribution follows

Digital Object Identifier 10.1109/MEMB.2007.907093

the exponential form over practically the entire range [22], [26]. Counterintuitively, the slower decaying tail of the distribution of heartbeat fluctuations for the night phase indicates higher probability of larger variations in the healthy heart dynamics during sleep hours in comparison with the daytime dynamics during wake state (Figure 2). Modeling approaches to heart rate dynamics based on stochastic feedback mechanisms suggest that the marked change in the distribution of the cumulative heartbeat variations we observe during transition from wake to sleep state may be due to the relative decrease of the sympathetic tone in relation to the parasympathetic inputs during sleep [27].

Sleep-Wake Differences in the Correlations of Heartbeat Fluctuations

As we observed sleep-wake differences in the form of the probability distributions of the amplitudes of the fluctuations in the heartbeat intervals (Figure 2), we next asked the question if there are characteristic differences in the temporal correlations of cardiac dynamics between sleep and wake state. We applied the detrended fluctuation analysis (DFA) method [28]. The advantage of the DFA method over conventional methods, such as power spectrum analysis, is that it avoids the spurious detection of apparent long-range correlations that are an artifact of nonstationarity related to linear and higher-order polynomial trends in the data [29]–[32].

We analyzed 30 datasets from 18 healthy subjects, 12 patients with congestive heart failure and six cosmonauts during long-term orbital flight. We analyzed the nocturnal and diurnal fractions of the dataset of each subject, which correspond to the 6 h from midnight to 6 a.m. and noon to 6 p.m.

We find that at scales above ≈ 1 min the data during wake hours display long-range power-law correlations over two decades, with average exponents $\alpha_W \approx 1.05$ for the healthy group and $\alpha_W \approx 1.2$ for the heart failure patients [33]. For the sleep data, we find a systematic crossover at scale $n \approx 60$ beats followed by a scaling regime extending over two decades characterized by a smaller exponent: $\alpha_S \approx 0.85$ for the healthy and $\alpha_S \approx 0.95$ for the heart failure group [33]. We find that for all individuals studied the heartbeat dynamics during sleep are characterized by a smaller exponent (Figure 3), suggesting stronger anticorrelations in heartbeat fluctuations during sleep compared with wake state.

The findings of stronger anticorrelations [33], as well as higher probability for larger heartbeat fluctuations during sleep [7], [22], [26], suggest that the observed dynamical characteristics in the heartbeat fluctuations during sleep and wake phases are related to intrinsic mechanisms of neuroautonomic control, and support a reassessment of the sleep as a surprisingly active dynamical state. Surprisingly, we note that for the regime of large time scales ($n > 60$ beats) the average sleep-wake scaling difference ($\alpha_W - \alpha_S \approx 0.2$ for both healthy and heart failure groups) is comparable with the scaling difference between health and disease. We also note that the scaling exponents for the heart failure group during sleep are close to the exponents observed for the healthy group during wake [33]. Since heart failure occurs when the cardiac output is not adequate to meet the metabolic demands of the body, one would anticipate that the manifestations of heart failure would be most severe during physical stress when metabolic demands are greatest, and least severe when metabolic demands are minimal, i.e., during rest or sleep. The scaling results we obtain are consistent with these physiological considerations: the heart failure subjects should be closer to normal during minimal activity. Of related interest, recent studies indicate that sudden death in individuals with underlying heart disease is most likely to occur in the hours just after awakening [34], [35]. For all cosmonauts during orbital flight, the values of the scaling exponent α during wake and sleep are consistent with those found for the healthy terrestrial group (Figure 3).

The sleep-wake changes in the scaling characteristics we observe possibly indicate different regimes of intrinsic neuroautonomic regulation of cardiac dynamics, which may switch on and off in accordance with circadian rhythms. These findings raise the intriguing possibility that the transition between the sleep and wake phases is a period of potentially increased neuroautonomic instability because it requires a transition from strongly to weakly anticorrelated regulation of the heart, i.e., a phase transition from one fractal state of self-organization over a range of time scales to another. This hypothesis triggered further investigations on the

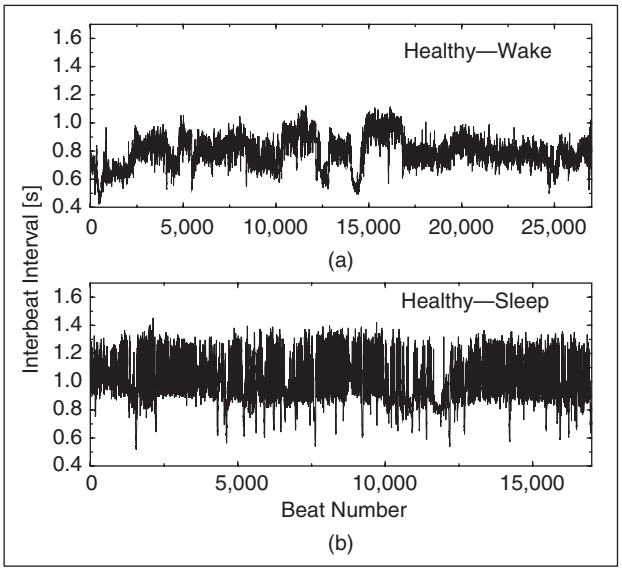

Fig. 1. Consecutive heartbeat intervals versus beat number for six hours recorded from the same healthy subject during (a) wake period: 12 p.m. to 6 p.m. and (b) sleep period: 12 a.m. to 6 a.m.

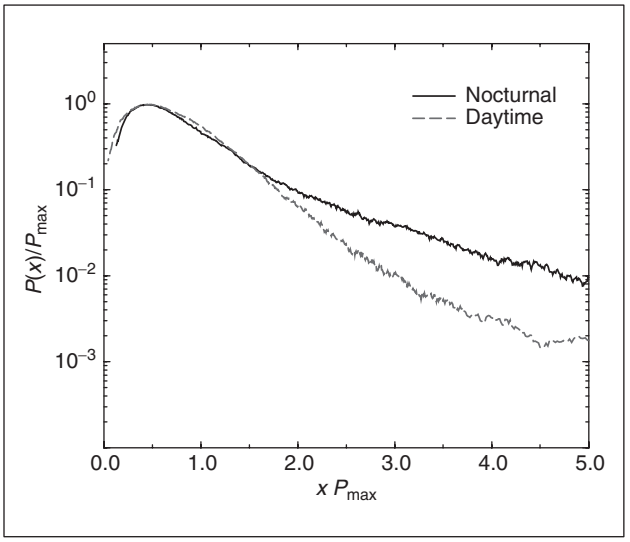

Fig. 2. Plots of the sleep- and wake-phase distributions of heartbeat variations obtained using the CVAA method (7), (26). Data are averaged over a subset of 18 healthy subjects after rescaling the individual distributions. Adapted from (22).

Changes in the physiological processes are associated with circadian rhythms and with different sleep stages.

potential influence of the circadian rhythms on cardiac vulnerability, as outlined in "Temporal Correlations in Heartbeat Dynamics Change with Circadiar Phase." These transitions in the scale-invariant temporal organization of the heartbeat fluctuations between sleep and wake state have been futher investigated and confirmed by recent studies [36]. We also note that similart transitions have been observed in the correlation scaling properties of heartbeat dynamics during rest and exercise [37], [38].

Temporal Correlations in Heartbeat Fluctuations Change with Sleep Stages

Healthy sleep consists of cycles of approximately one to two hours duration. Each cycle is characterized by a sequence of sleep stages usually starting with light sleep, followed by deep sleep, and rapid eye movement (REM) sleep [39]. While the specific functions of the different sleep stages are not yet well understood, many believe that deep sleep is essential for physical rest, while REM sleep is important for memory consolidation [39]. It is known that changes in the physiological processes are associated with circadian rhythms (wake or sleep state) and with different sleep stages. Thus, we next ask how cardiac dynamics of healthy subjects change during different sleep stages.

A recent study has confirmed our finding of lower value for the scaling exponent during sleep compared with wake and has further shown that different stages of sleep (e.g., light sleep, deep sleep, REM stages) could be associated with different temporal correlations in heartbeat fluctuations [40], suggesting a change in the mechanism of cardiac regulation in the process of sleep-stage transitions.

We employed a recently proposed approach of magnitude and sign analysis [41], [42] to further investigate how the linear and nonlinear properties of heartbeat dynamics change during different stages of sleep. We focus on the correlations of the sign and the magnitude of the heartbeat increments obtained from recordings of interbeat intervals from healthy subjects during sleep. We apply the DFA method [28] on both the sign and the magnitude time series. We find that the sign series exhibits anticorrelated behavior at short time scales, which is characterized by a correlation exponent α_{sign}, with smallest value for deep sleep, larger value for light sleep, and largest value for REM sleep (Figure 4). The magnitude series, on the other hand, exhibits uncorrelated behavior for deep sleep with $\alpha_{mag} \approx 1.5$, while long-range correlations are observed for light and REM sleep, with a larger exponent for REM sleep (Figure 4). The observed increase in the values of both the sign and magnitude correlation exponents from deep through light to REM sleep is systematic and significant [43]. We also observe that the values of the sign and magnitude exponents for REM sleep are very close to the values of these exponents for the wake state.

Our studies suggest that long-range correlated behavior for the magnitude series obtained from a long-range anticorrelated increment series relates to the nonlinear properties of the signal, while the sign series reflects the linear properties [41],

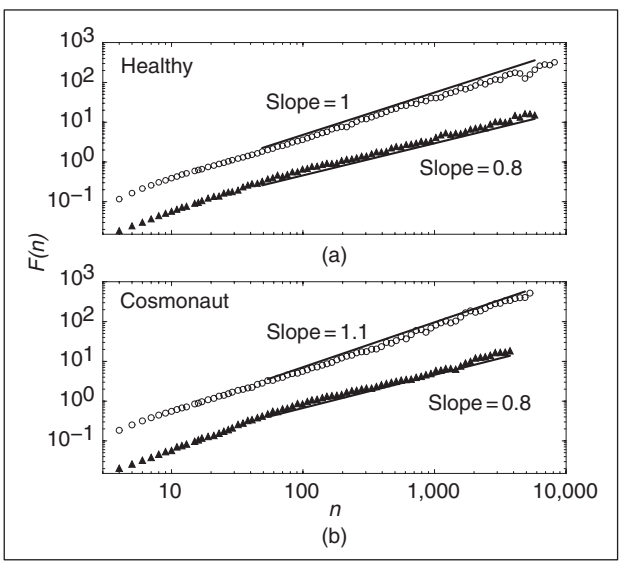

Fig. 3. Log-log plots of the DFA fluctuation function *F(n)* versus the time scale *n* (number of beats) for 6 h wake records (open circles) and sleep records (filled triangles) of (a) one typical healthy subject; (b) one cosmonaut during orbital flight. The slope indicates the scaling exponent α. Note the systematic lower exponent for the sleep phase (filled triangles), indicating stronger anticorrelations. Adapted from (32).

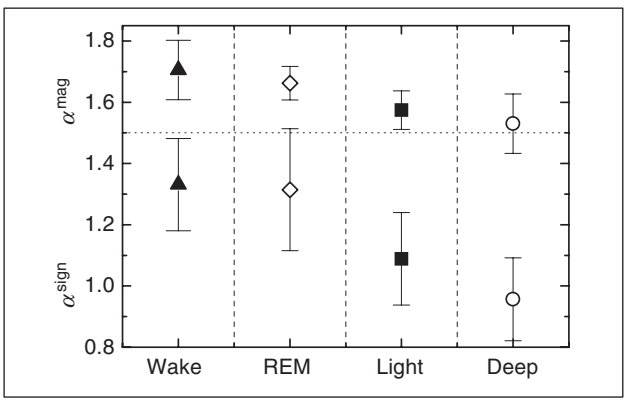

Fig. 4. The average values of the exponents α_{mag} for the integrated magnitude series and α_{sign} for the integrated sign series for the different phases (wake state, REM sleep, light sleep, and deep sleep). For each of the 24 records from 12 healthy subjects the corresponding second order DFA fluctuation functions $F(n)$ have been fit in the range of $8 \leq n \leq 13$ and $11 \leq n \leq 150$ heartbeats for α_{sign} and α_{mag}, respectively, where the most significant differences between the sleep stages occur. Adapted from (42).

[42]. Thus, our finding of positive power-law correlations for the magnitude of the heartbeat increments during REM sleep, and of loss of these correlations during deep sleep (Figure 4), indicates a different degree of nonlinearity in cardiac dynamics during different sleep stages. A stochastic model has been subsequently developed to account for the complex changes in the scaling and nonlinear features of heartbeat dynamics with sleep and wake state and across sleep stage transitions [44].

Temporal Correlations in Heartbeat Dynamics Change with Circadian Phase

Epidemiological studies have reported a robust day/night pattern in the incidence of adverse cardiovascular events with a peak at ≈ 10 a.m. [45]. This peak has been traditionally attributed to day/night patterns in behaviors including activity levels. We hypothesized that these dynamical scaling features of the healthy human heartbeat have an intrinsic circadian rhythm that brings them closer to the features observed under pathologic conditions at specific circadian phases.

We investigated heartbeat dynamics in healthy subjects (four males and one female; age: 20–33; mean: 25.8 years) recorded throughout a ten-day protocol in which the sleep/wake and activity cycle were desynchronized from the endogenous circadian cycle, enabling separation of internal circadian factors from behavior-related factors. Subjects' sleep-wake behavior

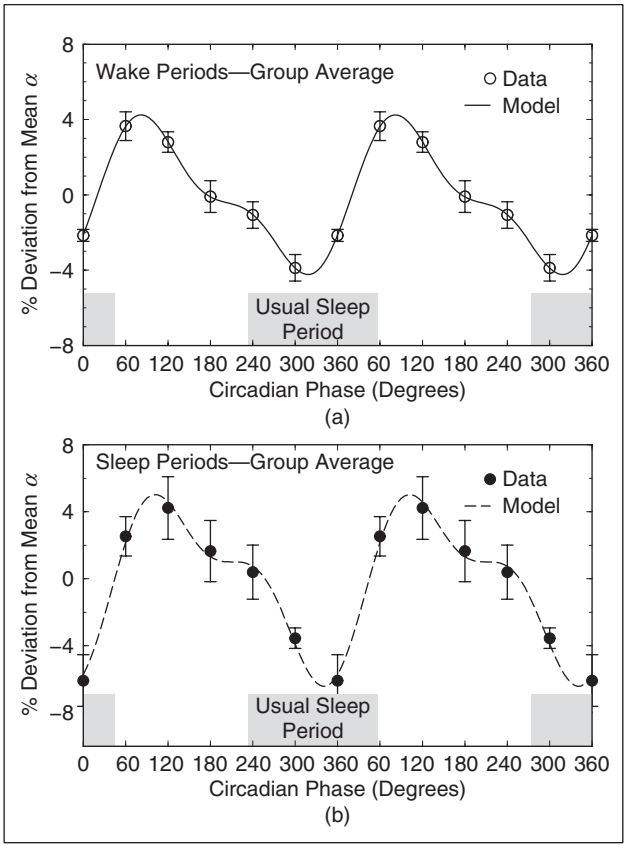

Fig. 5. Circadian rhythms in the group average of the scaling exponent α for (a) wake periods and for (b) sleep-opportunity periods. Consistent and significant circadian rhythms are observed for both wake periods (p-value = 0.01) and sleep-opportunity periods (p-value = 0.0003). Note the well-pronounced peak at between 60 and 90 circadian degrees (9–11 a.m.). Adapted from (45).

cycles are adjusted to 28 h [46]. This 28-h recurring sleep/wake schedule is repeated for seven cycles in the absence of bright light, so that the body clock oscillates at its inherent rate. Subjects have been asked to repeat the same schedule in all seven wake periods so that, statistically, the same behaviors occur at each circadian phase throughout all seven 28-h cycles.

We separated all interbeat interval data into 1-h windows, and for each window we calculate the value of the DFA scaling exponent and the mean heartbeat interval. Since the sleep and wake states have different effects on cardiac dynamics [22], [33], [40], [43], we analyzed wake and sleep-opportunity periods separately. Averaging the data according to the circadian phase yields effects caused only by the endogenous circadian rhythms independent of behavioral factors, because in the forced desynchrony protocol each behavior is represented at each circadian phase.

We find that the DFA scaling exponent characterizing the temporal correlations in heartbeat dynamics exhibits a significant circadian rhythm, with a sharp peak at the circadian phase corresponding to ≈ 10 a.m. (Figure 5), coinciding with the window of cardiac vulnerability reported in clinical studies [45]. We find that this peak in the value of the scaling exponent is independent of the scheduled behaviors and occurs during both sleep and awake periods scheduled across different circadian phases [46]. Since cardiac dynamics under pathologic conditions such as congestive heart failure are associated with a larger value of the scaling exponent, our findings suggest that circadian-mediated influences on cardiac control may be involved in cardiac vulnerability. Further, we find that the peak in the value of the correlation exponent at ≈ 10 a.m. is not related to the circadian-mediated influence on the mean activity levels, leading to changes in the average heartrate that displays a very different circadian rhythm with a peak in the window 5–9 p.m. [46].

Conclusions

We find that key scale-invariant features of heartbeat dynamics, which have been previously associated with the underlying mechnisms of cardiac regulation, change significantly with sleep-wake transition, across sleep stages and circadian phases under both healthy and pathologic conditions. Our findings indicate that sleep-wake and circadian cycles do not simply modulate basic physiologic functions by generating rhythms with a fixed periodicity, but also influence the neural regulation of fundamental physiologic systems such as the cardiovascular system simultaneously over a broad range of time scales. Our empirical observations suggest that the neural systems of sleep and circadin regulation play an important role in the scale-invariant fractal organization of cardiac dynamics (and perhaps also of other physiologic dynamics), which has been shown to breakdown with disease and advanced age.

Acknowledgments

The results reviewed here represent a collaborative research effort with contributions from many individuals, including Z. Chen, A. Bunde, A.L. Goldberger, S. Havlin, K. Hu, J.W. Kantelhardt, T. Penzel, M.G. Rosenblum, S.A Shea, H.E. Stanley. This work was supported by NIH (Grant No. 2RO1 HL 071972).

Plamen Ch. Ivanov received an M.S. degree in theoretical physics/condensed matter physics from Sofia University in 1988, and a Ph.D. in biophysics from Boston University in 1998. He is currently a senior research associate at the Center for Polymer Studies and the Physics Department at Boston

University, lecturer at the Division of Sleep Medicine at Harvard Medical School, Brigham and Women's Hospital, and an associate professor at the Institute of Solid State Physics, Bulgarian Academy of Sciences. His research interests include methods of analysis and modeling of integrated biological and physiological systems and networks; multiscale dynamical properties emerging from cellular level interactions; neural regulation; stochastic processes; and phase transitions. He has served as an editor of FNL in the period 2000–2002, and he is currently on the Editorial Board of the *Journal of Biological Physics*.

Address for Correspondence: Plamen Ch. Ivanov, Center for Polymer Studies and Department of Physics, Boston University, 590 Commonwealth Ave., Boston, Massachusetts 02215. E-mail: plamen@buphy.bu.edu.

References

[1] R. I. Kitney and O. Rompelman, *The Study of Heart-Rate Variability*, London, U.K.: Oxford Univ. Press, 1980.
[2] S. Akselrod, D. Gordon, F. A. Ubel, D. C. Shannon, A. C. Berger, and R. J. Cohen, "Power spectrum analysis of heart rate fluctuation: a quantitative probe of beat-to-beat cardiovascular control," *Science*, vol. 213, no. 4504, pp. 220–222, July 10, 1981.
[3] M. Kobayashi and T. Musha, "1/f fluctuation of heartbeat period," *IEEE Trans. Biomed. Eng.*, vol. 29, no. 6, p. 456, 1982.
[4] J. P. Saul, P. Albrecht, R. D. Berger, and R. J. Cohen, "Analysis of long term heart rate variability: Methods, 1/f scaling, and implications," *Comput. Cardiol.*, vol. 14, pp. 419–422, 1988.
[5] C.-K. Peng, J. Mietus, J. M. Hausdorff, S. Havlin, H. E. Stanley, and A. L. Goldberger, "Long-range anticorrelations and non-Gaussian behavior of the heartbeat," *Phys. Rev. Lett.*, vol. 70, no. 9, pp. 1343–1346, Mar 1, 1993.
[6] C.-K. Peng, S. Havlin, H. E. Stanley, and A. L. Goldberger, "Quantification of scaling exponents and crossover phenomena in nonstationary heartbeat time-series," *Chaos*, vol. 5, no. 1, pp. 82–87, Mar 1995.
[7] P. Ch. Ivanov, M. G. Rosenblum, C.-K. Peng, J. Mietus, S. Havlin, H. E. Stanley, and A. L. Goldberger, "Scaling behaviour of heartbeat intervals obtained by wavelet-based time-series analysis," *Nature*, vol. 383, no. 6598, pp. 323–327, Sep 26, 1996.
[8] P. Ch. Ivanov, L. A. N. Amaral, A. L. Goldberger, S. Havlin, M. G. Rosenblum, Z. R. Struzik, and H. E. Stanley, "Multifractality in human heartbeat dynamics," *Nature*, vol. 399, no. 6735, pp. 461–465, June 3, 1999.
[9] L. A. Lipsitz, J. Mietus, G. B. Moody, and A. L. Goldberger, "Spectral characteristics of heart-rate-variability before and during postural tilt—Relations to aging and risk of syncope," *Circulation*, vol. 81, no. 6, pp. 1803–1810, June 1990.
[10] D. T. Kaplan, M. I. Furman, S. M. Pincus, S. M. Ryan, L. A. Lipsitz, and A. L. Goldberger, "Aging and the complexity of cardiovascular dynamics," *Biophys. J.*, vol. 59, no. 4, pp. 945–949, Apr 1991.
[11] N. Iyengar, C.-K. Peng, R. Morin, A. L. Goldberger, and L. A. Lipsitz, "Age-related alterations in the fractal scaling of cardiac interbeat interval dynamics," *Am. J. Physiol.*, vol. 271, no. 4, pp. R1078–R1084, Oct 1996.
[12] A. L. Goldberger, L. A. N. Amaral, J. M. Hausdorff, P. Ch. Ivanov, C.-K. Peng, and H. E. Stanley, "Fractal dynamics in physiology: Alterations with disease and aging," *Proc. Natl. Acad. Sci. USA*, vol. 99, no. Suppl 1, pp. 2466–2472, Feb 19, 2002.
[13] R. M. Berne and M. N. Levy, *Cardiovascular Physiology*, 6th ed. St. Louis, MO: Mosby, 1996.
[14] M. Malik and A. J. Camm, Eds., *Heart Rate Variability*. Armonk, NY: Futura, 1995.
[15] H. Molgaard, K. E. Sorensen, and P. Bjerregaard, "Circadian variation and influence of risk factors on heart rate variability in healthy subjects," *Am. J. Cardiol.*, vol. 68, no. 8, pp. 777–784, Sep 15, 1991.
[16] A. Grossmann and J. Morlet, *Mathematics and Physics, Lectures on Recent Results*. Singapore: World Scientific, 1985.
[17] D. Gabor, "Theory of communication," *J. Inst. Elect. Eng.*, vol. 93, pp. 429–457, 1946.
[18] M. Meyer, A. Rahmel, C. Marconi, B. Grassi, P. Cerretelli, and J. E. Skinner, "Stability of heartbeat interval distributions in chronic high altitude hypoxia," *Integr. Physiol. Behav. Sci.*, vol. 33, no. 4, pp. 344–362, Oct–Dec 1998.
[19] J. Bhattacharya, P. P. Kanjilal, and S. H. Nizamie, "Decomposition of posterior alpha rhythm," *IEEE Trans. Biomed. Eng.*, vol. 47, no. 6, p. 738, 2000.
[20] J. Bhattacharya and H. Petsche, "Universality in the brain while listening to music," *Proc. R. Soc. Lond. B Biol. Sci.*, vol. 268, no. 1484, p. 2423, 2001.
[21] P. A. Ritto, J. J. Alvarado-Gil, and J. G. Contreras, "Scaling and wavelet-based analyses of the longterm heart rate variability of the Eastern Oyster," *Physica A*, vol. 349, no. 1-2, pp. 291–301, Apr 1, 2005.
[22] P. Ch. Ivanov, M. G. Rosenblum, C.-K. Peng, J. E. Mietus, S. Havlin, H. E. Stanley, and A. L. Goldberger, "Scaling and universality in heart rate variability distributions," *Physica A*, vol. 249, no. 1-4, pp. 587–593, Feb 1, 1998.
[23] K. Kiyono, Z. R. Struzik, N. Aoyagi, S. Sakata, J. Hayano, and Y. Yamamoto, "Critical scale invariance in a healthy human heart rate," *Phys. Rev. Lett.*, vol. 93, no. 17, p. 178103, Oct 22, 2004.
[24] H. E. Stanley, *Introduction to Phase Transitions and Critical Phenomena*. London: Oxford University Press, 1971.
[25] T. Vicsek, *Fractal Growth Phenomena*, 2nd ed. Singapore: World Scientific, 1992.
[26] P. Ch. Ivanov, A. L. Goldberger, S. Havlin, C.-K. Peng, M. G. Rosenblum, and H. E. Stanley, "Wavelets in medicine and physiology," in *Wavelets in Physics*, H. van der Berg, Ed. Cambridge: Cambridge University Press, 1998.
[27] P. Ch. Ivanov, L. A. N. Amaral, A. L. Goldberger, and H. E. Stanley, "Stochastic feedback and the regulation of biological rhythms," *Europhys. Lett.*, vol. 43, no. 4, pp. 363–368, Aug 15, 1998.
[28] C.-K. Peng, S. V. Buldyrev, S. Havlin, M. Simons, H. E. Stanley, and A. L. Goldberger, "On the mosaic organization of DNA sequences," *Phys. Rev. E, Stat. Phys. Plasmas Fluids Relat. Interdiscip. Top.*, vol. 49, no. 2, pp. 1691–1689, Feb 1994.
[29] K. Hu, P. Ch. Ivanov, Z. Chen, P. Carpena, and H. E. Stanley, "Effect of trends on detrended fluctuation analysis," *Phys. Rev. E, Stat. Phys. Plasmas Fluids Relat. Interdiscip. Top.*, vol. 64, no. 1, Art. No. 011114 Part 1, July 2001.
[30] Z. Chen, P. Ch. Ivanov, K. Hu, and H. E. Stanley, "Effect of nonstationarities on detrended fluctuation analysis," *Phys. Rev. E, Stat. Phys. Plasmas Fluids Relat. Interdiscip. Top.*, vol. 65, no. 4, Art. No. 041107 Part 1, Apr 2002.
[31] Z. Chen, K. Hu, P. Carpena, P. Bernaola-Galvan, H. E. Stanley, and P. Ch. Ivanov, "Effect of nonlinear filters on detrended fluctuation analysis," *Phys. Rev. E, Stat. Phys. Plasmas Fluids Relat. Interdiscip. Top.*, vol. 71, no. 1, Art. No. 011104 Part 1, Jan 2005.
[32] L. M. Xu, P. Ch. Ivanov, K. Hu, Z. Chen, A. Carbone, and H. E. Stanley, "Quantifying signals with power-law correlations: A comparative study of detrended fluctuation analysis and detrended moving average techniques," *Phys. Rev. E, Stat. Phys. Plasmas Fluids Relat. Interdiscip. Top.*, vol. 71, no. 5, Art. No. 051101 Part 1, May 2005.
[33] P. Ch. Ivanov, A. Bunde, L. A. N. Amaral, S. Havlin, J. Fritsch-Yelle, R. M. Baevsky, H. E. Stanley, and A. L. Goldberger, "Sleep-wake differences in scaling behavior of the human heartbeat: Analysis of terrestrial and long-term space flight data," *Europhys. Lett.*, vol. 48, no. 5, pp. 594–600, Dec 1999.
[34] R. W. Peters, L. B. Mitchell, M. M. Brooks, D. S. Echt, A. H. Barker, R. Capone, P. R. Liebson, and H. L. Greene, "Circadian pattern of arrhythmic death in patients receiving encainide, flecainide or moricizine in the cardiac-arrhythmia suppression trail (CAST)," *J. Am. Coll. Cardiol.*, vol. 23, no. 2, pp. 283–289, Feb 1994.
[35] S. Behrens, G. Ney, S. G. Fisher, R. D. Fletcher, M. R. Franz, and S. N. Singh, "Effects of amiodarone on the circadian pattern of sudden cardiac death (department of veterans affairs congestive heart failure-survival trial of anti-arrhythmic therapy)," *Am. J. Cardiol.*, vol. 80, no. 1, pp. 45–48, Jul 1, 1997.
[36] K. Kiyono, Z. R. Struzik, N. Aoyagi, F. Togo, and Y. Yamamoto, "Phase transition in a healthy human heart rate," *Phys. Rev. Lett.*, vol. 95, no. 5, Art. No. 058101, July 29, 2005.
[37] R. Karasik, N. Sapir, Y. Ashkenazy, P. Ch. Ivanov, I. Dvir, P. Lavie, and S. Havlin, "Correlation differences in heartbeat fluctuations during rest and exercise," *Phys. Rev. E, Stat. Phys. Plasmas Fluids Relat. Interdiscip. Top.*, vol. 66, no. 6, Art. No. 062902 Part 1, Dec 2002.
[38] M. Martinis, A. Knezevic, G. Krstacic, and E. Vargovic, "Changes in the Hurst exponent of heartbeat intervals during physical activity," *Phys. Rev. E, Stat. Phys. Plasmas Fluids Relat. Interdiscip. Top.*, vol. 70, no. 1, Art. No. 012903 Part 1, July 2004.
[39] M. A. Carskadon and W. C. Dement, *Principles and Practice of Sleep Medicine*, M. H. Kryger, T. Roth, and W. C. Dement, Eds. Philadelphia: Saunders, 1994, pp. 16–25.
[40] A. Bunde, S. Havlin, J. W. Kantelhardt, T. Penzel, J. H. Peter, and K. Voigt, "Correlated and uncorrelated regions in heart-rate fluctuations during sleep," *Phys. Rev. Lett.*, vol. 85, no. 17, pp. 3736–3739, Oct 23, 2000.
[41] Y. Ashkenazy, P. Ch. Ivanov, S. Havlin, C.-K. Peng, A. L. Goldberger, and H. E. Stanley, "Magnitude and sign correlations in heartbeat fluctuations," *Phys. Rev. Lett.*, vol. 86, no. 9, pp. 1900–1903, Feb 26, 2001.
[42] Y. Ashkenazy, S. Havlin, P. Ch. Ivanov, C.-K. Peng, V. Schulte-Frohlinde, and H. E. Stanley, "Magnitude and sign scaling in power-law correlated time series," *Physica A*, vol. 323, pp. 19–41, May 15, 2003.
[43] J. W. Kantelhardt, Y. Ashkenazy, P. Ch. Ivanov, A. Bunde, S. Havlin, T. Penzel, J. H. Peter, and H. E. Stanley, "Characterization of sleep stages by correlations in the magnitude and sign of heartbeat increments," *Phys. Rev. E, Stat. Phys. Plasmas Fluids Relat. Interdiscip. Top.*, vol. 65, no. 5, Art. No. 051908 Part 1, May 2002.
[44] J. W. Kantelhardt, S. Havlin, and P. Ch. Ivanov, "Modeling transient correlations in heartbeat dynamics during sleep," *Europhys. Lett.*, vol. 62, no. 2, p. 147, 2003.
[45] J. E. Muller, P. H. Stone, Z. G. Turi, J. D. Rutherford, C. A. Czeisler, C. Parker, W. K. Poole, E. Passamani, R. Roberts, T. Robertson, B. E. Sobel, J. T. Willerson, and E. Braunwald, "Circadian variation in the frequency of onset of acute myocardial infarction," *N. Eng. J. Med.*, vol. 313, no. 21, pp. 1315–1322, 1985.
[46] K. Hu, P. Ch. Ivanov, M. F. Hilton, Z. Chen, R. T. Ayers, H. E. Stanley, and S. A. Shea, "Endogenous circadian rhythm in an index of cardiac vulnerability independent of changes in behavior," *Proc. Natl. Acad. Sci.*, vol. 101, no. 52, pp. 18223–18227, Dec 28, 2004.

Scale-invariant aspects of cardiac dynamics - Observing sleep stages and circadian phases

By: Ivanov, PC (Ivanov, Plamen Ch.)

View ResearcherID and ORCID

IEEE ENGINEERING IN MEDICINE AND BIOLOGY MAGAZINE
Volume: 26 **Issue:** 6 **Pages:** 33-37
DOI: 10.1109/MEMB.2007.907093
Published: NOV-DEC 2007
Document Type: Article
View Journal Impact

Keywords

KeyWords Plus: HEART-RATE-VARIABILITY; TIME-SERIES; BEHAVIOR; FLUCTUATION; DISTRIBUTIONS; UNIVERSALITY; MAGNITUDE; PATTERN; RHYTHM; DEATH

Author Information

Reprint Address: Ivanov, PC (reprint author)

+ Boston Univ, Ctr Polymer Studies, Dept Phys, 590 Commonwealth Ave, Boston, MA 02215 USA.

Addresses:

+ [1] Univ Sofia, BU-1126 Sofia, Bulgaria

+ [2] Harvard Univ, Sch Med, Brigham & Womens Hosp, Div Sleep Med, Cambridge, MA 02138 USA

+ [3] Bulgarian Acad Sci, Inst Solid State Phys, BG-1040 Sofia, Bulgaria

E-mail Addresses: plamen@buphy.bu.edu

Funding

Funding Agency	Grant Number
NHLBI NIH HHS	2R01 HL 071972

Publisher

IEEE-INST ELECTRICAL ELECTRONICS ENGINEERS INC, 445 HOES LANE, PISCATAWAY, NJ 08855-4141 USA

Categories / Classification

Research Areas: Engineering; Medical Informatics
Web of Science Categories: Engineering, Biomedical; Medical Informatics

See more data fields

Citation Network

In Web of Science Core Collection

33

Times Cited

Create Citation Alert

All Times Cited Counts

34 in All Databases

See more counts

46

Cited References

View Related Records

Most recently cited by:

Xiong, Wanting; Faes, Luca; Ivanov, Plamen Ch.
Entropy measures, entropy estimators, and their performance in quantifying complex dynamics: Effects of artifacts, nonstationarity, and long-range correlations.
PHYSICAL REVIEW E (2017)

dos Santos Lima, Gustavo Zampier; Lopes, Sergio Roberto; Prado, Thiago Lima; et al.
Predictability of arousal in mouse slow wave sleep by accelerometer data.
PLOS ONE (2017)

View All

Use in Web of Science

Web of Science Usage Count

0 Last 180 Days **4** Since 2013

Learn more

This record is from:
Web of Science Core Collection

View Record in Other Databases:
View **medical data** (in MEDLINE ®)

Suggest a correction

If you would like to improve the quality of the data in this record, please suggest a correction.

84 of 127

Cited References: 46

Showing 30 of 46 **View All in Cited References page** *(from Web of Science Core Collection)*

1. **POWER SPECTRUM ANALYSIS OF HEART-RATE FLUCTUATION - A QUANTITATIVE PROBE OF BEAT-TO-BEAT CARDIOVASCULAR CONTROL** **Times Cited: 3,445**
   By: AKSELROD, S; GORDON, D; UBEL, FA; et al.
   SCIENCE Volume: 213 Issue: 4504 Pages: 220-222 Published: 1981

2. **Magnitude and sign scaling in power-law correlated time series** **Times Cited: 108**
   By: Ashkenazy, Y; Havlin, S; Ivanov, PC; et al.
   PHYSICA A-STATISTICAL MECHANICS AND ITS APPLICATIONS Volume: 323 Pages: 19-41 Published: MAY 15 2003

3. **Magnitude and sign correlations in heartbeat fluctuations** **Times Cited: 299**
   By: Ashkenazy, Y; Ivanov, PC; Havlin, S; et al.
   PHYSICAL REVIEW LETTERS Volume: 86 Issue: 9 Pages: 1900-1903 Published: FEB 26 2001

4. **Effects of Amiodarone on the circadian pattern of sudden cardiac death (department of veterans affairs congestive heart failure-survival trial of antiarrhythmic therapy)** **Times Cited: 11**
   By: Behrens, S; Ney, G; Fisher, SG; et al.
   AMERICAN JOURNAL OF CARDIOLOGY Volume: 80 Issue: 1 Pages: 45-48 Published: JUL 1 1997

5. Title: [not available] **Times Cited: 17**
   By: BERNE RM
   CARDIOVASCULAR PHYSL Published: 1996

6. **Decomposition of posterior alpha rhythm** **Times Cited: 13**
   By: Bhattacharya, J; Kanjilal, PP; Nizamie, SH
   IEEE TRANSACTIONS ON BIOMEDICAL ENGINEERING Volume: 47 Issue: 6 Pages: 738-747 Published: JUN 2000

7. **Universality in the brain while listening to music** **Times Cited: 33**
   By: Bhattacharya, J; Petsche, H
   PROCEEDINGS OF THE ROYAL SOCIETY B-BIOLOGICAL SCIENCES Volume: 268 Issue: 1484 Pages: 2423-2433 Published: DEC 7 2001

8. **Correlated and uncorrelated regions in heart-rate fluctuations during sleep** **Times Cited: 367**
   By: Bunde, A; Havlin, S; Kantelhardt, JW; et al.
   PHYSICAL REVIEW LETTERS Volume: 85 Issue: 17 Pages: 3736-3739 Published: OCT 23 2000

9. **Normal human sleep: an overview** **Times Cited: 109**
   By: Carskadon, M. A.; Dement, W. C.
   Principles and practice of sleep medicine Pages: 16-25 Published: 1994

Endogenous circadian rhythm in human motor activity uncoupled from circadian influences on cardiac dynamics

Plamen Ch. Ivanov*†‡, Kun Hu*†, Michael F. Hilton†§, Steven A. Shea†¶, and H. Eugene Stanley*

*Center for Polymer Studies and Department of Physics, Boston University, Boston, MA 02215; †Harvard Medical School and Division of Sleep Medicine, Brigham and Women' s Hospital, Boston, MA 02115; and §School of Population Health, University of Queensland, Brisbane QLD 4072, Australia

Contributed by H. Eugene Stanley, October 31, 2007 (sent for review September 27, 2007)

The endogenous circadian pacemaker influences key physiologic functions, such as body temperature and heart rate, and is normally synchronized with the sleep/wake cycle. Epidemiological studies demonstrate a 24-h pattern in adverse cardiovascular events with a peak at ≈10 a.m. It is unknown whether this pattern in cardiac risk is caused by a day/night pattern of behaviors, including activity level and/or influences from the internal circadian pacemaker. We recently found that a scaling index of cardiac vulnerability has an endogenous circadian peak at the circadian phase corresponding to ≈10 a.m., which conceivably could contribute to the morning peak in cardiac risk. Here, we test whether this endogenous circadian influence on cardiac dynamics is caused by circadian-mediated changes in motor activity or whether activity and heart rate dynamics are decoupled across the circadian cycle. We analyze high-frequency recordings of motion from young healthy subjects during two complementary protocols that decouple the sleep/wake cycle from the circadian cycle while controlling scheduled behaviors. We find that static activity properties (mean and standard deviation) exhibit significant circadian rhythms with a peak at the circadian phase corresponding to 5–9 p.m. (≈9 h later than the peak in the scale-invariant index of heartbeat fluctuations). In contrast, dynamic characteristics of the temporal scale-invariant organization of activity fluctuations (long-range correlations) do not exhibit a circadian rhythm. These findings suggest that endogenous circadian-mediated activity variations are not responsible for the endogenous circadian rhythm in the scale-invariant structure of heartbeat fluctuations and likely do not contribute to the increase in cardiac risk at ≈10 a.m.

cardiac vulnerability | circadian pacemaker | locomotor activity | scale invariance

Epidemiological studies demonstrate that myocardial infarction (1–4), stroke (5, 6), and sudden cardiac death (7) have a 24-h daily pattern with a broad peak at 9–11 a.m. This 24-h pattern is widely assumed to be due to day/night patterns in behaviors that affect cardiovascular variables, such as autonomic balance, blood pressure, and platelet aggregability, in vulnerable individuals (8). However, endogenous influences from the circadian pacemaker [suprachiasmatic nuclei of the hypothalamus (SCN)], independent from external behavioral effects, may also contribute to this daily pattern of adverse cardiovascular events. These circadian influences could occur via hormonal effects, direct neuronal links between the SCN and the sympathetic system (9) and through circadian modulation of the sympathovagal balance (10). Recently, we demonstrated (11) that dynamical scale-invariant features of heartbeat fluctuations [related to underlying mechanisms of cardiac control (12–17)], exhibit a significant endogenous circadian rhythm, independent from extrinsic scheduled behaviors and the sleep/wake cycle. These dynamical features of heartbeat fluctuations move closer to the features observed under pathologic conditions (13, 16, 18) at the endogenous circadian phase corresponding to 9–11 a.m. (11). These findings raise two plausible hypotheses for the endogenous pathways of circadian influence on cardiac dynamics: that the SCN directly influences cardiac regulation or that the SCN affects the intrinsic regulation of physical activity, which in turn influences cardiac dynamics (Fig. 1).

The output of integrated, multiple-component physiologic systems under neural regulation, such as activity and heart rate, often exhibit complex continuous fluctuations, even under healthy resting conditions and in the absence of external perturbations (14, 15, 19–22). Static properties (e.g., mean and standard deviation) as well as dynamic scale-invariant properties of these variables (e.g., long-range power-law correlations) relate to cardiac vulnerability. For instance, static measures of heartbeat fluctuations change with pathologic conditions (23–25); e.g., reduced vagal tone in congestive heart failure leads to much lower average interbeat interval (16, 18, 26). Furthermore, increased cardiac vulnerability is characterized by a smaller standard deviation of heartbeat fluctuations in pathologic conditions of impaired cardiac responsiveness (26, 27).

In terms of dynamic measures, studies have revealed that heartbeat fluctuations in healthy subjects possess a self-similar temporal structure related to the underlying cardiac control mechanism, which is characterized by long-range power-law correlations over a broad range of time scales (12–14). These dynamic scale-invariant features change with sleep/wake states (20, 21, 28, 29), sympathetic and parasympathetic blockade (30), and exercise (31, 32) and under pathologic conditions, such as congestive heart failure (13, 16, 18). Moreover, the scaling exponent associated with these power-law correlations is a robust marker sensitive to predicting mortality in patients with heart failure (26).

Scale-invariant dynamic patterns also have been recently found in the fluctuations of human motor activity, such as forearm motion and gait (22, 33, 34), with long-range power-law correlations on time scales of seconds to hours that are insensitive to changes in mean activity level and to fluctuations caused by random and scheduled extrinsic factors (22). Furthermore, this scale-invariant dynamic measure changes under pathologic conditions (35). These combined results suggest that scale-invariant dynamic changes in activity in humans are regulated by an intrinsic activity control mechanism.

Average motor activity clearly affects average heart rate, but it is not known how the dynamic scale-invariant measures of these two

Author contributions: P.Ch.I. and K.H. contributed equally to this work; P.Ch.I., K.H., M.F.H., and S.A.S. designed research; P.Ch.I., K.H., M.F.H., S.A.S., and H.E.S. performed research; P.Ch.I., K.H., M.F.H., S.A.S., and H.E.S. analyzed data; and P.Ch.I., K.H., M.F.H., S.A.S., and H.E.S. wrote the paper.

The authors declare no conflict of interest.

‡To whom correspondence may be addressed at: Center for Polymer Studies and Department of Physics, Boston University, 590 Commonwealth Avenue, Boston, MA 02215. E-mail: plamen@buphy.bu.edu.

¶To whom correspondence may be addressed at: Harvard Medical School and Division of Sleep Medicine, Brigham and Women's Hospital, 75 Francis Street, Boston, MA 02115. E-mail: sshea@hms.harvard.edu.

This article contains supporting information online at www.pnas.org/cgi/content/full/0709957104/DC1.

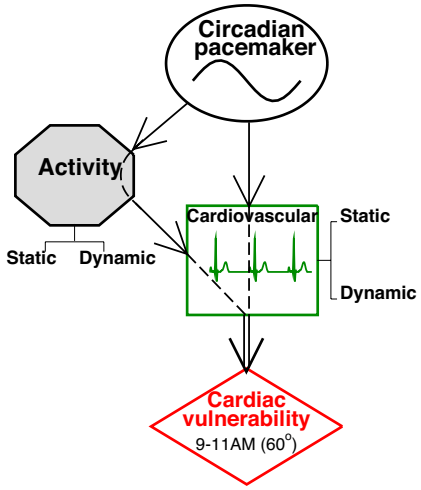

Fig. 1. Schematic diagram of two potential hypotheses for separate pathways of intrinsic circadian influence on the mechanism of cardiac control, which ultimately may lead to increased cardiac risk. (*i*) Direct circadian influence: Static and/or dynamic measures of heartbeat fluctuations have an intrinsic circadian rhythm that may contribute to the epidemiologically observed increase in cardiac vulnerability at 60° circadian phase (relative to CBT minimum at 0°). (*ii*) Indirect activity-mediated circadian influence on cardiac control: Static and dynamic measures of motor activity fluctuations exhibit an intrinsic circadian rhythm, which in turn may influence cardiac regulation leading to increased cardiac risk at particular circadian phases. Our results shown in Figs. 2 and 3 do not support the second hypothesis and suggest that the endogenous circadian variability in physical activity does not contribute to increased cardiac risk at 9–11 a.m. However, the temporal fractal organization of heartbeat fluctuations, quantified by the scale-invariant dynamic index α (Fig. 3), changes significantly under the direct influence of the circadian pacemaker with a pronounced peak at ≈60° circadian phase, suggesting that the endogenous circadian pacemaker may contribute to the increased cardiac vulnerability observed at this circadian phase (1, 11).

physiologic variables are related. For instance, are the dynamic changes in heartbeat fluctuations across the circadian cycle caused by dynamic changes in activity regulation across the circadian cycle (Fig. 1). In this study, we investigate activity and heartbeat data simultaneously recorded in healthy individuals across all circadian phases and determine whether circadian influences on static or dynamic features of heart rate regulation are uncoupled from the circadian influences on activity regulation by using two complementary protocols: (*i*) a forced desynchrony protocol (36–38) that decouples the sleep/wake cycle from the endogenous circadian cycle while controlling for (and averaging out) scheduled events and extrinsic behavioral influences; (*ii*) a constant-routine protocol, when the average and variance of activity levels are minimized in an attempt to uncouple the endogenous circadian influences on cardiac dynamics from activity variations. Because sudden onset of adverse cardiovascular events often occurs in ostensibly healthy, asymptomatic people (39, 40), the study of healthy subjects may provide information concerning circadian or activity-related mechanisms in cardiac vulnerability. Specifically, we examine whether circadian-mediated changes in the statistical indices of activity data exhibit a peak at the endogenous circadian phase corresponding to ≈10 a.m. [i.e., 60° circadian phase, with 0° defined as the core body temperature (CBT) minimum]. If endogenous activity fluctuations do exhibit circadian rhythms with a peak at 60°, it raises the possibility that such changes may be involved in the peak in cardiac vulnerability observed at this phase (Fig. 1) (1–3). To discern the separate intrinsic pathways of SCN influence on the mechanisms of cardiac control, i.e., the direct influence from the indirect activity-mediated influence, we compare how indices of activity and cardiac dynamics change with circadian phase.

Results

The group-averaged results for the static measures of activity and heartbeat RR intervals from wakefulness in the forced desynchrony protocol are presented in Fig. 2 *A–D*. The subjects exhibit a significant endogenous circadian rhythm in mean activity with a large amplitude equivalent to 60% of the average 24-h mean activity (Fig. 2*A*). This pronounced rhythm occurs despite constrains on the activity imposed by the scheduled events as well as being confined to a laboratory suite. The minimum of the mean activity level is at ≈0° circadian phase, corresponding to the endogenous circadian temperature minimum (which normally occurs during sleep in most individuals, although in this protocol only the scheduled wake episodes were analyzed). We find a broad peak in mean activity at 180–240° (corresponding to the habitual hours of 5–9 p.m.). We also find a significant circadian rhythm in the group average of the standard deviation of activity levels during wakefulness with a minimum and a maximum at the same circadian phases as we find for the mean activity levels (Fig. 2*B*).

Mean data for the average and standard deviation of RR interval recordings are presented for comparison with activity recordings in Fig. 2 *C* and *D*. The results in Fig. 2 *A–D* show a strong correlation between the circadian rhythms in the static measures of heart rate and those of activity fluctuations, with minima in the activity variables corresponding to the maxima in the static measures of the RR intervals. Thus, the minimum in the circadian rhythm for the mean interbeat interval (i.e., highest heart rate) coincides with the circadian maximum in the mean activity level (Fig. 2, compare *A* with *C*). Similarly, the circadian maximum in mean heartbeat interval (i.e., lowest heart rate) coincides with the circadian minimum in the mean activity level at 330–30°, corresponding to the habitual sleep period (Fig. 2, compare *A* with *C*). The circadian minimum in the heartbeat interval standard deviation (i.e., lowest heart rate variability) at ≈240° coincides with the circadian peak in the standard deviation of activity fluctuations (Fig. 2, compare *B* with *D*), whereas the circadian maximum in the heartbeat standard deviation at ≈0–20° circadian phase coincides with the minimum in the activity standard deviation (Fig. 2, compare *B* with *D*). Thus, during the forced desynchrony protocol that allows spontaneous activities, the static measures of activity and heart rate appear to be coupled.

The contrasting results from the constant-routine protocol are presented in Fig. 2 *E–H*. As expected, due to the design of the constant routine that greatly constrains activity, we find no significant circadian rhythms in the mean and standard deviation of activity (Fig. 2 *E* and *F*). Thus, the strong circadian rhythm in these static measures of activity (Fig. 2 *A* and *B*) can be volitionally or experimentally constrained. However, we find very similar and significant circadian rhythms in both the average RR interval and the standard deviation of RR intervals during the constant routine (Fig. 2 *G* and *H*), as occurred under the forced desynchrony protocol (compare with Fig. 2 *C* and *D*). Thus, although the static measures of activity and heart rate appear to be coupled across the circadian cycle, constraining mean activity does not affect the circadian rhythm of the RR intervals, suggesting that the circadian rhythm in the mean and standard deviation of RR intervals may not be simply a consequence of circadian changes in the mean and standard deviation of activity.

To determine how the circadian pacemaker influences dynamic control of motor activity, we examine the temporal organization in the fluctuations of activity values over a broad range of time scales (Fig. 3). We apply the detrended fluctuation analysis (DFA) method to quantify long-range temporal correlations in activity fluctuations after accounting for nonstationarities in data by subtracting underlying polynomial trends in the average activity level (41, 42). The scaling behavior in activity fluctuations as assessed by the DFA method is characterized by a scaling exponent $\alpha = 0.9$ (Fig. 3*A*), much greater than $\alpha = 0.5$ for white noise, indicating

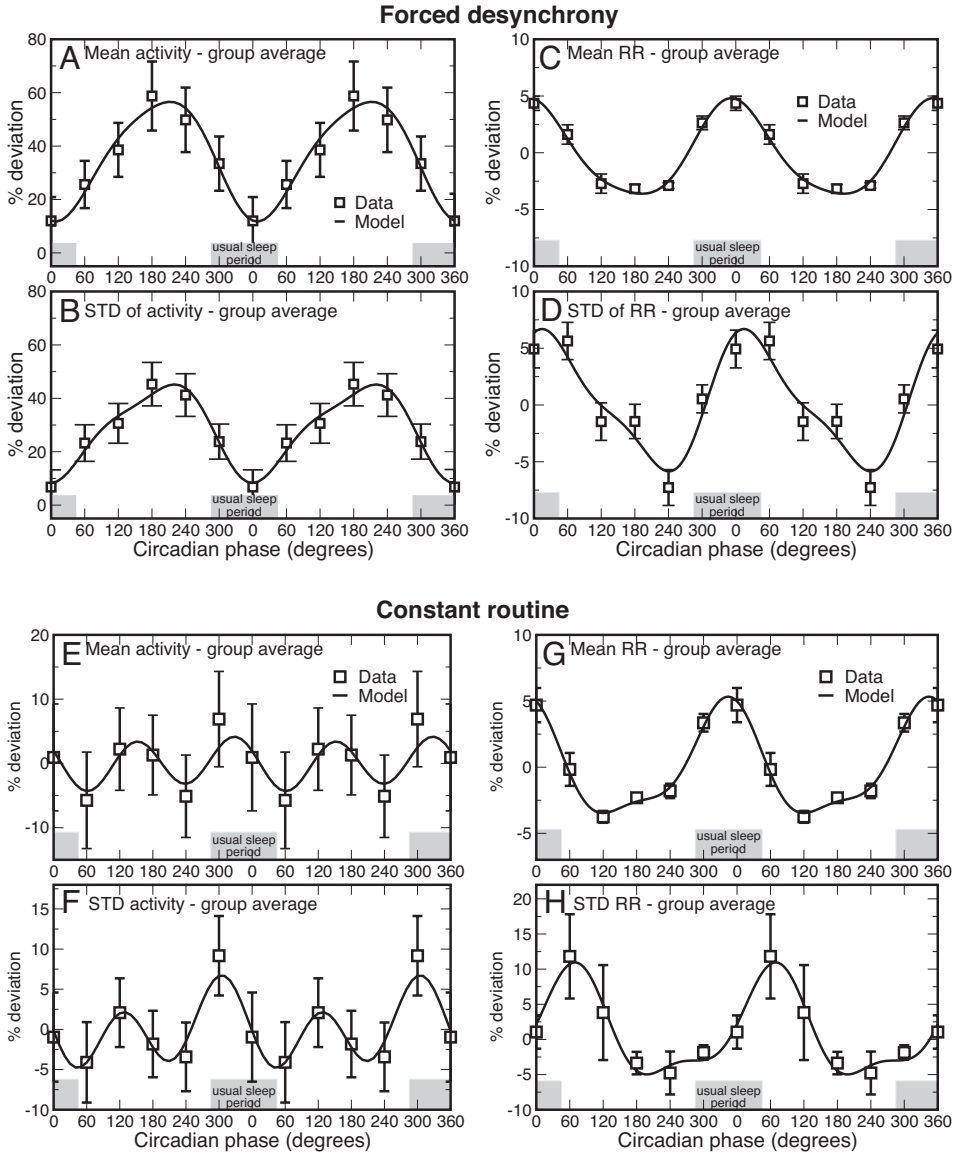

Fig. 2. Endogenous circadian rhythms in static measures of activity and heartbeat fluctuations. (*A* and *B*) Statistically significant circadian rhythms are observed during forced desynchrony in the mean activity levels ($P = 6.2 \times 10^{-4}$ obtained from the cosinor analysis) (*A*) and the standard deviation of activity fluctuations ($P = 8.5 \times 10^{-5}$) (*B*), with a maximum at 180–240° and a minimum at ≈0° circadian phase. Group-averaged data are shown as symbols (error bars represent standard error), and the cosinor analysis fits are shown as solid lines. The results are double-plotted to better visualize rhythmicity. The habitual sleep period when living outside of the laboratory is indicated by gray shaded boxes. The percent deviation in *A* takes only positive values because the mean activity is calculated over both wake and sleep periods, although this analysis includes data only from wakefulness when activity is usually higher. (*C* and *D*) Statistically significant circadian rhythms also are observed during forced desynchrony in the mean value ($P = 3.62 \times 10^{-10}$) (*C*) and the standard deviation ($P = 6.25 \times 10^{-5}$) (*D*) of heartbeat intervals RR, with a minimum at 180–240° and a peak during the habitual sleep period at ≈0° circadian phase (corresponding to minimum CBT). The mean heart rate data in *C* have previously been published (11) and are presented for comparison with activity data. Both activity and heartbeat data were analyzed during wakeful periods in the forced desynchrony protocol. (*E*–*H*) No significant circadian rhythms were observed during constant routine in the mean activity level (*E*) and the standard deviation (*F*) of activity fluctuations, whereas the circadian rhythms in the mean RR interval ($P = 1.6 \times 10^{-9}$) (*G*) and the standard deviation of heartbeat intervals ($P = 0.01$) (*H*) persist.

strong positive correlations and the presence of a robust scale-invariant organization embedded in activity fluctuations across a broad range of time scales. In Fig. 3*A*, we show the scaling behavior of activity fluctuations for a single subject at three different circadian phases corresponding to 9 a.m., 1 p.m., and 5 p.m. obtained during the forced desynchrony protocol. We observe a stable value for the slope of the scaling function $F(n)$ characterized by a scaling exponent $\alpha = 0.9$ for all three circadian phases, indicating that the scale-invariant/fractal temporal structure in activity fluctuations does not significantly change with circadian phase. Similarly for the group, we find no significant circadian rhythm in the average scaling exponent of activity fluctuations during the forced desynchrony protocol ($P = 0.91$) (Fig. 3*B*), although α varies somewhat between different 4-h bins.

This finding for activity fluctuations is in contrast to the significant circadian pattern in the scaling exponent α for the heartbeat interval fluctuations previously published in ref. 11 (Fig. 3*D*), indicating a strong circadian influence on cardiac dynamics. Moreover, the maximum value of α [i.e., a deviation that brings the scale-invariant features of cardiac dynamics closer to those observed under pathologic conditions (13, 16, 18)] occurs at between 60° and 90°, which corresponds to the window 9–11 a.m., where epidemiological studies have reported highest cardiac risk (1–4).

Results of the dynamic measures of activity and RR interval data from the constant-routine protocol are shown in Fig. 3 *E* and *F*. There is no significant circadian rhythm in the scaling exponent α of activity (Fig. 3*E*), whereas a strong circadian rhythm in α of RR intervals persists (Fig. 3*F*), with a similar circadian profile as observed for the forced desynchrony protocol (Fig. 3, compare *D* with *F*).

Discussion

Our investigations demonstrate the presence of a large-amplitude circadian influence upon the static measures (mean and standard deviation) of spontaneous physical activity. Specifically, during the forced desynchrony protocol we find a pronounced peak in the mean activity level and in the standard deviation of activity fluctuations at the circadian phase interval 180–240° (corresponding to the habitual afternoon and evening hours of 5–9 p.m.) and a minimum at ≈0° (corresponding to the lowest CBT, ≈5 a.m.) (Fig. 2 *A* and *B*). In the forced-desynchrony protocol, subjects repeated the same sleep/wake and behavior schedule (i.e., timing of meals and shower, etc.) in all wake periods so that statistically the same

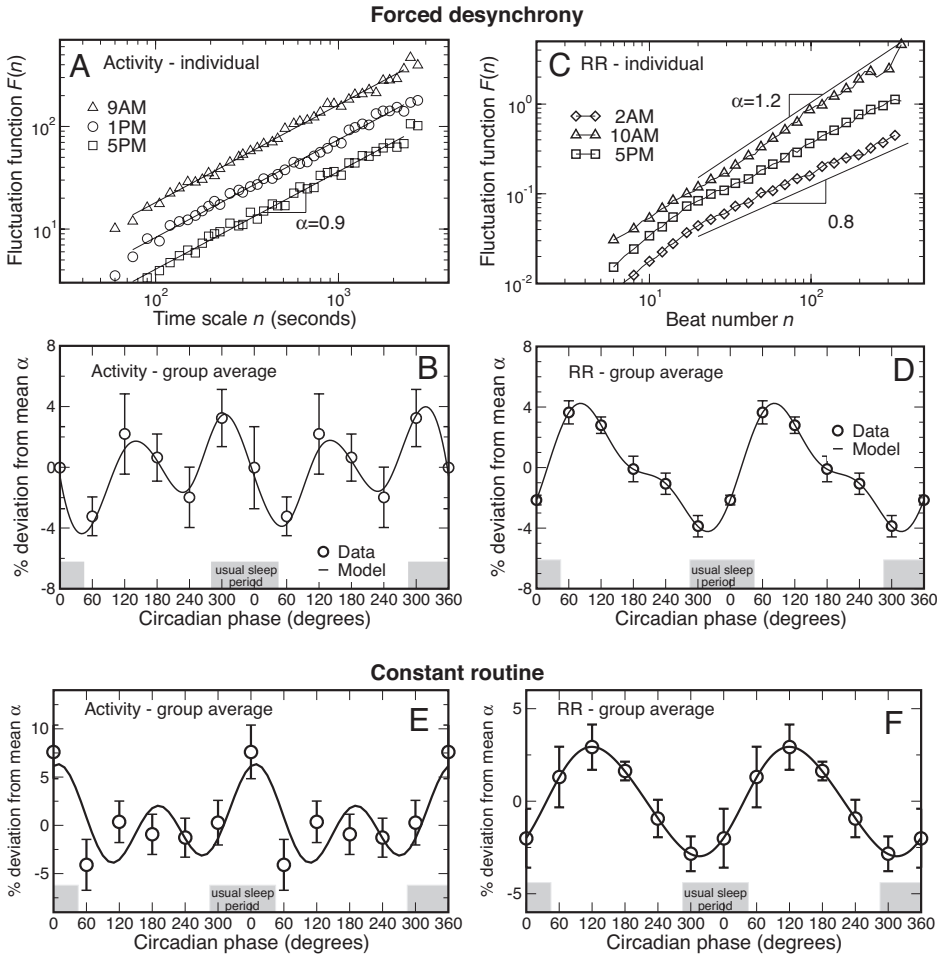

Fig. 3. Scale-invariant dynamic index of activity and heartbeat fluctuations as a function of the circadian phase. (*A* and *C*) Long-range power-law correlations during forced desynchrony in human motor activity fluctuations (*A*) and heartbeat fluctuations (*C*) as quantified by the DFA method (47–49) for one representative subject. Scaling curves $F(n)$ represent the DFA results for different data segments across different circadian phases during wake periods. The values for the exponent α are obtained by fitting $F(n)$ for activity fluctuations in the time scale range $60 < n < 2{,}600$ sec (*A*) and for heartbeat fluctuations in the range $20 < n < 400$ beats (*C*). For clarity, $F(n)$ curves are vertically offset. (*C* and *D*) The results for the exponent α of heartbeat data during forced desynchrony have previously been published (11) and are presented for comparison with activity data. (*B–F*) Cosinor analysis for the group-averaged scaling exponent α during the forced desynchrony (*B* and *D*) and constant-routine (*E* and *F*) protocols for activity fluctuations (*B* and *E*) and heartbeat fluctuations (*D* and *F*). Group-averaged data are shown as symbols (error bars represent standard error), and the cosinor analysis fits are shown as solid lines. (*B* and *D–F*) A significant circadian rhythm in the deviation of the α value is observed only for the heartbeat RR intervals during the forced-desynchrony protocol ($P = 0.01$) (*D*), with a pronounced peak at ≈60° corresponding to the 9–11 a.m. window of increased cardiac risk, and during the constant-routine protocol ($P = 0.004$) (*F*) but not for activity data (*B* and *E*). The habitual sleep period when living outside the laboratory is indicated by gray shaded boxes.

behaviors were evenly distributed across all circadian phases, thus allowing the statistical separation of scheduled behaviors across the wake periods from the influences of the endogenous circadian cycle. Although scheduled behaviors were evenly balanced across the circadian cycle, spontaneous activity was permitted with some mild constraints. With this technique, our findings demonstrate an endogenous circadian variation in mean spontaneous physical activity in humans. Moreover, this variation occurred despite constraints imposed by the laboratory schedule and laboratory environment, including no formal exercise and no unscheduled sleep, suggesting that the endogenous circadian rhythm is a very robust physiological drive. Although day/night activity patterns have been demonstrated in other mammalian species, and even though this mean activity pattern is often used as a circadian phase marker (e.g., ref. 43), generally behaviors, including the sleep/wake cycle, have not been decoupled from the endogenous circadian cycle in such prior animal studies.

We also observe a statistically significant endogenous circadian variation for both mean and standard deviation of the heart rate. The circadian rhythm in the heart rate static measures parallels the rhythm in activity, i.e., the circadian maximum and minimum phases for mean heart rate (inversely proportional to the heartbeat interval) correspond to the circadian peaks and troughs in mean activity level (Fig. 2 *A* and *C*). These findings suggest that the endogenous circadian system alters activity and heart rate regulation in ways that would be appropriate for the expected habitual behavior at that time of the day when living outside the laboratory, namely a lower heart rate when habitual sleep usually occurs. Notably, the lower heart rate at 330–30° is accompanied by an increased probability for large interbeat fluctuations, i.e., a peak in the standard deviation (Fig. 2*D*). Such circadian-mediated decrease of the mean heart rate coupled with an increase of the standard deviation between 3 and 7 a.m. suggests a reduced sympathovagal balance that may be cardioprotective. The apparent synchrony between the rhythms in the static measures of activity and heart rate, characterized by matching minima and maxima (Fig. 2 *A–D*), may reflect a physiological coupling between activity and cardiac control. Notably, it can be seen in Fig. 2 that there was no peak in any of the activity or RR interval static measures around the time of increased cardiac vulnerability (≈9–11 a.m.) (11). That is, the peak in static measures of activity (and heart rate) occur at 5–9 p.m., i.e., ≈9 h later, and there is a very gradual increase in the static characteristics of activity during the morning hours (Fig. 2 *A–D*). Thus, the circadian variation in the static measures of heart rate and activity fluctuations are unlikely to be a contributor to the increased cardiac risk in the time window of 9–11 a.m. (Fig. 1).

In the constant routine in which activity is minimal and constant and, thus, there is no circadian rhythm in the static measurements of activity data (Fig. 2 *E* and *F*), surprisingly we find that the significant circadian rhythm of heart rate persists (Fig. 2 *G* and *H*) and can therefore be uncoupled (be independent) from endogenous circadian rhythms of activity.

In contrast to the static measures of activity fluctuations, our investigations show no significant circadian rhythm in the scale-invariant dynamic index α of activity in either the forced desynchrony or constant-routine protocol (Fig. 3 *A*, *B*, and *E*). This finding suggests that a key measure of activity dynamics, which is related to the intrinsic nonlinear multiscale mechanism of activity

regulation (22), is not influenced by the circadian system. Although there is no significant 24-h rhythm, a significant 12-h rhythm ($P = 0.01$) is apparent in the dynamic index α of activity data but not in the heartbeat interval data (Fig. 3), providing further evidence of decoupling between activity and heart rate. Our findings in the forced desynchrony protocol of pronounced circadian rhythms in the static measures and absence of endogenous circadian modulation in the dynamic scale-invariant measure of activity fluctuations suggest that separate physiologic pathways may be involved in the circadian influence on these different elements of activity regulation.

In contrast to activity fluctuations, the scale-invariant temporal organization of heartbeat fluctuations, as quantified by the dynamic index α, exhibits a significant 24-h circadian pattern (Fig. 3*D*), characterized by a pronounced peak at 60–90°, bringing α closer to the values observed for subjects with congestive heart failure (13) around that time. Notably, this circadian period corresponds to the window 9–11 a.m. of highest cardiac risk (1). Furthermore, the minimum value of α occurs at 300–360°, corresponding to the habitual sleep period outside the laboratory (Fig. 3*D*), bringing the index α closer to the values observed for subjects during sleep (20). Because there is no significant circadian rhythm in the scaling index α of motor activity fluctuations, our results from both the forced desynchrony protocol (Fig. 3*B*) and constant routine (Fig. 3*E*) indicate that circadian influences on dynamic measures of activity are unlikely to contribute to the peak in α observed for heartbeat fluctuations at 9–11 a.m. and are therefore unlikely to contribute to increased cardiac vulnerability.

In summary, our results demonstrate the presence of an endogenous circadian rhythm in the average level and the standard deviation of human motor activity fluctuations, indicating that the circadian pacemaker affects the intrinsic regulation of physical activity. In contrast, the dynamic measure α, which quantifies the scale-invariant temporal structure in activity fluctuations, does not exhibit a significant circadian rhythm. The endogenous circadian variability in the static measures of activity is usually synchronized to the circadian changes in static measures of heart rate, yet the results from the constant-routine protocol demonstrate that the circadian rhythm in static and dynamics measures of the human heart rate can be decoupled from the rhythms in activity. Overall, our data from both forced desynchrony and constant-routine protocols provide no evidence for an activity-mediated circadian influence on either static or dynamic measures of cardiac control (indirect pathway on Fig. 1). Thus, central circadian influences on activity are unlikely to contribute to the observed increase of cardiac risk at given circadian phases. Rather, a direct endogenous circadian influence on cardiac neuroautonomic regulation, which affects the scale-invariant/fractal temporal organization of heartbeat fluctuations over a broad range of time scales, appears more likely to play a role for the peak in adverse cardiac events at ≈10 a.m. Provided a similar circadian rhythm in the dynamic scaling index α for RR intervals also is observed for subjects with cardiac disease, it would potentially contribute to increased risk, because a shift in the scaling exponent α of RR intervals to higher values closer to 1.5 has been robustly linked to pathologic conditions and higher mortality rate (13, 18, 26).

We note, that external behavioral factors, such as exercise, which are independent from the intrinsic circadian influence reported here and which were curtailed in this laboratory experiment, may also be an independent contributing factor to increased cardiac risk when living outside the laboratory environment. Moreover, if such specific activities have a day/night frequency distribution of occurrence, these behaviors could be implicated in the day/night pattern of adverse cardiovascular events. At the same time, our findings in the forced desynchrony of average activity level and standard deviation of activity fluctuations being endogenously driven by the circadian system to higher values in the interval 180–240° (corresponding to 5–9 p.m., the habitual afternoon and evening hours), may have implications when choosing the best time for physical exercise. It is not known to what degree the endogenous circadian rhythm of activity contributes to the day/night activity patterns when living in unconstrained conditions. It is conceivable that preferred times to be more active would coincide with the endogenous circadian rhythm of activity and would lead to a greater amplitude in the day/night pattern of activity in unconstrained conditions. Such a finding would have implications for the optimal time to perform work or volitional exercise and deserves further study.

Finally, our observations raise the possibility that the circadian system operates through a complex feedback mechanism (14, 17), which intrinsically coordinates activity regulation to reduce cardiac stress at particular circadian phases, e.g., by endogenously lowering the mean activity level and the standard deviation of activity fluctuations in the morning hours during the 9–11 a.m. window of elevated sympathetic response (10) and highest cardiac risk (1–4). This putative feedback mechanism of the circadian system may have a cardioprotective role. In contrast, maintaining the scale-invariant/fractal temporal structure in activity fluctuations unchanged across circadian phases may be evolutionary advantageous, as motor control response has to remain optimal over a broad range of time scales (frequencies) throughout the circadian cycle.

Data Collection and Methods

Subjects. We studied six healthy subjects (four male, two female) with a mean age of 25 years (range, 21–32 years) during a forced desynchrony protocol and nine healthy subjects (seven male, two female) with a mean age of 28 years (range, 21–36 years) during a constant-routine protocol. All subjects had no medical disorders other than mild asthma, as assessed by history, physical examination, overnight polysomnography, psychological examination, pulmonary function tests, a 12-lead ECG, and routine blood and urine chemistry.

Forced Desynchrony Protocol. We collected physiologic data throughout a 10-day ''forced desynchrony protocol,'' with subjects living in an individual suite conducting controlled daily behaviors (36–38). There were two initial baseline acclimatization days with 8-h sleep opportunities and 16 h of wakefulness. After a 48-h baseline, sleep periods were delayed by 4 h every day such that subjects were living on recurring 28-h ''days,'' with 9 h and 20 min of sleep opportunity and 18 h and 40 min of scheduled wakefulness. This 28-h recurring sleep/wake schedule was repeated for seven cycles [supporting information (SI) Fig. 4] in the absence of known zeitgebers, such as bright light, so that the body clock oscillated at its inherent rate. Light was kept constant and dim at <8 lux to avoid resetting the body clock, and the subjects had no external cues regarding the time of day. Room temperature was 23°C. Subjects repeated the same behavior schedule in all wake periods so that, statistically, the same scheduled behaviors, including the sleep/wake cycle, occurred evenly across all circadian phases by the end of the protocol. Thus, all scheduled activities become desynchronized from the endogenous circadian pacemaker (36–38), which allows separation of behavioral effects (sleep/wake cycle as well as scheduled activities) from circadian effects. During the periods of wakefulness, spontaneous activity was still possible although somewhat constrained, being limited to walking around the suite, sitting, and resting.

Constant-Routine Protocol. To assess intrinsic activity controllers (i.e., circadian or other neural centers) independent of scheduled and random external influences, activity recordings were made in the laboratory throughout a 38-h constant routine. Subjects were asked to remain awake and seated semirecumbent on a bed (45° torso elevation) in a constant environment with a room temperature of 23°C and dim (<8 lux) indoor light. The dietary intake consisted of a measured portion of food and drink every 2 hours containing ≈100 mEq of potassium and 150 mEq of sodium every 24 h and consisting of 25% fat, 25% protein, and 50% carbohydrates. Fluid intake was constant at 3.5 liters/day evenly distributed and consumed at 2-h intervals. These highly controlled and constant experimental conditions result in reduced average and variance of activity levels. Thus, all scheduled activities remained the same across the entire circadian cycle.

Measurements. As a marker of the endogenous circadian pacemaker, CBT, was recorded throughout the protocols by using a rectal temperature sensor (YSI 20463; Yellow Springs Instruments) with values stored to a computer once per minute. For an assessment of human motor activity, subjects wore a wristwatch-sized *Actiwatch* recorder (MiniMitter) that unobtrusively measured changes in

forearm acceleration in any plane (sensitive to $0.01 \times g$). Each data point recorded in the device's internal memory represents the value of changes in acceleration sampled at 32 Hz and integrated over a 15-s epoch length (44). For an assessment of the cardiac interbeat interval, a chest lead ECG was recorded on an ambulatory recording device (Vitaport; Temec Instruments) at 256 Hz throughout the forced desynchrony and constant routine protocols. Cardiac interbeat intervals were obtained from the ECG by using a QRS wave detector based on the Aristotle algorithm (45). Data on RR intervals from the forced desynchrony protocol have previously been published (11).

Estimation of Circadian Phases. CBT was used as the marker of the circadian phase (36, 46). Each subject's phase and period of the CBT circadian rhythm was estimated by nonlinear least-squares regression (38), and a circadian phase was assigned to hourly averages of activity and heartbeat data relative to the time of the minimum CBT (CBT minimum = 0° circadian phase corresponding to ≈5 a.m. in these subjects).

DFA. We used the DFA to estimate correlations in the activity and heartbeat interval fluctuations (47). Compared with traditional correlation analyses, such as autocorrelation, power-spectrum analysis, and Hurst analysis, the advantage of the DFA method is that it can accurately quantify the correlation property of signals masked by polynomial trends (41, 42). Details on the DFA method are presented in *SI Data Collection and Methods*.

Analysis of Circadian Rhythmicity in Activity and Cardiac Dynamics. We analyzed and compared activity and heartbeat data recorded only during the periods of wakefulness in the forced desynchrony and constant-routine protocols. We separated activity data during the wakeful periods into nonoverlapping segments of the same size, and, for each segment, we calculated the values of the DFA scaling exponent α (a dynamic scale-invariant measure of activity fluctuations), and the mean and the standard deviation of activity levels (static measures). We used different segment sizes for the different measures we estimated, i.e., 1-h segments for the mean and the standard deviation of activity levels and 4-h segments for the DFA scaling exponent α. We chose 4-h as the segment size for the DFA scaling exponent because the DFA method requires ≈1,000 data points for an accurate estimate of the long-range power-law correlations and the scaling exponent α (each 4-h segment contains 960 data points) (41, 42). For each 4-h data segment, we estimated the scaling exponent α over the same range of time scales, from 1 to 40 min. For each subject, we analyzed ≈124 h for wake periods throughout the forced desynchrony protocol (SI Fig. 4). Next, we assigned a circadian phase (determined from the regression analysis of CBT) for each DFA exponent value obtained from 4-h activity data segments as well as for each mean and standard deviation value obtained from 1-h activity data segments. Because the activity level is much lower (large percentage of zero values in the actigraphy recordings) and the motor control mechanism is quite different during sleep, we analyzed data only during wake periods in the forced desynchrony protocol. Similar recordings and analyses of RR interval data from the same individuals in the forced desynchrony protocol have previously been published (11). Details regarding the cosinor analysis, our data binning procedure across circadian phases, and data statistics for each bin are presented in *SI Data Collection and Methods*.

ACKNOWLEDGMENTS. We thank Zhi Chen for help in extracting data. This work was supported by National Institutes of Health Grants HL071972 (to H.E.S.), HL076446 (to S.A.S.), and HL076409 (to S.A.S.).

1. Muller JE, Stone PH, Turi ZG, Rutherford JD, Czeisler CA, Parker C, Poole WK, Passamani E, Roberts R, Robertson T, *et al.* (1985) *N Eng J Med* 313:1315–1322.
2. Goldberg RJ, Brady P, Muller JE, Chen ZY, Degroot M, Zonneveld P, Dalen JE (1990) *Am J Cardiol* 66:140–144.
3. Ridker PM, Manson JE, Buring JE, Muller JE, Hennekens CH (1990) *Circulation* 82:897–902.
4. Tofler GH, Stone PH, Maclure M, Edelman E, Davis VG, Robertson T, Antman EM, Muller JE (1990) *Am J Cardiol* 66:22–27.
5. Marler JR, Price TR, Clark GL, Muller JE, Robertson T, Mohr JP, Hier DB, Wolf PA, Caplan LR, Foulkes MA (1989) *Stroke* 20:473–476.
6. Willich SN, Pohjola-Sintonen S, Bhatia SJS, Shook TL, Tofler GH, Muller JE, Curtis DG, Williams GH, Stone PH (1989) *Circulation* 79:557–565.
7. Willich SN, Goldberg RJ, Maclure M, Perriello L, Muller JE (1992) *Am J Cardiol* 70:65–68.
8. Shea SA, Hilton MF, Muller JE (2007) in *Clinical Hypertension and Vascular Disease: Blood Pressure Monitoring in Cardiovascular Medicine and Therapeutics* (Humana, Totowa, NJ), pp 253–291.
9. Buijs RM, La Fleur SE, Wortel J, Van Heyningen C, Zuiddam L, Mettenleiter TC, Kalsbeek A, Nagai K, Niijima A (2003) *J Comp Neurol* 464:36–48.
10. Hilton MF, Umali MU, Czeisler CA, Wyatt JK, Shea SA (2001) *Comp Cardiol* 27:197–200.
11. Hu K, Ivanov PCh, Hilton MF, Zhi C, Ayers RT, Stanley HE, Shea SA (2004) *Proc Natl Acad Sci USA* 101(52):18223–18227.
12. Kobayashi M, Musha T (1982) *IEEE Trans Biomed Eng* 29:456–457.
13. Peng C-K, Havlin S, Stanley HE, Goldberger AL (1995) *Chaos* 5:82–87.
14. Ivanov PCh, Amaral LAN, Goldberger AL, Havlin S, Rosenblum MG, Stanley HE, Struzik ZR (2001) *Chaos* 11:641–652.
15. Ivanov PCh, Rosenblum MG, Peng C-K, Mietus J, Havlin S, Stanley HE, Goldberger AL (1996) *Nature* 383:323–327.
16. Goldberger AL (1996) *Lancet* 347:1312–1314.
17. Ivanov PCh, Nunes ALA, Goldberger AL, Stanley HE (1998) *Europhys Lett* 43:363–368.
18. Ho KKL, Moody GB, Peng C-K, Mietus JE, Larson MG, Levy D, Goldberger AL (1997) *Circulation* 96:842–848.
19. Ivanov PCh, Rosenblum MG, Amaral LAN, Struzik ZR, Havlin S, Goldberger AL, Stanley HE (1999) *Nature* 399:461–465.
20. Ivanov PCh, Bunde A, Amaral LAN, Havlin S, Fritsch-Yelle J, Baevsky RM, Stanley HE, Goldberger AL (1999) *Europhys Lett* 48:594–600.
21. Bunde A, Havlin S, Kantelhardt JW, Penzel T, Peter JH, Voigt K (2000) *Phys Rev Lett* 85:3736–3739.
22. Hu K, Ivanov PCh, Hilton MF, Chen Z, Stanley HE, Shea SA (2004) *Physica A* 337:307–318.
23. Wolf MM, Varigos GA, Hunt D, Sloman JG (1978) *Med J Aust* 2:52–53.
24. O'Brien IA, O'Hare P, Corrall RJ (1986) *Br Heart J* 55:348–354.
25. Tsuji H, Venditti FJ, Manders ES, Evans JC, Larson MG, Feldman CL, Levy D (1994) *Circulation* 90:878–883.
26. Huikuri HV, Makikallio TH, Peng CK, Goldberger AL, Hintze U, Moller M (2000) *Circulation* 101:47–53.
27. Bernaola-Galvan P, Ivanov PCh, Amaral LAN, Stanley HE (2001) *Phys Rev Lett* 87:168105.
28. Kantelhardt JW, Ashkenazy Y, Ivanov PCh, Bunde A, Havlin S, Penzel T, Peter JH, Stanley HE (2002) *Phys Rev E* 65:051908.
29. Penzel T, Kantelhardt JW, Grote L, Peter JH, Bunde A (2003) *IEEE Trans Biomed Eng* 50:1143–1451.
30. Amaral LAN, Ivanov PCh, Aoyagi N, Hidaka I, Tomono S, Goldberger AL, Stanley HE, Yamamoto Y (2001) *Phys Rev Lett* 86:6026–6029.
31. Karasik R, Sapir N, Ashkenazy Y, Ivanov PCh, Dvir I, Lavie P, Havlin S (2002) *Phys Rev E* 66:062902.
32. Martinis M, Knezevic A, Krstacis G, Vargovic E (2004) *Phys Rev E* 70:012903.
33. Housdorff JM, Purdon PL, Peng CK, Ladin Z, Wei JY, Goldberger AL (1996) *J Appl Physiol* 80:1448–1457.
34. Ashkenazy Y, Hausdorff JM, Ivanov PCh, Stanley HE (2002) *Physica A* 316:662–670.
35. Bartsch R, Plotnik M, Kantelhardt JW, Havlin S, Giladi N, Hausdorff JM (2007) *Physica A* 383:455–465.
36. Czeisler CA, Duffy JF, Shanahan TL, Brown EN, Mitchell JF, Rimmer DW, Ronda JM, Silva EJ, Allan JS, Emens JS, *et al.* (1999) *Science* 284:2177–2181.
37. Czeisler CA, Khalsa SB (2000) in *Principles and Practice of Sleep Medicine*, eds Kryger MH, Roth T, Dement WC (Saunders, Philadelphia), pp 354–375.
38. Dijk DJ, Czeisler CA (1994) *Neurosci Lett* 166:63–68.
39. Muller JE, Ludmer PL, Willich SN, Tofler GH, Aylmer G, Klangos I, Stone PH (1987) *Circulation* 75:131–138.
40. Aronson D (2001) *Chronobiol Int* 18:109–121.
41. Hu K, Ivanov PCh, Chen Z, Carpena P, Stanley HE (2001) *Phys Rev E* 64:011114.
42. Chen Z, Ivanov PCh, Hu K, Stanley HE (2002) *Phys Rev E* 65:041107.
43. Stephan FK, Zucker I (1972) *Proc Natl Acad Sci USA* 69:1583–1586.
44. Jean-Louis G, Mendlowicz MV, Gillin JC, Rapaport MH, Kelsoe JR, Zizi F, Landolt HP, Von Gizycki H (2000) *Physiol Behav* 70:49.
45. Moody MB, Mark RG (1982) in *Computers in Cardiology* (IEEE Comp Soc Press, Los Alamitos, CA), pp 39–44.
46. Brown EN, Czeisler CA (1992) *J Biol Rhythms* 7:177–202.
47. Peng C-K, Buldyrev SV, Havlin S, Simons M, Stanley HE, Goldberger AL (1994) *Phys Rev E* 49:1685–1689.
48. Nelson W, Tong YL, Lee JK (1979) *Chronobiologia* 6:305–323.

Endogenous circadian rhythm in human motor activity uncoupled from circadian influences on cardiac dynamics

By: Ivanov, PC (Ivanov, Plamen Ch.)[1]; Hu, K (Hu, Kun)[2,1]; Hilton, MF (Hilton, Michael F.)[3]; Shea, SA (Shea, Steven A.)[2]; Stanley, HE (Stanley, H. Eugene)[1]

View ResearcherID and ORCID

PROCEEDINGS OF THE NATIONAL ACADEMY OF SCIENCES OF THE UNITED STATES OF AMERICA
Volume: 104 **Issue:** 52 **Pages:** 20702-20707
DOI: 10.1073/pnas.0709957104
Published: DEC 26 2007
Document Type: Article
View Journal Impact

Abstract

The endogenous circadian pacemaker influences key physiologic functions, such as body temperature and heart rate, and is normally synchronized with the sleep/wake cycle. Epidemiological studies demonstrate a 24-h pattern in adverse cardiovascular events with a peak at approximate to 10 a.m. It is unknown whether this pattern in cardiac risk is caused by a day/night pattern of behaviors, including activity level and/or influences from the internal circadian pacemaker. We recently found that a scaling index of cardiac vulnerability has an endogenous circadian peak at the circadian phase corresponding to approximate to 10 a.m., which conceivably could contribute to the morning peak in cardiac risk. Here, we test whether this endogenous circadian influence on cardiac dynamics is caused by circadian-mediated changes in motor activity or whether activity and heart rate dynamics are decoupled across the circadian cycle. We analyze high-frequency recordings of motion from young healthy subjects during two complementary protocols that decouple the sleep/wake cycle from the circadian cycle while controlling scheduled behaviors. We find that static activity properties (mean and standard deviation) exhibit significant circadian rhythms with a peak at the circadian phase corresponding to 5-9 p.m. (approximate to 9 h later than the peak in the scale-invariant index of heartbeat fluctuations). In contrast, dynamic characteristics of the temporal scale-invariant organization of activity fluctuations (long-range correlations) do not exhibit a circadian rhythm. These findings suggest that endogenous circadian-mediated activity variations are not responsible for the endogenous circadian rhythm in the scale-invariant structure of heartbeat fluctuations and likely do not contribute to the increase in cardiac risk at approximate to 10 a.m.

Keywords

Author Keywords: cardiac vulnerability; circadian pacemaker; locomotor activity; scale invariance
KeyWords Plus: ACUTE MYOCARDIAL-INFARCTION; HEART-RATE-VARIABILITY; SCALING BEHAVIOR; MORNING INCREASE; TIME-SERIES; SLEEP; ONSET; FLUCTUATION; DEATH; MORTALITY

Author Information

Reprint Address: Ivanov, PC (reprint author)

+ Boston Univ, Ctr Polymer Studies, Dept Phys, 590 Commonwealth Ave, Boston, MA 02215 USA.

Addresses:

+ [1] Boston Univ, Ctr Polymer Studies, Dept Phys, Boston, MA 02215 USA

+ [2] Brigham & Womens Hosp, Harvard Med Sch, Div Sleep Med, Boston, MA 02115 USA

[3] Univ Queensland, Sch Populat Hlth, Brisbane, Qld 4072, Australia

E-mail Addresses: plamen@buphy.bu.edu; sshea@hms.harvard.edu

Funding

Funding Agency	Grant Number
NHLBI NIH HHS	HL071972 K24 HL076446-04 R01 HL076409 HL076446 HL076409 K24 HL076446-01 R01 HL071972 K24 HL076446

Publisher

NATL ACAD SCIENCES, 2101 CONSTITUTION AVE NW, WASHINGTON, DC 20418 USA

Journal Information

Impact Factor: Journal Citation Reports

Categories / Classification

Research Areas: Science & Technology - Other Topics

Web of Science Categories: Multidisciplinary Sciences

See more data fields

Cited References: 48

Showing 30 of 48 **View All in Cited References page** *(from Web of Science Core Collection)*

1. **Behavioral-independence features of complex heartbeat dynamics** **Times Cited: 186**
By: Amaral, LAN; Ivanov, PC; Aoyagi, N; et al.
PHYSICAL REVIEW LETTERS Volume: 86 Issue: 26 Pages: 6026-6029 Published: JUN 25 2001

2. **Impaired modulation of circadian rhythms in patients with diabetes mellitus: A risk factor for cardiac thrombotic events?** **Times Cited: 24**
By: Aronson, D
CHRONOBIOLOGY INTERNATIONAL Volume: 18 Issue: 1 Pages: 109-121 Published: 2001

3. **A stochastic model of human gait dynamics** **Times Cited: 87**
By: Ashkenazy, Y; Hausdorff, JA; Ivanov, PC; et al.
PHYSICA A-STATISTICAL MECHANICS AND ITS APPLICATIONS Volume: 316 Issue: 1-4 Pages: 662-670 Article Number: PII S0378-4371(02)01453-X Published: DEC 15 2002

4. **Fluctuation and synchronization of gait intervals and gait force profiles distinguish stages of Parkinson's disease** **Times Cited: 41**
By: Bartsch, Ronny; Plotnik, Meir; Kantelhardt, Jan W.; et al.
PHYSICA A-STATISTICAL MECHANICS AND ITS APPLICATIONS Volume: 383 Issue: 2 Pages: 455-465 Published: SEP 15 2007

5. **Scale invariance in the nonstationarity of human heart rate** **Times Cited: 132**

Eur. Phys. J. B **63**, 547–550 (2008)
DOI: 10.1140/epjb/e2008-00210-2

THE EUROPEAN PHYSICAL JOURNAL B

Influence of corruption on economic growth rate and foreign investment

Boris Podobnik[1,2,3,a], Jia Shao[3], Djuro Njavro[2], Plamen Ch. Ivanov[3,4,b], and H.E. Stanley[3]

[1] Department of Physics, Faculty of Civil Engineering, University of Rijeka, Rijeka, Croatia
[2] Zagreb School of Economics and Management, Zagreb, Croatia
[3] Center for Polymer Studies and Department of Physics, Boston University, Boston, 02215, USA
[4] Institute of Solid State Physics, Bulgarian Academy of Sciences, 1784 Sofia, Bulgaria

Received 9 December 2007 / Received in final form 23 April 2008
Published online 4 June 2008 –

Abstract. We analyze the dependence of the Gross Domestic Product (GDP) per capita growth rates on changes in the Corruption Perceptions Index (CPI). For the period 1999–2004 for all countries in the world, we find on average that an increase of CPI by one unit leads to an increase of the annual GDP per capita growth rate by 1.7%. By regressing only the European countries with transition economies, we find that an increase of CPI by one unit generates an increase of the annual GDP per capita growth rate by 2.4%. We also analyze the relation between foreign direct investments received by different countries and CPI, and we find a statistically significant power-law functional dependence between foreign direct investment per capita and the country corruption level measured by the CPI. We introduce a new measure to quantify the relative corruption between countries based on their respective wealth as measured by GDP per capita.

PACS. 89.90.+n Other topics in areas of applied and interdisciplinary physics

Corruption, defined as abuse of public power for private benefit, is a global phenomenon that affects almost all aspects of social and economic life. Examples of corruption include the sale of government property by public officials, bribery, embezzlement of public funds, patronage and nepotism. The World Bank estimates that over 10^9 US dollars annually are lost due to corruption, representing 5% of the world GDP. The African Union estimates that due to corruption, the African continent loses 25% of its GDP [1].

Previous studies have mainly reported a negative association between corruption level and country wealth [2–5], i.e., on average richer countries are less corrupt. There is ongoing debate concerning the relation between corruption and economic growth [6]. Some earlier studies suggest that corruption may even help the most efficient firms bypass bureaucratic obstacles and rigid laws [7], while recent papers do not find a significant negative association between economic growth and the level of corruption [2,3]. The majority of studies have found an insignificant negative association between the corruption level and foreign investments [3,8,9], without reporting a specific functional dependence.

In order to find a quantitative relation between corruption level and economic factors such as GDP growth rate and foreign direct investments, we analyze the Corruption Perceptions Index (CPI) [10] introduced by Transparency International, a global civil organization supported by government agencies, developmental organizations, foundations, public institutions, the private sector, and individuals. The CPI is a composite index ranging from 0 to 10, where 0 denotes the highest level of corruption and 10 denotes the lowest. For GDP per capita we use annual nominal GDP per capita in current prices in US dollars [11], and GDP per capita in constant dollars [12].

The CPI 2006 index is defined based on data gathered from 12 sources originating from 9 independent institutions. All sources measure the overall extent of corruption, where evaluation of the extent of corruption in different countries is done by experts, residents and non-residents. The ranks, and not the scores of countries, are the only information provided from each source. The CPI 2006 combines assessments for the past two years only. Each of the sources uses its own evaluation system, and for that reason the data are standardized before a single mean value for the CPI is determined for each country. This standardization is carried out in two steps, using two statistical methods: matching percentiles and beta-transformation [10].

Table 1 shows the first ten least corrupt countries as ranked by Transparency International according to the

[a] e-mail: bp@phy.hr
[b] e-mail: plamen@buphy.bu.edu

Table 1. Rank of countries (left column) by Transparency International for year 2006 with CPI values (right column) for each country.

1	Finland, Iceland, New Zealand	**9.6**
4	Denmark	**9.5**
5	Singapore	**9.4**
6	Sweden	**9.2**
7	Switzerland	**9.1**
8	Norway	**8.8**
9	Australia, Netherlands	**8.7**
11	United Kingdom	**8.6**
16	Germany	**8.0**
17	Japan	**7.6**
18	France, Ireland	**7.4**
20	Belgium, Chile, USA	**7.3**
37	Botswana	**5.6**
40	Italy	**5.0**
70	China, India, Mexico, Brazil, Senegal Ghana, Egypt, Peru, S.Arabia,	**3.3**
121	Russia	**2.5**

CPI values obtained in 2006 as well as some other countries. Besides some Western European countries, among the least corrupt ten countries are New Zealand, Singapore, and Australia. Chile and Botswana are the least corrupt countries in South America and Africa, whereas Singapore is the least corrupt Asian country. Table 1 provides information about corruption levels throughout the World in absolute terms, where each country, whether rich or poor, is given only its CPI value.

In the modern economy, globalization leads to economic competition and comparison between countries, so we compare the corruption levels for different groups of countries in the world. Normalizing the CPI value for year 2006 on the population in each country [13], we find a normalized CPI value for the world to be 3.7, for the countries in Europe we find 5.4, for Asia and Latin America we find 3.3, and for Africa 2.7.

An earlier study reported a power-law functional dependence between GDP per capita, GDP_{pc}, and CPI for all countries [5]:

$$CPI = N\ (GDP_{pc})^{\mu} \tag{1}$$

with scaling exponent $\mu \approx 0.23$ (see Fig. 1), and constant $N = 0.548$. This functional dependence spans multiple scales of wealth and remains stable over different time periods. The positive value of exponent μ indicates that richer countries are less corrupt. This power-law dependence provides information about the expected level of corruption for a given level of country wealth — e.g., a country above (or below) the fitting line is less (or more) corrupt than expected for its level of wealth. We may say that for a country above the fitting line the level of corruption is less than the expected level for the given country wealth [5].

This previous finding indicates that in order to compare the corruption level between two countries, countries may be compared not only in terms of absolute CPI values but also in terms of relative country wealth. To this end, we introduce a new measure of relative corruption which we call *Honesty per Dollar* (H_{pd}):

$$H_{pd} = \ln(CPI) - \mu \ln(GDP_{pc}) - \ln N, \tag{2}$$

equal to the difference between the actual CPI value and the value of CPI expected from the power-law fitting line (Fig. 1), where N is defined in equation (1).

We assume that all countries, with similar GDP per capita and falling on the power-law fitting line in Figure 1, have comparable levels of corruption when ($H_{pd} = 0$). Generally, the larger the value for H_{pd}, the better the performance of a country. For 2006 based on regression of the data for the entire world, we can calculate the values of the H_{pd} index for individual countries: $H_{pd}(UK) = 0.29$, $H_{pd}(USA) = 0.1$, $H_{pd}(Italy) = -0.23$, $H_{pd}(Greece) = -0.3$. The negative values of H_{pd} index for Italy and Greece, indicate that these two countries are relatively more corrupt than expected for their corresponding level of wealth (GDP per capita).

One of the reasons for a country to reduce corruption is to attract more foreign investments, and thus to additionally increase its GDP. This is because corruption generally increases start-up costs for new businesses. If investors can choose between two countries with different levels of corruption, they may choose not to start their business in a more corrupt country since the profit in that country will be reduced. In the previous study we have analyzed how the corruption level relates to foreign

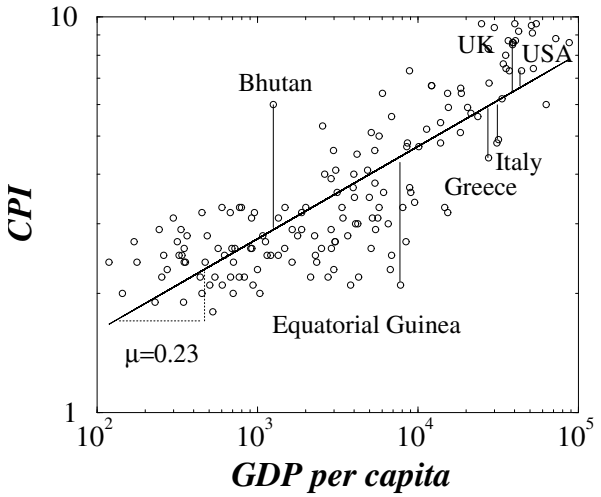

Fig. 1. Corruption level measured by Corruption Perceptions Index (CPI) versus country wealth measured by GDP per capita calculated for 2006 (in US dollars). We find the functional dependence can be fit by a power law 0.56 $(GDP_{pc})^{0.23}$ with positive exponent. The power law fit in log-log plot represents the expected level of CPI for a country with given GDP per capita. The countries that are above the line are less corrupt than expected. We define a new index, Honesty per Dollar (H_{pd}) to measure relative performance of a country when CPI and GDP per capita are simultaneously considered. Besides the USA, UK, Greece, and Italy, we show the countries with the extreme H_{pd} values, Bhutan and Equatorial Guinea (oil exporter).

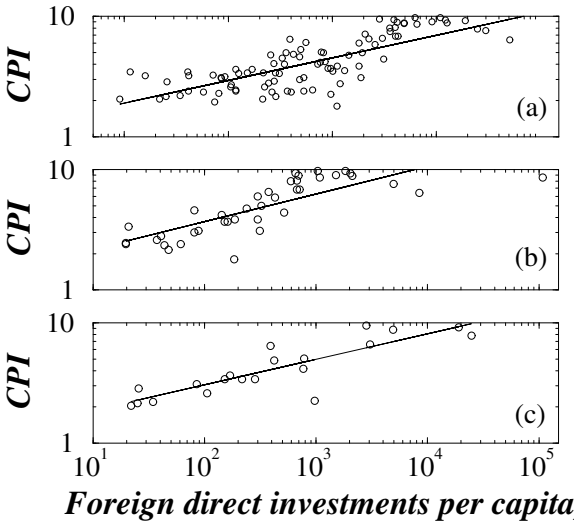

Fig. 2. Less corrupt countries receive more foreign investments. For the period 1999-2004, we show average foreign direct investments (FDI) per capita (in U.S. dollars) originating from all foreign countries, denoted by I, received by (a) World, (b) European, and (c) Asian countries versus corruption level measured by CPI. We find a statistically significant power-law dependence between I and CPI, $CPI \sim I^{\lambda}$ with scaling exponents: for the World $\lambda = 0.19$ ($\Delta = 0.016$), Europe $\lambda = 0.23$ ($\Delta = 0.029$), Asia $\lambda = 0.21$ ($\Delta = 0.029$). In the paranthesis we show the standard errors of the exponents. In the study we exclude Indonesia and Cameroon as countries with total negative value for FDI.

direct investments received by different countries from the United States [5]. For each continent we have found that the functional dependence between the US direct investments per capita, I, and the corruption levels across countries exhibits scale-invariant behavior characterized by a power law

$$CPI \sim I^{\lambda}. \quad (3)$$

Since $\lambda > 0$ for each continent, less corrupt countries have received on average more US investment per capita.

For each country in the world we analyze the foreign direct investments (FDI) received from all foreign countries (not only from the US). For each country we sum up the foreign direct investments over the period 1999–2004, and we calculate the average FDI per year per capita. In Figure 2 we show that the functional dependence between the average foreign direct investment per capita, I, and the corruption level measured by CPI exhibits power-law behavior $CPI \sim I^{\lambda}$ with a statistically significant scaling exponent $\lambda = 0.19$ and a standard error $\Delta = 0.016$ [14]. As for the case of the foreign direct investments originating from the US only [5], we find that less corrupt countries on average receive more foreign investments per capita than more corrupt countries.

We next repeat our analysis for different continents. Again we obtain a power-law dependence $CPI \sim I^{\lambda}$ with scaling exponents for Europe $\lambda = 0.23$ ($\Delta = 0.029$), for Asia $\lambda = 0.21$ ($\Delta = 0.029$), for Latin America $\lambda = 0.23$ ($\Delta = 0.085$) and for Africa $\lambda = 0.18$ ($\Delta = 0.059$).

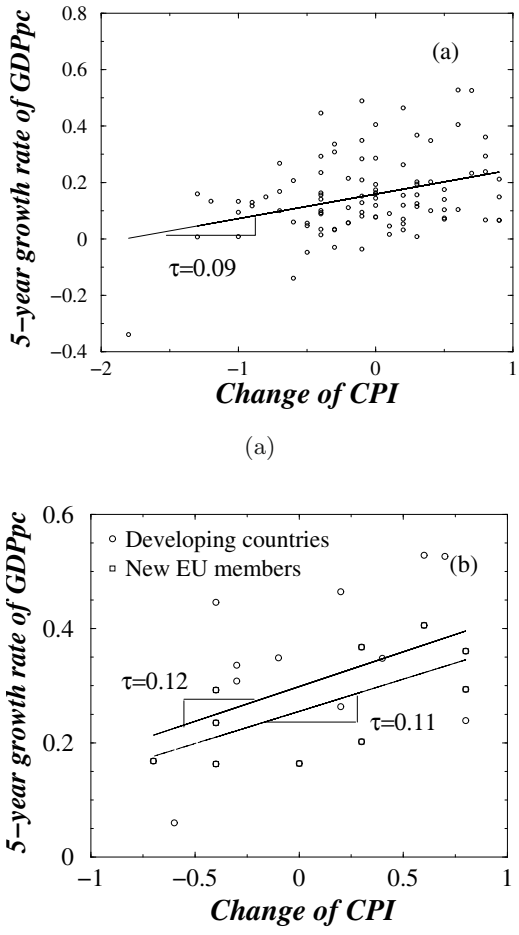

Fig. 3. Countries improving more corruption level generates larger GDP per capita growth rate. For the period 1999–2004, we plot growth rate of GDP per capita in constant dollars, defined as $\ln(GDP_{pc}(2004)) - \ln(GDP_{pc}(1999))$ versus difference of CPI. We analyze (a) world countries (except Belgium and Uruguay) and (b) 21 European transition countries. For each case we find a functional dependence that can be approximated by a straight line. For case (a), by using linear regression we obtain exponent $\tau = 0.09$ (five year period) with standard error $\Delta = 0.024$. For case (b), we obtain exponent $\tau = 0.12$ (five years period) with $\Delta = 0.049$. Thus, for (b) we find that — on yearly basis — increase of CPI by one is followed on average by increase of GDP per capita growth rate equal to ≈2.4%. Separately, for ten new EU members we obtain that the functional dependence between GDP per capita growth rates and change of CPI can be fit by linear regression with statistically significant exponent $\tau = 0.11$ and standard error $\Delta = 0.044$. Note that if Belgium and Uruguay (outliers) are included in (a), the estimated exponent in this regression is 0.052, where $\Delta = 0.022$.

The parameters obtained for each continent are statistically significant at the 5% level. Note that the scaling exponent $\lambda = 0.23$ we obtain for Europe when considering investments from all foreign countries is larger than the scaling exponent $\lambda = 0.14$ obtained for Europe when considering foreign investments only from the US reported in Ref. [5].

Finally, we investigate the relation between change in CPI and economic growth as measured by growth in the GDP per capita, defined as $\ln(GDP_{pc}(t)) - \ln(GDP_{pc}(t'))$, where t and t' are two different years. For the period 1999–2004 and countries ranked by Transparency International, we run regression fit between the growth rate of the GDP per capita in constant dollars as dependent variable and the change in CPI for this period as the explanatory variable. In Figure 3a we show GDP per capita growth rates versus change in CPI that can be fit by a linear regression with a slope $\tau \approx 0.09$. We find that an increase in CPI by one unit leads on average to a 1.7% increase in GDP per capita growth rate.

We perform the same analysis for 39 European countries ranked by Transparency International for the period 1999–2004 and we obtain a statistically *insignificant* dependence of GDP per capita growth rate on changes in CPI (exponent $\tau = 0.036$ and standard error $\Delta = 0.042$). Then we repeat the same analysis for 21 European countries with transition economies. In Figure 3b for the period 1999–2004 we show the GDP per capita growth rate in constant dollars versus change in CPI. We find a functional dependence that can be approximated by a straight line, where the slope 0.12 (standard error $\Delta = 0.049$) is statistically significant at the 5% level. This result shows that an increase of CPI by one unit is followed by additional annual increase of GDP per capita growth rate of approximately 2.4%. For all EU members, we find that the GDP per capita growth rate in constant dollars versus change of CPI is characterized by a similar statistically significant exponent $\tau = 0.11$ with error $\Delta = 0.044$ (see Fig. 3b).

In summary, we have observed a statistically significant power-law functional dependence between CPI and foreign direct investment per capita. This power-law dependence spans a broad range of scales in foreign direct investment (from hundreds to tens of thousands of dollars). We also find a statistically significant dependence between changes in CPI and GDP per capita growth rate, consistent with the interesting possibility that reducing the corruption level leads to significant growth in the wealth of country.

References

1. H. Boch, *Regional Brief*: available at `http://go.worldbank.org/3IGKDWFTG1`
2. J. Svensson, J. Economic Perspectives **19**, 19 (2005)
3. P. Mauro, Quarterly J. Economics **110**, 681 (1995)
4. V. Tanzi, H.R. Davoodi, *Corruption, Growth, and Public Finance*, Working Paper of the International Monetary Fund, Fiscal Affairs Department (2000)
5. J. Shao, P.Ch. Ivanov, B. Podobnik, H.E. Stanley, Eur. Phys. J. **56**, 157 (2007)
6. J.G. Lambsdorf, *Corruption in Empirical Research* — A review, Transparency International Working Paper, (1999)
7. N.H. Leff, American Behavioral Scientists **82**, 337 (1964)
8. D. Wheeler, A. Mody, J. International Economics **33**, 57 (1992)
9. S.J. Wei, Rev. Economics & Statistics **82**, 1 (2000)
10. The Corruption Perceptions Index (CPI) is published by Transparency International `www.transparency.org`
11. GDP per capita as current prices in US dollars are provided by the International Monetary Fund, WORLD ECONOMIC OUTLOOK Database, September 2006, `www.imf.org/external/pubs/ft/weo/2006`
12. Foreign Direct Investments data and GDP per capita as constant prices in US dollars are provided by `www.earthtrends.wri.com`
13. Population data are provided by `www.earthtrends.wri.com`
14. To test at the 0.05 significance level if exponent λ obtained from the regression line is statistically significant, we use t-ratio (t-value) defined as $t = \lambda/\sigma$, where σ represents the standard deviation of the coefficient λ. If t lies outside the interval $-t_{0.975}$ to $t_{0.975}$, where $t_{0.975}$ is a critical value, then λ is statistically significant ($\lambda \neq 0$)

Influence of corruption on economic growth rate and foreign investment

By: Podobnik, B (Podobnik, Boris)[1,2,3,4]; Shao, J (Shao, Jia)[3,4]; Njavro, D (Njavro, Djuro)[2]; Ivanov, PC (Ivanov, Plamen Ch.)[3,4,5]; Stanley, HE (Stanley, H. E.)[3,4]

View ResearcherID and ORCID

EUROPEAN PHYSICAL JOURNAL B
Volume: 63 **Issue:** 4 **Pages:** 547-550
DOI: 10.1140/epjb/e2008-00210-2
Published: JUN 2008
Document Type: Article
View Journal Impact

Abstract

We analyze the dependence of the Gross Domestic Product (GDP) per capita growth rates on changes in the Corruption Perceptions Index (CPI). For the period 1999-2004 for all countries in the world, we find on average that an increase of CPI by one unit leads to an increase of the annual GDP per capita growth rate by 1.7%. By regressing only the European countries with transition economies, we find that an increase of CPI by one unit generates an increase of the annual GDP per capita growth rate by 2.4%. We also analyze the relation between foreign direct investments received by different countries and CPI, and we find a statistically significant power-law functional dependence between foreign direct investment per capita and the country corruption level measured by the CPI. We introduce a new measure to quantify the relative corruption between countries based on their respective wealth as measured by GDP per capita.

Author Information

Reprint Address: Podobnik, B (reprint author)

+ Univ Rijeka, Fac Civil Engn, Dept Phys, Rijeka, Croatia.

Addresses:

+ [1] Univ Rijeka, Fac Civil Engn, Dept Phys, Rijeka, Croatia
[2] Zagreb Sch Econ & Management, Zagreb, Croatia
+ [3] Boston Univ, Ctr Polymer Studies, Boston, MA 02215 USA
+ [4] Boston Univ, Dept Phys, Boston, MA 02215 USA
+ [5] Bulgarian Acad Sci, Inst Solid State Phys, BU-1784 Sofia, Bulgaria

E-mail Addresses: bp@phy.hr; plamen@buphy.bu.edu

Publisher

SPRINGER, 233 SPRING ST, NEW YORK, NY 10013 USA

Journal Information

Impact Factor: Journal Citation Reports

Categories / Classification

Research Areas: Physics

Web of Science Categories: Physics, Condensed Matter

See more data fields

If you would like to improve the quality of the data in this record, please suggest a correction.

88 of 127

Cited References: 11

Showing 11 of 11 View All in Cited References page *(from Web of Science Core Collection)*

1. Title: [not available]
   By: BOCH H
   REGIONAL BRIEF
   Times Cited: 1

2. Title: [not available]
   Group Author(s): International Monetary Fund
   World Economic Outlook Database Published: 2006
   Times Cited: 20

3. Title: [not available]
   By: LAMBSDORF JG
   CORRUPTION EMPIRICAL Published: 1999
   Times Cited: 1

4. Title: [not available]
   By: LEFF NH
   AM BEHAV SCI Volume: 82 Pages: 337 Published: 1964
   Times Cited: 20

5. **CORRUPTION AND GROWTH**
   By: MAURO, P
   QUARTERLY JOURNAL OF ECONOMICS Volume: 110 Issue: 3 Pages: 681-712 Published: AUG 1995
   Times Cited: 2,203

6. **Quantitative relations between corruption and economic factors**
   By: Shao, Jia; Ivanov, Plamen Ch.; Podobnik, Boris; et al.
   EUROPEAN PHYSICAL JOURNAL B Volume: 56 Issue: 2 Pages: 157-166 Published: MAR 2007
   Times Cited: 32

7. **Eight questions about corruption**
   By: Svensson, J
   JOURNAL OF ECONOMIC PERSPECTIVES Volume: 19 Issue: 3 Pages: 19-42 Published: SUM 2005
   Times Cited: 426

8. Title: [not available]
   By: Tanzi, V.; Davoodi, H. R.
   Corruption, growth, and public finances Published: 2000
   Times Cited: 9

9. Title: [not available]
   Group Author(s): Transparency International
   Various years. Corruption Perceptions Index (CPI)
   Publisher: Transparency International, Berlin
   Times Cited: 6

10. **How taxing is corruption on international investors?**
    By: Wei, SJ
    REVIEW OF ECONOMICS AND STATISTICS Volume: 82 Issue: 1 Pages: 1-11 Published: FEB 2000
    Times Cited: 597